Atmospheric / Topographic Correction for Satellite Imagery

(ATCOR-2/3 User Guide, Version 8.2 BETA, February 2012)

R. Richter[1] and D. Schläpfer[2]
[1] DLR - German Aerospace Center, D - 82234 Wessling, Germany
[2]ReSe Applications, Langeggweg 3, CH-9500 Wil SG, Switzerland
DLR-IB 565-02/12

The cover image shows a true color subset of a Landsat-7 ETM+ scene with lake Constance at the Austrian-German-Swiss border (top left), acquired 2 June 2000. The top right image is the atmospherically corrected scene employing a haze removal over land and water. The haze removal over water is one of the new features of the 2011 release. The bottom part presents a zoomed view. The water mask is derived from the DEM file of this scene, because a unique water classification with exclusively spectral criteria is not possible in this scene. A correct water/land mask is critical for the quality of the separate haze removal algorithms over land and water.

ATCOR-2/3 User Guide, Version 8.2.0, February 2012

Authors:
R. Richter[1] and D. Schläpfer[2]
[1] DLR - German Aerospace Center, D - 82234 Wessling , Germany
[2] ReSe Applications, Langeggweg 3, CH-9500 Wil SG, Switzerland

© All rights are with the authors of this manual.

Distribution:
ReSe Applications Schläpfer
Langeggweg 3, CH-9500 Wil, Switzerland

Updates: see ReSe download page: www.rese.ch/download

The MODTRAN® trademark is being used with the expressed permission of the owner, the United States of America, as represented by the United States Air Force.

Contents

1 Introduction **11**

2 Basic Concepts in the Solar Region **14**
2.1 Radiation components . . . 16
2.2 BRDF correction . . . 19
2.3 Spectral calibration . . . 21
2.4 Inflight radiometric calibration . . . 23
2.5 De-shadowing . . . 24

3 Basic Concepts in the Thermal Region **27**

4 Workflow **29**
4.1 Menus Overview . . . 29
4.2 First steps with ATCOR . . . 31
4.3 Survey of processing steps . . . 34
4.4 Directory structure of ATCOR . . . 35
4.5 Convention for file names . . . 35
4.6 User-defined hyperspectral sensors . . . 37
4.6.1 Definition of a new sensor . . . 37
4.7 Spectral smile sensors . . . 40
4.8 Haze, cloud, water map . . . 42
4.9 Processing of multiband thermal data . . . 43
4.10 External water vapor map . . . 47

5 Description of Modules **48**
5.1 Menu: File . . . 49
5.1.1 Display ENVI File . . . 49
5.1.2 Show Textfile . . . 52
5.1.3 Select Input Image . . . 52
5.1.4 Import . . . 52
5.1.5 Plot Sensor Response . . . 53
5.1.6 Plot Calibration File . . . 53
5.1.7 Show System File . . . 53
5.1.8 Edit Preferences . . . 54
5.2 Menu: New Sensor . . . 56
5.2.1 Define Sensor Parameters . . . 57
5.2.2 Create Channel Filter Files . . . 57
5.2.3 BBCALC : Blackbody Function . . . 59

5.2.4 RESLUT : Resample Atm. LUTS from Database . . . 59
5.3 Menu: Atm. Correction . . . 61
5.3.1 The ATCOR main panel . . . 61
5.3.2 ATCOR2: multispectral sensors, flat terrain . . . 61
5.3.3 ATCOR3: multispectral sensors, rugged terrain . . . 61
5.3.4 ATCOR2: User-defined Sensors . . . 62
5.3.5 ATCOR3: User-defined Sensors . . . 62
5.3.6 SPECTRA module . . . 65
5.3.7 Aerosol Type . . . 66
5.3.8 Visibility Estimate . . . 66
5.3.9 Inflight radiometric calibration module . . . 66
5.3.10 Shadow removal panels . . . 69
5.3.11 Panels for Image Processing . . . 72
5.3.12 Start ATCOR Process (Tiled / from ∗.inn) . . . 77
5.4 Menu: Topographic . . . 78
5.4.1 Slope/Aspect . . . 78
5.4.2 Skyview Factor . . . 78
5.4.3 Shadow Mask . . . 79
5.4.4 DEM Smoothing . . . 80
5.5 Menu: Filter . . . 82
5.5.1 Resample a Spectrum . . . 82
5.5.2 Spectral Polishing: Statistical Filter . . . 82
5.5.3 Spectral Polishing: Radiometric Variation . . . 83
5.5.4 Spectral Smile Interpolation . . . 84
5.6 Menu: Simulation . . . 87
5.6.1 TOA/At-Sensor Radiance Cube . . . 87
5.6.2 At-Sensor Apparent Reflectance . . . 87
5.6.3 Resample Image Cube . . . 88
5.7 Menu: Tools . . . 89
5.7.1 Solar Zenith and Azimuth . . . 89
5.7.2 SPECL: Spectral Reflectance Classification . . . 90
5.7.3 SPECL for User Defined Sensors . . . 90
5.7.4 Nadir normalization (Wide FOV Imagery) . . . 90
5.7.5 Quick Topographic (no atm.) Correction . . . 91
5.7.6 Add a Blue Spectral Channel . . . 92
5.7.7 Spectral Smile Detection . . . 92
5.7.8 Spectral Calibration (Atm. Absorption Features) . . . 94
5.7.9 Calibration Coefficients with Regression . . . 96
5.7.10 Convert High Res. Database (New Solar Irradiance) . . . 97
5.7.11 Convert .atm for another Irradiance Spectrum . . . 97
5.8 Menu: Help . . . 99
5.8.1 Help Options . . . 99

6 Batch Processing Reference **100**
6.1 Using the batch mode . . . 100
6.2 Batch modules, keyword-driven modules . . . 101

7 Value Added Products **108**
7.1 LAI, FPAR, Albedo . . . 108
7.2 Surface energy balance . . . 110

8 Sensor simulation of hyper/multispectral imagery **116**

9 Implementation Reference and Sensor Specifics **121**
9.1 The Monochromatic atmospheric database . . . 121
9.1.1 Visible / Near Infrared region . . . 121
9.1.2 Thermal region . . . 122
9.1.3 Database update with solar irradiance . . . 123
9.1.4 Sensor-specific atmospheric database . . . 124
9.1.5 Resample sensor-specific atmospheric LUTs with another solar irradiance . . . 124
9.2 Supported I/O file types . . . 125
9.3 Preference parameters for ATCOR . . . 127
9.4 Job control parameters of the "inn" file (former "ini") . . . 130
9.5 Problems and Hints . . . 136
9.6 Metadata files (geometry and calibration) . . . 138
9.6.1 Landsat-7 ETM+ . . . 138
9.6.2 SPOT . . . 139
9.6.3 ALOS AVNIR-2 . . . 141
9.6.4 Ikonos . . . 141
9.6.5 Quickbird . . . 142
9.6.6 IRS-1C/1D Liss . . . 143
9.6.7 IRS-P6 . . . 143
9.6.8 ASTER . . . 143
9.6.9 DMC (Disaster Monitoring Constellation) . . . 144
9.6.10 RapidEye . . . 144
9.6.11 GeoEye-1 . . . 145
9.6.12 WorldView-2 . . . 145

10 Theoretical Background **146**
10.1 Basics on radiative transfer . . . 146
10.1.1 Solar spectral region . . . 146
10.1.2 Integrated Radiometric Correction (IRC) . . . 153
10.1.3 Spectral solar flux, reflected surface radiance . . . 154
10.1.4 Thermal spectral region . . . 155
10.2 Masks for haze, cloud, water, snow . . . 159
10.3 Quality layers . . . 163
10.4 Standard atmospheric conditions . . . 165
10.4.1 Constant visibility (aerosol) and atmospheric water vapor . . . 165
10.4.2 Aerosol retrieval and visibility map . . . 166
10.4.3 Water vapor retrieval . . . 171
10.5 Non-standard conditions . . . 173
10.5.1 Empirical methods for BRDF correction . . . 173
10.5.2 Haze removal over land . . . 177
10.5.3 Haze or sun glint removal over water . . . 179
10.5.4 Cirrus removal . . . 180

10.5.5 De-shadowing . . . 183
10.6 Summary of atmospheric correction steps . . . 189
10.6.1 Algorithm for flat terrain . . . 189
10.6.2 Algorithm for rugged terrain . . . 190
10.7 Spectral classification of reflectance cube . . . 191
10.8 Accuracy of the method . . . 191

References **193**

A Altitude Profile of Standard Atmospheres **199**

B Comparison of Solar Irradiance Spectra **202**

List of Figures

2.1 Visibility, AOT, and total optical thickness, atmospheric transmittance. 15
2.2 Schematic sketch of solar radiation components in flat terrain. 17
2.3 Nadir normalization of an image with hot-spot geometry. 19
2.4 BRDF correction in rugged terrain imagery. 20
2.5 Geometric function G for three thresholds of β_T. 21
2.6 Wavelength shifts for an AVIRIS scene. 22
2.7 Radiometric calibration with multiple targets using linear regression. 24
2.8 Sketch of a cloud shadow geometry. 25
2.9 De-shadowing of an Ikonos image of Munich. 25
2.10 Zoomed view of central part of Figure 2.9. 26

3.1 Atmospheric transmittance in the thermal region. 27
3.2 Radiation components in the thermal region. 28

4.1 Top level graphical interface of ATCOR. 29
4.2 Top level graphical interface of ATCOR: "File". 30
4.3 Top level graphical interface of ATCOR: "New Sensor". 30
4.4 Topographic modules. 30
4.5 Top level graphical interface of ATCOR: "Atmospheric Correction". 31
4.6 ATCOR panel for flat terrain imagery. 32
4.7 Image processing options. Right panel appears if a cirrus band exists. 33
4.8 Panel for DEM files. 34
4.9 Typical workflow of atmospheric correction. 35
4.10 Input / output image files during ATCOR processing. 36
4.11 Directory structure of ATCOR. 37
4.12 Template reference spectra from the 'spec_lib' library. 38
4.13 Directory structure of ATCOR with hyperspectral add-on. 39
4.14 Supported analytical channel filter types. 39
4.15 Optional haze/cloud/water output file. 43
4.16 Path radiance and transmittace of a SEBASS scene derived from the ISAC method. 45
4.17 Comparison of radiance and temperature at sensor and at surface level. 46

5.1 Top level menu of the satellite ATCOR. 48
5.2 The File Menu 49
5.3 Band selection dialog for ENVI file display 49
5.4 Display of ENVI imagery 51
5.5 Simple text editor to edit plain text ASCII files 52
5.6 Plotting the explicit sensor response functions 53

5.7 Plotting a calibration file . . . 54
5.8 Displaying a calibration file (same file as in Fig. 5.7) . . . 54
5.9 Panel to edit the ATCOR preferences . . . 55
5.10 The *'New Sensor'* Menu . . . 56
5.11 Sensor definition files: the three files on the left have to be provided/created by the user. . . . 56
5.12 Definition of a new sensor . . . 58
5.13 Spectral Filter Creation . . . 59
5.14 Black body function calculation panel . . . 60
5.15 Panels of RESLUT for resampling the atmospheric LUTs. . . . 60
5.16 The *'Atm. Correction'* Menu . . . 61
5.17 ATCOR panel. . . . 62
5.18 Panel for DEM files. . . . 63
5.19 Panel to make a decision in case of a DEM with steps. . . . 63
5.20 Influence of DEM artifacts on the solar illumination image. . . . 64
5.21 SPECTRA module. . . . 65
5.22 Radiometric calibration: target specification panel. . . . 67
5.23 Radiometric CALIBRATION module. . . . 68
5.24 Normalized histogram of unscaled shadow function. . . . 69
5.25 Panel to define the parameters for interactive de-shadowing. . . . 70
5.26 Quicklook of de-shadowing results. . . . 71
5.27 Image processing options. Right panel appears if a cirrus band exists. . . . 72
5.28 Emissivity selection panel. . . . 72
5.29 Options for haze processing. . . . 73
5.30 Reflectance ratio panel for dark reference pixels. . . . 73
5.31 BRDF panel. . . . 74
5.32 Value added panel for a flat terrain. . . . 75
5.33 Value added panel for a rugged terrain. . . . 75
5.34 LAI / FPAR panel . . . 76
5.35 Job status window. . . . 76
5.36 ATCOR Tiled Processing . . . 77
5.37 Topographic modules. . . . 78
5.38 Slope/Aspect Calculation panel . . . 79
5.39 Panel of SKYVIEW. . . . 80
5.40 Example of a DEM (left) with the corresponding sky view image (right). . . . 81
5.41 Panel of SHADOW. . . . 81
5.42 Panel of DEM smoothing . . . 81
5.43 Filter modules. . . . 82
5.44 Resampling of a (reflectance) spectrum. . . . 82
5.45 Statistical spectral polishing. . . . 83
5.46 Radiometric spectral polishing. . . . 84
5.47 Spectral smile interpolation . . . 86
5.48 Simulation modules menu. . . . 87
5.49 Apparent Reflectance Calculation . . . 88
5.50 The tools menu. . . . 89
5.51 Calculation of sun angles. . . . 89
5.52 SPECL: spectral classification of reflectance cube. . . . 90
5.53 Example of classification with SPECL. . . . 90

5.54 Nadir normalization. . . . 91
5.55 Topographic correction only, no atmospheric correction. . . . 92
5.56 Spectral smile detection . . . 94
5.57 SPECTRAL_CAL.: spectral calibration . . . 95
5.58 CAL_REGRESS.: radiometric calibration with more than one target . . . 96
5.59 Convert monochromanic database to new solar reference function . . . 97
5.60 Convert atmlib to new solar reference function . . . 98
5.61 The help menu. . . . 99

7.1 Water vapor partial pressure. . . . 112
7.2 Air emissivity. . . . 113

8.1 Weight factors of hyperspectral bands. . . . 117
8.2 Sensor simulation in the solar region. . . . 118
8.3 Graphical user interface of program "HS2MS". . . . 119
8.4 TOA radiances for three albedos. . . . 120

9.1 Monochromatic atmospheric database. . . . 122
9.2 Solar irradiance database. . . . 124
9.3 User interface to convert database from one to another solar irradiance. . . . 125
9.4 GUI panels of the satellite version of program RESLUT. . . . 126
9.5 SPOT orbit geometry. . . . 140
9.6 Solar and view geometry. . . . 141

10.1 Radiation components, illumination and viewing geometry. . . . 147
10.2 Schematic sketch of solar radiation components in flat terrain. . . . 149
10.3 Radiation components in rugged terrain, sky view factor. . . . 151
10.4 Solar illumination geometry and radiation components. . . . 152
10.5 Radiation components in the thermal region. . . . 156
10.6 Schematic sketch of visibility determination with reference pixel. . . . 167
10.7 Correlation of reflectance in different spectral regions. . . . 168
10.8 Rescaling of the path radiance with the blue and red band. . . . 169
10.9 Optical thickness as a function of visibility and visibility index. . . . 170
10.10 Reference and measurement channels for the water vapor method. . . . 171
10.11 APDA ratio with an exponential fit function for the water vapor. . . . 172
10.12 Nadir normalization of an image with hot-spot geometry. . . . 174
10.13 Geometric functions for empirical BRDF correction. . . . 176
10.14 Haze removal method. . . . 178
10.15 Subset of Ikonos image of Dresden, 18 August 2002. . . . 179
10.16 Haze removal over water, ALOS-AVNIR2 . . . 180
10.17 Scatterplot of apparent reflectance of cirrus (1.38 μm) band versus red band. . . . 182
10.18 Sketch of a cloud shadow geometry. . . . 183
10.19 Flow chart of processing steps during de-shadowing. . . . 184
10.20 Normalized histogram of unscaled shadow function. . . . 186
10.21 Cloud shadow maps of a HyMap scene. . . . 187
10.22 De-shadowing of a Landsat-7 ETM+ scene. . . . 189
10.23 Weighting of q function for reference pixels. . . . 190
10.24 Examples of template reflectance spectra employed by the SPECL code. . . . 191

List of Tables

4.1 Example of a sensor definition file (no thermal bands). . . . 40
4.2 Sensor definition file: instrument with thermal bands. . . . 40
4.3 Sensor definition file: smile sensor without thermal bands. . . . 41
4.4 Class label definition of "hcw" file. . . . 44

7.1 Heat fluxes for the vegetation and urban model. . . . 114

9.1 Elevation and tilt angles for Ikonos. . . . 142
9.2 Elevation and tilt angles for Quickbird. . . . 142
9.3 Radiometric coefficients c1 for ASTER. . . . 144

10.1 Class labels in the hcw file. . . . 159
10.2 Visibility iterations on negative reflectance pixels (red, NIR bands). . . . 166

A.1 Altitude profile of the dry atmosphere. . . . 199
A.2 Altitude profile of the midlatitude winter atmosphere. . . . 200
A.3 Altitude profile of the fall (autumn) atmosphere. . . . 200
A.4 Altitude profile of the 1976 US Standard. . . . 200
A.5 Altitude profile of the subarctic summer atmosphere. . . . 201
A.6 Altitude profile of the midlatitude summer atmosphere. . . . 201
A.7 Altitude profile of the tropical atmosphere. . . . 201

Chapter 1

Introduction

The objective of any radiometric correction of airborne and spaceborne imagery of optical sensors is the extraction of physical earth surface parameters such as spectral albedo, directional reflectance quantities, emissivity, and temperature. To achieve this goal, the influence of the atmosphere, solar illumination, sensor viewing geometry, and terrain information have to be taken into account. Although a lot of information from airborne and satellite imagery can be extracted without radiometric correction, the physical model based approach as implemented in ATCOR offers advantages, especially when dealing with multitemporal data and when a comparison of different sensors is required. In addition, the full potential of imaging spectrometers can only be exploited with this approach.

Although physical models can be quite successful to eliminate atmospheric and topographic effects they inherently rely on an accurate spectral and radiometric sensor calibration and on the accuracy and appropriate spatial resolution of a digital elevation model (DEM) in rugged terrain. In addition, many surfaces have a bidirectional reflectance behavior, i.e., the reflectance depends on the illumination and viewing geometry. The usual assumption of an isotropic or Lambertian reflectance law is appropriate for small field-of-view (FOV $< 30^o$, scan angle $< \pm 15^o$) sensors if viewing does not take place in the solar principal plane. However, for large FOV sensors and / or data recording close to the principal plane the anisotropic reflectance behavior of natural surfaces causes brightness gradients in the image. These effects can be removed with an empirical method that normalizes the data to nadir reflectance values. In addition, for rugged terrain areas illuminated under low local solar elevation angles, these effects also play a role and can be taken care of with an empirical method included in the ATCOR package.

The ATCOR software was developed to cover about 80% of the typical cases with a reasonable amount of coding. It is difficult if not impossible to achieve satisfactory results for all possible cases. Special features of ATCOR are the consideration of topographic effects and the capability to process thermal band imagery.

There are two ATCOR models available, one for satellite imagery, the other one for airborne imagery ([68], [69]). The satellite version of ATCOR supports all major commercially available small-to-medium FOV sensors with a sensor-specific atmospheric database of look-up tables (LUTs) containing the results of pre-calculated radiative transfer calculations. New sensors will be added on demand. The current list of supported sensors is available at this web address. A simple interface has been added to provide the possibility to include user-defined instruments. It is mainly intended for hyperspectral sensors where the center wavelength of channels is not stable and a re-calculation

of atmospheric LUTs is required, e.g., Hyperion, Chris-Proba.

An integral part of all ATCOR versions is a large database containing the results of radiative transfer calculations based on the Modtran®5 code (Berk et al. 1998, 2008). While ATCOR uses the AFRL MODTRAN code to calculate the database of atmospheric look-up tables (LUT), the correctness of the LUT's is the responsibility of ATCOR.

Historical note:
For historic reasons, the satellite codes are called ATCOR-2 (flat terrain, two geometric degrees-of-freedom DOF [56]) and ATCOR-3 (three DOF's, mountainous terrain [59]). They support all commercially available small to medium FOV satellite sensors with a sensor-specific atmospheric database. The scan angle dependence of the atmospheric correction functions within a scene is neglected here.

The airborne version is called ATCOR-4, to indicate the four geometric DOF's x, y, z, and scan angle [62]. It includes the scan angle dependence of the atmospheric correction functions, a necessary feature, because most airborne sensors have a large FOV up to 60°- 90°. While satellite sensors always operate outside the atmosphere, airborne instruments can operate in altitudes of a few hundred meters up to 20 km. So the atmospheric database has to cover a range of altitudes. Since there is no standard set of airborne instruments and the spectral / radiometric performance might change from year to year due to sensor hardware modifications, a monochromatic atmospheric database was compiled based on the Modtran®5 radiative transfer code. This database has to be resampled for each user-defined sensor.

Organization of the manual:

Chapters 2 and 3 contain a short description of the basic concepts of atmospheric correction which will be useful for newcomers. Chapter 2 discusses the solar spectral region, while chapter 3 treats the thermal region. Chapter 4 presents the workflow in ATCOR, and chapter 5 contains a detailed description of the graphical user interface panels of the major modules. Chapter 6 describes the batch processing capabilities with ATCOR. It is followed by chapters on value added products available with ATCOR, sensor simulation, miscellaneous topics, and a comprehensive chapter on the theoretical background of atmospheric correction. In the appendix, the altitude profile of the standard atmospheres and a short intercomparison of the various solar reference functions is given.

Information on the IDL version of ATCOR can be found on the internet: `http://www.rese.ch`.

What is new in the 2012 version:

- In mountainous terrain the height resolution of the radiative transfer functions is improved from 100 m to 20 m.
- The skyview calculation now supports a user-defined angular increment for azimuth/elevation and a pixel undersampling factor. The default azimuth/elevation increment is 30°/ 10° to be compatible with the previous version. The new recommendated values are 10° and 5° for azimuth and elevation, respectively. For a large scene an undersampling factor of 3 is recommended to avoid an excessive calculation time.

- The water vapor retrieval can be performed with channels in the 820 nm atmospheric absorption region. This is a useful enhancement for VIS/NIR spectrometers covering the spectrum from 400 - 900 nm. The previous version only supported a retrieval if channels exist in the 940 nm or 1130 nm region.
- Water vapor retrieval with band regression: the previous version supported the calculation of the water vapor map for ground elevations up to 2.5 km, now extrapolation is provided up to elevations of 3.5 km.
- An external water vapor map is accepted for instruments that have the capability i.e., necessary spectral bands) to derive the water vapor map. If 'scene1.bsq' is the name of the input scene and the name of the external water vapor map is 'scene1_wv.bsq' (in the same folder as the input scene) then it is automatically used and the internal calculation is bypassed.
- The correction of dark areas caused by topographic shadow has been improved.
- A positive spectral reflectance correlation factor b defines the relationship $\rho(blue) = b\ \rho(red)$ for the dark reference pixels. If $b > 0$ then the surface reflectance of the reference pixels (dense dark vegetation: DDV) in the blue band is used to modify the aerosol type (if necessary) to fulfill this equation. This option is retained in the 2012 version, but a new option with $b < 0$ is added. In this case, the program still calculates the visibility/AOT (aerosol optical thickness) map based on dark reference pixels, but retains the selected aerosol type.
- The tiling capability for large scenes is improved: while the previous version did not allow the first tile to consist only of background pixels, the new version handles any spatial distribution of background pixels in a large scene. It calculates the visibility map for the tile with the lowest percentage of background pixels, and processes the remaining tiles with the same average visibility to avoid potential brightness steps at tile borders.
- The IRC (Integrated Radiometric Correction) method [40, 41] of combined atmospheric / topographic correction in rugged terrain is included as one additional option, see chapter 10.1.2.

Chapter 2

Basic Concepts in the Solar Region

Standard books on optical remote sensing contain an extensive presentation on sensors, spectral signatures, and atmospheric effects where the interested reader is referred to (Slater 1980 [80], Asrar 1989 [2], Schowengert 1997 [78]).
This chapter describes the basic concept of atmospheric correction. Only a few simple equations (2.1-2.21) are required to understand the key issues. We start with the radiation components and the relationship between the at-sensor radiance and the digital number or grey level of a pixel. Then we are already able to draw some important conclusions about the radiometric calibration. We continue with some remarks on how to select atmospheric parameters. Next is a short discussion about the thermal spectral region. The remaining sections present the topics of BRDF correction, spectral / radiometric calibration, and de-shadowing. For a discussion of the haze removal method the reader is referred to chapter 10.5.2.

Two often used parameters for the description of the atmosphere are 'visibility' and 'optical thickness'.

Visibility and optical thickness

The visibility (horizontal meteorological range) is approximately the maximum horizontal distance a human eye can recognize a dark object against a bright sky. The exact definition is given by the Koschmieder equation:

$$VIS = \frac{1}{\beta}\, ln\frac{1}{0.02} = \frac{3.912}{\beta} \tag{2.1}$$

where β is the extinction coefficient (unit km^{-1}) at 550 nm. The term 0.02 in this equation is an arbitrarily defined contrast threshold. Another often used concept is the optical thickness of the atmosphere (δ) which is the product of the extinction coefficient and the path length x (e.g., from sea level to space in a vertical path) :

$$\delta = \beta\, x \tag{2.2}$$

The optical thickness is a pure number. In most cases, it is evaluated for the wavelength 550 nm. Generally, there is no unique relationship between the (horizontal) visibility and the (vertical) total optical thickness of the atmosphere. However, with the MODTRAN® radiative transfer code a certain relationship has been defined between these two quantities for clear sky conditions as shown in Fig. 2.1 (left) for a path from sea level to space. The optical thickness can be defined separately for the different atmospheric constituents (molecules, aerosols), so there is an optical thickness due

to molecular (Rayleigh) and aerosol scattering, and due to molecular absorption (e.g., water water, ozone etc.). The total optical thickness is the sum of the thicknesses of all individual contributors :

$$\delta = \delta(molecular\ scattering)\ +\ \delta(aerosol)\ +\ \delta(molecular\ absorption) \tag{2.3}$$

The MODTRAN® visibility parameter scales the aerosol content in the boundary layer (0 - 2 km altitude). For visibilities greater than 100 km the total optical thickness asymptotically approaches a value of about 0.17 which (at 550 nm) is the sum of the molecular thickness ($\delta = 0.0973$) plus ozone thickness ($\delta = 0.03$) plus a very small amount due to trace gases, plus the contribution of residual aerosols in the higher atmosphere (2 - 100 km) with $\delta = 0.04$. The minimum optical thickness or maximum visibility is reached if the air does not contain aerosol particles (so called "Rayleigh limit") which corresponds to a visibility of 336 km at sea level and no aerosols in the boundary layer and higher atmosphere. In this case the total optical thickness (molecular and ozone) is about $\delta = 0.13$. Since the optical thickness due to molecular scattering (nitrogen and oxygen) only depends on pressure level it can be calculated accurately for a known ground elevation. The ozone contribution to the optical thickness usually is small at 550 nm and a climatologic/geographic average can be taken. This leaves the aerosol contribution as the most important component which varies strongly in space and time. Therefore, the aerosol optical thickness (AOT) at 550 nm is often used to characterize the atmosphere instead of the visibility.

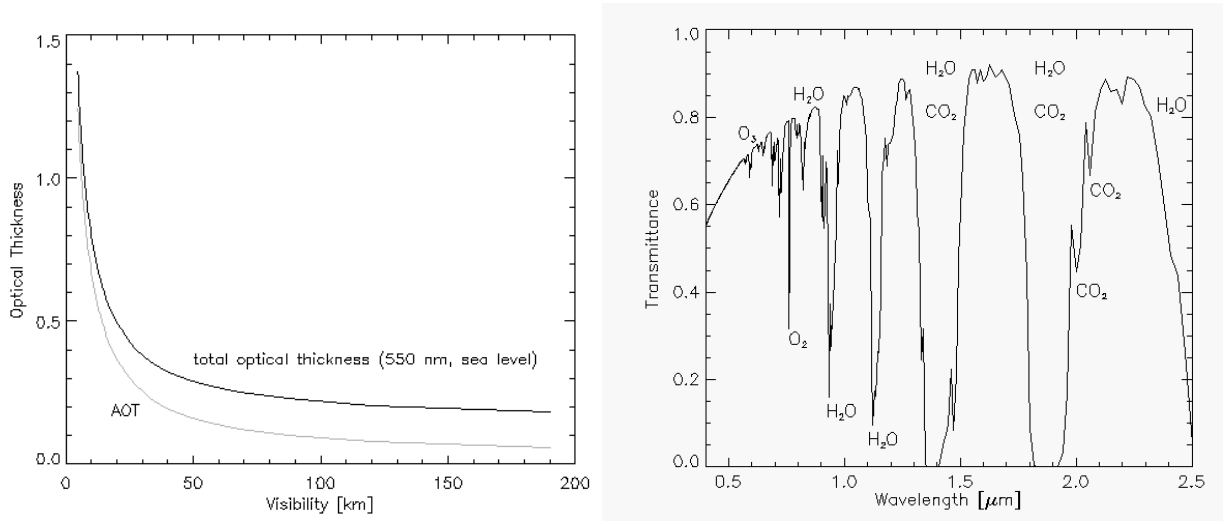

Figure 2.1: *Visibility, AOT, and total optical thickness, atmospheric transmittance.*

The atmospheric (direct or beam) transmittance for a vertical path through the atmosphere can be calculated as :

$$\tau = e^{-\delta} \tag{2.4}$$

Fig. 2.1 (right) shows an example of the atmospheric transmittance from 0.4 to 2.5 μm. The spectral regions with relatively high transmittance are called "atmospheric window" regions. In absorbing regions the name of the molecule responsible for the attenuation of radiation is included.

Apparent reflectance

The apparent reflectance describes the combined earth/atmosphere behavior with respect to the reflected solar radiation:

$$\rho(apparent) = \frac{\pi \ d^2 \ L}{E \ cos\theta_s} \tag{2.5}$$

where d is the earth-sun distance in astronomical units, $L = c_0 + c1 \ DN$ is the at-sensor radiance, c_0, c_1, DN, are the radiometric calibration offset, gain, and digital number, respectively. E and θ_s are the extraterrestrial solar irradiance and solar zenith angle, respectively. For imagery of satellite sensors the apparent reflectance is also named top-of-atmosphere (TOA) reflectance.

2.1 Radiation components

We start with a discussion of the radiation components in the solar region, i.e., the wavelength spectrum from 0.35 - 2.5 μm. Figure 2.2 shows a schematic sketch of the total radiation signal at the sensor. It consists of three components:

1. path radiance (L_1), i.e., photons scattered into the sensor's instantaneous field-of-view, without having ground contact.
2. reflected radiation (L_2) from a certain pixel: the direct and diffuse solar radiation incident on the pixel is reflected from the surface. A certain fraction is transmitted to the sensor. The sum of direct and diffuse flux on the ground is called global flux.
3. reflected radiation from the neighborhood (L_3), scattered by the air volume into the current instantaneous direction, the adjacency radiance. As detailed in [65] the adjacency radiation L_3 consists of two components (atmospheric backscattering and volume scattering) which are combined into one component in Fig. 2.2 to obtain a compact description.

Only radiation component 2 contains information from the currently viewed pixel. The task of atmospheric correction is the calculation and removal of components 1 and 3, and the retrieval of the ground reflectance from component 2.

So the total radiance signal L can be written as :

$$L = L_{path} + L_{reflected} + L_{adj} (= L_1 + L_2 + L_3) \tag{2.6}$$

The path radiance decreases with wavelength. It is usually very small for wavelengths greater than 800 nm. The adjacency radiation depends on the reflectance or brightness difference between the currently considered pixel and the large-scale (0.5-1 km) neighborhood. The influence of the adjacency effect also decreases with wavelength and is very small for spectral bands beyond 1.5 μm [65].

For each spectral band of a sensor a linear equation describes the relationship between the recorded brightness or digital number DN and the at-sensor radiance (Fig. 2.2) :

$$L = c_0 + c_1 * DN \tag{2.7}$$

The c_0 and c_1 are called radiometric calibration coefficients. The radiance unit in ATCOR is $mWcm^{-2}sr^{-1}\mu m^{-1}$. For instruments with an adjustable gain setting g the corresponding equation is :

$$L = c_0 + \frac{c_1}{g} * DN \tag{2.8}$$

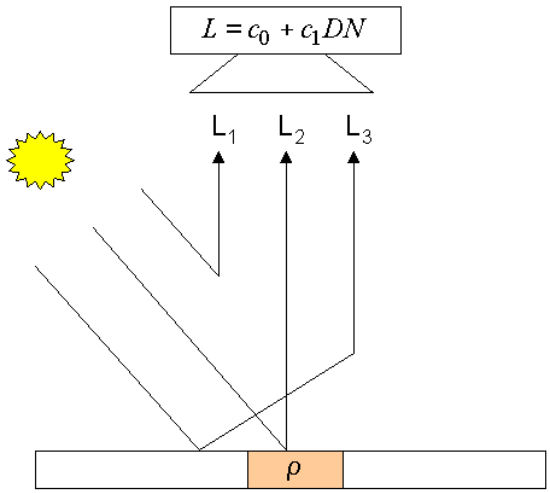

Figure 2.2: *Schematic sketch of solar radiation components in flat terrain.*
L_1 : path radiance, L_2 : reflected radiance, L_3 : adjacency radiation.

During the following discussion we will always use eq. (2.7). Disregarding the adjacency component we can simplify eq. (2.6)

$$L = L_{path} + L_{reflected} = L_{path} + \tau\rho E_g/\pi = c_0 + c_1 DN \tag{2.9}$$

where τ, ρ, and E_g are the ground-to-sensor atmospheric transmittance, surface reflectance, and global flux on the ground, respectively. Solving for the surface reflectance we obtain :

$$\rho = \frac{\pi\{d^2(c_0 + c_1 DN) - L_{path}\}}{\tau E_g} \tag{2.10}$$

The factor d^2 takes into account the sun-to-earth distance (d is in astronomical units), because the LUT's for path radiance and global flux are calculated for d=1 in ATCOR. Equation (2.9) is a key formula to atmospheric correction. A number of important conclusions can now be drawn:

- An accurate radiometric calibration is required, i.e., a knowledge of c_0 , c_1 in each spectral band.
- An accurate estimate of the main atmospheric parameters (aerosol type, visibility or optical thickness, and water vapor) is necessary, because these influence the values of path radiance, transmittance, and global flux.
- If the visibility is assumed too low (optical thickness too high) the path radiance becomes high, and this may cause a physically unreasonable negative surface reflectance. Therefore, dark surfaces of low reflectance, and correspondingly low radiance $c_0 + c_1 DN$, are especially sensitive in this respect. They can be used to estimate the visibility or at least a lower bound. If the reflectance of dark areas is known the visibility can actually be calculated. The interested reader may move to chapter 10.4.2, but this is not necessary to understand the remaining part of the chapter.
- If the main atmospheric parameters (aerosol type or scattering behavior, visibility or optical thickness, and water vapor column) and the reflectance of two reference surfaces are measured,

the quantities L_{path}, τ, ρ, and E_g are known. So, an "inflight calibration" can be performed to determine or update the knowledge of the two unknown calibration coefficients $c_0(k)$, $c_1(k)$ for each spectral band k, see section 2.4.

Selection of atmospheric parameters

The optical properties of some air constituents are accurately known, e.g., the molecular or Rayleigh scattering caused by nitrogen and oxygen molecules. Since the mixing ratio of nitrogen and oxygen is constant the contribution can be calculated as soon as the pressure level (or ground elevation) is specified. Other constituents vary slowly in time, e.g., the CO_2 concentration. ATCOR calculations were performed for a concentration of 380 ppmv. Ozone may also vary in space and time. Since ozone usually has only a small influence ATCOR employs a fixed value of 330 DU (Dobson units, corresponding to the former unit 0.33 atm-cm, for a ground at sea level) representing average conditions. The three most important atmospheric parameters that vary in space and time are the aerosol type, the visibility or optical thickness, and the water vapor. We will mainly work with the term *visibility* (or meteorological range), because the radiative transfer calculations were performed with the Modtran®5 code (Berk et al., 1998, 2008), and visibility is an intuitive input parameter in MODTRAN®, although the aerosol optical thickness can be used as well. ATCOR employs a database of LUTs calculated with Modtran®5.

Aerosol type

The aerosol type includes the absorption and scattering properties of the particles, and the wavelength dependence of the optical properties. ATCOR supports four basic aerosol types: rural, urban, maritime, and desert. The aerosol type can be calculated from the image data provided that the scene contains vegetated areas. Alternatively, the user can make a decision, usually based on the geographic location. As an example, in areas close to the sea the maritime aerosol would be a logical choice if the wind was coming from the sea. If the wind direction was toward the sea and the air mass is of continental origin the rural, urban, or desert aerosol would make sense, depending on the geographical location. If in doubt, the rural (continental) aerosol is generally a good choice. The aerosol type also determines the wavelength behavior of the path radiance. Of course, nature can produce any transitions or mixtures of these basic four types. However, ATCOR is able to adapt the wavelength course of the path radiance to the current situation provided spectral bands exist in the blue-to-red- region and the scene contains reference areas of known reflectance behavior. The interested reader may read chapter 10.4.2 for details.

Visibility estimation

Two options are available in ATCOR:

- An interactive estimation in the SPECTRA module (compare chapter 5). The spectra of different targets in the scene can be displayed as a function of visibility. A comparison with reference spectra from libraries determines the visibility. In addition, dark targets like vegetation in the blue-to-red spectrum or water in the red-to-NIR can be used to estimate the visibility.

- An automatic calculation of the visibility can be performed if the scene contains dark reference pixels. The interested reader is referred to chapter 10.4.2 for details.

Water vapor column

The water vapor content can be automatically computed if the sensor has spectral bands in water vapor regions (e.g., 920-960 nm). The approach is based on the differential absorption method

and employs bands in absorption regions and window regions to measure the absorption depth, see chapter 10.4.3. Otherwise, if a sensor does not possess spectral bands in water vapor regions, e.g. Landsat TM or SPOT, an estimate of the water vapor column based on the season (summer / winter) is usually sufficient. Typical ranges of water vapor columns are (sea-level-to space):

tropical conditions:	wv=3-5 cm (or g cm^{-2})
midlatitude summer:	wv= 2-3 cm
dry summer, spring, fall:	wv=1-1.5 cm
dry desert or winter:	wv=0.3-0.8 cm

2.2 BRDF correction

The reflectance of many surface covers depends on the viewing and solar illumination geometry. This behavior is described by the bidirectional reflectance distribution function (BRDF). It can clearly be observed in scenes where the view and / or sun angles vary over a large angular range.

Since most sensors of the satellite version of ATCOR have a small field-of-view, these effects will only play a role in rugged terrain and for the wide FOV sensors such as IRS-1D WiFS or MERIS.

For flat terrain scenes across-track brightness gradients that appear after atmospheric correction are caused by BRDF effects, because the sensor's view angle varies over a large range. In extreme cases when scanning in the solar principal plane, the brightness is particularly high in the hot spot angular region where retroreflection occurs, see Figure 2.3, left image, left part. The opposite scan angles (with respect to the central nadir region) show lower brightness values. A simple method, called nadir normalization or across-track illumination correction, calculates the brightness as a function of scan angle, and multiplies each pixel with the reciprocal function.

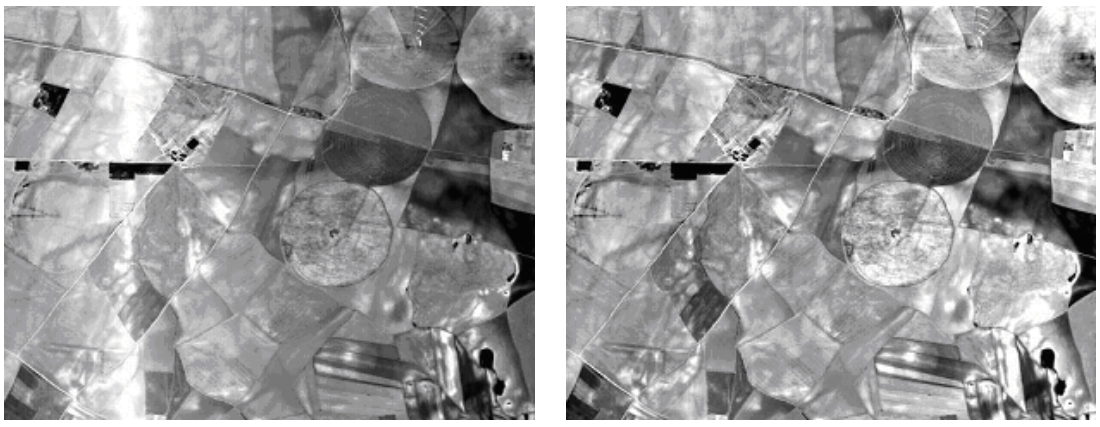

Figure 2.3: *Nadir normalization of an image with hot-spot geometry.*
Left: reflectance image without BRDF correction. Right: after empirical BRDF correction.

The BRDF effect can be especially strong in rugged terrain with slopes facing the sun and others oriented away from the sun. In areas with steep slopes the local solar zenith angle β may vary from 0° to 90°, representing geometries with maximum solar irradiance to zero direct irradiance,

i.e., shadow. The angle β is the angle between the surface normal of a DEM pixel and the solar zenith angle of the scene. In mountainous terrain there is no simple method to eliminate BRDF effects. The usual assumption of an isotropic (Lambertian) reflectance behavior often causes an overcorrection of faintly illuminated areas where local solar zenith angles β range from 60°- 90°. These areas appear very bright, see Figure 2.4, left part.

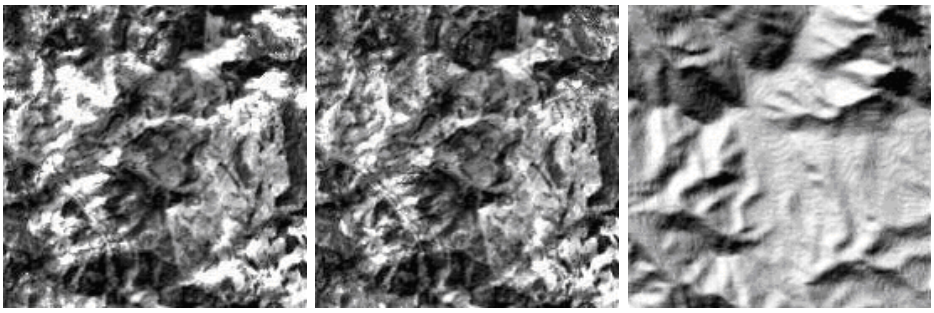

Figure 2.4: *BRDF correction in rugged terrain imagery.*
Left: image without BRDF correction. Center: after BRDF correction with threshold angle β_T = 65°. Right: illumination map = $cos\beta$.

To avoid a misclassification of these bright areas the reflectance values have to be reduced (Fig. 2.4, center part). In ATCOR empirical geometry-dependent functions are used for this purpose. For details the interested reader is referred to chapter 10.5.1, but the main idea is also discussed here. In the simplest cases, the empirical BRDF correction employs only the local solar zenith angle β_i and a threshold β_T to reduce the overcorrected surface reflectance ρ_L with a factor G, compare Figure 2.5.

$$\rho_{corrected} = \rho_L G \tag{2.11}$$

where

$$G = \{cos\beta_i / cos\beta_T\}^b \quad \geq g \tag{2.12}$$

The exponent b is in the range 1/3 to 1, see chapter 10.5.1 for details. So the reflectance is only decreased for local solar zenith angles $\beta_i > \beta_T$ until the minimum value $G = g$ is reached. The parameters β_T and g may be scene-dependent and can be set by the user. In many cases the default g=0.25 works fine and only the threshold angle β_T has to be adapted.

Choice of β_T

The threshold illumination angle β_T should have some margin to the solar zenith angle to retain the original natural variation of pixels with illumination angles close to the solar zenith angle. The threshold angle can be specified by the user and the following empirical rules are recommended:

- $\beta_T = \theta_s + 20°$ if $\theta_s < 45°$
- If $45 \leq \theta_s \leq 20°$ then $\beta_T = \theta_s + 15°$
- If $\theta_s > 55°$ then $\beta_T = \theta_s + 10°$

These rules are automatically applied if $\beta_T = 0$, e.g., during batch processing.

The angle β_T can actually be calculated from the imagery as demonstrated by the following example. When processing the scene with ATCOR the map of local solar zenith angles is stored in

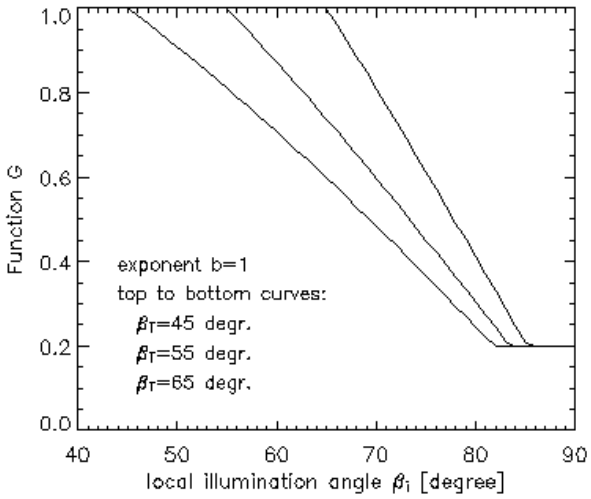

Figure 2.5: *Geometric function G for three thresholds of β_T.*
The reflectance is not modified for $\beta_i \leq \beta_T$, ($\beta_T = 45°, 55°, 65°$), and reduced for $\beta_i > \beta_T$ until the minimum value g=0.2 is reached.

a separate file "*ilu". If the output file after atmospheric / topographic correction contains bright overcorrected areas this file should be linked to the "*ilu" file using any available standard image processing software. The "*ilu" file contains the illumination map β_i scaled as byte data:

$$ilu = 100 * cos\beta_i \tag{2.13}$$

$$\beta_i = arccos(ilu/100) \tag{2.14}$$

Let us assume an example:
A pixel in a dark area of the "*ilu" image has the value ilu=32, i.e., $\beta_i = 71°$. The overcorrected reflectance value be $\rho_L = 80\%$ and this value shall be reduced to 40%, a value typical for the flat-terrain neighborhood. Then the threshold angle has to be specified such that $cos\beta_i/cos\beta_T = 0.5$ (with exponent b=1 in equation (2.12), in this case $\beta_T = 50°$. So, if the desired reflectance reduction factor is G then the required threshold angle can be calculated from eq. (2.12 with b=1):

$$\beta_T = arccos(\frac{cos\beta}{G}) = arccos\frac{ilu}{100G} \tag{2.15}$$

In many cases a separate treatment of BRDF effects for soil/rock and vegetation provides better results. For this purpose, two modes of BRDF correction are available for vegetation, compare the graphical user interface of Figure 5.31. The first mode is superior in most cases.

Reference [67] contains a comparison of different topographic correction methods for several Landsat-TM, ETM+, and SPOT-5 scenes from different areas. The proposed empirical ATCOR approach performed best in most of these cases, but no method ranked first in all cases.

2.3 Spectral calibration

This section can be skipped if data processing is only performed for imagery of broad-band sensors. Sensor calibration problems may pertain to spectral properties, i.e., the channel center positions

and / or bandwidths might have changed compared to laboratory measurements, or the radiometric properties, i.e., the offset (c_o) and slope (c_1) coefficients, relating the digital number (DN) to the at-sensor radiance $L = c_0 + c_1 * DN$. Any spectral mis-calibration can usually only be detected from narrow-band hyperspectral imagery as discussed in this section. For multispectral imagery, spectral calibration problems are difficult or impossible to detect, and an update is generally only performed with respect to the radiometric calibration coefficients, see chapter 2.4.

Surface reflectance spectra retrieved from narrow-band hyperspectral imagery often contain spikes and dips in spectral absorption regions of atmospheric gases (e.g., oxygen absorption around 760 nm, water vapor absorption around 940 nm). These effects are most likely caused by a spectral mis-calibration. In this case, an appropiate shift of the center wavelengths of the channels will remove the spikes. This is performed by an optimization procedure that minimizes the deviation between the surface reflectance spectrum and the corresponding smoothed spectrum. The merit function to be minimized is

$$\chi^2(\delta) = \sum_{i=1}^{n} \{\rho_i^{surf}(\delta) - \rho_i^{smooth}\}^2 \tag{2.16}$$

where $\rho_i^{surf}(\delta)$ is the surface reflectance in channel i calculated for a spectral shift δ, ρ_i^{smooth} is the smoothed (low pass filtered) reflectance, and n is the number of bands in each spectrometer of a hyperspectral instrument. So the spectral shift is calculated independently for each spectrometer. In the currently implemented version, the channel bandwidth is not changed and the laboratory values are assumed valid. More details of the method are described in [26]. A spectral re-calibration should precede any re-calibration of the radiometric calibration coefficients; see section 5.7.8 for details about this routine.

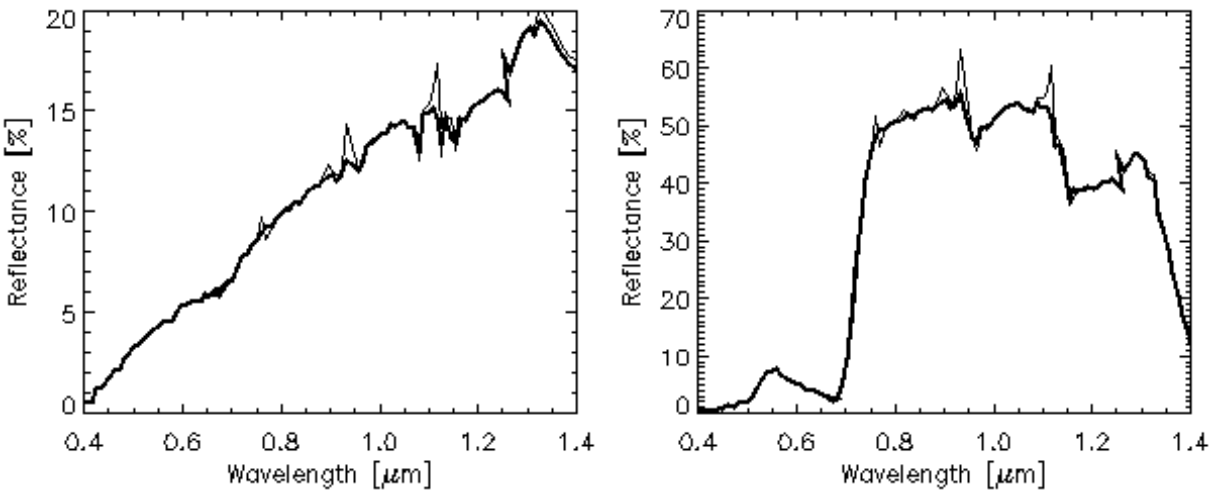

Figure 2.6: *Wavelength shifts for an AVIRIS scene.*

Figure 2.6 shows a comparison of the results of the spectral re-calibration for a soil and a vegetation target retrieved from an AVIRIS scene (16 Sept. 2000, Los Angeles area). The flight altitude was 20 km above sea level (asl), heading west, ground elevation 0.1 km asl, the solar zenith and azimuth angles were 41.2°and 135.8°. Only part of the spectrum is shown for a better visual comparison

of the results based on the original spectral calibration (thin line) and the new calibration (thick line). The spectral shift values calculated for the 4 individual spectrometers of AVIRIS are 0.1, -1.11, -0.88, and -0.21 nm, respectively.

2.4 Inflight radiometric calibration

Inflight radiometric calibration experiments are performed to check the validity of the laboratory calibration. For spaceborne instruments processes like aging of optical components or outgassing during the initial few weeks or months after launch often necessitate an updated calibration. This approach is also employed for airborne sensors because the aircraft environment is different from the laboratory and this may have an impact on the sensor performance. The following presentation only discusses the radiometric calibration and assumes that the spectral calibration does not change, i.e., the center wavelength and spectral response curve of each channel are valid as obtained in the laboratory, or it was already updated as discussed in chapter 2.3. Please refer to section 5.3.9 for further detail about how to perform an inflight calibration.

The radiometric calibration uses measured atmospheric parameters (visibility or optical thickness from sun photometer, water vapor content from sun photometer or radiosonde) and ground reflectance measurements to calculate the calibration coefficients c_0 , c_1 of equation (2.7) for each band. For details, the interested reader is referred to the literature (Slater et al., 1987 [82], Santer et al. 1992, Richter 1997). Depending of the number of ground targets we distinguish three cases: a single target, two targets, and more than two targets.

Calibration with a single target

In the simplest case, when the offset is zero ($c_0 = 0$), a single target is sufficient to determine the calibration coefficient c_1:

$$L_1 = c_1 DN_1^* = L_{path} + \tau \rho_1 E_g / \pi \tag{2.17}$$

L_{path} , τ, and E_g are taken from the appropriate LUT's of the atmospheric database, ρ_1 is the measured ground reflectance of target 1, and the channel or band index is omitted for brevity. DN_1^* is the digital number of the target, averaged over the target area and already corrected for the adjacency effect. Solving for c_1 yields:

$$c_1 = \frac{L_1}{DN_1^*} = \frac{L_{path} + \tau \rho_1 E_g / \pi}{DN_1^*} \tag{2.18}$$

Remark: a bright target should be used here, because for a dark target any error in the ground reflectance data will have a large impact on the accuracy of c_1.

Calibration with two targets

In case of two targets a bright and a dark one should be selected to get a reliable calibration. Using the indices 1 and 2 for the two targets we have to solve the equations:

$$L_1 = c_0 + c_1 * DN_1^* \qquad\qquad L_2 = c_0 + c_1 * DN_2^* \tag{2.19}$$

This can be performed with the c_0&c_1 *option* of ATCOR's calibration module, see chapter 5. The result is:

$$c_1 = \frac{L_1 - L_2}{DN_1^* - DN_2^*} \tag{2.20}$$

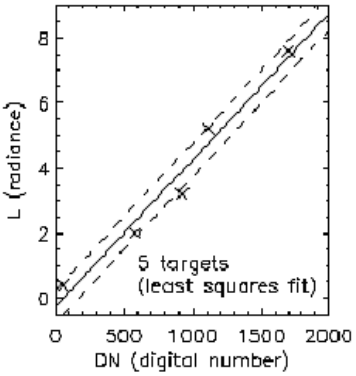

Figure 2.7: *Radiometric calibration with multiple targets using linear regression.*

$$c_0 = L_1 - c_1 * DN_1^* \tag{2.21}$$

Equation (2.20) shows that DN_1^* must be different from DN_2^* to get a valid solution, i.e., the two targets must have different surface reflectances in each band. If the denominator of eq. (2.20) is zero ATCOR will put in a 1 and continue. In that case the calibration is not valid for this band. The requirement of a dark and a bright target in all channels cannot always be met.

Calibration with n > 2 targets

In cases where n > 2 targets are available the calibration coefficients can be calculated with a least squares fit applied to a linear regression equation, see figure 2.7. This is done by the "cal_regress" program of ATCOR. It employs the "*.rdn" files obtained during the single-target calibration (the "c1 option" of ATCOR's calibration module. See section 5.7.9 for details about how to use this routine.
Note: If several calibration targets are employed, care should be taken to select targets without spectral intersections, since calibration values at intersection bands are not reliable. If intersections of spectra cannot be avoided, a larger number of spectra should be used, if possible, to increase the reliability of the calibration.

2.5 De-shadowing

Remotely sensed optical imagery of the Earth's surface is often contaminated with cloud and cloud shadow areas. Surface information under cloud covered regions cannot be retrieved with optical sensors, because the signal contains no radiation component being reflected from the ground. In shadow areas, however, the ground-reflected solar radiance is always a small non-zero signal, because the total radiation signal at the sensor contains a direct (beam) and a diffuse (reflected skylight) component. Even if the direct solar beam is completely blocked in shadow regions, the reflected diffuse flux will remain, see Fig. 2.8. Therefore, an estimate of the fraction of direct solar irradiance for a fully or partially shadowed pixel can be the basis of a compensation process called de-shadowing or shadow removal. The method can be applied to shadow areas cast by clouds or buildings.

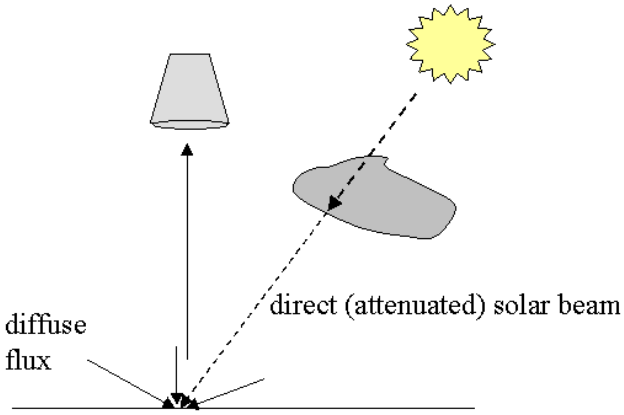

Figure 2.8: *Sketch of a cloud shadow geometry.*

Figure 2.9 shows an example of removing building shadows. The scene covers part of the central area of Munich. It was recorded by the Ikonos-2 sensor (17 Sept. 2003). The solar zenith and azimuth angles are 46.3°and 167.3°, respectively. After shadow removal the scene displays a much lower contrast, of course, but many details can be seen that are hidden in the uncorrected scene, see the zoom images of figure 2.10. The central zoom image represents the shadow map, scaled between 0 and 1000. The darker the area the lower the fractional direct solar illumination, i.e. the higher the amount of shadow. Some artifacts can also be observed in Figure 2.9, e.g., the Isar river at the bottom right escaped the water mask, entered the shadow mask, and is therefore overcorrected.

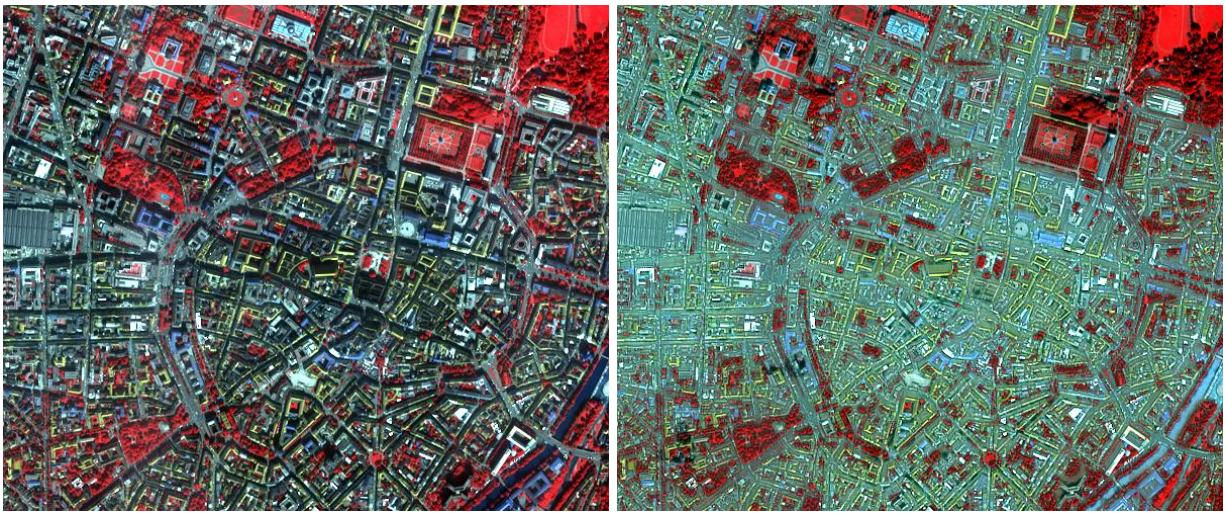

Figure 2.9: *De-shadowing of an Ikonos image of Munich.*
©European Space Imaging GmbH 2003. Color coding: RGB = bands 4/3/2 (800/660/550 nm). Left: original, right: de-shadowed image.

The proposed de-shadowing technique works for multispectral and hyperspectral imagery over land

Figure 2.10: *Zoomed view of central part of Figure 2.9.*
Courtesy of European Space Imaging, Color coding: RGB = bands 4/3/2.
Left: original, center: shadow map, right: de-shadowed image.

acquired by satellite / airborne sensors. The method requires a channel in the visible and at least one spectral band in the near-infrared (0.8-1 μm) region, but performs much better if bands in the short-wave infrared region (around 1.6 and 2.2 μm) are available as well. A fully automatic shadow removal algorithm has been implemented. However, the method involves some scene-dependent thresholds that might be optimized during an interactive session. In addition, if shadow areas are concentrated in a certain part of the scene, say in the lower right quarter, the performance of the algorithm improves by working on the subset only.

The de-shadowing method employs masks for cloud and water. These areas are identified with spectral criteria and thresholds. Default values are included in a file in the ATCOR path, called "preferences/preference_parameters.dat". As an example, it includes a threshold for the reflectance of water in the NIR region, ρ=5% . So, a reduction of this threshold will reduce the number of pixels in the water mask. A difficult problem is the distinction of water and shadow areas. If water bodies are erroneously included in the shadow mask, the resulting surface reflectance values will be too high.

Details about the processing panels can be found in section 5.3.10.

Chapter 3

Basic Concepts in the Thermal Region

Fig. 3.1 (left) presents an overview of the atmospheric transmittance in the 2.5 - 14 μm region. The main absorbers are water vapor and CO_2 which totally absorb in some parts of the spectrum. In the thermal region (8 - 14 μm) the atmospheric transmittance is mainly influenced by the water vapor column, ozone (around 9.6 μm) and CO_2 (at 14 μm). Fig. 3.1 (right) shows the transmittance for three levels of water vapor columns w=0.4, 1.0, 2.9 cm, representing dry, medium, and humid conditions. The aerosol influence still exists, but is strongly reduced compared to the solar spectral region because of the much longer wavelength. So an accurate estimate of the water vapor column is required in this part of the spectrum to be able to retrieve the surface properties, i.e., spectral emissivity and surface temperature.

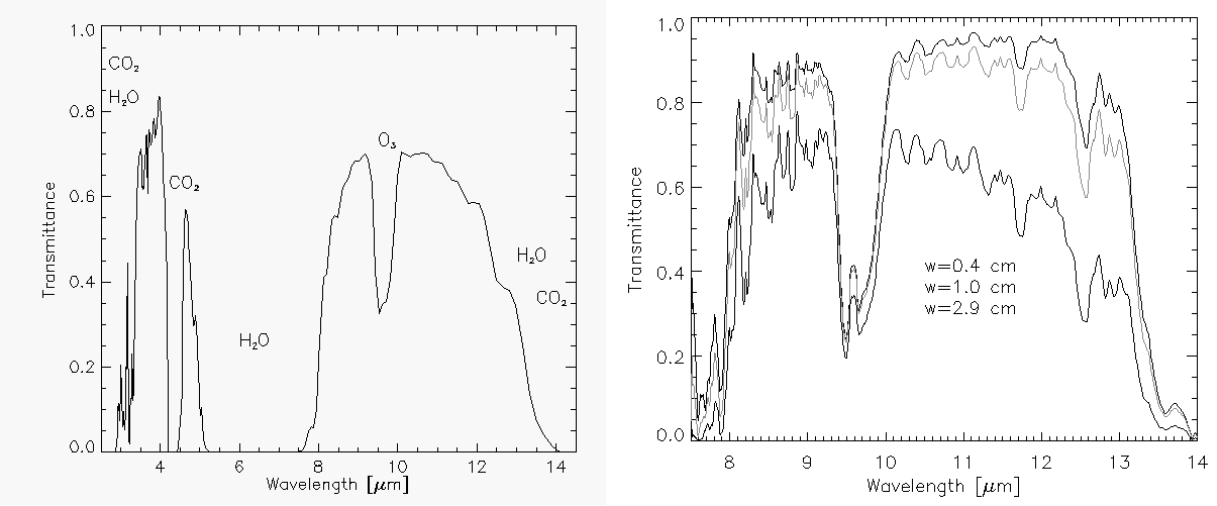

Figure 3.1: *Atmospheric transmittance in the thermal region.*

Similar to the solar region, there are three radiation components: thermal path radiance (L_1), i.e., photons emitted by the atmospheric layers, emitted surface radiance (L_2), and reflected radiance (L_3).
In the thermal spectral region from 8 - 14 μm the radiance signal can be written as

$$L = L_{path} + \tau\epsilon L_{BB}(T) + \tau(1-\epsilon)F/\pi \tag{3.1}$$

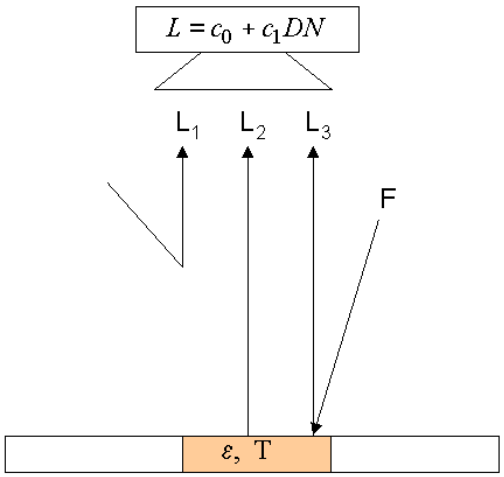

Figure 3.2: *Radiation components in the thermal region.*
$L_1 = L_P$, $L_2 = \tau\ \epsilon\ L_{BB}(T)$, $L_3 = \tau\ (1-\epsilon)\ F/\pi$.

where L_{path} is the thermal path radiance, i.e., emitted and scattered radiance of different layers of the air volume between ground and sensor, τ is the atmospheric ground-to-sensor transmittance, ϵ is the surface emissivity ranging between 0 and 1, $L_{BB}(T)$ is Planck's blackbody radiance of a surface at temperature T, and F is the thermal downwelling flux of the atmosphere, see Fig. 3.2. So the total signal consists of path radiance, emitted surface radiance, and reflected atmospheric radiation. The adjacency radiation, i.e., scattered radiation from the neighborhood of a pixel, can be neglected because the scattering efficiency decreases strongly with wavelength.

For most natural surfaces the emissivity in the 8-12 μm spectral region ranges between 0.95 and 0.99. Therefore, the reflected downwelling atmospheric flux contributes only a small fraction to the signal. Neglecting this component for the simplified discussion of this chapter we can write

$$L_{BB}(T) = \frac{L - L_{path}}{\tau\epsilon} = \frac{c_0 + c_1 DN - L_{path}}{\tau\epsilon} \tag{3.2}$$

In the thermal region the aerosol type plays a negligible role because of the long wavelength, and atmospheric water vapor is the dominating parameter. So the water vapor, and to a smaller degree the visibility, determine the values of L_{path} and τ. In case of coregistered bands in the solar and thermal spectrum the water vapor and visibility calculation may be performed with the solar channels. In addition, if the surface emissivity is known, the temperature T can be computed from eq. (3.2) using Planck's law.

For simplicity a constant emissivity $\epsilon = 1.0$ or $\epsilon = 0.98$ is often used and the corresponding temperature is called brightness temperature. The kinetic surface temperature differs from the brightness temperature if the surface emissivity does not match the assumed emissivity. With the assumption $\epsilon = 1.0$ the kinetic temperature is always higher than the brightness temperature. As a rule of thumb an emissivity error of 0.01 (one per cent) yields a surface temperature error of 0.5K.

For rugged terrain imagery no slope/aspect correction is performed for thermal bands, only the elevation-dependence of the atmospheric parameters is taken into account.

Chapter 4

Workflow

This chapter familiarizes the user with ATCOR 2/3's workflow and with the program's basic functionality using the graphical user interface. A detailed description of all modules and user interface panels is given in the subsequent chapter 5.
ATCOR may also be used in batch mode for most of its functions. A description of the batch mode can be found in chapter 6.

4.1 Menus Overview

To start ATCOR, double click the file 'atcor.sav'. It will be opened through IDL or the IDL virtual machine and the graphical user interface of Fig. 4.1 will pop up. Alternatively, type *atcor* on the IDL command line after having added the *atcor*-directory to the IDL search path. A large number of processing modules is available from this level as described in chapter 5. Most of them can be used without reading a detailed manual description because they contain explanations in the panels themselves. However, the next section guides the ATCOR newcomer during the atmospheric correction of a sample scene. The functions in the *"File"* menu allow the display of an image file, the on-screen display of calibration files, sensor response curves etc, see Fig. 4.2. More details about this menu are given in chapter 5.1.

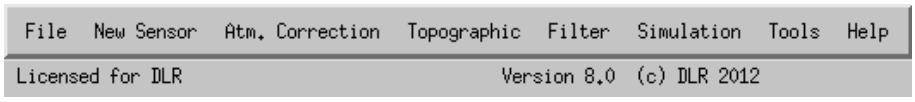

Figure 4.1: *Top level graphical interface of ATCOR.*

The *"New Sensor"* menu of Fig. 4.1 is available if the module for hyperspectral (or user-defined) sensors is licensed. It contains routines to create spectral filter curves (rectangular, Gaussian, etc) from a 3-column ASCII file (band number, center wavelength, bandwidth, one line per channel) provided by the user, calculates atmospheric look-up tables (LUTs) for new sensors, and computes the radiance/temperature functions for thermal bands; see Fig. 4.3 and chapter 5.2.

The menu *"Atm. Correction"* gives access to the ATCOR core processes for atmospheric correction in flat and rugged terrain. For both, multispectral and hyperspectral instruments. It also gives access to the tiled processing. It is further described in section 4.2 below and chapter 5.3.

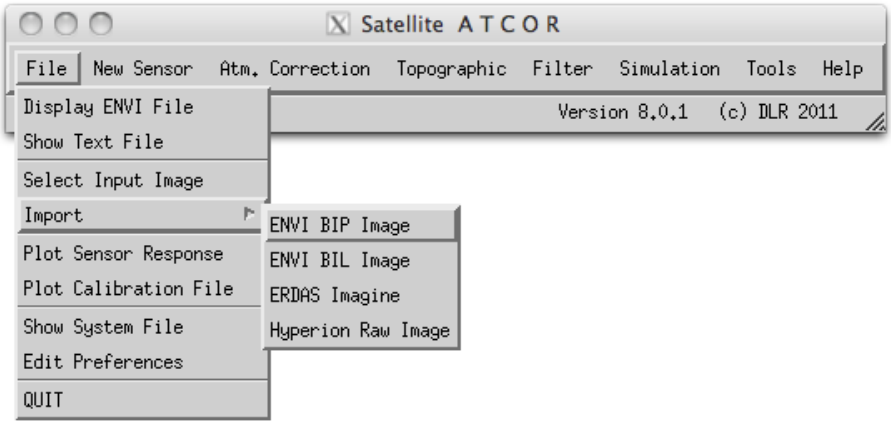

Figure 4.2: *Top level graphical interface of ATCOR: "File".*

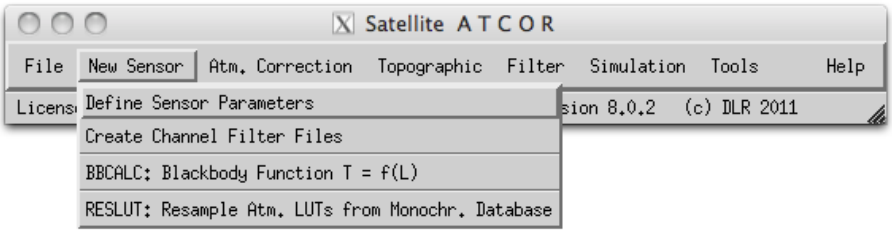

Figure 4.3: *Top level graphical interface of ATCOR: "New Sensor".*

The *"Topographic"* menu contains programs for the calculation of slope/aspect images from a digital elevation model, the skyview factor, and topographic shadow. Furthermore, it supports the smoothing of DEMs and its related layers, see chapter 5.4.

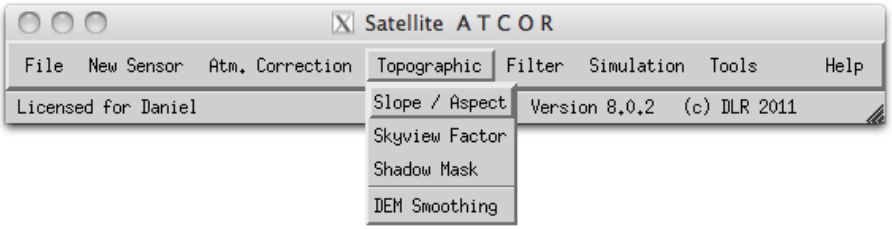

Figure 4.4: *Topographic modules.*

The *"Filter"* menu provides spectral filtering of single spectra (reflectance, emissivity, radiance) provided as ASCII files, spectral filtering of image cubes, and spectral polishing; see chapter 5.5.

The *"Simulation"* menu provides programs for the simulation of at-sensor radiance scenes based on surface reflectance (or emissivity and temperature) images; see chapter 5.6.

The *"Tools"* menu contains a collection of useful routines such as the calculation of the solar

zenith and azimuth angles, spectral classification, nadir normalization for wide field-of-view imagery, adding of a synthetic blue channel for multispectral sensors without a blue band (e.g. SPOT), spectral calibration, conversion of the monochromatic atmospheric database from one to another solar irradiance spectrum, BIL to BSQ conversion, and more; see chapter 5.7.

Finally, the *"Help"* menu allows browsing of the ATCOR user manual, provides a link to web resources, and displays license and credits information, see chapter 5.8.

4.2 First steps with ATCOR

The *'Atm.Correction'* button of Fig. 4.5 displays the choices *'ATCOR2: multispectral sensors, flat terrain'* and *'ATCOR3: multispectral sensors, rugged terrain'*. If the add-on for user-defined (mainly hyperspectral) sensors is included, then the buttons *'ATCOR2: hyperspectral sensors, flat terrain'* and *'ATCOR3: hyperspectral sensors, rugged terrain'* will also appear, compare Fig. 4.5. The last button starts the ATCOR processing in the image tiling mode, i.e., the image is divided into sub-images in x and y direction as specified by the user. This mode is intended for large scenes, compare section 5.3.12, and the *'*.inn'* file with the processing parameters must already exist.

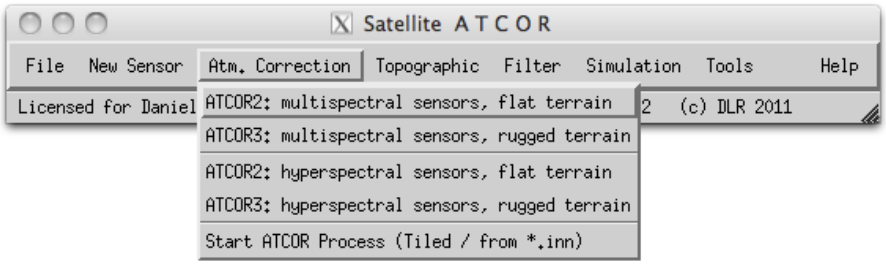

Figure 4.5: *Top level graphical interface of ATCOR: "Atmospheric Correction".*

Let us start with a scene from a flat terrain area where no digital elevation model (DEM) is needed. Then the panel of Fig. 4.6 will pop up. First, the 'INPUT IMAGE FILE' has to be selected. ATCOR requires the band sequential format (BSQ) for the image data with an ENVI header. The TIFF format is supported with some restrictions, see chapter 9.2. Next the acquisition date of the image has to be updated with the corresponding button. We work from top to bottom to specify the required information. The scale factor defines the multiplication factor for surface reflectance (range 0 - 100%) in the output file. A scale factor of 1 yields the output as float data (4 bytes per pixel). However, a scale factor of 100 is recommended if the input data is 16 bit (2 bytes) per pixel, so a surface reflectance value of say 20.56% is coded as 2056 and is stored as a 2 byte integer which means the file size is only half of the float file size. If the input data is 8 bit data then a scale factor of 4 is recommended, i.e., a surface reflectance of 20.56% will be coded as 82.

If the input file name is *"image.bsq"* then the default output file name for the atmospherically corrected image is *"image_atm.bsq"*. The user may modify the output name, but it is recommended to keep the *"_atm.bsq"* qualifier to facilitate the use of subsequent programs. Then the sensor view geometry has to be specified as well as the sensor and the calibration file. The atmospheric file contains the look-up table (LUT) results of the radiative transfer calculations, separately for the

solar and thermal region. These LUTs are calculated for a nadir view, but for tilt sensors the files *"phasefct*.bin"* in the *"../atcor/bin"* directory contain the path radiance as a function of the scattering angle, and the appropriate file is automatically included.

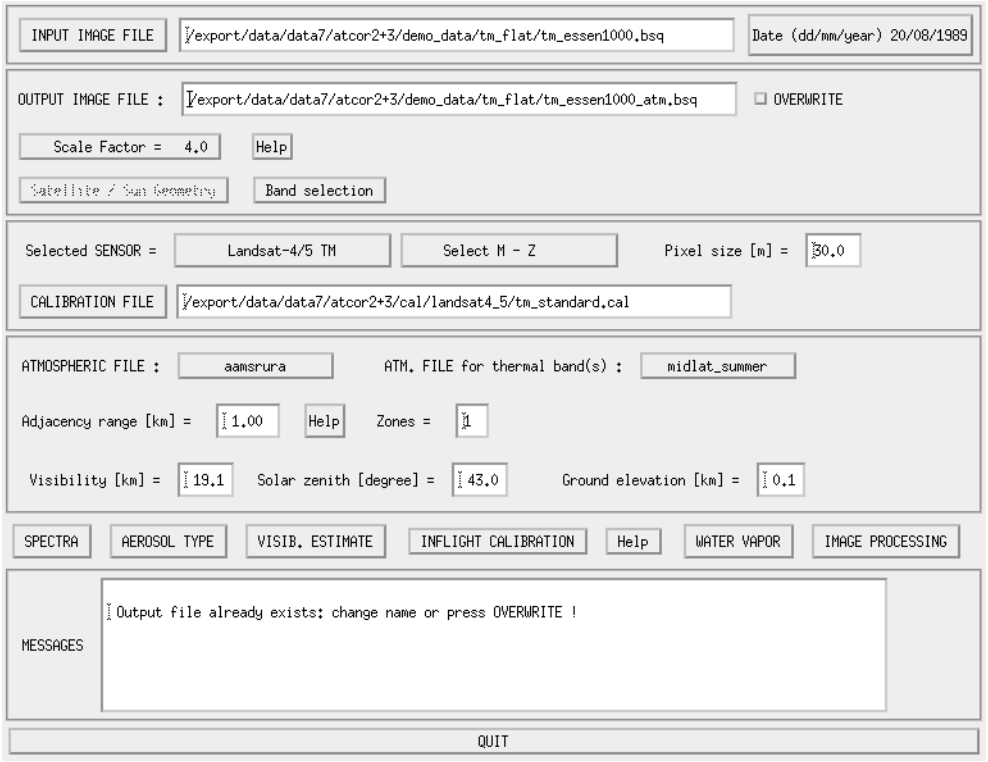

Figure 4.6: *ATCOR panel for flat terrain imagery.*

Note that for a new user-specified sensors, these LUTs have to be calculated once prior to the first call of ATCOR. This is done with the module RESLUT (see section 5.2.4) available under the 'New Sensor' menu.

It is recommended to check the quality of the atmospheric correction before processing the image data. For that purpose, the SPECTRA module should be used where the surface reflectance of small user-defined boxes can be evaluated and compared with library spectra, compare chapter 5.3.6. In case of calibration problems, the spectral calibration module, available from the 'Tools' button of Fig. 4.1, and the radiometric (inflight) calibration may be employed before finally processing the image data. The *'AEROSOL TYPE'* button provides an estimate for the recommended aerosol type (e.g. rural, maritime, urban) derived from the scene. This module also provides a visibility value for each aerosol type based on reference pixels (dark vegetation) in the scene. The *'VISIB. ESTIMATE'* button provides a visibility value for the selected aerosol type by checking dark scene pixels in the red band (vegetation, water) and NIR band (water). It is assumed that the lowest reflectance in the red band is 0.01 (1 percent) and 0.0 in the NIR band. Therefore, the obtained visibility value usually can be considered as a lower bound. The higher visibility value (of *'AEROSOL TYPE'* and *'VISIB. ESTIMATE'*) is recommended as a start visibility for the *SPECTRA* module.

The *'Inflight Calibration'* is described in chapter 5.3.9. This module is usually not required for first use of the software.

The *'WATER VAPOR'* button can be used to test the appropriate band combinations for the retrieval of a water vapor map without a calculation of the surface reflectance cube.

Th button *IMAGE PROCESSING* starts the atmospheric correction process from the entered parameters. A series of sequential panels are displayed after this button is pressed. Fig. 4.7 shows the panel with the image processing options. Some options may not be accessible, they are blocked if the required spectral bands are missing.

In case of a mountainous terrain the ATCOR3 button has to be selected (Fig. 4.1, "Atm.Correction"). This panel is similar to Fig. 4.6, but an additional panel for the specification of the DEM files will appear (Fig. 4.8). The user has to provide the DEM file matched to the size of the input image. The slope and aspect files can be calculated from the corresponding module under "Topographic" (Fig. 4.1). These two files may need a special treatment as discussed in chapter 5.3.11. Therefore, they are not automatically created from the elevation file. The "skyview" file and cast shadow file are optional, only required in extremely steep terrain. The "skyview" calculation can also be found under the "Topographic" label of Fig. 4.1.

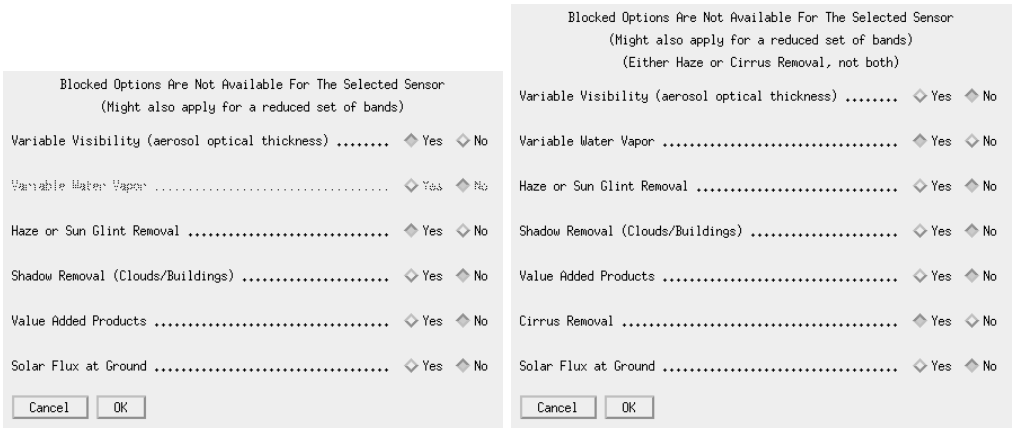
Blocked Options Are Not Available For The Selected Sensor
(Might also apply for a reduced set of bands)
Variable Visibility (aerosol optical thickness) ..... Yes No
Variable Water Vapor ..... Yes No
Haze or Sun Glint Removal ..... Yes No
Shadow Removal (Clouds/Buildings) ..... Yes No
Value Added Products ..... Yes No
Solar Flux at Ground ..... Yes No
Cancel OK
Blocked Options Are Not Available For The Selected Sensor
(Might also apply for a reduced set of bands)
(Either Haze or Cirrus Removal, not both)
Variable Visibility (aerosol optical thickness) ..... Yes No
Variable Water Vapor ..... Yes No
Haze or Sun Glint Removal ..... Yes No
Shadow Removal (Clouds/Buildings) ..... Yes No
Value Added Products ..... Yes No
Cirrus Removal ..... Yes No
Solar Flux at Ground ..... Yes No
Cancel OK

Figure 4.7: *Image processing options. Right panel appears if a cirrus band exists.*

Depending on the selected image processing option some additional panels may pop up. Most of them are listed in chapter 5.7.4, but they are self-explaining and will not be discussed here. They also contain default settings which can be used in most cases. When the main panel (Fig. 4.6) is left and the "SPECTRA" or "IMAGE PROCESSING" sections are entered, all information is written to a processing initialization (*.inn*) file, e.g., *"image.inn"*. When reloading the input file this information is read from the *.inn* file, so a new specification of all processing parameters is not necessary. Therefore, this *.inn* file can also be used for a batch processing, see chapter 6.

The remaining sub-chapters of chapter 4 may be skipped during the first reading if the definition of user-defined (hyperspectral) sensors is not relevant. These sub-chapters can be consulted if specific questions arise, e.g., about batch job processing.

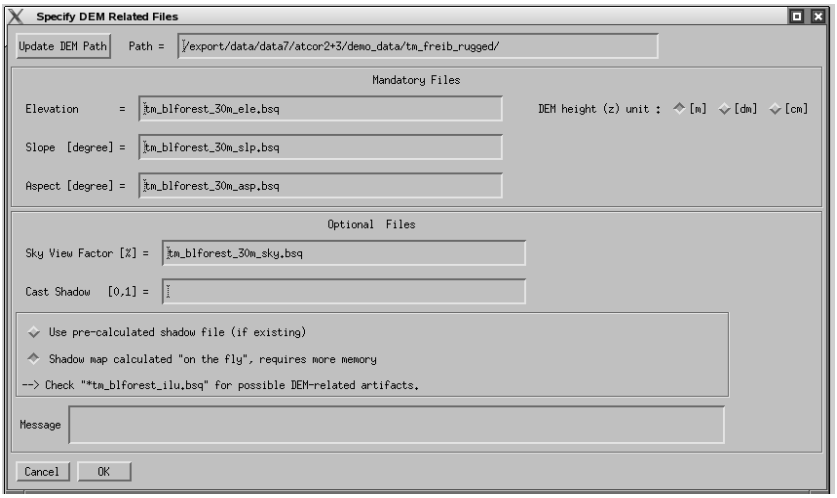

Figure 4.8: *Panel for DEM files.*

4.3 Survey of processing steps

Figure 4.9 shows the typical workflow of atmospheric correction. A detailed description of the corresponding graphicical user interface for each module is given in chapter 5. First, the image is loaded with possibly some additional information (DEM files). Then the sensor has to be defined, the radiometric calibration file, and a basic atmosphere/aerosol type combination, e.g. a summer atmosphere with a rural aerosol. It is recommended to check the validity of the calibration and to estimate the visibility (and perhaps the atmospheric water vapor column wv) before processing the image cube. The SPECTRA module can be employed for this purpose, see chapter 5.3.6. Reflectance spectra of scene targets can be displayed as a function of visibility and water vapor (the winter, fall, summer, and tropical atmospheres have different wv contents, see appendix A) and compared with field or library spectra. If calibration problems exist in a few channels a copy of the calibration file can be edited in these channels to match the reference spectrum. If there are problems in many channels the inflight radiometric calibration module should be used to generate a calibration file as discussed in chapter 5.3.9.
When the calibration file is OK the user can continue with the image processing. Depending on the available sensor channels there are options to process the imagery with constant or variable visibility and atmospheric water vapor. For large FOV sensors an option is available to correct for across-track illumination (BRDF) effects. This is especially useful if the image recording took place in the solar principal plane. In addition, a spectral polishing can be performed for the atmospherically and / or BRDF corrected data as indicated by the dotted lines of figure 4.9 . The polishing requires hyperspectral imagery. Finally, a classification may be performed.

Figure 4.10 shows the input / output image files associated with ATCOR processing. On the left part the flat terrain case is treated, on the right part the rugged terrain case. In mountainous terrain, the DEM, DEM slope and aspect files are required. Optional input are the skyview file and the shadow map, the latter can also be calculated on-the-fly. The slope and aspect files can be calculated from ATCOR's interactive menu, or run as a batch job (*slopasp_batch* see chapter 6.2). The skyview file has to be computed with the *skyview* program, see chapter 5.4.2.

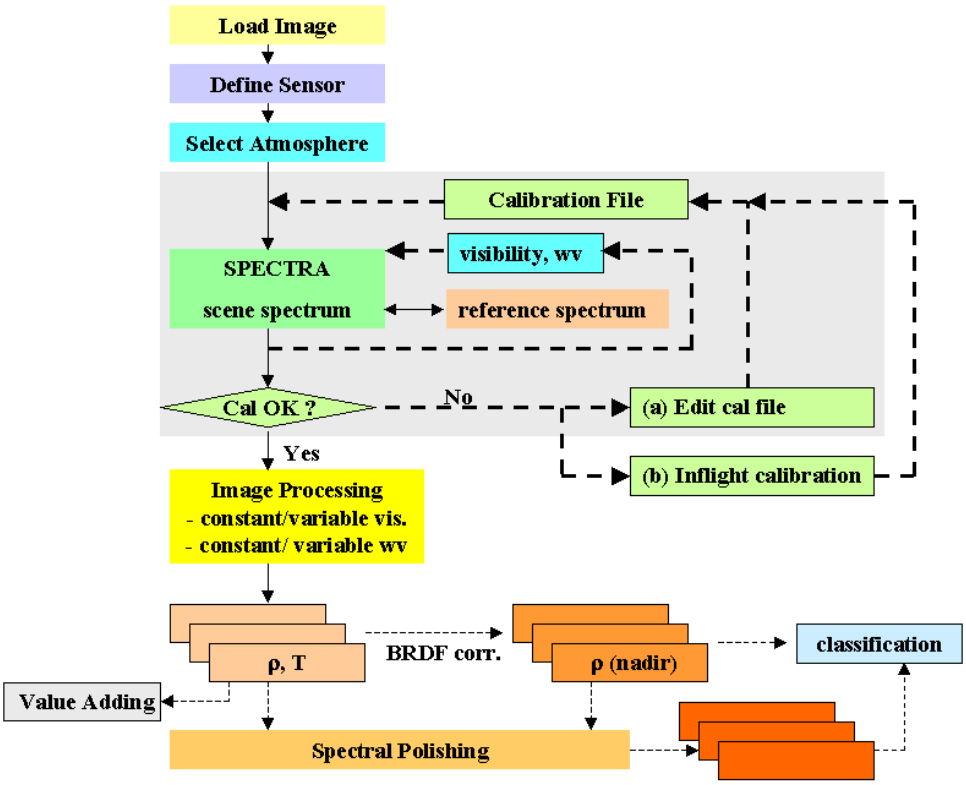

Figure 4.9: *Typical workflow of atmospheric correction.*

4.4 Directory structure of ATCOR

Figure 4.11 shows the directory structure of the satellite version of ATCOR. There are a number of sub-directories with the following content: The 'bin' directory holds the ATCOR program with all modules as listed in chapter 5. The 'cal' directory holds all supported satellite sensors in sensor-specific sub-directories. The sensor definition is contained in two files: one contains the extraterrestrial solar irradiance (e.g. *'e0_solar_aster.spc'*), the second one contains the radiometric calibration coefficients, e.g., *'aster.cal'*. The *'atm_lib'* contains the results of the atmospheric database after resampling with the sensor-specific spectral response curves. The *'spec_lib'* is a directory containing prototype reflectance spectra of water, soils, vegetation, asphalt etc. Here the user can also put field measurements of surface reflectance spectra resampled for the appropriate sensor. This is useful for inflight calibration or comparison of scene spectra with ground spectra. Finally, the *'demo_data'* contains some demo imagery to be able to run ATCOR immediately.

4.5 Convention for file names

Although file names are arbitrary it is useful to agree on some conventions to facilitate the search of files, especially concerning the extensions of file names.

Input images to ATCOR must have the band sequential format (BSQ), therefore it is recommended to employ the *'.bsq'* as an extension, e.g. *'image1.bsq'* . Then in this example the default output file name of ATCOR will be *'image1_atm.bsq'* and a log report of the processing is available in

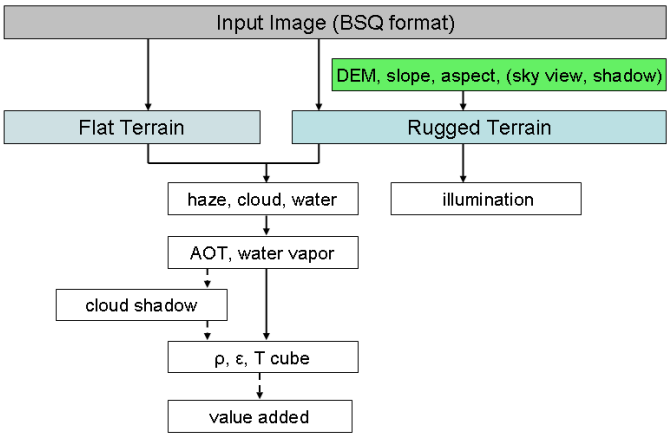

Figure 4.10: *Input / output image files during ATCOR processing.*

'image1_atm.log'.

Once an image is processed with ATCOR all input parameters are saved in a file *'*.inn'* that is automatically loaded should the image be processed again.

The recommended extension for the radiometric calibration files is *'.cal'* . Other extensions are *'*_ele.bsq'* for the digital elevation file, *'*_slp.bsq'* for the DEM slope file, *'*_asp.bsq'* for the DEM aspect, *'*_sky.bsq'* for the sky view file, *'*_ilu.bsq'* for the solar illumination file in rugged terrain, and *'_cla.bsq'* for the classification map of SPECL. The visibility index map is named *'*_visindex.bsq'*, the aerosol optical thickness is *'*_aot.bsq'*, the cloud/building shadow map is named *'*_fshd.bsq'*, and the atmospheric water vapor map *'*_wv.bsq'*.

Thermal band imagery

In case of thermal band imagery the surface temperature and emissivity are stored in separate files. Surface temperature is appended to the reflectance cube, i.e. is included as the last channel in the *'*_atm.bsq'* file, e.g., *'image1_atm.bsq'*.

The surface temperature calculation is based on an assumption for the emissivity. A constant emissivity or a surface cover-dependent emissivity can be selected as options. The simple case of a 3-class emissivity file (vegetation $\epsilon = 0.97$, soil $\epsilon = 0.96$, others $\epsilon = 0.98$) is calculated on the fly. Its output file name is *'image1_atm_emi3.bsq'*, the *'3'* indicating the 3 classes.

In case of standard sensors with multiple thermal bands, e.g. ASTER, the spectral emissivity channels are not computed and ATCOR uses only one of the thermal bands, band 13 in case of ASTER. If ASTER band 13 is offered as a single-channel input file to ATCOR the emissivity is set to a constant value of $\epsilon = 0.98$ for the surface brightness temperature calculation. If all reflective bands and the thermal bands of ASTER are geocoded and offered as a 14-channel file to ATCOR then the 3-class emissivity option is also available.
If a user is interested in derived surface emissivity data, the corresponding instrument (e.g., ASTER) has to be defined as a user-specified sensor, see chapter 4.6.

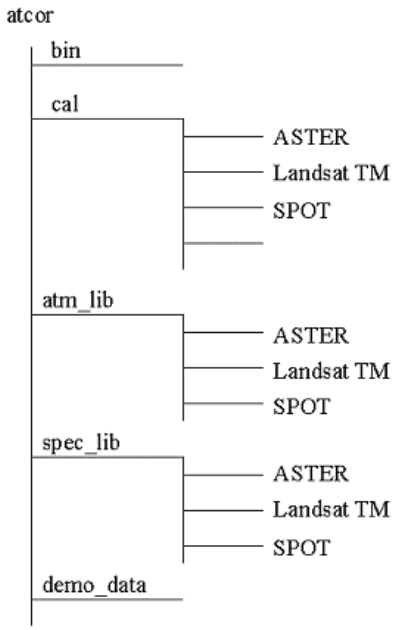

Figure 4.11: *Directory structure of ATCOR.*

4.6 User-defined hyperspectral sensors

Examples of satellite hyperspectral sensors are Hyperion and CHRIS/Proba. Since the channel center wavelength of these instruments may change from scene to scene, they have to be treated as user-specified sensors, and a flexible interface has been implemented to enable the calculation of atmospheric LUTs adapted to the spectral channel properties. This interface is similar to the one for the airborne ATCOR, and the corresponding part of the airborne ATCOR user manual is repeated here. The hyperspectral tool is an optional add-on to the satellite ATCOR. Although it is mainly intended for hyperspectral sensors it can of course also be employed for user-defined multispectral instruments.

The first step is the definition of a new 'sensor' subdirectory, compare Figure 4.13 and Fig. 5.11. It serves as the start folder of further subdirectories for the user-defined hyperspectral sensors, e.g., 'chris_m1'. A few sensor description files have to be provided by the user, as explained in the next section.

4.6.1 Definition of a new sensor

A few steps have to be taken to include a new satellite sensor in ATCOR. They are supported by the respective panels. On the level of the ATCOR installation directory, the following steps are to be taken:

- A new sensor subdirectory in the *".../atcor/sensor/"* folder has to be created. This is easiest done using the routine *Define Sensor Parameters* as described in chapter 5.2.1. Please make sure this name does not agree with an existing multispectral sensor name in the *"../atcor/cal/"* folder. This process may also be done manually by copying and adapting an existing user-defined sensor or one of the samples provided (or use the function above to make the changes).

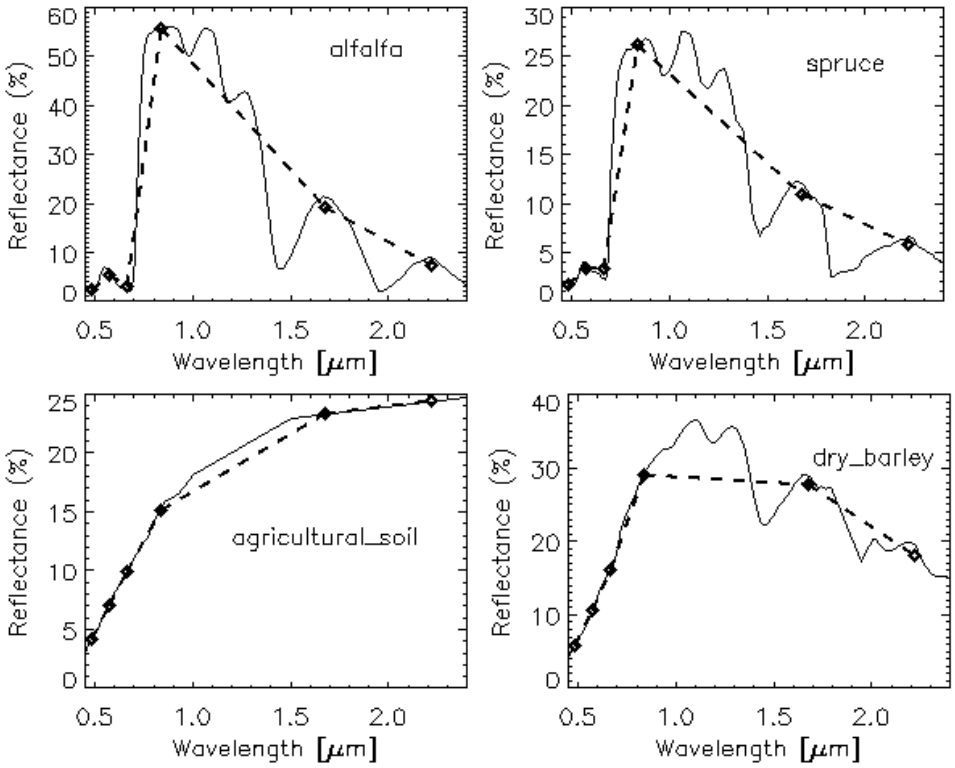

Figure 4.12: *Template reference spectra from the 'spec_lib' library.*
The dashed spectra are resampled with the Landsat-5 TM filter curves.

- A sensor-definition file must be specified. Just copy any of the existing files, e.g., *"sensor_chris_m1.dat"*, and modify the appropriate lines, see the next table.

- A wavelength file *('*.wvl')* has to be specified. It is a simple ASCII file with three columns (band number, center wavelength, and bandwidth), compare Fig. 5.11. Center wavelength and bandwidth may be given in the *nm* or μm unit. The first line may contain an optional header with text. This wavelength file will be used to create the spectral response function for each band as a numerical table (the *'band*.rsp'* files), compare Fig. 5.11.
  Eight analytical filter shapes can be selected from the top level graphical interface (Fig. 4.1 when pressing the 'New Sensor', then 'Create Channel Filter Files' button. Then the menu of Fig. 4.14 will pop up, and one of these 8 filter shapes can be selected. Filter numbers 1 to 4 are of the Butterworth type, the slow drop-off for the Butterworth order 1 is truncated at the 0.05 response and set to zero. The filter type 9 (parameter *filter_type* in Table 4.3) is reserved for arbitrary user-specified channel filter functions (the *'band*.rsp'* files).

- A calibration file (e.g., *"chris_m1.cal"*) has to be provided in the new sensor sub-directory.

- The RESLUT (*resample atmospheric LUTs*) program has to be run to generate the atmospheric LUTs for the new sensor employing the monochromatic atmospheric database in *".../atcor/atm_database/"*. These resampled *'*.atm'* files will automatically be placed in a sub-directory of *'.../atcor/atm_lib/'* with the name of the selected sensor. RESLUT will also create the resampled spectrum of the extraterrestrial solar irradiance in the appropriate

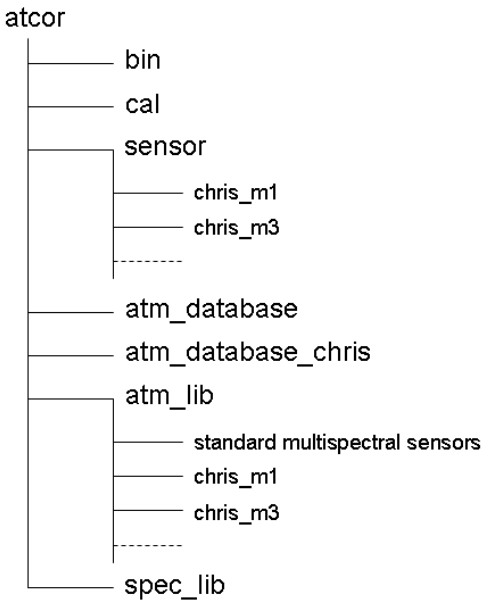

Figure 4.13: *Directory structure of ATCOR with hyperspectral add-on.*

".../sensor/chris_m1/" folder, see chapter 9.1.4, e.g., *"e0_solar_chris_m1.spc"*.

Remember that the sensors might have to be specified as scene-dependent if the center wavelengths and/or bandwidths change, so you might need sensor subdirectories such as *"chris_m1_11april2003"* or *"chris_m1_scene3_29june2004"*.

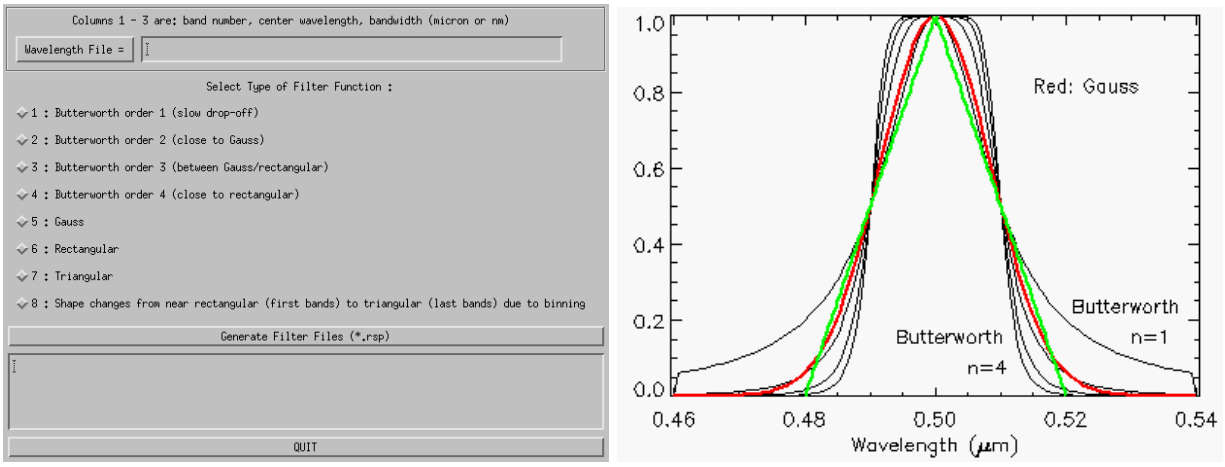

Figure 4.14: *Supported analytical channel filter types.*

The next two tables present examples of a sensor definition file for an instrument without thermal bands and with thermal bands, respectively.
Line 1 is retained to be compatible with the airborne version of ATCOR. Line 6 is a required dummy to be compatible with previous versions.

5.0	6000	across-track FOV [degree], pixels per line (dummy to agree with airborne ATCOR)
1	128	first, last reflective band (0.35-2.55 μm)
0	0	first, last mid IR band (2.6 -7.1 μm)
0	0	first, last thermal band (7.1 -14 μm)
1		flag for tilt capability (1=yes, 0=no)
0		required dummy

Table 4.1: *Example of a sensor definition file (no thermal bands).*

4.0	3000	cross-track FOV [degree], pixels per line (dummy to agree with airborne ATCOR
1	72	first, last reflective band (0.35-2.55 μm)
73	73	first, last mid IR band (2.6 -7.1 μm)
74	79	first, last thermal band (7.1 -14 μm)
0		flag for tilt capability (1=yes, 0=no)
0		no gain settings (required dummy)
77		temperature band (itemp_band=77)

Table 4.2: *Sensor definition file: instrument with thermal bands.*

Any mid-IR bands are skipped in the processing, the surface temperature band (itemp_band) is appended after the reflective bands as the last channel of the *"_atm.bsq"* output file.

4.7 Spectral smile sensors

Imaging systems can employ different techniques to record a scene: the whiskbroom design uses a rotating or oscillating mirror to collect an image line in across-track direction (with one or a few detector elements per spectral band). The forward direction is provided by the motion of the platform. Secondly, a pushbroom linear array can perform the same task without moving optical elements, but the number of array lines (each recording a certain spectral channel) in the focal plane is limited. The third imaging technique employs an area detector array where one direction collects the spatial information (across-track) and the orthogonal direction covers the spectral dimension. The advantage of the last two techniques is a longer pixel dwell time and a potentially improved signal-to-noise ratio (SNR). The drawback is a substantial increase in the spectral and radiometric characterization, i.e., a change of the channel center wavelength across the columns of the array (spectral "smile"), spatial misregistration ("keystone"), and detector non-uniformity problems [48], [17], [70]. Typical representatives of the whiskbroom type are Landsat TM/ ETM, HyMap, AVIRIS, and Daedalus. These instruments almost show no spectral smile, i.e., the channel center position and bandwidth do not depend on column pixel location. Spaceborne hyperspectral instruments showing the "smile" effect are Hyperion and CHRIS/Proba, airborne instruments are for example CASI-1500 and APEX.

This section describes the ATCOR input files required for smile sensors. There are only two changes compared to the "non-smile" instruments:

- The sensor definition file, e.g., *"sensor_chris_mode3.dat"*, needs one more line (see Table 4.3) containing the parameters *ismile* (=1 if smile sensor, otherwise 0) and *filter_type* (a number between 1 and 9 for the type of channel filter function) compare section 4.6.1 and Fig. 4.14.

The filter types 1 to 8 are analytical functions, filter type 9 is reserved for arbitrary user-defined channel filter functions (the *'band*.rsp'* files). Center wavelength and bandwidth for each channel are defined in the wavelength file (*'*.wvl'*) pertaining to the center pixel=column of the detector array.

- For each spectral channel j the channel center wavelength $\lambda_c(j)$ depends on the image column or pixel position x. The absolute value of $\lambda_c(j)$ is specified in the wavelength file used to generate the spectral channel response functions, and it is also included in the sensor-specific solar irradiance file (e.g., *"e0_solar_chris_mode3.spc"*). If n is the number of image columns, the change $\Delta(x, j)$ of the center wavelength $\lambda_c(j)$ with the pixel position x can be described as a 4th order polynomial (using the nm unit):

$$\Delta(x, j)[nm] = a_0(j) + a_1(j) \cdot x + a_2(j) \cdot x^2 + a_3(j) \cdot x^3 + a_4(j) \cdot x^4 \tag{4.1}$$

$$\lambda_c(x, j) = \lambda_c(j) + \Delta(x, j) \tag{4.2}$$

The first left-hand image pixel is x=0, the last right-hand image pixel is x=(n-1). The coefficients $a_i(j)$ have to be stored in an ASCII file, corresponding to the band sequence. The first column must contain the wavelength or band number, followed by the five channel-dependent coefficients (beginning with a_0 and ending with a_4), one line per channel. The fixed file name is *smile_poly_ord4.dat* and it has to be located in the corresponding sensor sub-directory. In the ideal case these coefficients should be derived from laboratory measurements. Since an accurate description is only required for channels in atmospheric absorption regions, the 5 coefficients can be set to zero for the remaining regions, but they must be provided for each channel. If all 5 coefficients are set to zero for a certain channel, this channel is processed in the "non-smile" mode which will expedite the processing.

2.0	512	across-track FOV [degree], pixels per line
1	128	first, last reflective band (0.35-2.55 μm)
0	0	first, last mid IR band (2.6 -7.1 μm)
0	0	first, last thermal band (7.1 -14 μm)
0		no tilt in flight direction
0		required dummy
1	5	1=smile sensor, 5 = Gaussian spectral channel filter

Table 4.3: *Sensor definition file: smile sensor without thermal bands.*

Imagery from smile sensors must be processed in the raw geometry (IGM Image Geometry Map) to preserve the original image columns. During the surface reflectance retrieval the atmospheric / topographic correction is performed on a per column basis, i.e., to each image column its appropriate center wavelength /bandwidth is associated. For the nadir pixel the channel center and bandwidth are defined in the sensor's wavelength file (*'*.wvl'*), for off-nadir pixels the center wavelength is shifted according to eq. 4.1. Currently, the change in spectral bandwidth with image column is assumed to be negligible.

The per-column processing typically implies a factor of 8 increase in processing time. The following steps are to be performed:

1. Define a sensor (∗wvl, ∗cal, ∗rsp files, RESLUT) using the original set of wavelengths (pre-launch values, as provided with the data from the data provider),

2. Run the smile detection tool (compare Section 5.7.7, using the sensor defined in 1 and appropriate absorption features, to derive the polynomial coefficients *smile_poly_ord4.dat* for smile correction in step 3; alternatively: enter the smile polynomial factors from laboratory calibration. *Note:* if two detectors are in the sensor system, this should be done separately for VNIR and SWIR, option 'repeat values', resolution 0.02 nm. Combine the two files for VNIR and SWIR manually into one file afterwards.

3. Using the same sensor as above, run the atmospheric correction with the smile correction option switched 'ON'; (after putting the new file *smile_poly_ord4.dat* into the sensor definition directory),

4. Apply the spectral polishing routine (see Section 5.5.2 and 5.5.3, and

5. Run the Spectral Smile Interpolation module (see Section 5.5.4 on the atmospherically corrected image.

4.8 Haze, cloud, water map

Although the surface reflectance cube (and temperature / emissivity for thermal channels) is the main result of the atmospheric correction, some additional products are often requested. One of these products is a map of the haze, cloud, water and land pixels of a scene. This map not only delivers a basic scene classification, but it may also contain information about potential processing problems. For example, if turbid water pixels are not included in the water mask, the haze mask may also be not appropriate and consequently, results of the haze removal over land might be of poor quality. Such a pre-classification as part of the atmospheric correction has a long history [37, 38, 55, 56, 57, 39, 44]. It is also employed as part of NASA's automatic processing chain for MODIS [45] using the classes land, water, snow/ice, cloud, shadow, thin cirrus, sun glint, etc.

Therefore, the calculated haze/cloud/water map is a useful optional output of ATCOR. It is enabled by setting the parameter $ihcw = 1$ in the *preference_parameters.dat* file (see chapter 9.3). If the file name of the imagery is *"image.bsq"* the corresponding map is named *"image_out_hcw.bsq"*. It is a 1-channel false-color coded ENVI file. In principle, if a certain mask of *"image_out_hcw.bsq"* (say haze pixels) contains artifacts, it may be edited, and if the edited file is named *"image_hcw.bsq"* it will automatically be used for the ATCOR processing. This means ATCOR can repeat the processing with an improved (edited) haze mask.
The file *"image_hcw.bsq"* can also be provided by an external (ATCOR-independent) source. In any case, if this files exists, ATCOR will skip its internal calculations of these masks and use the pre-calculated map.
The haze/cloud/water file contains the following classes (see Table 4.4):

- land
- water
- boundary layer haze (two classes: thin-to-medium haze, and medium-to-thick haze)
- cirrus clouds (three classes: thin, medium, and thick cirrus, provided a narrow channel around 1.38 μm exists)

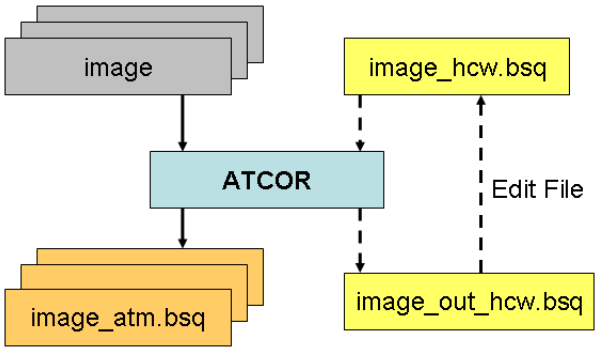

Figure 4.15: *Optional haze/cloud/water output file.*

- cloud over land, cloud over water
- snow (requires a 1.6 μm channel)
- saturated pixels using the criterion $T > 0.9 * DN_{max}$ where T is a threshold set at 0.9 times the maximum digital number. This criterion is only used for 8 bit and 16 bit (signed or unsigned) data, no threshold is defined for 32 bit (integer or float) data. As an example, for an 8 bit/pixel data encoding we obtain T = 0.9*255 = 230, and pixels with a grey value greater than 230 are flagged as (truly or potentially) saturated.
  Although the saturation nominally starts at DN_{max} some sensors already show a non-linear behavior around $0.9 * DN_{max}$, so the factor 0.9 is a precaution to be on the safe side.
  This saturation check is performed for two channels in the visible region (blue band around 470-500 nm, and a green band around 550 nm). For multispectral sensors, the blue band is usually the critical one concerning saturation. For hyperspectral sensors with many blue bands the one closest to 450 nm is taken. Although the haze/cloud/water file contains saturated pixels based on two visible bands, the percentage of saturated pixels for all bands will be given in the corresponding *".log"* file. However, the check of the blue and green channel normally captures all saturated pixels.

Note: cloud (or building) shadow pixels are not included here, they are stored separately (file *image_fshd.bsq"*).

4.9 Processing of multiband thermal data

Several options have been implemented to process multiband thermal data, see chapter 10.1.4 for details. Apart from the final products (surface temperature and emissivity) intermediate products are available such as surface radiance, at-sensor blackbody temperature, and surface blackbody temperature. The intermediate products might be useful to trace back spectral or radiometric problems. If *image.bsq* denotes the file name of the input image then the following products are available:

- *image_atm_emi3.bsq* : 3 or 4 emissivity classes obtained from an on-the-fly (in memory) pre-classification (vegetation, soil, sand, water). The pre-classification requires daytime data acquisition and spectral bands in the solar region. This file has one channel with the emissivity values for the specified thermal band, or in case of ANEM the pixel-dependent values assign the maximum emissivity of all available thermal bands.

label	definition
0	geocoded background
1	shadow
2	thin cirrus (water)
3	medium cirrus (water)
4	thick cirrus (water)
5	land
6	saturated
7	snow
8	thin cirrus (land)
9	medium cirrus (land)
10	thick cirrus (land)
11	thin-medium haze/land
12	medium-thick haze/land
13	thin-medium haze/water
14	medium-thick haze/water
15	cloud/land
16	cloud/water
17	water

Table 4.4: *Class label definition of "hcw" file.*

- *image_atm_emiss.bsq* contains the spectral emissivity map for all thermal channels.
- *image_atm_emiss_lp3.bsq* is the same emissivity map but filtered with a 3-channel low pass filter to smooth spectral noise features (requires at least 10 thermal bands).
- *image_atm_emiss_lp5.bsq* is the same emissivity map but filtered with a 5-channel low pas filter to smooth spectral noise features (requires at least 30 thermal bands).
- *image_atm_isac_emiss.bsq* : emissivity cube for the ISAC algorithm.
- *image_at_sensor_channel_tmax.bsq* : map of channel numbers with maximum at-sensor temperature.
- *image_at_surface_channel_tmax.bsq* : map of channel numbers with maximum surface temperature.
- *image_at_sensor_tbb.bsq* : at-sensor brightness temperature cube
- *image_at_surface_tbb.bsq* : at-surface brightness temperature cube.

The last channel of *image_atm.bsq* contains the surface temperature map evaluated with the appropriate emissivity, the preceding thermal channels in this file contain the surface radiance.
In case of the ISAC algorithm an additional file *image_isac_lpath_trans.dat* contains the spectral path radiance and transmittance estimates for the scene. Fig. 4.16 shows an example of these spectra derived from a SEBASS scene.

Fig. 4.17 presents the at-sensor/at-surface radiance and brightness temperatures. The at-sensor products clearly show the atmospheric absorption features which are removed in the at-surface

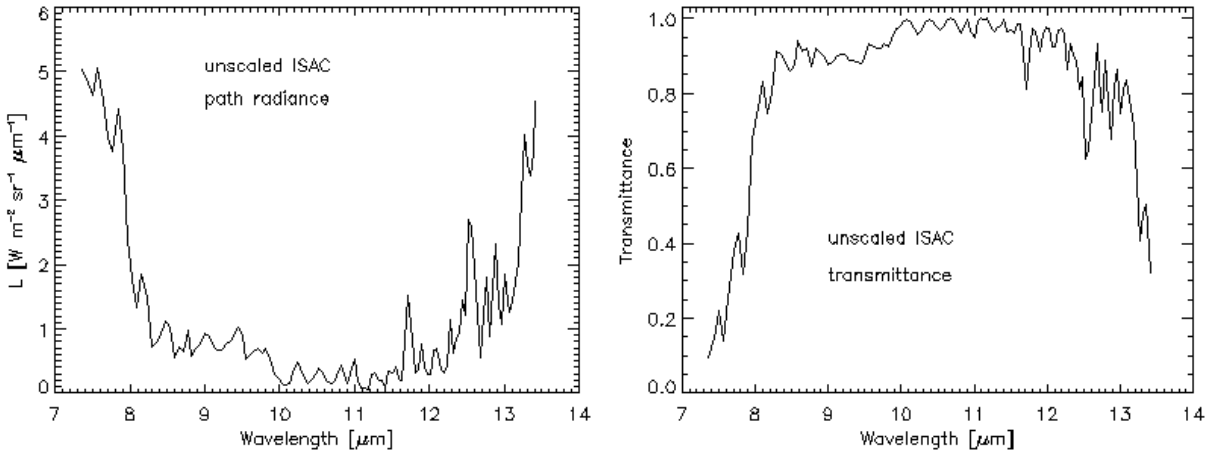

Figure 4.16: *Path radiance and transmittace of a SEBASS scene derived from the ISAC method.*

quantities, apart from small residual effects. The bottom graphic presents the corresponding surface emissivity spectrum.

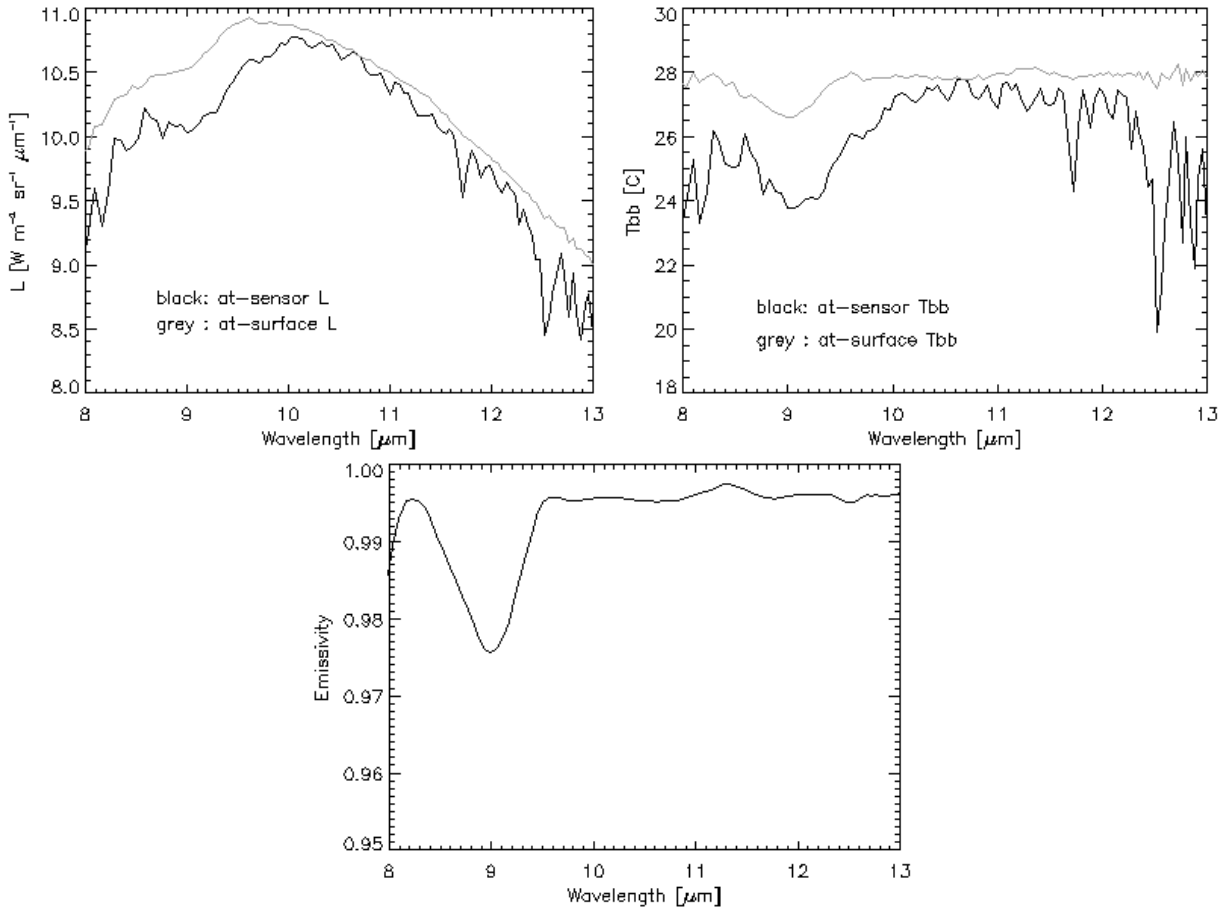

Figure 4.17: *Comparison of radiance and temperature at sensor and at surface level.*

4.10 External water vapor map

Sometimes, it is convenient to use an external water vapor map, even if this map could be derived from the scene. If the scene is named *"scene.bsq"* then the external map should be named *"scene_wv.bsq"* and it must have the same number of image lines and pixels per line as the scene. If this file is available in the same directory as the scene, it will be automatically used during the processing and the usage is also documented in the log file (*"scene_atm.log"*). Note: this feature is only supported for instruments that are able to retrieve the water vapor column with the intrinsic channels, because the prerequisite is the availability of the corresponding LUTs.

Chapter 5

Description of Modules

For most ATCOR modules a convenient graphical user interface is available, but batch jobs can also be submitted. If the atcor binary *atcor.sav* is opened by the IDL virtual machine or when *"atcor"* is typed on the IDL command line a menu with pull-down buttons pops up, see Figure 5.1, with a thematic grouping of modules. A detailed discussion of the interactive panel-driven modules is given hereafter whereas a description of the batch commands can be found in chapter 6.

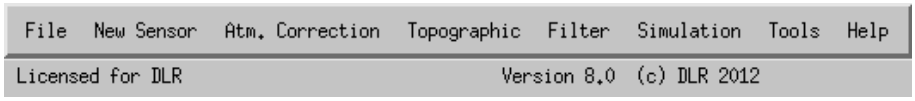

Figure 5.1: *Top level menu of the satellite ATCOR.*

5.1 Menu: File

The menu *'File'* offers some collaborative tools for handling of the data and ENVI files. Below, a short description of the individual functions is given:

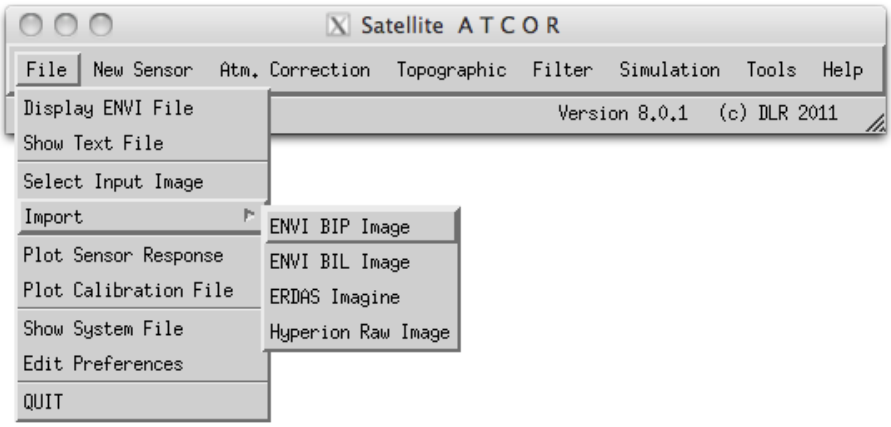

Figure 5.2: *The File Menu*

5.1.1 Display ENVI File

Use this function for displaying a band sequential ENVI-formatted file in a simple way [1]

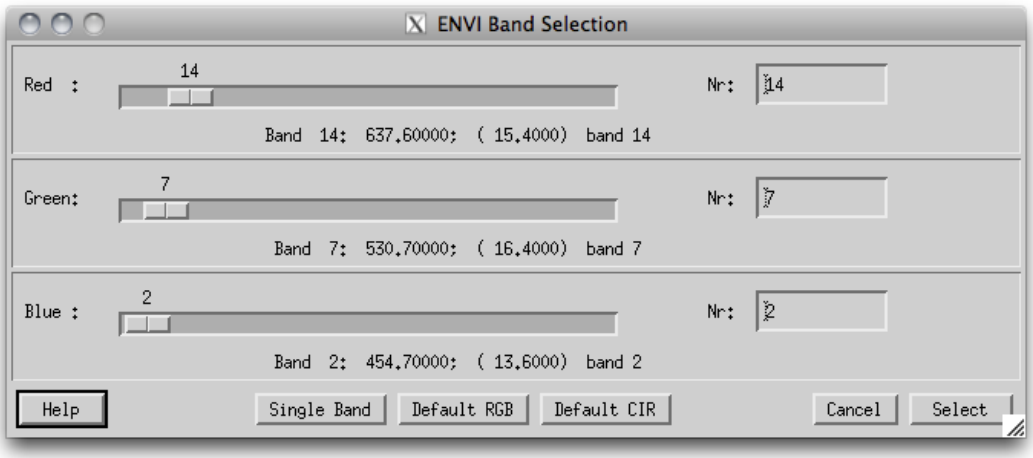

Figure 5.3: *Band selection dialog for ENVI file display*

An initial dialog allows to select the band(s) to display - either a true color, CIR color, or a single band mode may be selected. .

After display, the following options are available within from the menu:

[1] The ENVI format is a raw binary file, accompanied by an ASCII header ∗.hdr; in ATCOR it should be stored in band sequential order.

File:Display ENVI Image Displays an additional ENVI image in a new window (sorry, no linking available)

File:Show ENVI Header Displays the ENVI header of the current image in a new editable window. This allows to make changes to the ENVI header. Note that the file needs to be loaded from scratch if changes have been made.

File:Band Selection Allows to select a new combination of spectral bands and updates the display.

File:Display TIFF Image Loads a multi-band TIFF image in a new window.

File:Close Closes the window.

Edit:Equalize Image Performs a histogram equalization on the three bands.

Edit:Scale Image Applies standard linear scaling on the imagery on 5 levels.

Edit:Scale Zoom Applies standard linear scaling on the imagery on 5 levels based on the statistics of the Zoom Window.

Edit:No Scaling Reverts to unscaled display of the image.

Edit:Scale to Range Scales a single-band image linearly to a range entered as lower and upper limit (only applicable in single band displays).

Edit:Load Color Table Applies standard linear scaling on the imagery on 5 levels.

Profile:Horizontal Opens a window for a horizontal profile through the image (of the first band only). The profile is updated for the cursor location in the zoom window whenever the zoom window is clicked.

Profile:Vertical Opens a window for a vertical profile through the image (of the first band only).

Profile:Spectrum Opens a window for a spectrum of the image (for images with 4 and more bands only).

Export Allows to export the currently displayed image to one of the given image data formats.The displayed image may be exported as a scaled 8bit/24bit image to the available standard image formats.

Note: when clicking in the zoom window, the current image value and location is displayed, or a small plot of the spectrum at this pixel location is created (same as the function *Profile:Spectrum* of above). The menu in the such loaded window allows to save the spectrum to an ASCII table, to adapt the graph's properties and font size, configure the display and to output the graph to an appropriate graphics format.

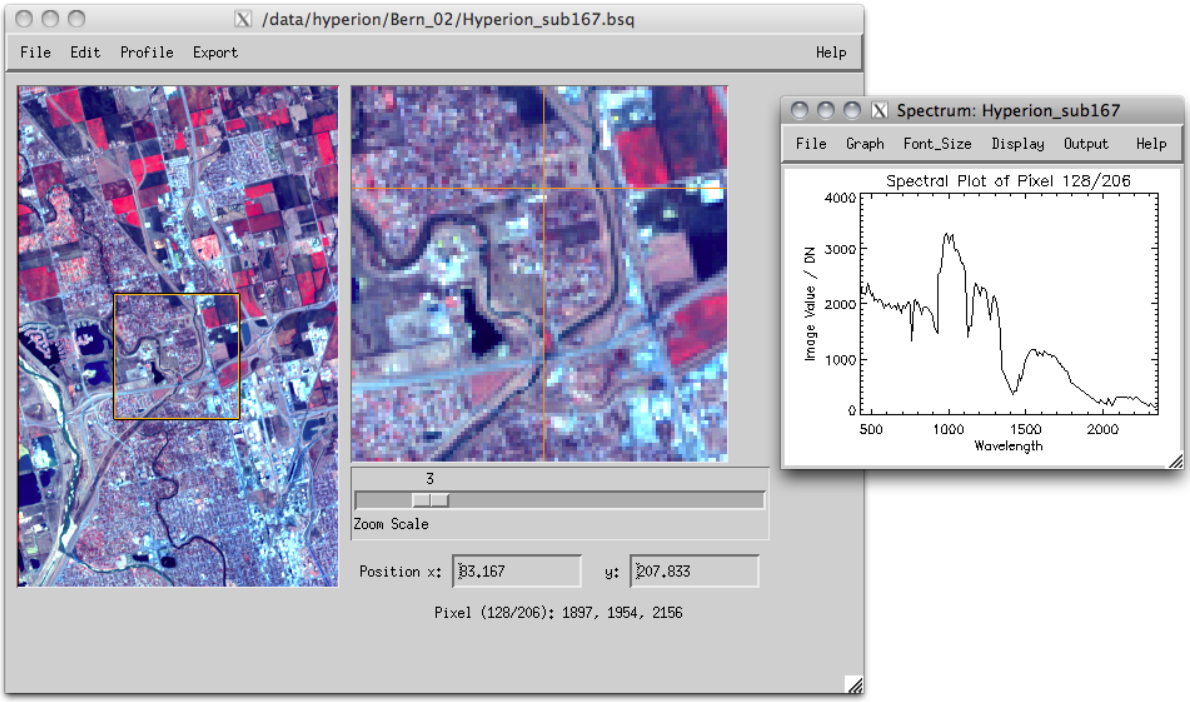

Figure 5.4: *Display of ENVI imagery*

5.1.2 Show Textfile

Use this function if you need to edit a plain text file which comes together with the data to be processed. The file is opened in a simple editor and may be changed and saved. The function comes handy if an ENVI header needs to be checked or updated (e.g.). Selecting the 'Save' or the 'Save As' function in the submenu will allow to overwrite the file or to create a new one.

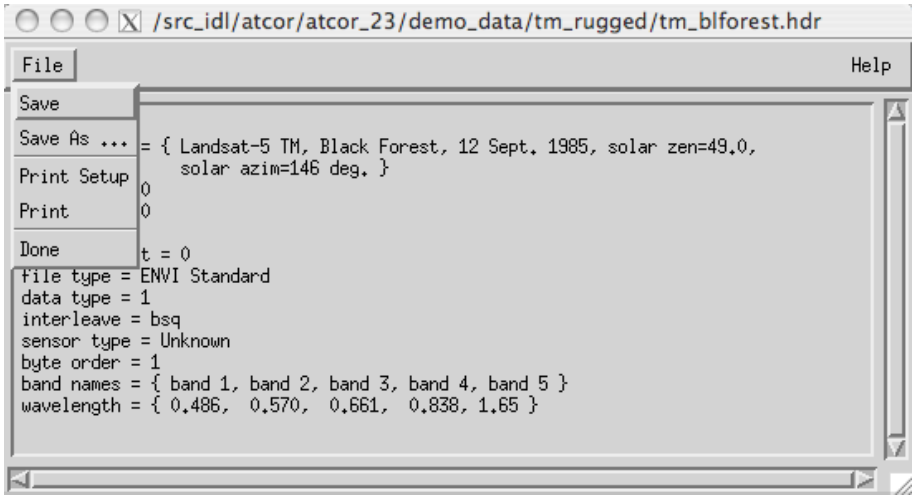

Figure 5.5: *Simple text editor to edit plain text ASCII files*

5.1.3 Select Input Image

This function allows to select the basis input image (i.e., the band sequential uncorrected image data in ENVI format). It is useful to define the starting point including the default paths of the images for further processing.

5.1.4 Import

A small number of standard formats is supported for importing data layers to be used with ATCOR:

ENVI BIP Image Imports and transforms an ENVI image in BIP (band interleaved by pixel) format to the ATCOR default BSQ (band sequential) format.

ENVI BIL Image Imports and transforms an ENVI image in BIL (band interleaved by line) format to the ATCOR default BSQ (band sequential) format.

Erdas Imagine Imports an uncompressed image in ERDAS Imagine format to ENVI format (specifically suited for DEM data import).

Hyperion Raw Image Imports a Hyperion image in ENVI format, 242 spectral bands for use with ATCOR. The number of bands is reduced to 167 according to the sensor definition provided with the software.

5.1.5 Plot Sensor Response

In the panel *Plot Sensor Response*, one may select the respective sensor response from within the available response functions in the ATCOR installation (or elsewhere). When selecting a response file, the related bands are loaded automatically and the total number of bands is displayed. The band range for display can be adjusted manually afterwards.

Normalization of the curves can be such that the area below the curves is constant (same weight of the functions) or the maximum is at 1 for all curves. The displayed graph may be adjusted in appearance and size and finally being exported to a standard graphics file for further use.

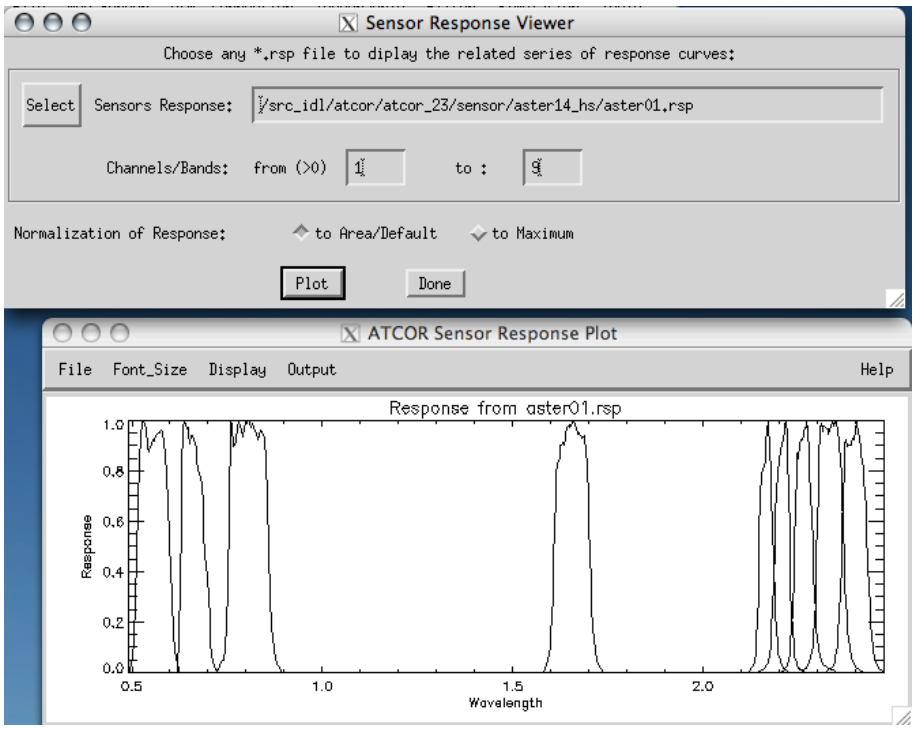

Figure 5.6: *Plotting the explicit sensor response functions*

5.1.6 Plot Calibration File

When selecting this function, the dialog defaults to the atcor installation for the selection of a $*$.cal file to be displayed. Both, gain and offset are then plotted in the same graph to get an overview of their relative values.

5.1.7 Show System File

This is the same function as 'Show Textfile' but defaults always to the ATCOR installation in order to allow to select an ATCOR system file from within the installation, such as the cal-files, the solar reference files, the sensor definition files. The function then allows to adjust and save the respective text contents of the selected file.

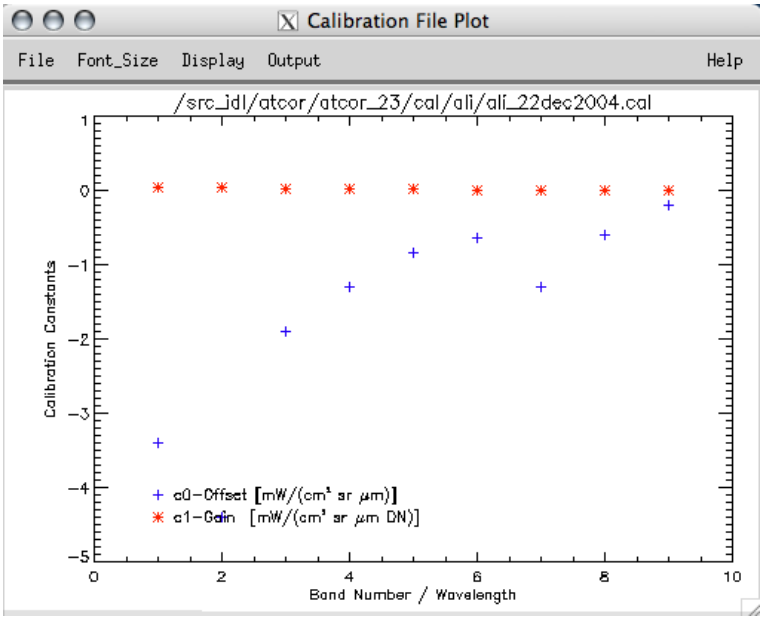

Figure 5.7: *Plotting a calibration file*

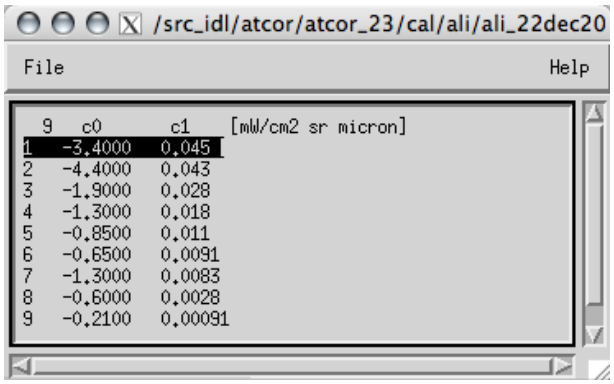

Figure 5.8: *Displaying a calibration file (same file as in Fig. 5.7)*

5.1.8 Edit Preferences

The default settings of ATCOR may be edited through this panel. The updated preferences are then written to the ASCII file as displayed at the top of the panel. The preferences persist for the user who started the ATCOR application the next time the system is started and also for batch processing.

NOTE: Preferences are set when one of the ATCOR modules has been opened. So, one should select one of the options from within the menu 'Atm. Correction' before editing the preferences.

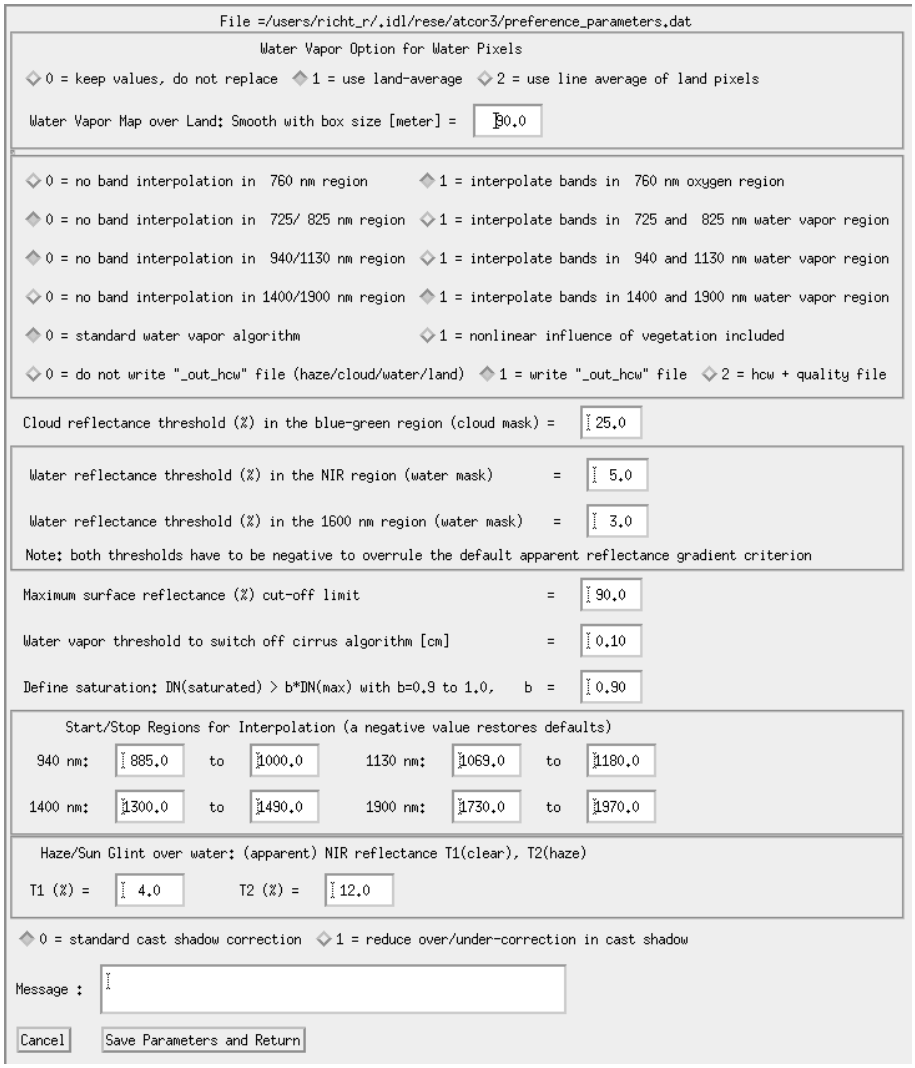
File =/users/richt_r/.idl/rese/atcor3/preference_parameters.dat
Water Vapor Option for Water Pixels
0 = keep values, do not replace
1 = use land-average
2 = use line average of land pixels
Water Vapor Map over Land: Smooth with box size [meter] = 90.0
0 = no band interpolation in 760 nm region
1 = interpolate bands in 760 nm oxygen region
0 = no band interpolation in 725/ 825 nm region
1 = interpolate bands in 725 and 825 nm water vapor region
0 = no band interpolation in 940/1130 nm region
1 = interpolate bands in 940 and 1130 nm water vapor region
0 = no band interpolation in 1400/1900 nm region
1 = interpolate bands in 1400 and 1900 nm water vapor region
0 = standard water vapor algorithm
1 = nonlinear influence of vegetation included
0 = do not write "_out_hcw" file (haze/cloud/water/land)
1 = write "_out_hcw" file
2 = hcw + quality file
Cloud reflectance threshold (%) in the blue-green region (cloud mask) = 25.0
Water reflectance threshold (%) in the NIR region (water mask) = 5.0
Water reflectance threshold (%) in the 1600 nm region (water mask) = 3.0
Note: both thresholds have to be negative to overrule the default apparent reflectance gradient criterion
Maximum surface reflectance (%) cut-off limit = 90.0
Water vapor threshold to switch off cirrus algorithm [cm] = 0.10
Define saturation: DN(saturated) > b*DN(max) with b=0.9 to 1.0, b = 0.90
Start/Stop Regions for Interpolation (a negative value restores defaults)
940 nm: 885.0 to 1000.0
1130 nm: 1069.0 to 1180.0
1400 nm: 1300.0 to 1490.0
1900 nm: 1730.0 to 1970.0
Haze/Sun Glint over water: (apparent) NIR reflectance T1(clear), T2(haze)
T1 (%) = 4.0
T2 (%) = 12.0
0 = standard cast shadow correction
1 = reduce over/under-correction in cast shadow
Message :
Cancel
Save Parameters and Return

Figure 5.9: *Panel to edit the ATCOR preferences*

5.2 Menu: New Sensor

The menu *'New Sensor'* is used to create a new sensor from calibration information, if the sensor is not supported as standard sensor by ATCOR.

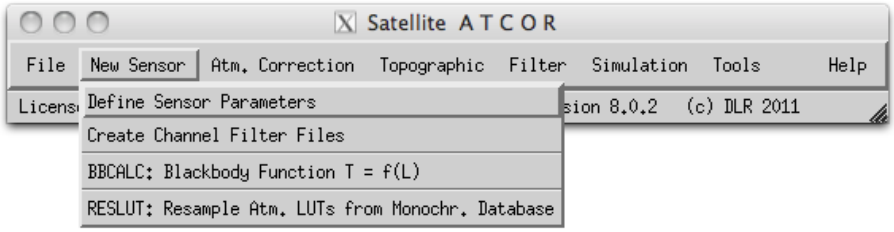

Figure 5.10: *The 'New Sensor' Menu*

Fig. 5.11 shows the three required steps to include a new user-defined (usually hyperspectral) sensor to ATCOR. The example uses a sensor with 96 spectral bands, denoted as 'sensor_x96'. A sub-directory of '.../atcor/sensor/' has to be created (named 'x96') and the three files as displayed in Fig. 5.11 have to be placed in this sub-directory. This procedure is supported by the Function 'Define Sensor Parameters'. After execution of steps 1 and 2, the new sensor will be automatically detected when ATCOR is started. Details about the sensor definition files are explained in chapter 4.5. Template files of several sensors are included in the distribution.

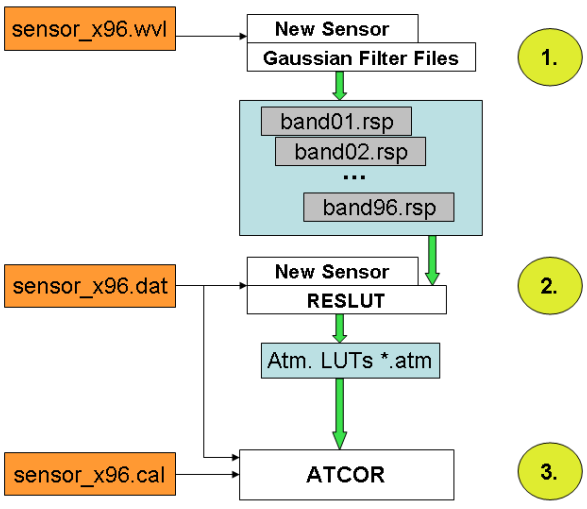

Figure 5.11: *Sensor definition files: the three files on the left have to be provided/created by the user.*

5.2.1 Define Sensor Parameters

This panel is the first step if a new sensor is to be defined. The panel as displayed in Fig. 5.12 allows the below options.

Sensor Selection

Select : Select any of the already defined sensors from within ATCOR note: a sensor is selected by on sensor file within a sensor directory.

New : A new sensor is created within the ATCOR installation, which results in a new directory in the 'sensor' directory of the installation.

Rename : The current sensor is renamed (both directory and sensor∗.dat file)

Delete : Allows to delete any sensor directory and all of its contents.

Inputs

Sensor Type This is to be selected first, smile sensor and thermal sensors require additional inputs (as displayed in the panel).

Sensor Total FOV [**deg**] : edge to edge FOV in across track direction in degrees.

Number of Across Track Pixels: : Nominal number of pixels in the unrectified data.

First, last Reflective Band: Band numbers (starting at one) - none: 0

First, last Mid IR Band: Band numbers (starting at one) - none: 0

First, last Thermal IR Band: Band numbers (starting at one) - none: 0

Thermal Sensor: Temperature Band Number: Spectral band used for temperature retrieval algorithm (Optional -according to sensor type)

Smile Sensor Response Type , required for convolution when sensor definition is not given explicetely, may be: 'Butterworth Order 1 (slow drop-off)', 'Butterworth Order 2 (close to Gauss)' 'Butterworth Order 3 (between Gauss/Rect)', 'Butterworth Order 4 (close to Rectangular)' 'Gaussian ' 'Rectangular ', 'Triangular ', 'Decreasing Binning (from Rectangular to Triangular)', or ' - Arbitrary - '

Outputs

A new sensor_∗.dat file, and possibly 'sensor' directory is created.
ATTENTION: this routine requires write-access to the sensor directory of the ATCOR installation.

5.2.2 Create Channel Filter Files

ATCOR requires the spectral response of all bands of a sensor being present as a spectral filter file (response file) ∗.rsp . For spectroscopic instruments, the band characteristics are often only available by band center and width at FWHM (Full width half maximum). This function creates the response curves from the latter information (compare Fig. 5.13).

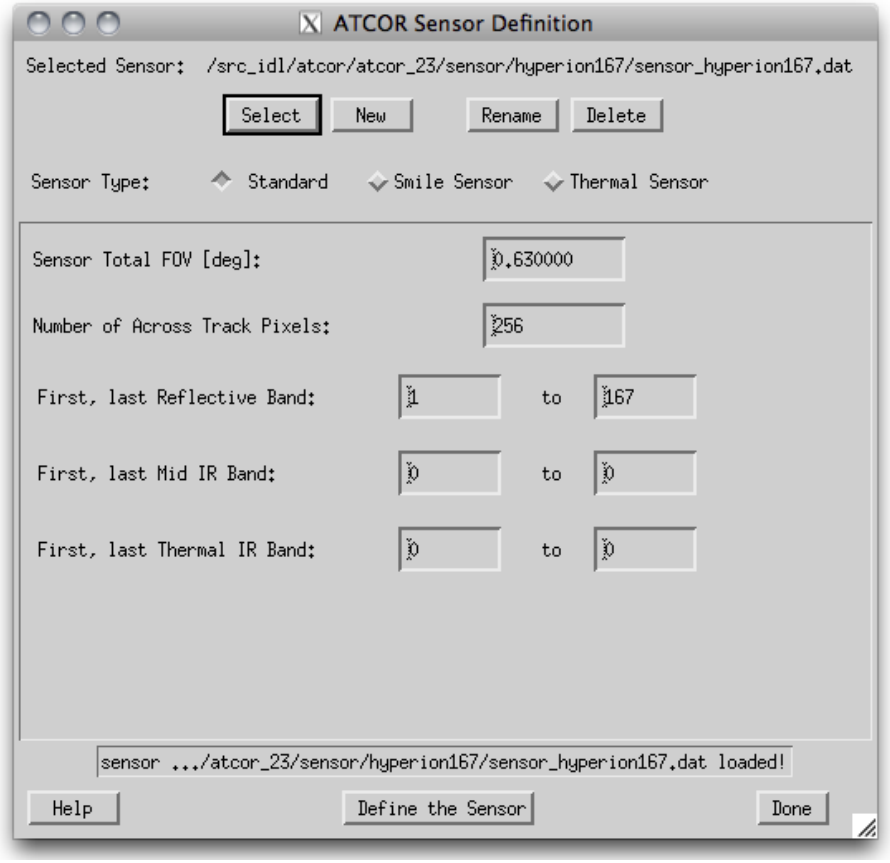

Figure 5.12: *Definition of a new sensor*

Inputs

Wavelength File A wavelength reference file. Format: ASCII, 3 columns, no header; column 1: band number; column2: center wavelength; column 3: band width. Unit: [nm].

Type of Filter Function The type defines the basic shape of each of the created response curves.
Options are: Butterworth Order 1 (slow drop-off)
Butterworth Order 2 (close to Gauss)
Butterworth Order 3 (between Gauss/Rect)
Butterworth Order 4 (close to Rectangular)
Gaussian
Rectangular
Triangular
Decreasing Binning (from Rectangular to Triangular)

Outputs

A numbered series of band_*.rsp files are created at the same location as the wavelength reference file is situated. The files contain wavelength reference and the relative response in two ASCII formatted columns.

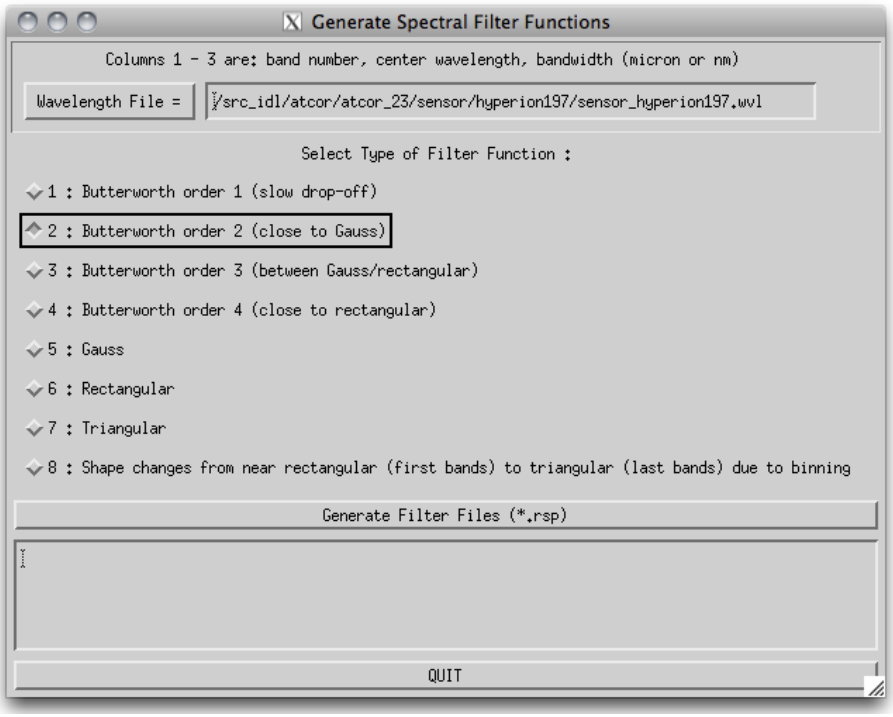
Generate Spectral Filter Functions
Columns 1 - 3 are: band number, center wavelength, bandwidth (micron or nm)
Wavelength File =
/src_idl/atcor/atcor_23/sensor/hyperion197/sensor_hyperion197.wvl
Select Type of Filter Function :
1 : Butterworth order 1 (slow drop-off)
2 : Butterworth order 2 (close to Gauss)
3 : Butterworth order 3 (between Gauss/rectangular)
4 : Butterworth order 4 (close to rectangular)
5 : Gauss
6 : Rectangular
7 : Triangular
8 : Shape changes from near rectangular (first bands) to triangular (last bands) due to binning
Generate Filter Files (*.rsp)
QUIT

Figure 5.13: *Spectral Filter Creation*

5.2.3 BBCALC : Blackbody Function

This routine calculates the blackbody function as described in section 10.1.4, weighted by the spectral response curve of the thermal band used for the temperature retrieval (compare Fig. 5.14).

Inputs

Spectral response file Select the ∗.rsp file of the spectral band in the thermal IR to be used for temperature retrieval.

Exponential Fit - Limits The lower and the higher limit of the temperatures for which a fitting function should be created.

Unit of radiance output Select the unit either per micron or without normalization.

Outputs

A file ∗_hs.bbfit is created containing the fitting parameters.

5.2.4 RESLUT : Resample Atm. LUTS from Database

The monochromatic database of atmospheric LUTs has to be resampled for the specific channel filter functions of each sensor. Details are given in chapters 4.6.1 to 9.1.4. Figure 5.15 repeats the panels of the LUT-resampling program RESLUT. The resampling has to be done separately for the

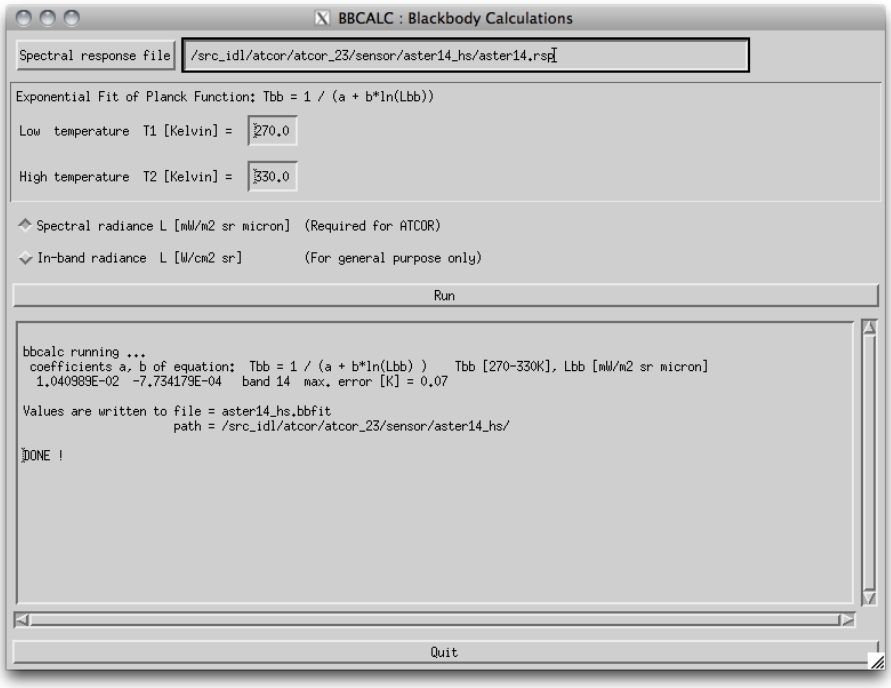
BBCALC : Blackbody Calculations
Spectral response file
/src_idl/atcor/atcor_23/sensor/aster14_hs/aster14.rsp
Exponential Fit of Planck Function: Tbb = 1 / (a + b*ln(Lbb))
Low temperature T1 [Kelvin] =
270.0
High temperature T2 [Kelvin] =
330.0
Spectral radiance L [mW/m2 sr micron] (Required for ATCOR)
In-band radiance L [W/cm2 sr] (For general purpose only)
Run
bbcalc running ...
coefficients a, b of equation: Tbb = 1 / (a + b*ln(Lbb)) Tbb [270-330K], Lbb [mW/m2 sr micron]
1.040989E-02 -7.734179E-04 band 14 max. error [K] = 0.07
Values are written to file = aster14_hs.bbfit
path = /src_idl/atcor/atcor_23/sensor/aster14_hs/
DONE !
Quit

Figure 5.14: *Black body function calculation panel*

reflective and thermal region. Only the required range of flight altitudes and aerosol types should be selected.

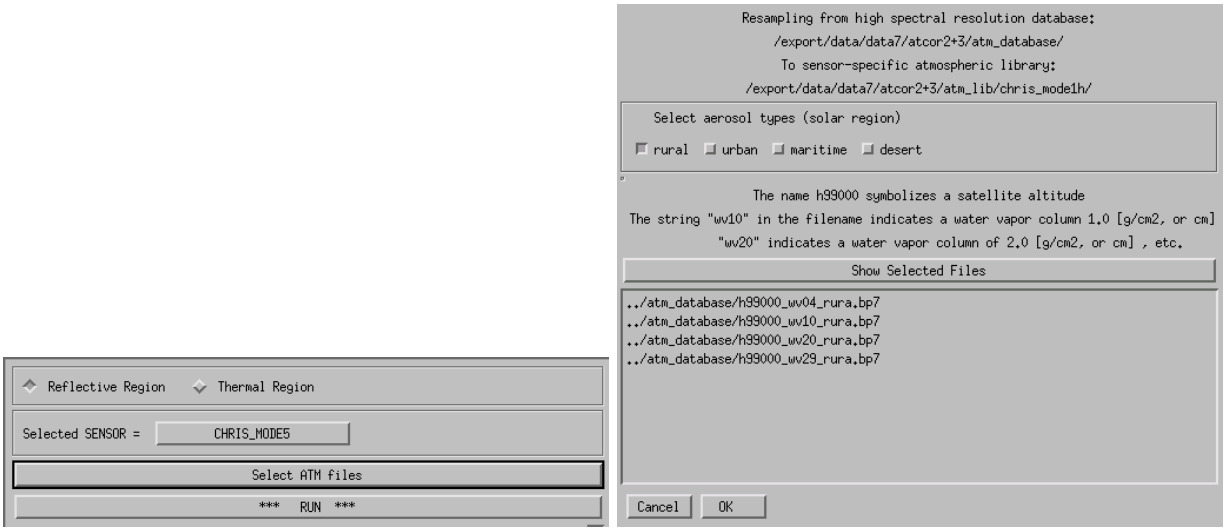

Figure 5.15: *Panels of RESLUT for resampling the atmospheric LUTs.*

5.3 Menu: Atm. Correction

The menu *'Atm. Correction'* contains the main processing modules of ATCOR, i.e., the panels for ATCOR2 and ATCOR3 in both, used-defined and pre-defined, usually multispectral and hyperspectral modes. In this section, the main panels are first shortly described. Thereafter, the subroutines *SPECTRA* and *IFCALI* and all panels related to them are explained.

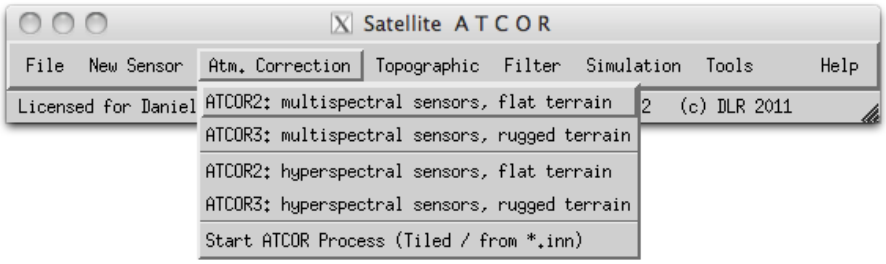

Figure 5.16: *The 'Atm. Correction' Menu*

5.3.1 The ATCOR main panel

Figure 5.17 (top) shows the input parameters required for ATCOR. The lower part of the panel contains buttons for selecting SPECTRA, determining the aerosol type, employing inflight radiometric CALIBRATION, and starting the image processing. The processing options are shown in the separate panel as described in section 5.3.11. The trivial panels, e.g., band selection, spatial subimage etc. will not be shown here. The panels should be filled or clicked in the top-down direction. The message widget at the bottom will display hints, warnings, or errors.

5.3.2 ATCOR2: multispectral sensors, flat terrain

The panel as decribed above and in figure 5.17 will appear when ATCOR2 is selected.

5.3.3 ATCOR3: multispectral sensors, rugged terrain

In case of the rugged terrain version of ATCOR the panel for the DEM files has to be specified in addition (Figure 5.18). It pops up after the input file has been specified. A quick quality check is performed on the DEM files. The solar illumination file is calculated and if its standard deviation is large the panel of Figure 5.19 pops up with a warning. In this case the DEM elevation file (and the derived files of DEM slope, aspect etc) probably have a lot of large steps. The DEM resolution is often not appropriate for high spatial resolution imagery, and integer coded DEM's might have to be resampled and stored as float data. Appropiate action for resampling or low pass filtering is recommended in these cases, see the tips in chapter 9.5. Figure 5.20 shows an example in terms of the DEM illumination. The top image is obtained after low pass filtering the original elevation file, the central image is the illumination based on the original DEM, and the bottom shows a 100 pixel transsect of the original elevation data revealing the steps. The original DEM had a resolution of 30 m, was coded as 16 bit integer, and initially resampled to the 6 m pixel size of the image with integer arithmetic. After reprocessing the elevation file the other DEM derived files should also be reprocessed.

Figure 5.17: *ATCOR panel.*

The pixel size of the DEM files must be the same as the image pixel size specified on the main panel, see figure 5.17. The physical units of pixel size (m) and adjacency range (km) are also used to calculate the equivalent number of pixels needed to cover the adjacency range.

5.3.4 ATCOR2: User-defined Sensors

The menus for user_defined (usually hyperspectral) sensors share the same functionalities as described above for multispectral systems in both flat and rugged terrain options. The major difference is the requirement of a specific sensor definition; ie. the sensor definition is editable and adjustable. The ATCOR2 variant is recommended to speed up processing time and for fast checks as hyperspectral image processing may be very time consuming in rugged terrain.

5.3.5 ATCOR3: User-defined Sensors

This routine is to be taken if highest accuracy is required in terrain for imaging spectroscopy instruments. The functionality is analoguous as described for the other panels.

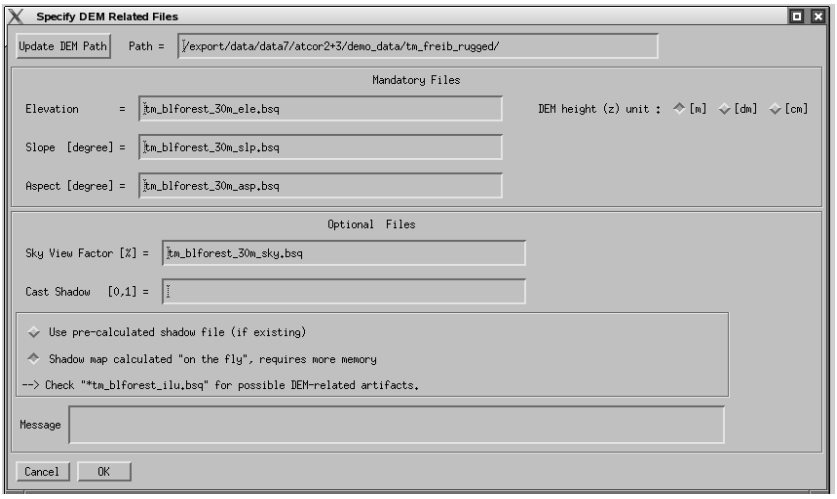

Figure 5.18: *Panel for DEM files.*

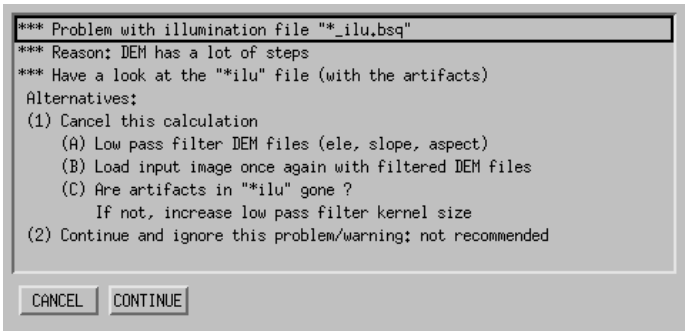
*** Problem with illumination file "*_ilu.bsq"
*** Reason: DEM has a lot of steps
*** Have a look at the "*ilu" file (with the artifacts)
Alternatives:
(1) Cancel this calculation
(A) Low pass filter DEM files (ele, slope, aspect)
(B) Load input image once again with filtered DEM files
(C) Are artifacts in "*ilu" gone ?
If not, increase low pass filter kernel size
(2) Continue and ignore this problem/warning: not recommended
CANCEL
CONTINUE

Figure 5.19: *Panel to make a decision in case of a DEM with steps.*

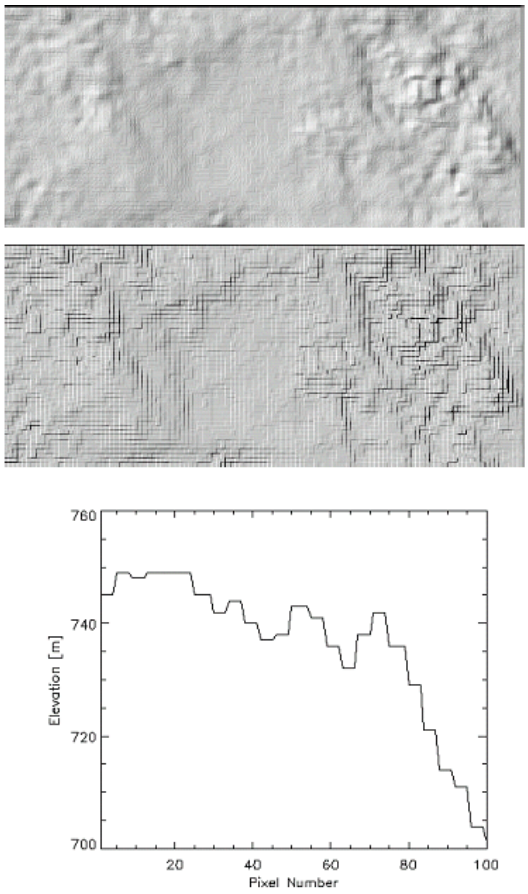

Figure 5.20: *Influence of DEM artifacts on the solar illumination image.*
Top: illumination with low pass filtered DEM; middle: illumination based on original DEM; bottom: 100 m transsect using original DEM, pixel size is 6 m.

5.3.6 SPECTRA module

The SPECTRA module (see figure 5.21) serves to extract spectra of different targets of the scene as a function of the visibility. It is started from within one of the four possible ATCOR main panels. These spectra can be compared to field spectra or library spectra to estimate the visibility. Scene-derived spectra also may indicate calibration errors in certain channels. In that case, a copy of the sensor calibration file can be edited to match the retrieved reflectance with the field / library spectrum or the inflight calibration module may be employed (see chapter 5.3.9).

In most cases it is useful to check some scene-derived target spectra, e.g. water, vegetation, or soils, before starting the processing of the image cube at the risk of *"blind"* processing and obtaining wrong results.

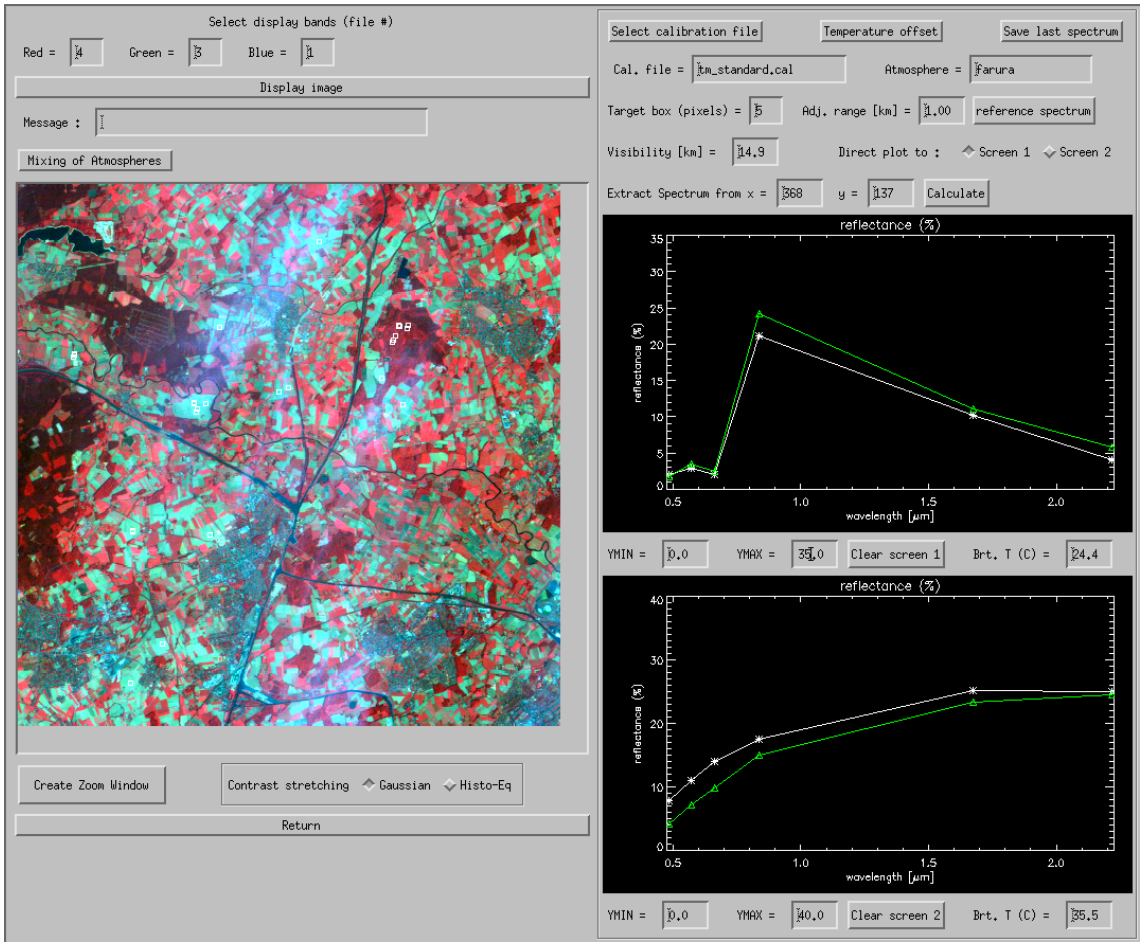

Figure 5.21: *SPECTRA module.*

To obtain a target spectrum of the scene click at any position in the image. In figure 5.21 the solid white-line spectrum at the top shows a coniferous forest signature, the green line represents a spruce reference spectrum taken from the *spec_lib* directory, already resampled for the Landsat-5 TM sensor. The symbols mark the TM center wavelengths. A reference spectrum can be loaded when clicking the corresponding button at the top right of the panel. The bottom graphics shows soil and water spectra taken from the scene and a soil reference spectrum from the *spec_lib* library.

An exact match of scene spectra and library spectra cannot be expected, but the trends (spectral shapes) should be consistent.

The parameter *Visibility* can be set in the corresponding widget near the center of the panel and its influence on the retrieved spectrum will be shown when placing the target box in the scene. To vary the atmospheric water vapor content the user should switch to the main panel and select a different atmosphere, e.g. switch from the mid-latitude summer atmosphere (with a column wv=2.9 cm) to a tropical atmosphere (with wv=4.1 cm), compare chapter 6. Most multispectral satellite sensors do not have spectral bands placed in water vapor regions, so the retrieved reflectance signature will show a rather small dependence on the water vapor estimate. For sensors with water vapor bands, e.g., Hyperion or MOS-B, the retrieved reflectance spectrum strongly depends on the water vapor content. In this case, the water vapor map can be derived during the image processing (see the panel of figure 5.17) as part of the reflectance retrieval. Note that the water vapor is not retrieved from the image pixel for correction in the SPECTRA module as it is done in the image processing for hyperspectral systems.

The button *"Save last spectrum"* (upper right corner of figure 5.21) can be used to save the selected surface reflectance spectrum. A sequence of target DN spectra can also be generated here that is required as input to the spectral calibration module (currently only available for the hyperspectral add-on module). Up to 9 targets can be defined to be used in the spectral calibration. They have to be labeled consecutively, e.g. *"target1"*, *"target2"*, etc. These output file names (without file name extension) have to be specified after pressing the button *"Save last spectrum"*. For each target name three files will be generated, e.g., *"target1.dat"* (surface reflectance spectrum), *"target1.txt"* (a description file), and *"target1_dn1.dat"* (the DN spectrum). The sequence of *"target*_dn*.dat"* files is used in the spectral calibration module.

5.3.7 Aerosol Type

The aerosol type is a parameter which is fixed for atmospheric correction. This routine searches automatically for the best suited aerosol type for the currently selected image. This type can then be used when selecting the atmospheric file.

5.3.8 Visibility Estimate

ATCOR uses the *Dark Dense Vegetation (DDV)* approach to calculate the best visibility for an image. This button allows to calculate the visibility estimate for the whole image without going into the image processing. Note, that for variable visibility options, the visibility will be calculated anyhow from the image in the image processing.

5.3.9 Inflight radiometric calibration module

This chapter presents the GUI for the inflight calibration, which may also be invoked from one of the four possible ATCOR main panels. The purpose is the calculation of the radiometric calibration coefficients for spectral bands in the solar region based on measured ground reflectance spectra. The user should be familiar with chapter 2.4 before using this function.

Note: a ground reflectance spectrum from a field spectrometer has to be resampled with the channel filter curves of the selected sensor. The field spectrometer file format should be converted into a simple ASCII file containing the wavelength (nm or μm) in the first column and reflectance in

the second column. The resampling can then be done with the sequence "Filter", "Resample a Spectrum" from the ATCOR main panel. The result is an ASCII file with 2 columns: the first contains the channel center wavelength (the nm and μm unit is allowed), the second contains the resampled reflectance value (either in the 0 - 1 or 0 - 100% range).

If "target1" is the name of the target, ATCOR provides three ASCII files with information on target / background properties and the derived calibration file. These are the output of the "c1" option of ATCOR's calibration module,

- File "target1.adj" contains the original target DN_1, the adjacency corrected DN_1^*, and the ground reflectance data for each band.
- File "target1.rdn" (radiance versus digital number) contains the band center wavelength, target radiance L_1 and corresponding digital number. This file can be used as input to a regression program "cal_regress" that allows the calculation of the calibration coefficients with a least squares fit in case of multiple targets (more than two).
- File "target1.cal" contains three columns: band center wavelength, offset or bias set to zero ($c_0 = 0$), and c_1 according to equation (2.18).

Remark: a bright target should be used here, because for a dark target any error in the ground reflectance data will have a large impact on the accuracy of c_1.

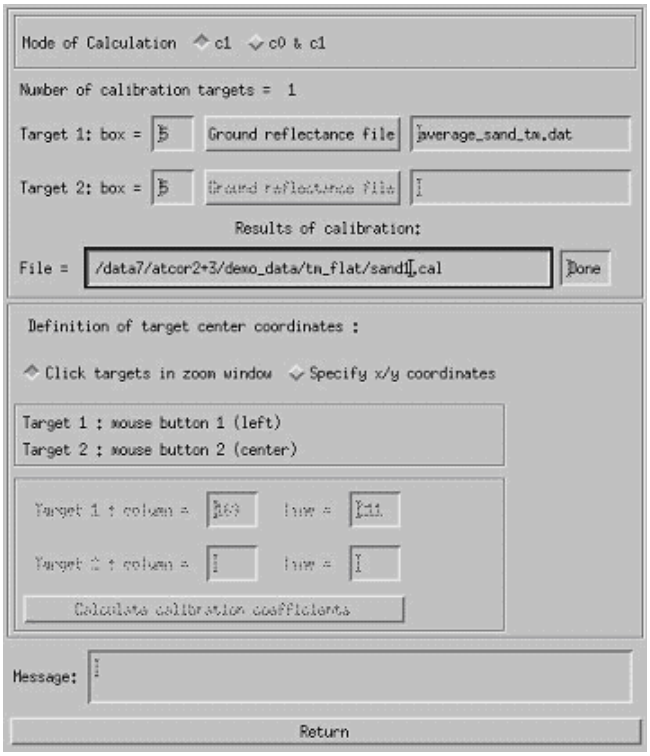

Figure 5.22: *Radiometric calibration: target specification panel.*

At the top line of the menu of figure 5.22 the mode of calibration is specified: one or two targets can be employed by selecting the button 'c1' or 'c0 & c1, respectively. If a calibration is intended

for n > 2 targets, each target has to be specified separately in the 'c1' mode, which creates a file 'target_i.rdn' (i=1, 2, ..., n) with the name 'target_i' specified by the user. These files contain the radiance and corresponding digital number spectrum as a 2-column ASCII table, and they are employed in the batch module *cal_regress* (see chapter 5) to calculate a least squares regression for the calibration coefficients. Next the target box size and the corresponding ground reflectance file have to be specified. The button for the file name of target 2 is insensitive, because the single target mode was selected here. Then the file name for the calibration results should be specified. The default name is *"test.cal"*. However, it is recommended to include the name of the ground target here. Now the target(s) can be clicked in the zoom window that pops up automatically. Target 1 has to be clicked with mouse button 1 (mb1, left), target 2 with mouse button 2 (mb2, center). The zoom window is moved in the main window by pressing mb1 (for target 1) and mb2 (for target 2). Alternatively, the target coordinates (x / y = column / line) can be specified.

In addition to the file *"xxx.cal"* the files *"xxx.rdn"* (radiance versus digital number), and *"xxx.adj"* (original and adjacency corrected DN's) are automatically created.

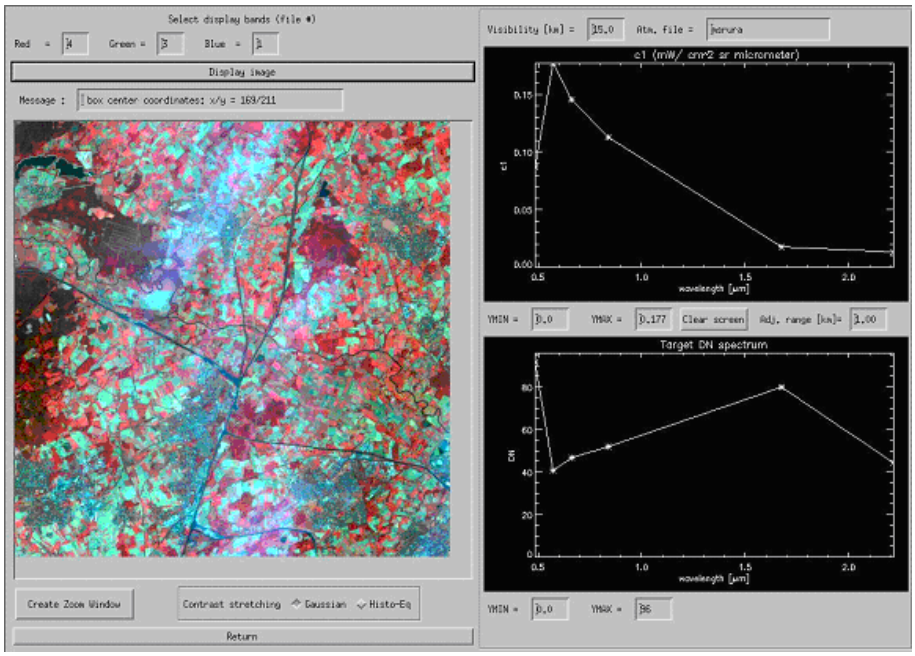

Figure 5.23: *Radiometric CALIBRATION module.*

The appearance of the inflight calibration module is similar to the SPECTRA module. In the left part the image is loaded. A zoom window can be created and two contrast stretching options (Gaussian and histogram equalization) are available. In the right part two windows are provided to display the c1 spectrum and the box-averaged target DN spectrum. The ymin / ymax widgets allow the user to scale the graphical display. The parameters visibility and adjacency range can be varied and their influence on the calibration curve can be studied.

5.3.10 Shadow removal panels

The interactive session of the de-shadowing method enables the setting of three parameters that influence the results, compare Figures 5.24, 5.25:

1. a threshold Φ_T for the unscaled shadow function Φ = PhiU to define the core size of the shadow regions, see chapter 10.5.5 for details.

2. the maximum range Φ_{max} for re-scaling the unscaled shadow function Φ = PhiU into the (0,1) interval of the scaled shadow function.

3. the last parameter sets the minimum value of the scaled shadow function Φ^* = PhiS, typically in the range PhiS=0.02 - 0.10, i.e., the darkest shadow pixels of the scene are treated as being illuminated with a fraction PhiS of the direct solar irradiance.

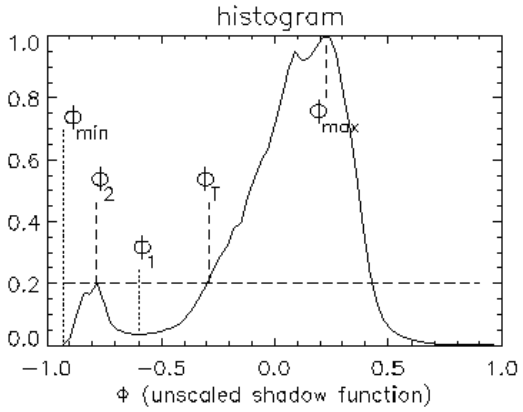

Figure 5.24: *Normalized histogram of unscaled shadow function.*

The first two parameters are most important. The last parameter is not very critical, and a default value in the range PhiS=0.04 - 0.08 covers most cases of interest.
The linear type of re-scaling of PhiU is recommened. The "exponential" option exaggerates the de-shadowing results, but it can be used to enhance the trends for a quick visual inspection.
When pressing the button "Run Interactive De-Shadowing", a reduced size image of the original scene, the shadow mask, and the de-shadowed image will pop up with the histogram of PhiU containing the threshold for core areas (point 1 of Fig. 5.25), the range of re-scaling of PhiU (point 2), and the current value for PhiS (point 3). Now these three parameters can be modified, and the results will again be shown as the corresponding quicklook image and histogram. When good results have been obtained the parameters can be saved and the final image processing can take place.
Figure 5.26 presents an example with two iterations. Results for iteration 1 contain too many shadow pixels (black areas in the central section of the image), therefore the threshold = -0.15 was decreased to -0.38 (parameter 1 of Fig. 5.25). After de-shadowing, most areas in the shadow mask were overcorrected in iteration 1, therefore the maximum range = 0.40 was decreased to 0.19 (parameter 2 of Fig. 5.25, see diagonal line from lower left to upper right in histogram of Fig. 5.26). The shadow mask for iteration 2 is appropriate, and no overcorrection effects can be observed.

Note: when leaving the panel of Fig. 5.25 it is possible to edit the cloud shadow map before continuing the scene processing, using any available image processing software. Then the edited

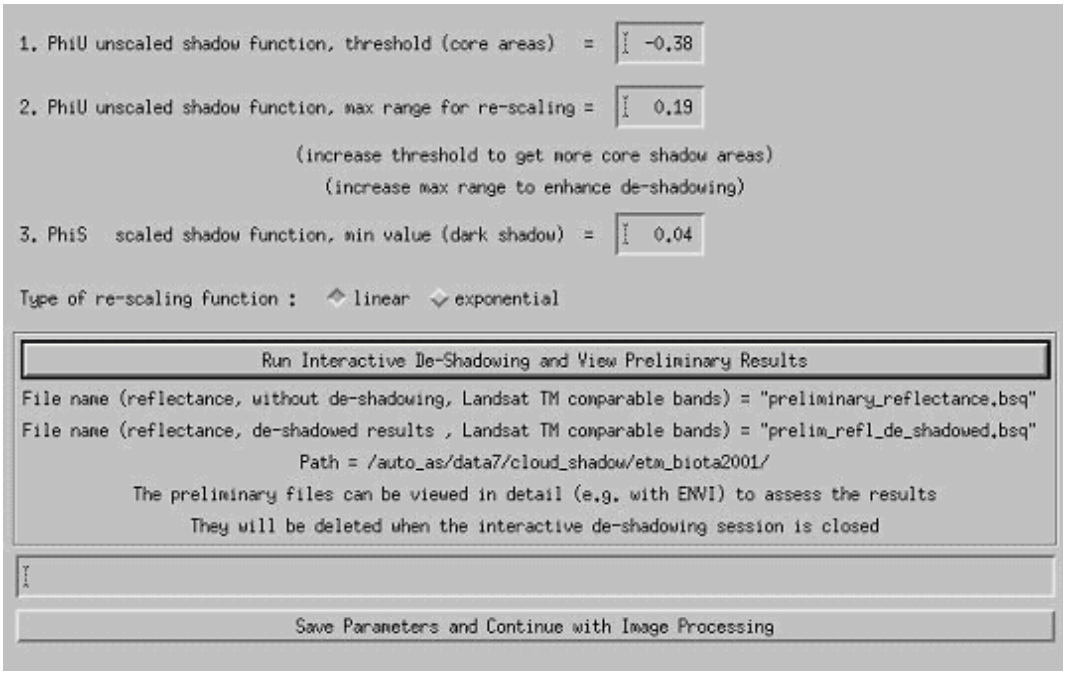
1. PhiU unscaled shadow function, threshold (core areas) = -0.38
2. PhiU unscaled shadow function, max range for re-scaling = 0.19
(increase threshold to get more core shadow areas)
(increase max range to enhance de-shadowing)
3. PhiS scaled shadow function, min value (dark shadow) = 0.04
Type of re-scaling function : linear exponential
Run Interactive De-Shadowing and View Preliminary Results
File name (reflectance, without de-shadowing, Landsat TM comparable bands) = "preliminary_reflectance.bsq"
File name (reflectance, de-shadowed results , Landsat TM comparable bands) = "prelim_refl_de_shadowed.bsq"
Path = /auto_as/data7/cloud_shadow/etm_biota2001/
The preliminary files can be viewed in detail (e.g. with ENVI) to assess the results
They will be deleted when the interactive de-shadowing session is closed
Save Parameters and Continue with Image Processing

Figure 5.25: *Panel to define the parameters for interactive de-shadowing.*

map is employed for the processing. This provides some flexibility because it is difficult to calculate a satisfactory shadow map in all cases.

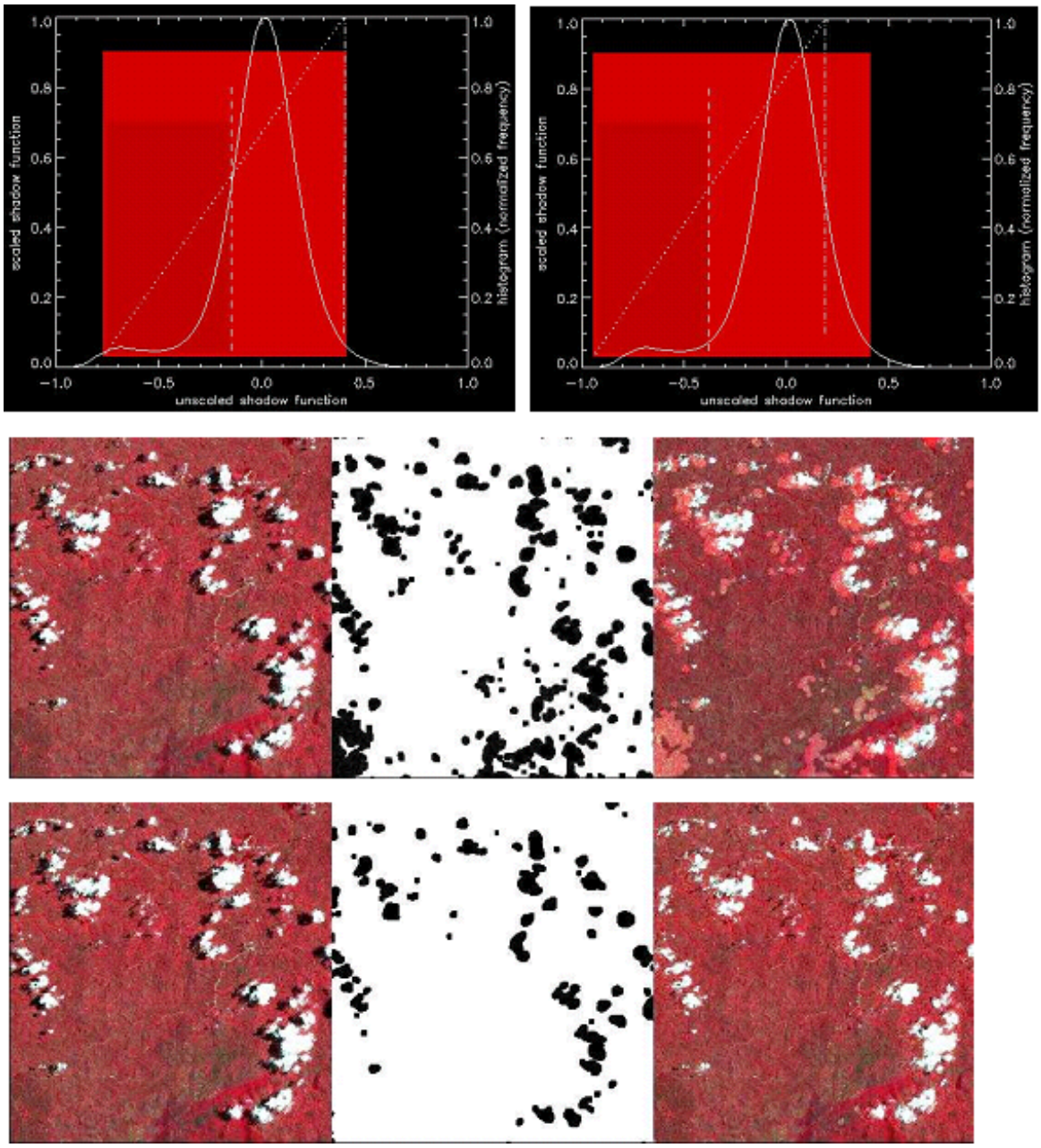

Figure 5.26: *Quicklook of de-shadowing results.*
Top left: histogram of PhiU (threshold=-0.15, range=0.40), iteration 1. Top right: histogram of PhiU (threshold= -0.38, range=0.19), iteration 2. Center: results for iteration 1, left-to-right: original, shadow mask, de-shadowed image. Bottom: results for iteration 2.

5.3.11 Panels for Image Processing

When pressing the button *"IMAGE PROCESSING"* in one of the main panel (figure 5.17) some additional panels will pop up. First, the processing options are to be selected (see figure 5.27).

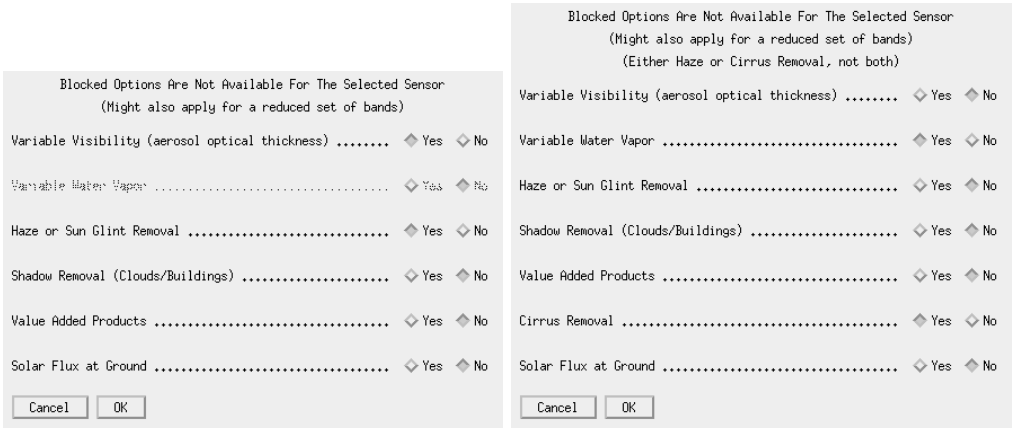
Blocked Options Are Not Available For The Selected Sensor
(Might also apply for a reduced set of bands)
Variable Visibility (aerosol optical thickness) ..... Yes No
Variable Water Vapor ..... Yes No
Haze or Sun Glint Removal ..... Yes No
Shadow Removal (Clouds/Buildings) ..... Yes No
Value Added Products ..... Yes No
Solar Flux at Ground ..... Yes No
Cancel OK
Blocked Options Are Not Available For The Selected Sensor
(Might also apply for a reduced set of bands)
(Either Haze or Cirrus Removal, not both)
Variable Visibility (aerosol optical thickness) ..... Yes No
Variable Water Vapor ..... Yes No
Haze or Sun Glint Removal ..... Yes No
Shadow Removal (Clouds/Buildings) ..... Yes No
Value Added Products ..... Yes No
Cirrus Removal ..... Yes No
Solar Flux at Ground ..... Yes No
Cancel OK

Figure 5.27: *Image processing options. Right panel appears if a cirrus band exists.*

Options that are not allowed for a specific sensor will appear insensitive. If the haze removal option is selected in combination with *"Variable Visibility"* the visibility index (proportional to total optical thickness) map is coded with the values 0-182. The value visindex=0 corresponds to visibility 190 km, each integer step of 1 corresponds to an AOT increase of 0.006. The array serves as a fast method of addressing the radiative transfer quantities (transmittance, path radiance etc) in case of a spatially varying visibility, i.e., in combination with the DDV algorithm. IF the *"Haze or Sunglint Removal"* button is selected the next panel will ask for haze removal over land (option 1), haze or sunglint removal over water (option 2), or haze removal over land and water (option 3).

In case of thermal bands, an emissivity selection panel will appear:

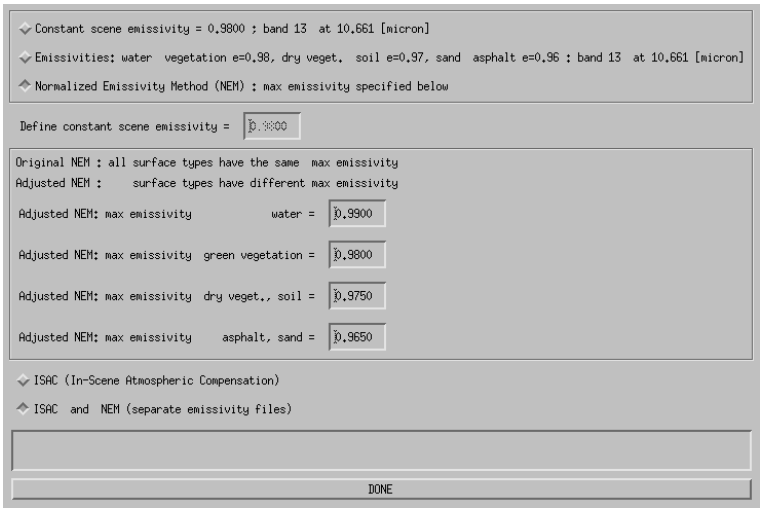
Constant scene emissivity = 0.9800 ; band 13 at 10.661 [micron]
Emissivities: water vegetation e=0.98, dry veget. soil e=0.97, sand asphalt e=0.96 ; band 13 at 10.661 [micron]
Normalized Emissivity Method (NEM) : max emissivity specified below
Define constant scene emissivity = 0.9800
Original NEM : all surface types have the same max emissivity
Adjusted NEM : surface types have different max emissivity
Adjusted NEM: max emissivity water = 0.9900
Adjusted NEM: max emissivity green vegetation = 0.9800
Adjusted NEM: max emissivity dry veget., soil = 0.9750
Adjusted NEM: max emissivity asphalt, sand = 0.9650
ISAC (In-Scene Atmospheric Compensation)
ISAC and NEM (separate emissivity files)
DONE

Figure 5.28: *Emissivity selection panel.*

The first two options are available for instruments with only a single thermal band, the NEM and ISAC options require multiple thermal bands and are not shown if there are less than 5 thermal bands. The surface classes (water, vegetation, soil etc) are calculated on-the-fly employing the surface reflectance spectra from the reflective bands.

Figure 5.29 shows the panel with the two options for haze over land processing as explained in chapter 10.5.2.

Compact Smaller Area Haze Mask
Large Area Haze Mask (superior in most cases)
Correct Thin to Medium Haze
Correct Thin to Moderately Thick Haze (superior in most cases)
DONE

Figure 5.29: *Options for haze processing.*

The panel of figure 5.30 pops up when the spatially varying visibility option was selected and if the sensor has a 2.2 μm (or 1.6 μm) band (or at least a red and NIR band) required for the automatic masking of the dark reference pixels, compare chapter 10.4.2.

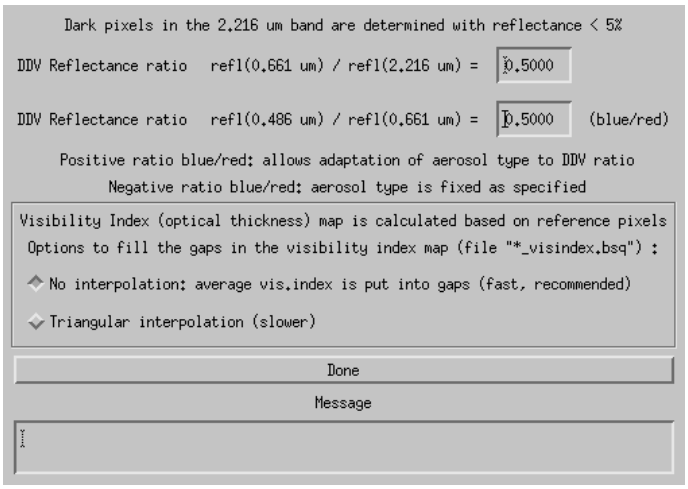
Dark pixels in the 2.216 um band are determined with reflectance < 5%
DDV Reflectance ratio refl(0.661 um) / refl(2.216 um) = 0.5000
DDV Reflectance ratio refl(0.486 um) / refl(0.661 um) = 0.5000 (blue/red)
Positive ratio blue/red: allows adaptation of aerosol type to DDV ratio
Negative ratio blue/red: aerosol type is fixed as specified
Visibility Index (optical thickness) map is calculated based on reference pixels
Options to fill the gaps in the visibility index map (file "*_visindex.bsq") :
No interpolation: average vis.index is put into gaps (fast, recommended)
Triangular interpolation (slower)
Done
Message

Figure 5.30: *Reflectance ratio panel for dark reference pixels.*

The panel of figure 5.31 pops up for rugged terrain and contains the input parameters to BRDF correction as discussed in chapter 2.2.

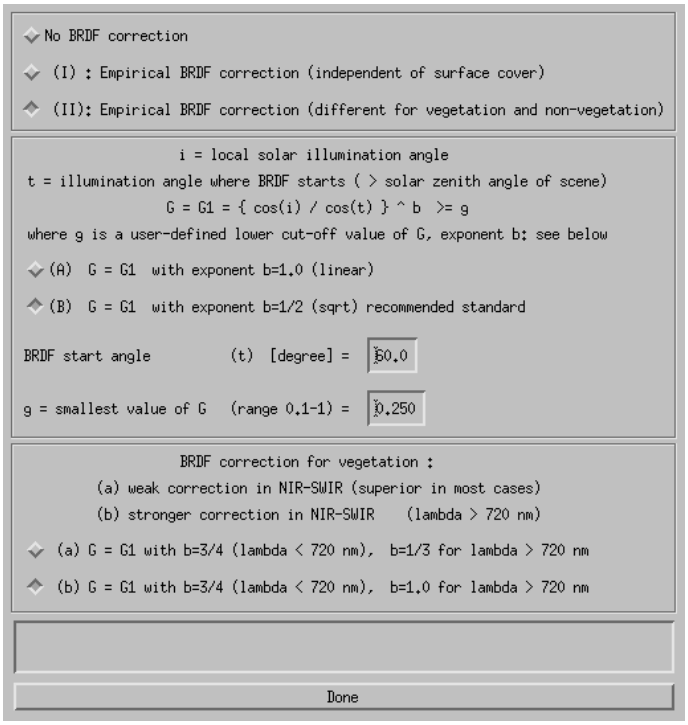
No BRDF correction
(I) : Empirical BRDF correction (independent of surface cover)
(II): Empirical BRDF correction (different for vegetation and non-vegetation)
i = local solar illumination angle
t = illumination angle where BRDF starts (> solar zenith angle of scene)
G = G1 = { cos(i) / cos(t) } ^ b >= g
where g is a user-defined lower cut-off value of G, exponent b: see below
(A) G = G1 with exponent b=1.0 (linear)
(B) G = G1 with exponent b=1/2 (sqrt) recommended standard
BRDF start angle (t) [degree] = 60.0
g = smallest value of G (range 0.1-1) = 0.250
BRDF correction for vegetation :
(a) weak correction in NIR-SWIR (superior in most cases)
(b) stronger correction in NIR-SWIR (lambda > 720 nm)
(a) G = G1 with b=3/4 (lambda < 720 nm), b=1/3 for lambda > 720 nm
(b) G = G1 with b=3/4 (lambda < 720 nm), b=1.0 for lambda > 720 nm
Done

Figure 5.31: *BRDF panel.*

Figures 5.32 and 5.33 are associated with the value added products as described in chapter 7. This value added file contains up to 10 channels if the sensor has thermal bands. In case of a flat terrain, the air temperature has to be specified. For a rugged terrain, air temperature at some base elevation and the air temperature gradient as well as water vapor have to be defined.

If the value added option is selected another panel pops up (Figure 5.34). It contains parameters for the leaf area index (LAI model) and FPAR model as described in chapter 7.

Finally, a job status window indicates the processing progress.

Note:
The job status window of ATCOR shows the percentage of processed image data and the estimated remaining time. The time estimate is based on the processing time for the current band. The time per band increases for channels in atmospheric water vapor regions, it decreases in regions where interpolation is applied, e.g., around 1400 nm. However, the time also depends on other factors such as the overall CPU load in case of multi-user machines, or the traffic on net-worked machines. Accordingly, the estimate for the remaining time is not always continuously decreasing, but may increase sometimes.

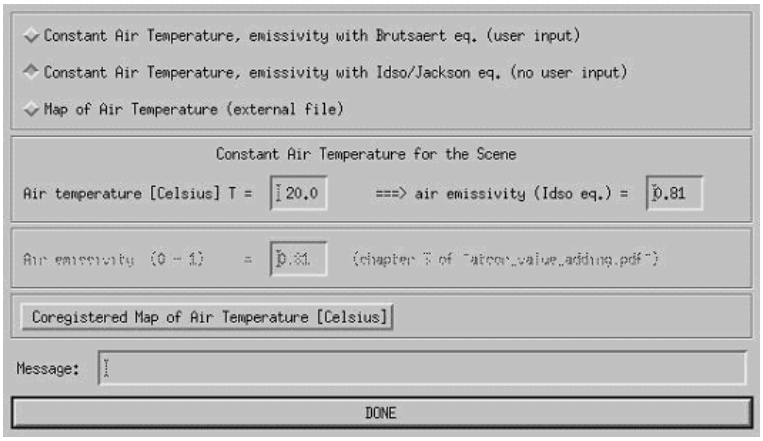
Constant Air Temperature, emissivity with Brutsaert eq. (user input)
Constant Air Temperature, emissivity with Idso/Jackson eq. (no user input)
Map of Air Temperature (external file)
Constant Air Temperature for the Scene
Air temperature [Celsius] T = 20.0
===> air emissivity (Idso eq.) = 0.81
Air emissivity (0 - 1) = 0.84
(chapter 3 of "atcor_value_adding.pdf")
Coregistered Map of Air Temperature [Celsius]
Message:
DONE

Figure 5.32: *Value added panel for a flat terrain.*

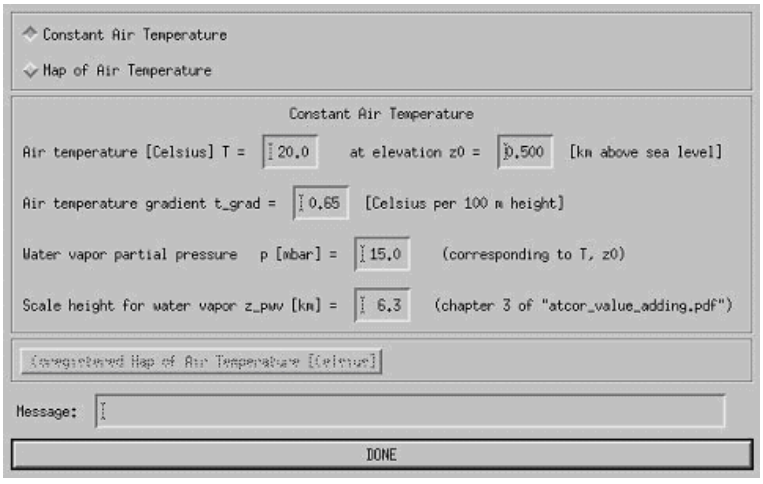
Constant Air Temperature
Map of Air Temperature
Constant Air Temperature
Air temperature [Celsius] T = 20.0
at elevation z0 = 0.500
[km above sea level]
Air temperature gradient t_grad = 0.65
[Celsius per 100 m height]
Water vapor partial pressure p [mbar] = 15.0
(corresponding to T, z0)
Scale height for water vapor z_pwv [km] = 6.3
(chapter 3 of "atcor_value_adding.pdf")
Coregistered Map of Air Temperature [Celsius]
Message:
DONE

Figure 5.33: *Value added panel for a rugged terrain.*

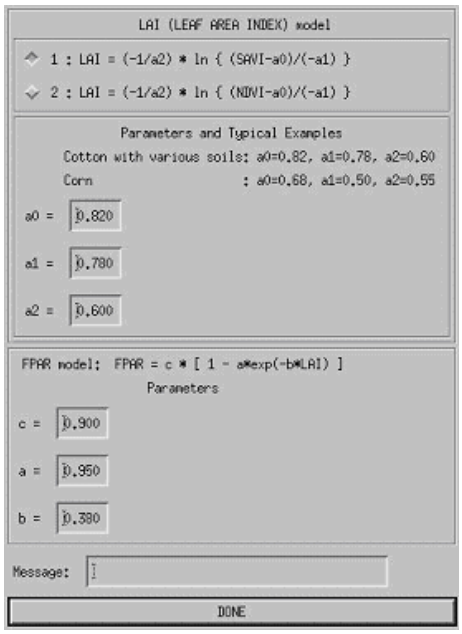
LAI (LEAF AREA INDEX) model
1 : LAI = (-1/a2) * ln { (SAVI-a0)/(-a1) }
2 : LAI = (-1/a2) * ln { (NDVI-a0)/(-a1) }
Parameters and Typical Examples
Cotton with various soils: a0=0.82, a1=0.78, a2=0.60
Corn : a0=0.68, a1=0.50, a2=0.55
a0 = 0.820
a1 = 0.780
a2 = 0.600
FPAR model: FPAR = c * [1 - a*exp(-b*LAI)]
Parameters
c = 0.900
a = 0.950
b = 0.380
Message:
DONE

Figure 5.34: *LAI / FPAR panel*

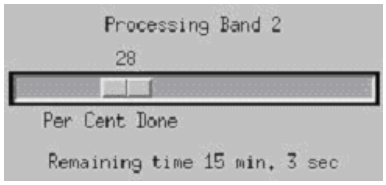

Figure 5.35: *Job status window.*

5.3.12 Start ATCOR Process (Tiled / from ∗.inn)

This is a way to start a tiled process of ATCOR from within the ATCOR GUI (instead of the standard batch-based process 'atcor_tile').

The process requires that an ∗.inn file has been created before by going through the atcor GUI or by editing a respective ASCII file manually or by using the routine *write_atcor_inn_file.pro* provided in the directory *docu* of the ATCOR installation.

The below parameters are to be entered for processing:

- Input file name: name of image data cube to be processed. The file must be accompanied by a valid ∗.inn file for processing.
- Name of output cube to be created.
- Number of tiles in X and Y dimensions - the total number of tiles to process is then X x Y tiles.
- ATCOR method: selection between flat processing and rugged processing - for the latter the DEM has to be prepared and ready.

After starting the process using the 'run' button, the messages are printed to the prompt (or the console) if available. Error and status messages may also be found in the *.log file during and after processing.

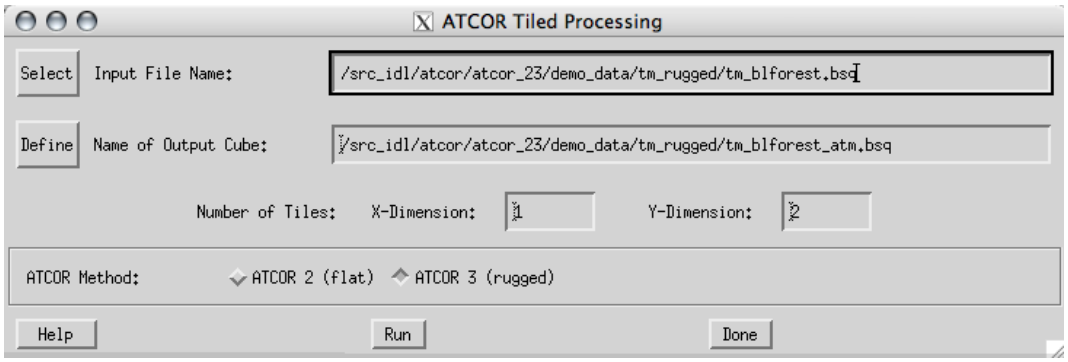

Figure 5.36: *ATCOR Tiled Processing*

5.4 Menu: Topographic

The *"Topographic"* menu contains programs for the calculation of slope/aspect images from a digital elevation model, the skyview factor, and topographic shadow. Furthermore, it supports the smoothing of DEMs and its related layers.

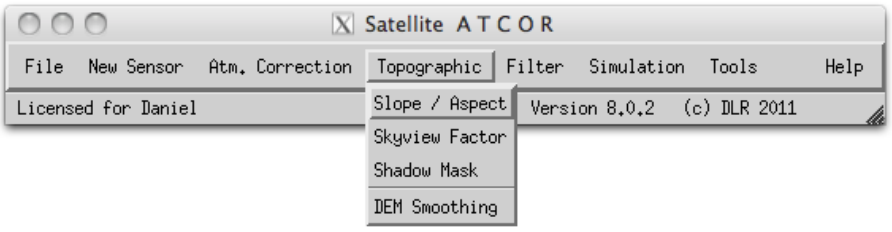

Figure 5.37: *Topographic modules.*

5.4.1 Slope/Aspect

Slope and aspect are to be calculated from the DEM before ATCOR is run for rugged terrain. This menu function as depicted in Fig. 5.38 allows to calculate both layers in one step.

Inputs

Input DEM file The standard DEM file used for atmospheric correction. This DEM should be in meters

Output file names The names for the output files are entered automatically and can't be changed as ATCOR asks these files to be named exactly according to the conventions.

Kernel Size Box Size of the kernel in number of pixels; the slope and aspect is calculated as gradient of the pixels at the edges of this box - the default value is 3 pixels (i.e. direct neighbours of center pixel).

DEM resolution This is the pixel size, a default of 30m is assumed. This needs to be entered manually.

DEM height unit The unit of the values in the DEM, usually a DEM is stored in meters, but sometimes an integer DEM is stored as dm or cm data in order to preserve disk space.

Outputs

The two files of slope and aspect are created, same size as DEM, integer data.

5.4.2 Skyview Factor

The sky view factor of a DEM is calculated with a ray tracing program and ranges from vsky = 0 to 1, with 1 indicating a full hemispherical view. Data in the sky view file are scaled from 0 to 100% and coded as byte. The sky view factor determines the fraction of the hemispherical diffuse

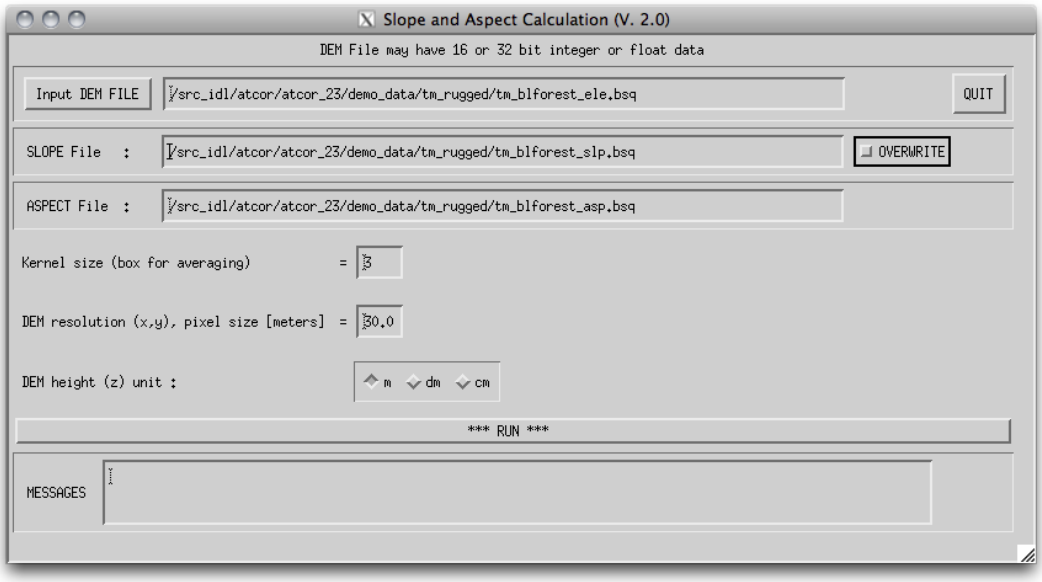

Figure 5.38: *Slope/Aspect Calculation panel*

sky flux and 1-vsky(x,y) determines the fraction of radiation reflected from surrounding mountains onto the considered pixel, see chapter 10.1.1. This program is also available in the batch mode, see chapter 6.2.

Input parameters besides the DEM file are:

- DEM horizontal resolution in meters: the x and y resolution must be the same.
- DEM height unit: supported units are m, dm, and cm.
- Angular resolution (degrees) in azimuth and elevation.
- The undersampling factor of the DEM in pixels. For large DEM's the skyview processing may be very time consuming unless an undersampling is chosen here.

Figure 5.39 shows the GUI panel, and figure 5.40 presents a skyview image derived from a DEM image. An angular azimuth / elevation resolution of 10 degrees / 5 degrees is recommended. For large images it causes a high execution time which can be reduced by selecting an undersampling factor of 3 pixels. A high angular resolution is more important than a low undersampling factor.

5.4.3 Shadow Mask

The calculation of the shadow map is done by ATCOR after reading the DEM files. If the shadow map is computed *"on-the-fly"* it is kept in memory, and it is not stored as a separate file. If the user wants to inspect the DEM shadow map the program *"shadow"* has to be started before running ATCOR. The program accepts float values of the solar zenith and azimuth angles. The output file name of the DEM shadow map includes the zenith and azimuth angles rounded to integer values. The DEM shadow map is a binary file where shadow pixels are coded with 0 and sunlit pixels with 1. It includes self shadowing and cast shadow effects. Self shadowing consists of pixels oriented away from the sun with slopes steeper than the solar elevation angle. The cast shadow calculation

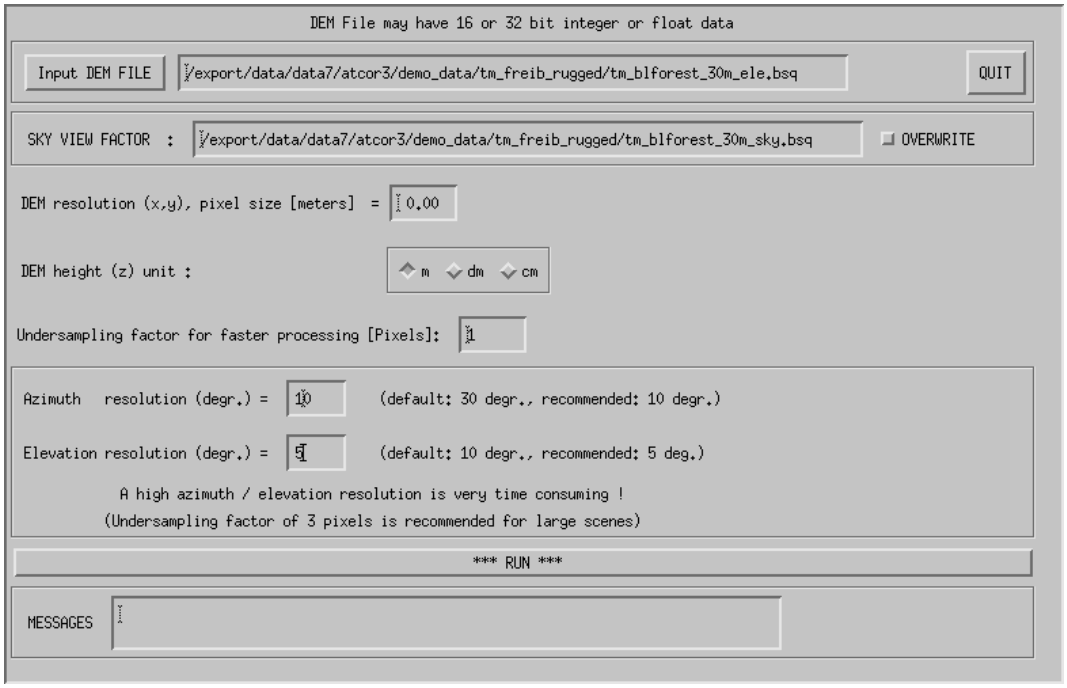

Figure 5.39: *Panel of SKYVIEW.*

is based on a ray tracing algorithm and includes shadow regions caused by higher surrounding mountains. Figure 5.41 shows the GUI panel.

5.4.4 DEM Smoothing

Smooth a DEM (or any other single-band image) in order to remove artifacts in the atmospherically corrected imagery. All related DEM-layers are automatically smoothed as well (e.g. slope / aspect / skyview). Alternatively, this task coud be done with any image processing software.

Inputs:

Input DEM/file Name Usually a DEM _* ele.bsq is selected here; but any other single band ENVI image or the *_ilu.bsq file is also accepted. The routine searches automatically for related files (i.e. *_sky, *_slp , and/or *_asp) and smoothes them with the same parameters.

Diameter of DEM Filter: Size of filter box in pixels (diameter)

Output Name: Name of Elevation file output (auxiliary layer names will be derived from that)

Outputs:
ENVI file(s) smoothed or filtered by the given factor and method:

Smooth: uses the standard smoothing (i.e., lowpass-filter) in the spatial domain.

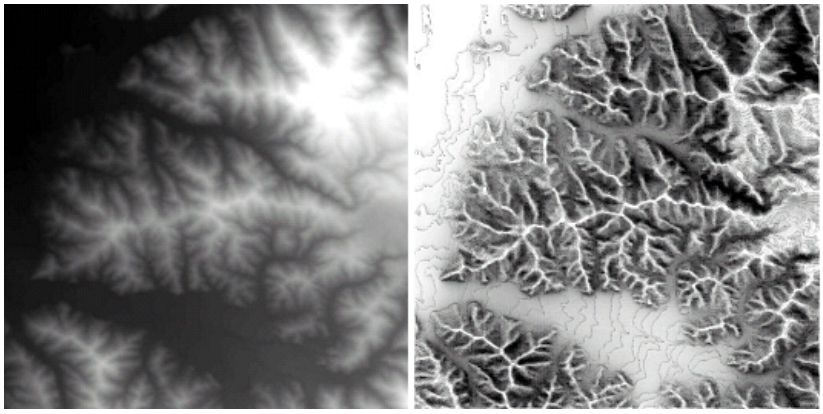

Figure 5.40: *Example of a DEM (left) with the corresponding sky view image (right).*

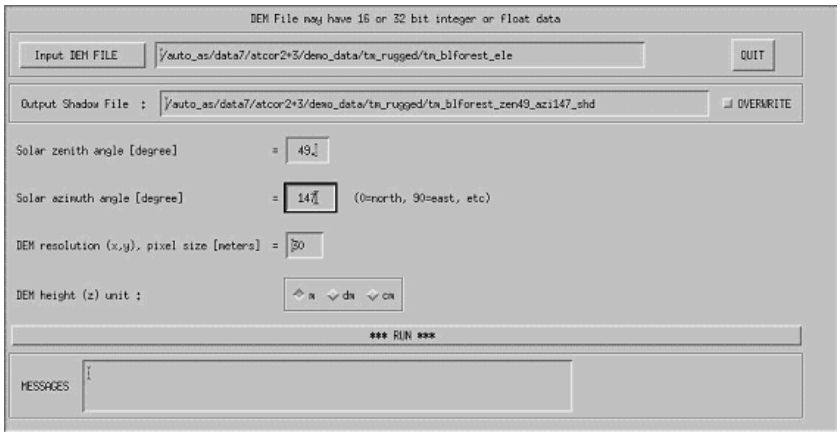

Figure 5.41: *Panel of SHADOW.*

Median: uses a median filter for data correction, e.g., to remove noise or outliers from the DEM.

ATTENTION: The $*$_ilu file is not smoothed automatically by this routine. If the ilu has already been calculated before, it should be either removed or be smoothed directly.

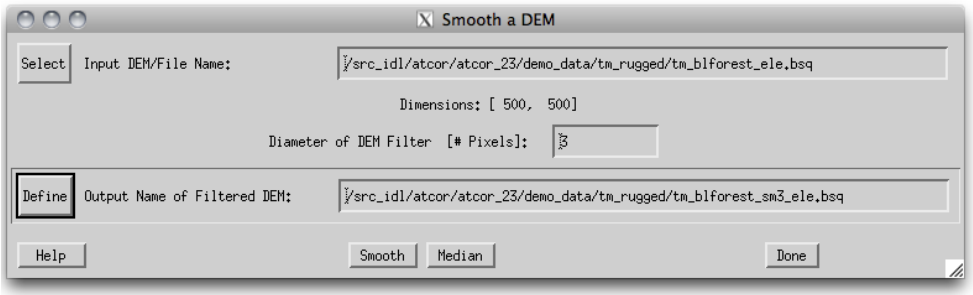

Figure 5.42: *Panel of DEM smoothing*

5.5 Menu: Filter

The *"Filter"* menu provides spectral filtering of single spectra (reflectance, emissivity, radiance) provided as ASCII files, spectral filtering of image cubes, and spectral polishing.

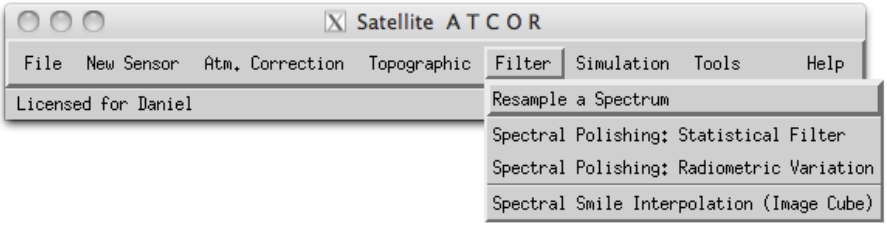

Figure 5.43: *Filter modules.*

5.5.1 Resample a Spectrum

This program serves for the general purpose of resampling. It requires an ASCII file with two columns as input. The first column is wavelength (nm or μm unit), the second is reflectance, or emissivity, or something else, e.g. spectral radiance. The reflectance range can be 0 - 1 (the intrinsic reflectance unit) or the percent range (0 - 100). Figure 5.44 shows the graphical user interface. The input spectrum is high spectral resolution data. After specifying the first band of the sensor the resampling is performed for all spectral bands, and the result is written to an output file, again with two columns (wavelength and resampled spectrum).

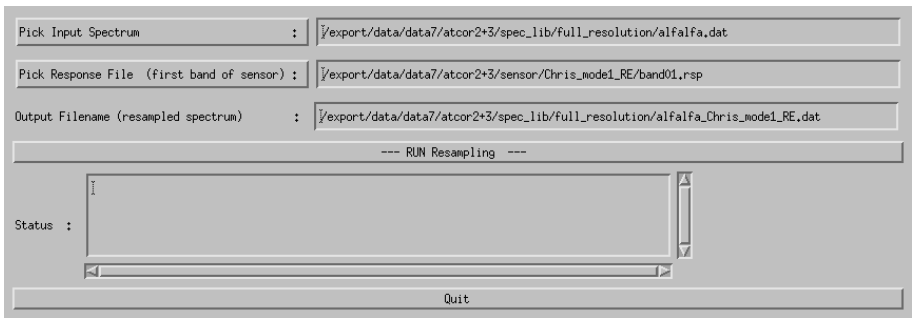

Figure 5.44: *Resampling of a (reflectance) spectrum.*

5.5.2 Spectral Polishing: Statistical Filter

Remove spectral artifacts in high spectral resolution imaging spectroscopy data.

Inputs:

Input file name A hyperspectral image cube, usually the output of atmospheric correction $*$_atm.bsq

Sensor Spectral Response Defines the first band of the sensor response $*$rsp. This field may be left empty - in that case, the wavelength information from the ENVI header is used if the

wavelengths tag is properly given. if no wavelength reference is there, a spectrally equidistant succession of the spetral bands is assumed.
Note: the Savitzky-Golay filter is not wavelength-aware and uses always the assumption of equidistant, constantly increasing bands.

Number of polishing bands on each side Adjacent bands to be used for calculation on each side of the target band; e.g. factor 3 uses 7 bands for polishing (3 on each side plus central band).

Smoothing Factor smoothing applied stand alone or in combination with the derivative filter:
0: no smoothing
1: slight smoothing (filter: 1/4/1)
2: moderate smoothing (filter: 1/2/1)
3: standard smoothing (filter: 1/1/1)
4 and more: standard smoothing with moving average

Polishing Filter Type Four options are available for statistical spectral polishing: *Derivative Filter:* all spectral bands of the given window size are taken into account to calculate derivative used to reconstruct the value of the center band.
Neighbour Derivative: all spectral bands except for the center itself are taken into account to calculate derivative used to reconstruct the value of the center band.
Lowpass Filter: Only the smoothing is performed, no derivatives are calculated.
Savitzky-Golay: Filter to perform a numerical polinomial fit of 4th degree through the selected total window size.

Output:
A cube containing the spectrally filtered copy of the original image data cube is generated (compare Paper Earsel, SIG-IS Workshop, Edinburgh, 2011).

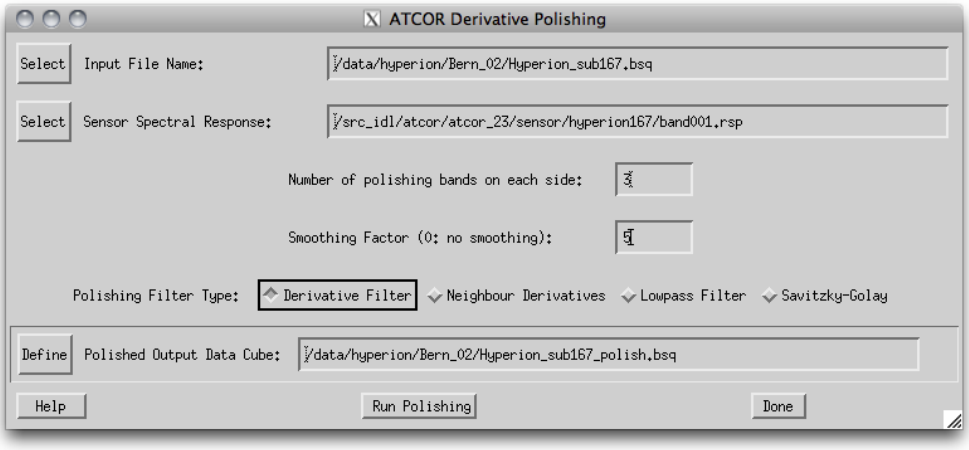

Figure 5.45: *Statistical spectral polishing.*

5.5.3 Spectral Polishing: Radiometric Variation

A module that was originally developed for the airborne version of ATCOR is the spectral polishing. The algorithm is only intended for hyperspectral imagery.

Figure 5.46: *Radiometric spectral polishing.*

Input to the spectral polishing program is the reflectance cube calculated with ATCOR. It employs the vegetation index ($0 < NDVI < 0.33, NDVI = (\rho_{NIR} - \rho_{RED})/(\rho_{NIR} + \rho_{RED})$) to mask soil pixels. A soil spectrum is a slowly varying function of wavelength, therefore a spectral smoothing will only remove spikes without disturbing the spectral shape. Then the average reflectance spectrum over all soil pixels is calculated and smoothed with a 5-channel filter except for the atmospheric water vapor regions where a linear interpolation is performed. The ratio of the filtered to the original soil spectrum is the spectral polishing function applied to all image pixels. If *"xxx_atm.bsq"* is the atmospherically corrected input image, then *"xxx_atm_polish.bsq"* is the polished output reflectance cube, and the spectral polishing function is stored in *"xxx_atm_polish.dat"*, an ASCII file with two columns containing the center wavelength of each channel and the polishing factor. Figure 5.46 shows the GUI panel.

5.5.4 Spectral Smile Interpolation

For sensors affected by *"spectral smile"* the surface reflectance cube is calculated accounting for the smile shift function in the column (across-track) direction of the detector array. The smile shift is specified as a 4th-order polynomial function, i.e. the file *"smile_poly_ord4.dat"* in the corresponding sensor folder, see chapter 4.7. Due to the smile shift the wavelength values of a spectral channel vary slightly in across-track direction. The "smile interpolation" function allows the specification of a common center wavelength for each channel. Then for each channel all pixel reflectances are interpolated to this new reference wavelength. Since the smile shift between adjacent bands does not vary significantly, a linear interpolation can be applied. If $\lambda_j(i)$ denotes the center wavelength of band i and column j, and $\rho_j(i)$ the surface reflectance of a column j pixel, then the new interpolated reflectance is

$$\rho_j^{(new)}(i, \lambda_{ref}(i)) = \rho_j(i) + \frac{(\lambda_{ref}(i) - \lambda_j(i)) \;\; (\rho_j(i+1) - \rho_j(i-1))}{\lambda_j(i+1) - \lambda_j(i-1)} \tag{5.1}$$

where $\lambda_{ref}(i)$ is the user-defined reference center wavelength for band i. There are three options for the reference wavelength grid:

1. use wavelength corresponding to the center of the detector array,
2. use average wavelength over all detector columns (per band),
3. use nominal wavelength specified in the (ENVI) header of the reflectance cube.

This tool is available in the interactive mode (main menu, then "Filter", then *"Spectral Smile Interpolation (Image Cube)"* and in the batch mode (*"smile_interp3_batch"*, see chapter 6.2).
This routine is used after smile-aware atmospheric correction. I applies a linear interpolation on the reflectance data in order to bring the spectral bands to a common reference in across track direction. The inputs are as follows (see Fig. 5.47):

Inputs:

Input Image A hyperspectral image cube, usually the output of atmospheric correction in smile mode *_atm.bsq

Smile polynomial file The file 'smile_poly_ord4.dat' as of the sensor definition used for the smile-aware atmospheric correction.

Options Three options for the spectral reference wavelength grid to be used for interpolation may be selected:
center of detector array: The spectral position of the center pixel in across track direction of the detector is taken as the reference wavelength for each spectral band.
average over all detector columns: For each spectral band, the average of all (smiled) center wavelengths is calculated and used as the new reference wavelength.
nominal position (ENVI header) the nominal position as provided in the ENVI header file is taken as the reference.

Output:
A cube containing the spectrally interpolated image data is generated and the ENVI header is updated (for options 1 and 2).

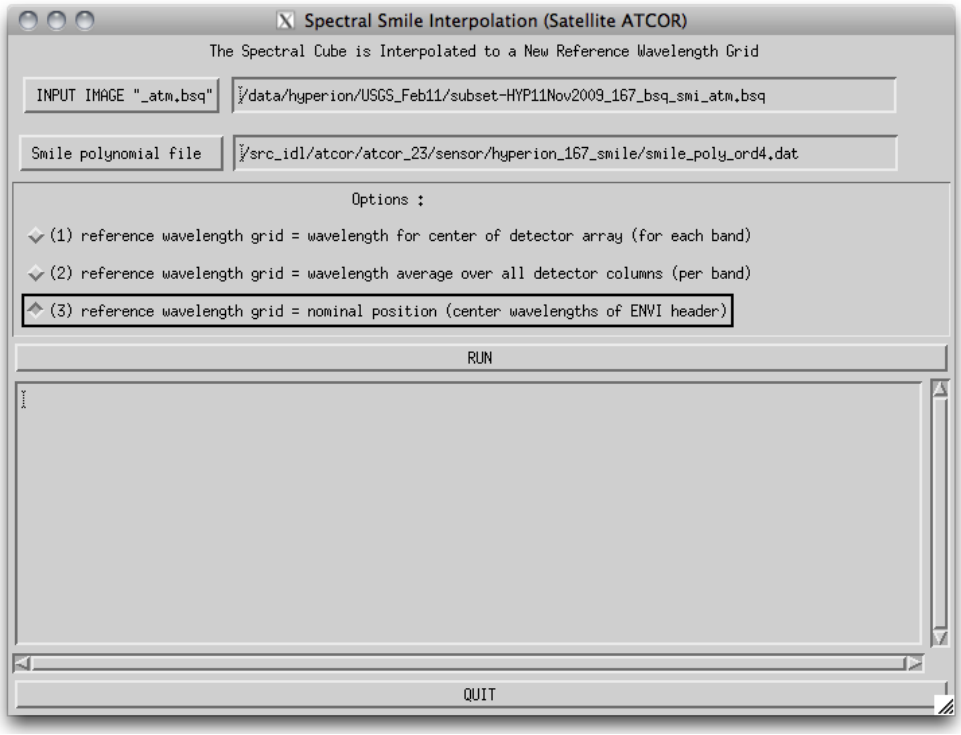
Spectral Smile Interpolation (Satellite ATCOR)
The Spectral Cube is Interpolated to a New Reference Wavelength Grid
INPUT IMAGE "_atm.bsq"
/data/hyperion/USGS_Feb11/subset-HYP11Nov2009_167_bsq_smi_atm.bsq
Smile polynomial file
/src_idl/atcor/atcor_23/sensor/hyperion_167_smile/smile_poly_ord4.dat
Options :
(1) reference wavelength grid = wavelength for center of detector array (for each band)
(2) reference wavelength grid = wavelength average over all detector columns (per band)
(3) reference wavelength grid = nominal position (center wavelengths of ENVI header)
RUN
QUIT

Figure 5.47: *Spectral smile interpolation*

5.6 Menu: Simulation

The *"Simulation"* menu provides programs for the simulation of at-sensor radiance scenes based on surface reflectance (or emissivity and temperature) images.

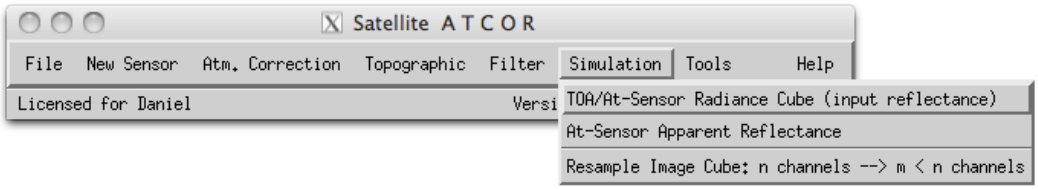

Figure 5.48: *Simulation modules menu.*

5.6.1 TOA/At-Sensor Radiance Cube

This routine calculates an At-Sensor Radiance Cube from an reflectance image cube. All parameters used for the processing are generated from the ∗.inn file of the input cube. If the function is called, the cube is opened and the ∗.inn file is read, which results in an at-sensor cube ∗_toarad.bsq . Note that this routine does not consider adjacency effects and is a simple forward propagation based on the given parameters and the given standard model.

No specific panel is displayed. The routine asks for the input reflectance image. All other information is taken from the *.inn file. Please make sure that the reflectance image spectral definition corresponds exactly to the chosen atmospheric library and sensor definition as of the *.inn file.

5.6.2 At-Sensor Apparent Reflectance

This routine calculates an at-sensor apparent reflectance from a calibrated at-sensor radiance image cube. This routines alculates for each image band the following output:

$$\rho_{app} = (DN * c_1 + c_0) * \pi * d^2/(E_0 * cos(\theta_0)) \tag{5.2}$$

where:
DN: stored data values
c_1: gain for conversion of DN to at sensor radiance
c_0: offset for conversion to at sensor radiance
d: relative sun-earth distance (average:d=1)
E_0: solar irradiance, top of atmosphere (NOT at aircraft altitude)
θ_0: solar zenith angle

Inputs:

- input file name
- calibration file name (∗.cal)
- solar radiation file (e0_solar_∗.spc)
- output file name

- scale factor (see below)
- date of the year, given exactly as 'day/month', eg. 26/7 for July, 26th, used for sun-earth distance calculation
- solar zenith angle (use 'Tools : Solar Zenith and Azimuth' for its calculation)

Output:
A cube containing the scaled apparent reflectance in [%] is stored. The data format is driven by the scaling factor as follows:

- scale < 10 : byte
- scale $>= 10$: integer
- scale $>= 500$: unsigned integer
- scale $<= 1.$: floating point (effective value, unit: [%]) (wavelength reference and FWHM are taken from the file e0_solar_*.spc)

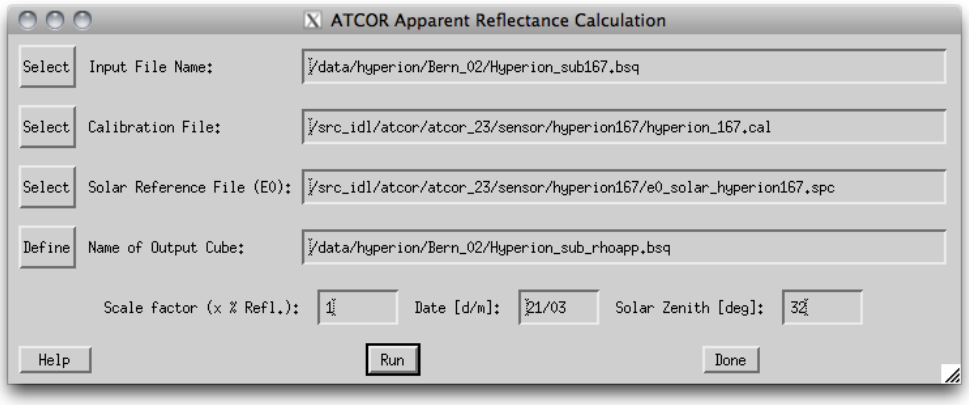

Figure 5.49: *Apparent Reflectance Calculation*

5.6.3 Resample Image Cube

This routine allows to simulate a multispectral image from imaging spectroscopy data. A detailed description of this routine is given in chapter 8.

5.7 Menu: Tools

The *"Tools"* menu contains contains a collection of useful routines such as the calculation of the solar zenith and azimuth angles, spectral classification, nadir normalization for wide field-of-view imagery, adding of a synthetic blue channel for multispectral sensors with a blue band (e.g. SPOT) which is done for the atmospherically corrected surface reflectance image, spectral calibration, conversion of the monochromatic atmospheric database from one to another solar irradiance spectrum, and BIL to BSQ conversion.

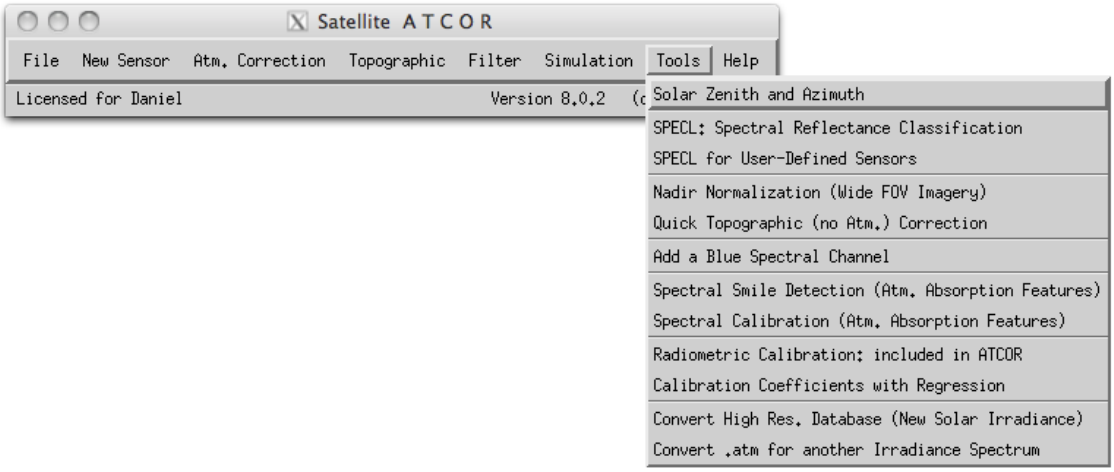

Figure 5.50: *The tools menu.*

5.7.1 Solar Zenith and Azimuth

The routine SOLAR_GEOMETRY is used to calculate the zenith and azimuth angle for the image location and acquisition time. All explanations concerning the definition of angles are included in the panel (Fig. 5.51).

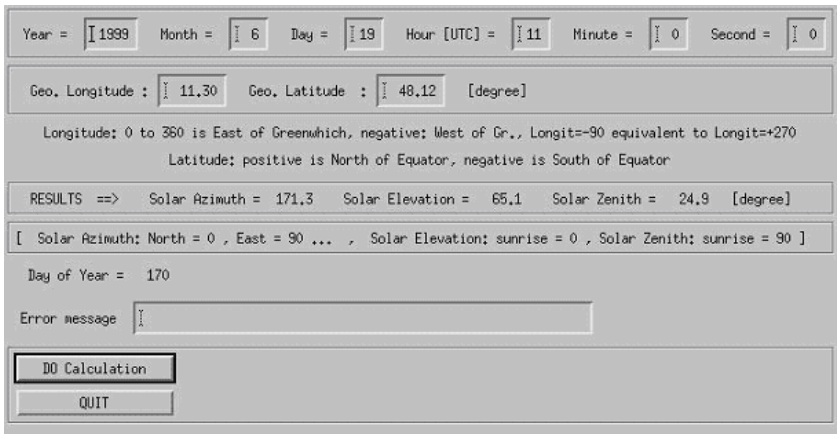
Year = 1999
Month = 6
Day = 19
Hour [UTC] = 11
Minute = 0
Second = 0
Geo. Longitude : 11.30
Geo. Latitude : 48.12
[degree]
Longitude: 0 to 360 is East of Greenwhich, negative: West of Gr., Longit=-90 equivalent to Longit=+270
Latitude: positive is North of Equator, negative is South of Equator
RESULTS ==> Solar Azimuth = 171.3 Solar Elevation = 65.1 Solar Zenith = 24.9 [degree]
[Solar Azimuth: North = 0 , East = 90 ... , Solar Elevation: sunrise = 0 , Solar Zenith: sunrise = 90]
Day of Year = 170
Error message
DO Calculation
QUIT

Figure 5.51: *Calculation of sun angles.*

5.7.2 SPECL: Spectral Reflectance Classification

SPECL is a spectral classification based on reflectance data. The program compares each pixel spectrum to a list of template spectra. It is assigned to the class with the best match or put into the class *"undefined"* with class label 0.
Figures 5.52 and 5.53 show the panel of the SPECL program and a sample output.

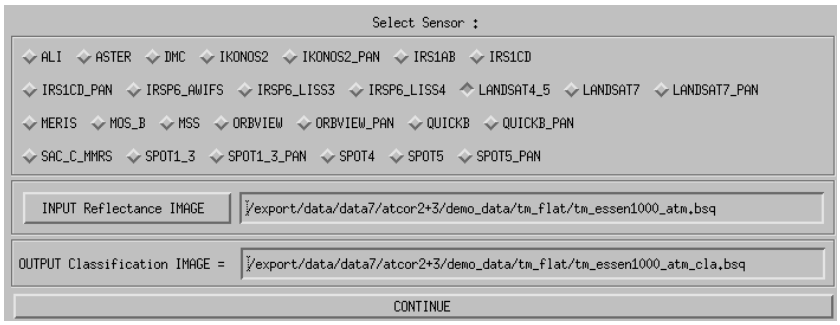
Select Sensor :
ALI ASTER DMC IKONOS2 IKONOS2_PAN IRS1AB IRS1CD
IRS1CD_PAN IRSP6_AWIFS IRSP6_LISS3 IRSP6_LISS4 LANDSAT4_5 LANDSAT7 LANDSAT7_PAN
MERIS MOS_B MSS ORBVIEW ORBVIEW_PAN QUICKB QUICKB_PAN
SAC_C_MMRS SPOT1_3 SPOT1_3_PAN SPOT4 SPOT5 SPOT5_PAN
INPUT Reflectance IMAGE
/export/data/data7/atcor2+3/demo_data/tm_flat/tm_essen1000_atm.bsq
OUTPUT Classification IMAGE =
/export/data/data7/atcor2+3/demo_data/tm_flat/tm_essen1000_atm_cla.bsq
CONTINUE

Figure 5.52: *SPECL: spectral classification of reflectance cube.*

Figure 5.53: *Example of classification with SPECL.*
Left: true color image of Landsat TM, right: result of classification.

5.7.3 SPECL for User Defined Sensors

This function is the same as described above in Section 5.7.2 and Figure 5.53. The only difference being that the available sensors are the ones defined in the 'sensor' directory of the ATCOR installation, i.e., the self-defined sensors.

5.7.4 Nadir normalization (Wide FOV Imagery)

This module (NADIR_REFL) performs an empirical BRDF correction by normalizing the across-track radiance gradients to the nadir brightness value (see chapters 2.2, 10.5.1). Figure 5.54 shows the corresponding GUI panel.

The nadir normalization was originally implemented for the airborne version of ATCOR and requires a minimum field-of-view of 20°. Therefore, it might also be of interest for some of the supported satellite sensors, e.g. IRS-1C WiFS or MERIS.

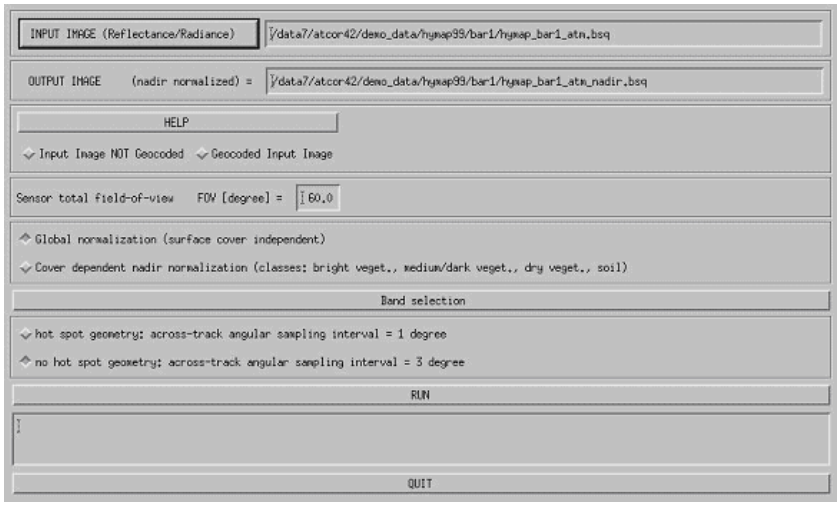
INPUT IMAGE (Reflectance/Radiance)
/data7/atcor42/demo_data/hymap99/bar1/hymap_bar1_atm.bsq
OUTPUT IMAGE (nadir normalized) =
/data7/atcor42/demo_data/hymap99/bar1/hymap_bar1_atm_nadir.bsq
HELP
Input Image NOT Geocoded
Geocoded Input Image
Sensor total field-of-view FOV [degree] =
60.0
Global normalization (surface cover independent)
Cover dependent nadir normalization (classes: bright veget., medium/dark veget., dry veget., soil)
Band selection
hot spot geometry: across-track angular sampling interval = 1 degree
no hot spot geometry: across-track angular sampling interval = 3 degree
RUN
QUIT

Figure 5.54: *Nadir normalization.*

5.7.5 Quick Topographic (no atm.) Correction

The quick topographic correction routine (TOPOCOR) tries to eliminate the slope/aspect topographic effects and neglects the atmospheric influence. The program runs very fast and the output image contains the modified digital numbers. Processing with TOPOCOR can be done with or without display of images. The DEM slope and aspect files have to be specified on a separate panel that pops up after the input image has been specified. The topographic correction implemented here multiplies the DN value with a factor f that depends on the local solar zenith angle β and a weighting coefficient w. The wavelength-depending weighting w is based on a typical value of the ratio of the direct to diffuse solar flux on the ground.

$$f = 1 - (1 - cos\Theta_S/cos\beta)w \qquad if \quad \lambda < 1.1\mu m \tag{5.3}$$

$$f = cos\Theta_S/cos\beta \qquad if \quad \lambda \geq 1.1\mu m \tag{5.4}$$

Θ_S is the solar zenith angle of the scene. For $\lambda \geq 1.1\mu m$ the diffuse flux is neglected, i.e., w=1. The factor f is 1 for a flat terrain and some bounds were employed to prevent overcorrection. So for each pixel the new digital number is calculated as

$$DN(new) = DN * f \tag{5.5}$$

The method was compared with the standard Minnaert correction (eq. 5.6) and was superior in most cases. Figure 5.55 shows the GUI panel.

$$f = \{\frac{cos\Theta_S}{cos\beta}\}^{log(cos\Theta_S/cos\beta)} \tag{5.6}$$

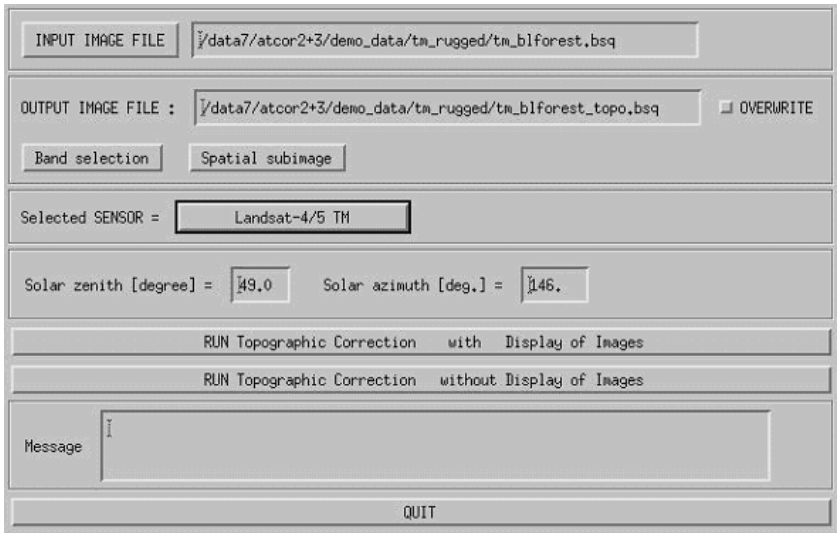

Figure 5.55: *Topographic correction only, no atmospheric correction.*

5.7.6 Add a Blue Spectral Channel

This routine (MAKEBLUE) adds a blue spectral channel for multispectral imagery not containing a blue band. The band is calculated from empirical relationships from the green, red, and NIR bands which ought to be present. The routine simply asks for an input multispectral image to be processed.
NOTE: the input image should have at least 3 bands and the first three bands are assumed to be the triple GREEN/RED/NIR.

5.7.7 Spectral Smile Detection

This routine uses sharp atmospheric absorption features and Fraunhofer lines for inflight smile (i.e., spectral across-track non-uniformity) detection. The calculation is done by correlation analysis of a number of spectral bands in the vicinity of selected absorption features. The outputs may be used for smile-aware atmospheric correction.

Initially, the smile characterization for each spectrometer channel is derived from laboratory measurements. From such data, the wavelength shift with respect to the center pixel of the detector array can be parametrized using a 4th order polynomial fit. However, in case of instrument changes during the mission, a spectral re-calibration might be necessary from the image data or from onboard calibration facilities using well-defined absorption features. Onboard spectral calibration devices such as interference or rare earth filters would be well suited for this purpose. However, such devices are often not available in sensor systems. Therefore, atmospheric gas absorption features or solar Fraunhofer lines have to be taken as a reference from the imagery itself. Its major steps are:

1. A calibrated image is averaged in along track direction, leading to a signature image of the size of the detector array.

2. The surface reflectance is calculated (atmospheric correction) and smoothed.

3. The spectral bands within the spectral matching range are selected.

4. Spectral shifts with intervals between 0.01-0.05 nm are calculated and applied to the selected spectral band response functions.

5. An appropriate pre-calculated fine-spectral resolution atmospheric LUT is selected which serves for the calculation of at-sensor radiance values for the series of spectrally shifted response functions using the surface reflectance spectrum from step (2).

6. The derived spectral signatures are correlated to the observed column-averaged signal in the image, such that the best fitting spectral shift $\Delta\lambda_j = \Delta_j$ can be found for each image column j, i.e., the Δ_j with the highest Pearson's correlation coefficient is selected. This is equivalent to minimizing the merit function

$$\chi^2(\Delta_j) = \sum_{\Delta_j=\lambda_k-5nm}^{\lambda_k+5nm} \left[L_I(j,k) - L_R(\lambda_k + \Delta_j, k)\right]^2, \tag{5.7}$$

   where $L_I(j,k)$ is the average at-sensor radiance of the image for column j and channel k, and $L_R(\lambda_k + \Delta_j, k)$ is the corresponding reference radiance for a wavelength shift Δ_j within a 5 nm interval around λ_k.

7. A 4th order polynomial is fitted through the calculated spectral points and the respective polynomial parameters of eq. 4.1 are stored.

8. The polynomial parameters are interpolated and optionally extrapolated to all other bands within the same detector or spectrometer unit. Optionally, the polynomial coefficients can be set to zero in atmospheric absorption regions to expedite the processing.

Once the coefficients have been determined, they are converted into the required file format and are placed in the respective sensor folder for a subsequent fully automatic radiometric and atmospheric processing.
Fig. 5.56 shows the panel of the smile detection module. The input files (scene, high-resolution atmospheric database, sensor spectral response) and the output file has to be specified in the upper part of the panel. Then the 'smile detection resolution', 'search range', and 'band range' can be specified. Next are parameters pertaining to the scene (visibility, solar zenith angle, and ground elevation. Up to 12 atmospheric or Fraunhofer feature wavelengths can be selected. The 'Interpolation Type' refers to the interpolation of the smile polynomial between feature wavelengths. Extrapolation can be done by extrapolating the trend, repeating the values of the last band calculated or by setting the polynomial to zero at the borders of the spectral range of the instrument.
The module will perform the calculation when pressing the "Run' button. Results of the smile detection can be viewed with 'Plot Smile'. Here the relative smile curves with respect to the center of the detector array can be plotted or the absolute wavelength smile curves.

Outputs:
An ASCII-file which may be used as smile description file in the respective sensor directory. Note that this file should be named smile_poly_ord4.dat in order to be automatically recognized by ATCOR.
As a side output, an IDL save dump (∗.sav) is written in parallel which contains all used parameters and the effectively calculated smile results.

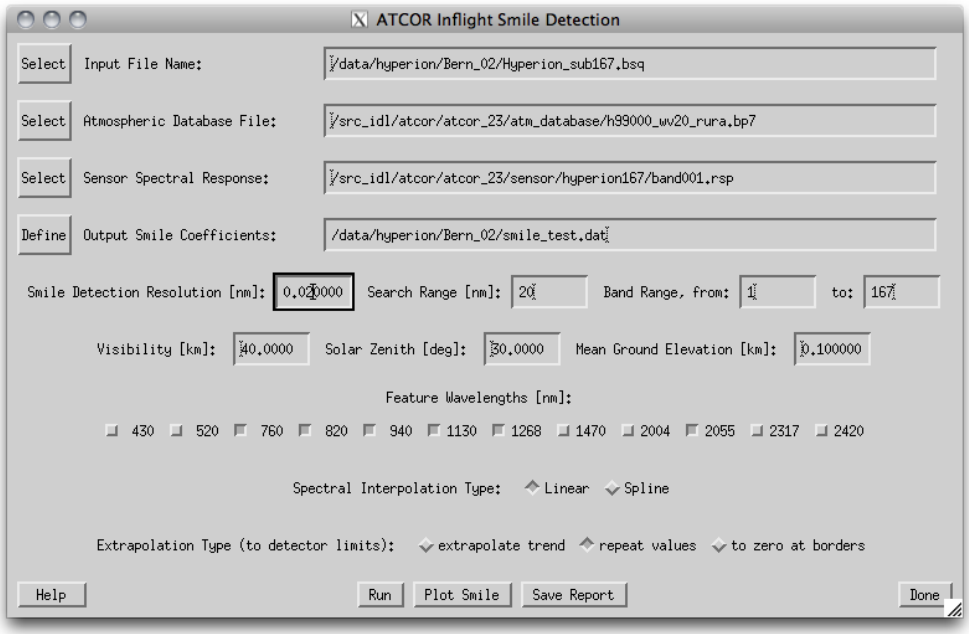

Figure 5.56: *Spectral smile detection*

5.7.8 Spectral Calibration (Atm. Absorption Features)

The program (SPECTRAL_CAL) is only intended for hyperspectral sensors and employs atmospheric absorption features to detect and remove possible wavelength calibration errors (see chapter 2.3). For this purpose, a certain number of target spectra have to be selected in the SPECTRA module.
Input to the spectral calibration module are the DN spectra of selected fields saved as ASCII files in the SPECTRA module by pressing the button "Save last spectrum". The files should be numbered consecutively, starting with a name such as "location_target1", without extension. The next target has to be named "location_target2" etc. For each target field three files will generated, for example:

- "location_target1.dat" : contains surface reflectance spectrum,
- "location_target1.txt" : contains target coordinates, and processing parameters (visibility, water vapor column, etc.),
- "location_target1_dn1.dat" : contains the DN spectrum.

For a given location (scene) up to 9 targets can be extracted and used for the spectral calibration. The geometry, scene visibility and average water vapor content of the targets enter as parameters to the spectral calibration, see Fig. 5.57. The water vapor content has to be averaged from the values found in the "location_target*.txt" files. The first target DN file has to be selected by the user, the remaining target files are automatically found provided the nomenclature with a consecutive numbering is applied. The result of the spectral calibration are files with the spectral shifts per spectrometer and the new center wavelengths of all channels. The spectral bandwidth of channels is not modified.

The DN spectra will be employed in an optimization procedure that minimizes the spikes of the derived surface reflectance spectra in the atmospheric absorption regions.
The first target DN file has to be entered at the top left button of the GUI panel (Figure 5.57). The other target files are automatically searched and employed if the nomenclature of chapter 2.3 is employed. Further input data are the sensor definition, the range of bands per spectrometer, solar geometry and atmospheric parameters. Output is a file with the spectral channel center wavelength shifts per spectrometer, and a new wavelength file containing the updated wavelengths for each channel.

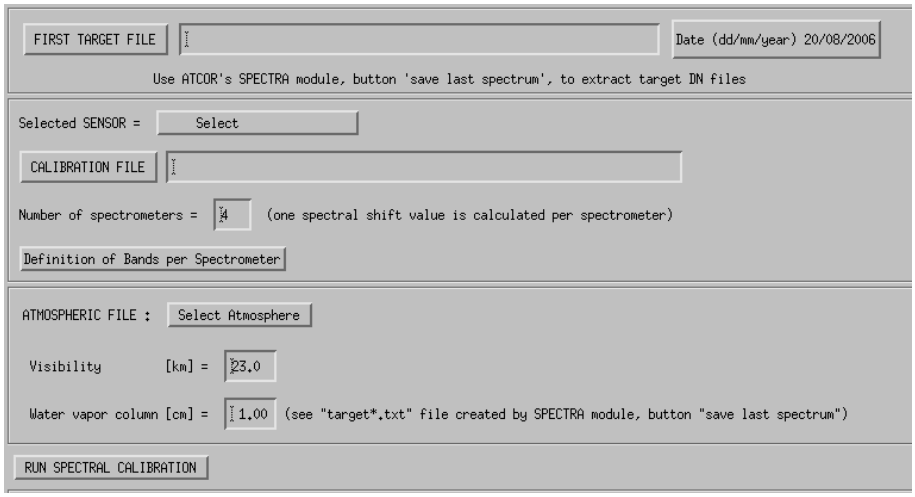
FIRST TARGET FILE
Date (dd/mm/year) 20/08/2006
Use ATCOR's SPECTRA module, button 'save last spectrum', to extract target DN files
Selected SENSOR =
Select
CALIBRATION FILE
Number of spectrometers =
4
(one spectral shift value is calculated per spectrometer)
Definition of Bands per Spectrometer
ATMOSPHERIC FILE :
Select Atmosphere
Visibility [km] =
23.0
Water vapor column [cm] =
1.00
(see "target*.txt" file created by SPECTRA module, button "save last spectrum")
RUN SPECTRAL CALIBRATION

Figure 5.57: *SPECTRAL_CAL.: spectral calibration*

The results of the spectral shift are summarized in a file *"spectral_calibration_results*.txt"* where the wavelength shift is listed for each spectrometer and each target. The final shift is taken as the average of all target wavelength shifts. In addition, a new wavelength file *"sensor_new.wvl"* is created containing the channel center wavelengths and the FWHMs (bandwidth as full width at half maximum). A copy of the original radiometric calibration file (e.g., *"xxx.cal"*) is provided for convenience (e.g., *"xxx_new.cal"*) which contains the original radiometric calibration coefficients and the updated channel center wavelengths.

In case of originally non-Gaussian filter curves, the output FWHM values of *"sensor_new.wvl"* represent the equivalent Gaussian FWHM values, even though the spectral re-calibration is based on the original (non-Gaussian) filter curves. The corresponding sensor with the new spectral calibration has to be added to the list of existing sensors (see chapter 4.5) to process imagery with the updated spectral calibration. In case of non-Gaussion filter curves, the original channel response files (*"band*.rsp"*) should be copied to the new sensor directory applying the appropriate wavelength shifts. For sensors with Gaussian filter curves the *'gauss_rsp"* module (see chapter 5) can be applied to the *"sensor_new.wvl"* file to generate the corresponding *"band*.rsp"* files. Note that a change of the spectral calibration usually requires a radiometric re-calibration.

5.7.9 Calibration Coefficients with Regression

This routine employs the "*.rdn" files obtained during the single-target calibration (the "c1 option" of ATCOR's calibration module to create a calibration file by rlinear regression.

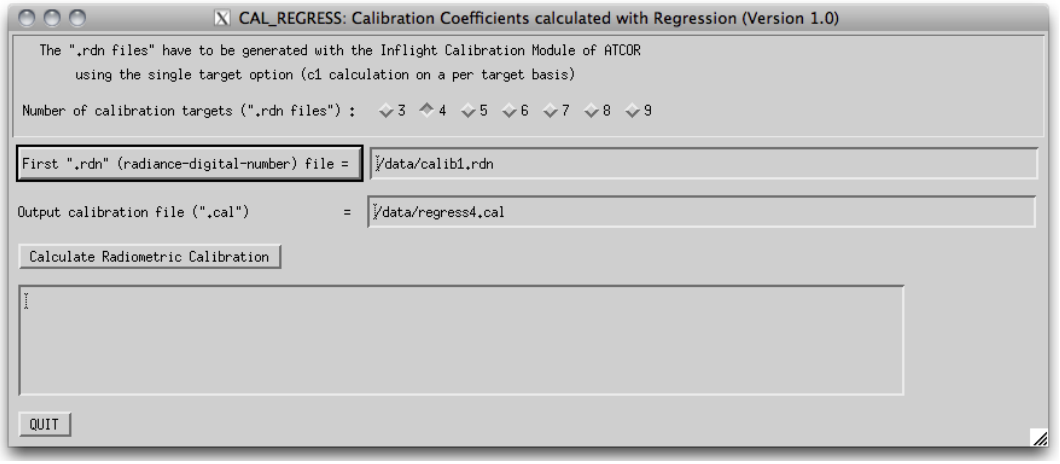
CAL_REGRESS: Calibration Coefficients calculated with Regression (Version 1.0)
The ".rdn files" have to be generated with the Inflight Calibration Module of ATCOR
using the single target option (c1 calculation on a per target basis)
Number of calibration targets (".rdn files") : 3 4 5 6 7 8 9
First ".rdn" (radiance-digital-number) file =
/data/calib1.rdn
Output calibration file (".cal") =
/data/regress4.cal
Calculate Radiometric Calibration
QUIT

Figure 5.58: *CAL_REGRESS.: radiometric calibration with more than one target*

So for n > 2 the single-target calibration is to be performed n times and the resulting "*.rdn" files (radiance versus digital number) are offered as input to the "cal_regress" program.

Inputs:

Number of calibration targets: A maximum of 9 calibration targets may be selected. The files *.rdn should having been calculated beforehand and the need to be calculated consecutively, e.g., calib1.rdn, calib2.rdn, ...

First *.rdn file: Name of the first *.rdn file of the series to be used for regression

Output Name" Name of the calibration output to be created.

Output:

The output of this program is an ASCII file "name.cal" with three columns (center wavelength, c_0 , c_1) where "name" is specified by the user.

Note: If several calibration targets are employed, care should be taken to select targets without spectral intersections, since calibration values at intersection bands are not reliable. If intersections of spectra cannot be avoided, a larger number of spectra should be used, if possible, to increase the reliability of the calibration.

5.7.10 Convert High Res. Database (New Solar Irradiance)

The standard solar irradiance curve used with ATCOR is the Fontenla database (2011). However, there's some uncertainty about the solar irradiance and people may want to use ATCOR with a different solar reference function. This module (CONVERT_DB3) converts the complete high resolution atmospheric database from the current definition to a new irradiance function. Normally, the standard database is converted (this function does not apply to the thermal IR), but also the specific CHRIS database may be selected. In the panel (see Fig. 5.59), the two databases may be selected on the basis of the directory (f1) and the new reference function e0_solar∗.dat.

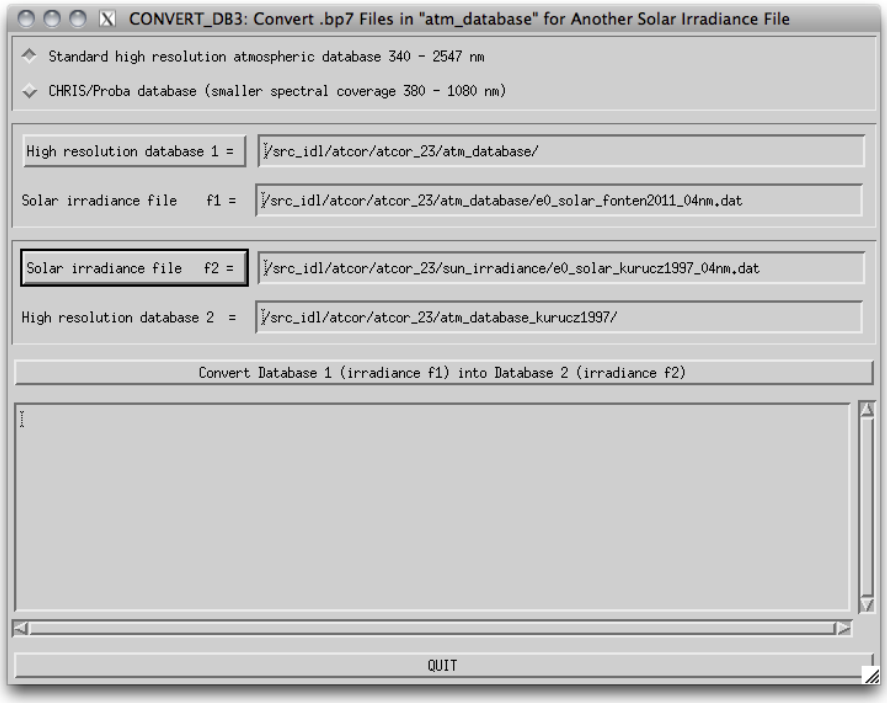
CONVERT_DB3: Convert .bp7 Files in "atm_database" for Another Solar Irradiance File
Standard high resolution atmospheric database 340 - 2547 nm
CHRIS/Proba database (smaller spectral coverage 380 - 1080 nm)
High resolution database 1 =
/src_idl/atcor/atcor_23/atm_database/
Solar irradiance file f1 =
/src_idl/atcor/atcor_23/atm_database/e0_solar_fonten2011_04nm.dat
Solar irradiance file f2 =
/src_idl/atcor/atcor_23/sun_irradiance/e0_solar_kurucz1997_04nm.dat
High resolution database 2 =
/src_idl/atcor/atcor_23/atm_database_kurucz1997/
Convert Database 1 (irradiance f1) into Database 2 (irradiance f2)
QUIT

Figure 5.59: *Convert monochromanic database to new solar reference function*

5.7.11 Convert .atm for another Irradiance Spectrum

The conversion as described in module 5.7.10 can be applied to a sensor-specific atmospheric library of a self-defined sensor using this function. In the panel as of Fig. 5.60, the sensor has first to be entered and the new solar function e0_solar∗.dat is to be selected before the conversion may be applied.

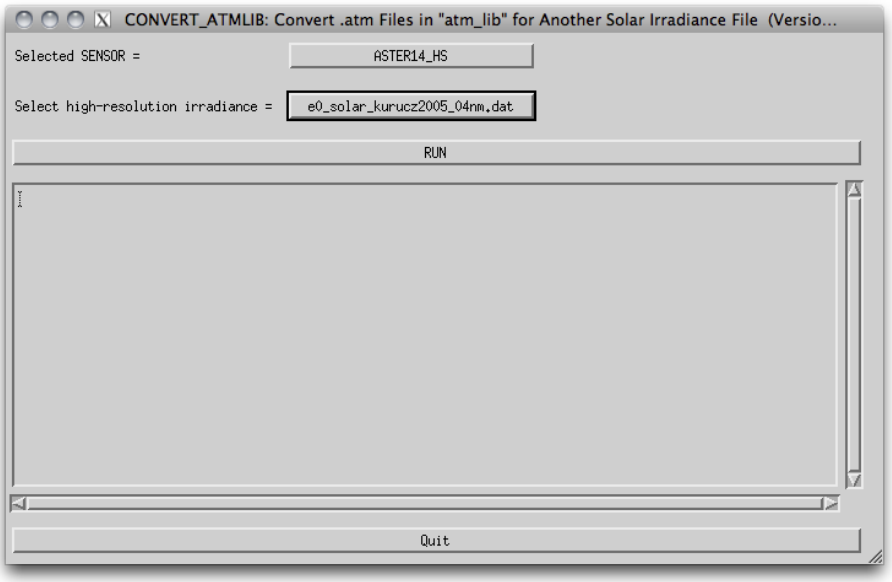

Figure 5.60: *Convert atmlib to new solar reference function*

5.8 Menu: Help

Finally, the *"Help"* menu allows browsing of the ATCOR user manual, provides a linke to the web resources, and displays license information.

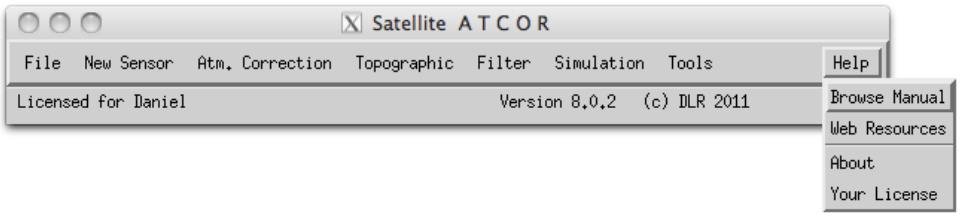

Figure 5.61: *The help menu.*

5.8.1 Help Options

The options of the *help* menu are listet below:

Browse Manual Opens this manual in the default PDF display application of your machine.

Web Resources Opens the html document *atcor3_webresources.htm* in the systems default applications for viewing HTML-documents.

About Provides basic information about the copyright and also displays the build-number of the software (please provide the build-number for debugging purposes in case the ATCOR support is contacted).

Your License Provides information about the licensed features in your license key and also displays which license key is currently active.

Chapter 6

Batch Processing Reference

For most ATCOR modules a convenient graphical user interface is available, but batch jobs can also be submitted. A detailed discussion of the interactive panel-driven modules is given in chapter 5.

6.1 Using the batch mode

ATCOR can process scenes in the batch mode. For large scenes the tiling option is also available in batch mode which splits a big scene into a number of smaller sub-scenes, processes the sub-scenes, and finally merges them into one file. A prerequite for the tiling is that enough IDL memory is available to keep one image channel and the sub-scene channel in memory. Also note that a full IDL developer license is required in order to make use of the batch commands on the IDL prompt.

The batch mode can be accessed after the processing parameters have been specified in the interactive graphical user interface (GUI) panel, i.e., after the SPECTRA module has been accessed or after one of the image processing options has been selected. Thus, the GUI panel creates an *'*.inn'* file containing all input parameters.
The batch mode can be started after quitting the interactive session, using the same IDL window. It can also be started in a new IDL session after typing 'atcor' on the IDL command line. Then continue with:

>atcor2_batch, input='/data1/examples/example_image.bsq' (case of flat terrain) or
>atcor3_batch, input='/data1/examples/example_image.bsq' (case of rugged terrain)

At this stage, all required input parameters are already available in the *'*.inn'* file, in this specific case *'example_image.inn'*.

The submitted job is a 'quasi batch' job, the corresponding IDL window is used for error and status messages and it may <u>not</u> be closed during the run time of the job. A log file is created during processing, e.g. *'example_image_atm.log'*, which contains information about the job status. It contains three message levels (I=Info, W=Warning, E=Error) followed by a two digit number (between 0 and 99) and a space, e.g. 'W19 ', followed by the appropriate information. These three message levels can easily be parsed by a separate user program if desired. Other information in the log file is marked with the hashmark symbol in the first column.

In the tiling mode the user has to specify the number of tiles in x=column direction (ntx) and in y=line direction (nty), e.g.,

>atcor2_tile, input='/data1/examples/example_image.bsq', ntx=3, nty=2

In this case the image is split into 3*2=6 tiles, each tile is processed separately, finally all tiles are merged into one output file, and the sub-scenes are deleted. The maximum size of each tile depends on the available memory for a specific machine because ATCOR performs most calculations in memory loading one or two complete bands of the scene. A typical tile size for modern machines is 3000*3000 pixels = 9 Mpixels to 5000*5000 pixels = 25 Mpixels. The user has to try and find out the appropiate tile size. As an example, with a 9 Mpixel tile size and a 30 Mpixel scene the image has to be split into 4 sub-scenes. Assuming that the number of image columns and lines is approximately the same, one would choose the keywords 'ntx=2, nty=2' in this example. Of course, processing of much smaller tiles is also possible, e.g., 'ntx=20, nty=10', but this is not recommended because of potential image border effects, i.e., larger visibility differences for the small tiles might lead to seams at the tile borders.

The TIFF input data format is supported, however, channels in the TIFF file must have the increasing band order, and the maximum number of bands should be less than 10. If all channels are in one input TIFF file (example: "image.tif"), the output TIFF after atmospheric correction will also hold all channels (example: "image_atm.tif").

An IDL routine called *'write_atcor3_inn_file'* is available to users who want to generate the *'*.inn'* file without the ATCOR GUI.

Note: :
On the IDL command line, the command 'atcor' has to be typed first to load the 'atcor.sav' file. Then the 'atcor2_tile' or 'atcor3_tile' commands will execute the tile processing. A simple trick can be used to start the 'atcor_tile' programs directly on the IDL command line without having to type 'atcor' first: just copy the 'atcor.sav' file to 'atcor2_tile.sav' and 'atcor3_tile.sav'. The same can be done for 'atcor2_batch.sav' and 'atcor3_batch.sav'. For the Linux/Unix operation systems a symbolic link is sufficient, e.g., *ln -s atcor.sav atcor2_batch.sav*.
For Linux/Unix users with a full IDL license a batch job can be started directly from the shell, e.g.: idl -e "atcor2_batch, input='/export/data/data7/demo_data/tm_essen.bsq' "

6.2 Batch modules, keyword-driven modules

Most of the modules are available in both modes (interactive and batch). If the *'atcor.sav'* file is copied to *'atcor2_batch.sav'* and *'atcor3_batch.sav'*, a batch job can be started immediately from the IDL command line, otherwise *'atcor'* has to be typed first. Hereafter, a description of the batch modules and keyword-driven modules is given.
In order to make the batch options available, you first have to type `"atcor"`on the IDL command line, then the ATCOR GUI selection panel pops up. (alternatively, you may use the command `restore,"atcor.sav"`). Disregard this panel and continue on the IDL command line with the name of the batch job module where all the input parameters have to be specified via key words. Current batch programs are:

- *slopasp_batch, input=filename, [pixelsize=10.0, kernel=3, dem_unit=0]*
  The 'filename' should have the last four characters as "_ele" and the extension ".bsq". Two output files (slope and aspect) are generated from the elevation file, e.g., "example_DEM25m_slp.bsq" and "example_DEM25m_asp.bsq". The values are coded in degrees. The keyword *pixelsize* is not required if this information is included in the map info of the ENVI header. The keywords *kernel* and *dem_unit* can be omitted if the default values *kernel=3*, and *dem_unit=0* are used. The unit of *pixelsize* is 'meter'. For the elevation height unit three options exist: *dem_unit=0* : height unit is 'meters', =1 for 'dm', =2 for 'cm'.
  Note: Before running ATCOR with a DEM, please check the results of the slope image. We often encounter severe horizontal and vertical striping in the slope image in case of low quality DEMs or if coarse DEMs of 25 m have to be resampled to say 5 m. Additional appropriate filtering is required in these cases! A simple way might be to try a larger kernel size, e.g., *kernel=5* or *kernel=7*. A simple check on the derived DEM solar illumination file is also performed at the start of ATCOR, see the discussion below.
  A TIFF input elevation file is converted into the corresponding ENVI elevation file.

- *skyview_batch, input=filename, pixelsize=10.0, [dem_unit=0, unders=unders, azi_inc=azi_inc, ele_inc=ele_inc]*
  'filename' is the full file name including the path, 'filename' should have the last four characters as "_ele" and the extension ".bsq" to indicate a digital elevation file and to enable an automatic processing, e.g., "example_DEM25m_ele.bsq". 'pixelsize' is specified in meters, 'dem_unit' is the integer code for the DEM height unit (0 represents [m], 1 means [dm], 2 means [cm]). The option *dem_unit=0* is default and can be omitted. The keyword "unders" specifies the undersampling factor (in pixels) to reduce the execution time for very large files. The default angular azimuth resolution is azi_inc=10 degrees and the default elevation increment is ele_inc=30 degrees. However, the recommended resolution is 10 degrees for azimuth and 5 degrees for elevation. In case of large files, an undersampling factor > 1 can be specified to reduce the execution time. Usually an undersampling factor of 3 is sufficient. A high angular resolution is more important than a low undersampling factor. The output file replaces the ending "_ele" with the ending "_sky", e.g., "example_DEM25m_sky.bsq".
  A TIFF input elevation file is converted into the corresponding ENVI elevation file.

- *shadow_batch, input=filename, pixelsize=10.0, solze=30.5, solaz=160.8, dem_unit=0,* The keywords have the same meaning as for *skyview_batch*, 'solze' is the solar zenith angle [degr.], and 'solaz' is the solar azimuth angle [degr.]. In particular, 'filename' should have the last four characters as "_ele" and the ".bsq" extension. The output file replaces the ending "_ele" with the ending "_shd" e.g., "example_DEM25m_zen31_azi161_shd.bsq". The rounded zenith and azimuth angles will be included in the "*shd" file name. Note: The shadow and skyview calculations can be omitted in gently undulated terrain. Example: for maximum slopes of 25°and a solar zenith angle of 40°no DEM shadow is possible. Also, the local trigonometric sky view factor, employed if the *"_sky.bsq"* file is missing, is sufficiently accurate, compare figure 10.3.
  A TIFF input elevation file is converted into the corresponding ENVI elevation file.

- *atcor2_batch, input=filename [, output=file, vis=vis, tiff2envi=tiff2envi]* or
  atcor2_tile, input=filename, ntx=3, nty=2 [, output=file, vis=vis, tiff2envi=tiff2envi]
  The "2" in *atcor2_batch* means the code for flat terrain, i.e. no DEM is employed. The 'filename' must be fully qualified, i.e. it includes the path, e.g., "/data2/project1/image1.bsq". The file should have the band sequential (BSQ) file structure. A corresponding "*.inn" file,

e.g., "/data2/project1/image1.ini" must be available that contains all processing parameters. This file will be generated during the interactive session. It may be also be created by the user, e.g. employing the program "write_atcor3_inn_file.pro" that is available on request. The default output file name without the output keyword specification is the input name with an "_atm.bsq" appended, e.g., "/data2/project1/image1_atm.bsq".
The keyword *output* can be used to specify the full output name, or only the output path, the latter option is recommended. In that case, all output files are written to the specified output directory, and the reflectance output file name is the name of the input file with "_atm.bsq" appended. Example: output="/data4/project1/" then the output reflectance file will be "/data4/project1/image1_atm.bsq".

The corresponding tile program *atcor2_tile* in this example is called to split the image into 3 sub-images in x direction, and 2 in y direction, compare chapter 5.3.12.
The optional keyword 'vis' can be used to overwrite the visibility value in the ".inn" file. For a constant visibility per scene (npref=0 in the "*.inn" file), the input 'vis' value is the start value that will be iterated as described in chapter 10.4.1. In case of a variable scene visibility (npref=1) the 'vis' parameter is ignored if the scene contains enough dark reference pixels. If not, the program switches to the constant visibility mode and 'vis' is used as a start value.

An optional keyword *output* can be used to define the output directory and name of the output reflectance file. If the keyword specifies only the output path, which is recommended, then all output files are written to the specified output directory, and the reflectance output file name is the name of the input file with "_atm.bsq" appended.

The optional keyword 'vis' can be used to overwrite the visibility value in the ".inn" file. For a constant visibility per scene (npref=0 in the "*.inn" file), the input 'vis' value is the start value that will be iterated as described in chapter 10.4.1. In case of a variable scene visibility (npref=1) the 'vis' parameter is ignored if the scene contains enough dark reference pixels. If not, the program switches to the constant visibility mode and 'vis' is used as a start value. A negative vis value means the value abs(vis) is used for processing even if it causes a large percentage of negative reflectance pixels.

The optional keyword *tiff2envi* can be used if the input file has the TIFF format. *tiff2envi=1* produces an automatic conversion of the input TIFF file (e.g., "image1.tif") into the corresponding ENVI file (e.g., "image1_envi.bsq"). This file is used as a temporary input file to ATCOR and it will be automatically deleted when the ATCOR run is finished. Two output surface reflectance files will be generated if *tiff2envi=1*, an ENVI file ("image1_envi_atm.bsq") and a TIFF file ("image1_atm.tif"). The ENVI output is needed if the spectral classification (SPECL) module is run, otherwise it may be deleted by the user.
The default for a TIFF input file is *tiff2envi=0*, i.e., the ENVI file conversion is switched off and no intermediate files are created. This will save disk space and some file conversion time. However, if the "image1.ini" file specifies the de-hazing or de-shadowing option, then *tiff2envi* is reset to 1 to enable the creation of of the needed additional intermediate ENVI files. For non-TIFF files, the tiff2envi keyword is ignored.

If each input band is in a separate TIFF file, the files should be labeled consecutively, e.g., "image_band1.tif", "image_band2.tif", etc. The output of ATCOR will be the corresponding

surface reflectance files "image_band1_atm.tif", "image_band2_atm.tif", etc.
A keyword *'tiff2envi'* can be specified as a parameter of the batch job. If not specified, the default is *'tiff2envi=0'* which means no intermediate disk files will be created, only the final "*_atm.tif". With the keyword *'tiff2envi=1'* the temporary file "image_envi.bsq" is automatically created and it contains the input data in the ENVI bsq (band sequential) format. The standard output name of the atmospheric correction is "image_envi_atm.bsq", and of course "image_atm.tif". The "image_envi.bsq" is deleted after processing, but "image_envi_atm.bsq" is kept, because it is required for a run of the spectral classification (SPECL module). The user has to delete this file manually if the SPECL module is not employed. The setting *'tiff2envi=0'* is automatically replaced with *'tiff2envi=1'* if the ".inn" file specifies the de-hazing or de-shadowing option, because these require additional disk files. In case of tiling and a TIFF input file the program automatically switches to *'tiff2envi=1'* because the intermediate tile images must have the ENVI bsq format.

- *atcor3_batch, input=filename [, output=file, vis=vis, tiff2envi=tiff2envi]* or
  atcor3_tile, input=filename, ntx=3, nty=2 [, output=file, vis=vis, tiff2envi=tiff2envi]
  The "3" in *atcor3_batch* means the code for rugged terrain, i.e. a DEM is employed as well as other DEM related files, e.g., slope, aspect, skyview. Otherwise, the same explanations hold as for the "flat" terrain ATCOR.
  The corresponding tile program *atcor3_tile* in this example is called to split the image into 3 sub-images in x direction, and 2 in y direction, compare chapter 5.3.12. The keywords *output* and *vis* are described in *atcor2_batch* above.

- Note: optional keywords for *atcor2_batch, atcor3_batch, atcor2_tile, atcor3_tile.*
  There are four keywords concerning spectral interpolation to overwrite the interpolation settings in file *"preference_parameters.dat"*:
  - i725=-1: no interpolation for 725/820 nm channels, i725=1: interpolation.
  - i760=-1: no interpolation for 760 nm channels, i760=1: interpolation.
  - i940=-1: no interpolation for 940 nm channels, i940=1: interpolation.
  - i1400=-1: no interpolation for 1400/1900 nm channels, i1400=1: interpolation.

- *toarad, input=filename, [pixelsize=pixelsize, sz=solar_zenith, atmfile=atmfile, elev=elevation, vis=visibility, adjrange=adjrange, scalef=scalef]*
  The keywords in brackets are optional, the meaning of all keywords is described in chapter 8. Information on all missing keywords is taken from the corresponding ".inn" file. If the keyword *elev* is missing and the corresponding "*.inn" file contains the DEM files (elevation, slope, aspect) then the simulation is performed for a rugged terrain, otherwise for a flat terrain, compare chapter 8.

- *cal_regress, ntargets=4, outfile='regression4'*
  This program uses the "*.rdn" files to calculate a regression for the c0, c1 radiometric calibration, see chapters 2.4 and 5.3.9. The above example is for the case of n=4 targets, and the output file will be *"regression4.cal"* in the directory of the *"*.rdn"* files which are prompted with a dialog pickfile panel. A graphical user interface for this program is available in the "Tools" pull-down menu of ATCOR labeled "Calibration Coefficients with Regression".

- *makeblue, input=filename*
  The program computes a synthetic blue channel for sensors without a blue spectral band. If

it is started from the the interactive panel ('Tools') a dialog pickfile box pops up prompting for the input file name. If *'makeblue'* is started on the IDL command line, the input file name must be fully qualified, i.e., the path has to be included. The input has to be atmospherically corrected data, i.e., an "*_atm.bsq" file, where the blue band is missing, e.g. imagery of SPOT, IRS-1D, DMC. The output file contains a synthetic blue band as the first image channel calculated from the green, red, and NIR bands on a pixel by pixel basis. The output file name is "*_blue_atm.bsq". This product is a useful supplement to be able to create a true color image of the scene.
The calculation of the surface reflectance in the synthetic blue band consists of three steps:

1. The blue band reflectance (index 1) is extrapolated from the green (index 2) and red (index 3) band reflectance :

$$\rho_1 = \rho_2 + (\rho_2 - \rho_3) * (\lambda_2 - \lambda_1)/(\lambda_3 - \lambda_2) \tag{6.1}$$

   where the center wavelength of the blue band is taken as $\lambda_1 = 480$ nm. This represents the typical spectral behavior of soils and some artificial surfaces (asphalt, concrete).

2. The red and NIR (index 4) bands are employed to compute the ratio vegetation index VI $= \rho_4/\rho_3$. Pixels with $VI > 2.5$ and $\rho_4 > 10\%$ are defined as vegetation and the blue band reflectance is calculated as :

$$\rho_1 = \rho_3/2 \tag{6.2}$$

3. Finally, water pixels are masked with the criterion $\rho_4 \leq 7\%$, where the large threshold of 7% is employed to account for potential turbid water bodies, and the blue band reflectance is calculated as :

$$\rho_1 = 1.2 * \rho_2 \tag{6.3}$$

- *specl2_batch, input=filename, sensor='xx'* or
  specl2_tile, input=filename, sensor='xx', ntx=ntx, nty=nty
  The spectral classification based on template reflectance spectra is also available in the batch mode and with the tiling option. The 'xx' is a keyword for the sensor type, e.g., 'xx'='landsat7' for Landsat-7 ETM. The complete list of sensor keywords is shown when typing *specl2_batch* on the IDL command line without the sensor specification. The ntx, nty keywords have the meaning explained for the ATCOR tile programs above.

- *smile_interp3_batch, input=filename, fpoly=fpname, option=number [, silent=silent]*
  Purpose: The atmospheric correction accounts for the column-dependent smile shift as specified in the *"smile_poly_ord4.dat"* of the corresponding sensor folder, but the image columns of each band belong to slightly different wavelengths.
  This function interpolates the pixel reflectance values for each band to a specified reference wavelength. Three options exist for the reference wavelength grid:

  1. use wavelength corresponding to the center of the detector array,
  2. use average wavelength over all detector columns (per band),
  3. use nominal wavelength specified in the (ENVI) header of the reflectance cube.

  The new reference center wavelengths are included in the header of the output file. If the input filename is *"/path1/image_atm.bsq"* the output name is *"/path1/image_atm_smcorr.bsq"* indicating the *"smile corrected"* common wavelength grid.
  Function parameters are: "filename" is the full name of the surface reflectance file, "fpname"

is the full name of *"smile_poly_ord4.dat"*, i.e., including the path, 'number' is the above option number (1 - 3), and if the keyword 'silent' is set the progress about the band processing is not issued to the command line.
This module is also available in the interactive mode (see main menu, 'Filter', *"Spectral Smile Interpolation (Image Cube)"*, chapter 5.5).

- *at_derpolish, infile, outfile, nbin, respfile *.rsp, smooth =.., /lowpass, /adj*

  Derivative polishing routine.

  PARAMETERS:
  infile: file of reflectances to be filtered
  outfile: name of output file to be created
  nbin: number of adjacent bands to use for filtering (nbin=1

  KEYWORDS:
  respfile: response file used for wavelength reference (default: ENVI header values) lowpass: perform lowpass filtering only
  smooth: smooth the outputs by a lowpass filter of size 'smooth' after derivative filtering
  adj: use only adjacent bands (excluding current) fro derivatives

- *at_rhoapp, infile, calfile, e0solar [,outfile, scale=.., zen=.., date=..]*

  Apparent reflectance calculation.

  PARAMETERS:
  calfile: Atcor calibration file to be used for conversion of the cube
  e0solar: File containing the solar irradiance for the sensor (atcor file)
  outfile: name of output

  KEYWORDS:
  scale: scale for processing (same convention as for ATCOR, scale=1.0 is floating point output)
  zen: solar zenith angle (default: 0 degrees), in degrees
  date: date as two-elemt array [day,month]

- *at_smiledetect, incube, dbfile, respfile, resol, outfile, featureflags=[..], vis=.., zen=.., ele=..,chlist=.., results=.., /spline=spline,zeroborder=[0—1—2], range=.., /overwrite*

  Smile detection routine.

  PARAMETERS:
  incube: input data cube
  dbfile: raw database file to be used for convolution (no height interpolation)
  respfile: response file (e.g., band001.rsp)
  resol: internal resolution for the calculation
  outfile: name of output file for smile coefficients

KEYWORDS:
featureflags: bytarr(n_feat), 12 feature regions, featureflags[i] = 1 if feature is set, else 0;
vis: visibility [km]
zen: solar zenith angle [deg]; zenith at 0 deg.
ele: average ground elevation [km]
chlist: list of bands which are used for smile detection and for interpolation of the results numbering starting at 0.
results: write idl save dump of all results in a file named *.sav together with the regular output
spline = 1, spline channel interpolation, =0 linear channel interpolation of smile coefficients
zeroborder : 2 set smile coefficients to 0 at spectral borders
(first, last channel) 1 repeat smile coefficients outside of interpolated values
range : search range, default = 20 nm
overwrite: silently overwrites the older output

- *at_smoothdem, infile, dist, outfile, /median*

  DEM smoothing routine.

  PARAMETERS:
  infile: input data cube (single band ENVI image)
  dist: size of smoothing filter
  outfile: name of output file

  KEYWORDS:
  median: use median filter instead of default low pass filter.

Chapter 7

Value Added Products

As a "by-product" of atmospheric correction a number of useful quantities can readily be calculated. The first group of value added products include vegetation indices (based on surface reflectance instead of at-sensor radiance), simple parametrizations of the leaf area index, and wavelength-integrated reflectance (albedo). The second group comprises quantities relevant for surface energy balance investigations which are a useful supplement for studies in landscape ecology and related fields, e.g., as input for regional modeling of evapotranspiration. These include global radiation on the ground, absorbed solar radiation, net radiation, and heat fluxes. Emphasis is put on simple models based on the reflectance / temperature cube derived during the atmospheric correction. No additional data (with the exception of air temperature) is taken into account. All value added products are written to a file with up to 11 bands. The file structure is band sequential. If the input file name is "example.bsq", the output reflectance file name is "example_atm.bsq", and the value added file name is "example_atm_flx.bsq", the 'flx' indicating the most important part of the calculation, i.e., the radiation and heat fluxes.

7.1 LAI, FPAR, Albedo

Many vegetation indices have been introduced in the literature. Only two are presented here, because these are often used for simple parametrizations of the leaf area index (LAI), the fraction of absorbed photosynthetically active radiation (FPAR), and surface energy fluxes (Baret and Guyot 1991, Choudury 1994). The normalized difference vegetation index (NDVI) is defined as

$$NDVI = \frac{\rho_{850} - \rho_{650}}{\rho_{850} + \rho_{650}} \tag{7.1}$$

where ρ_{650} and ρ_{850} are surface reflectance values in the red (650 nm) and NIR (850 nm) region, respectively. The soil-adjusted vegetation index (SAVI) is defined as (Huete 1988, Baret and Guyot 1991, with L=0.5) :

$$SAVI = \frac{(\rho_{850} - \rho_{650}) * 1.5}{(\rho_{850} + \rho_{650} + 0.5)} \tag{7.2}$$

The leaf area index (LAI) can often be approximated with an empirical three-parameter relationship employing a vegetation index (VI=SAVI or VI=NDVI)

$$VI = a_0 - a_1 \; exp(-a_2 \; LAI) \tag{7.3}$$

Solving for LAI we obtain

$$LAI = -\frac{1}{a_2}\ ln(\frac{a_0 - VI}{a_1}) \tag{7.4}$$

Sample sets of parameters are a_0=0.82, a_1=0.78, a_2=0.6 (cotton with varied soil types), a_0=0.68, a_1=0.50, a_2=0.55 (corn), and a_0=0.72, a_1=0.61, a_2=0.65 (soybean) with VI=SAVI (Choudury et al. 1994).
Note: Since it is difficult to take into account the parameters for different fields and different seasons it is suggested to use a fixed set of these three parameters for multitemporal studies. Then, the absolute values of LAI may not be correct, but the seasonal trend can be captured.

Plants absorb solar radiation mainly in the 0.4 - 0.7 μm region, also called PAR region (photosynthetically active radiation, ASRAR 1989). The absorbed photosynthetically active radiation is called APAR, and the fraction of absorbed photosynthetically active radiation is abbreviated as FPAR. These terms are associated with the green phytomass and crop productivity. A three-parameter model can be employed to approxiate APAR and FPAR (Asrar et al. 1984, Asrar 1989, Wiegand et al, 1990, 1991).

$$FPAR = C[1 - A\ exp(-B\ LAI)] \tag{7.5}$$

Typical values are C=1, A=1, B=0.4. Again, since it is difficult to account for the crop- and seasonal dependence of these parameters, a constant set may be used for multitemporal datasets to get the typical FPAR course as a function of time.

The wavelength-integrated surface reflectance (in a strict sense the *hemispherical - directional reflectance*), is used as a substitute for the surface albedo (*bi-hemispherical reflectance*). It is calculated as :

$$a = \frac{\int_{0.3\mu m}^{2.5\mu m} \rho(\lambda) d\lambda}{\int_{0.3\mu m}^{2.5\mu m} d\lambda} \tag{7.6}$$

Since most satellite sensors cover only part of the 0.3 - 2.5 μm region the following assumptions are being made for extrapolation. Extrapolation for the 0.30-0.40 μm region:

- $\rho_{0.3-0.4\mu m} = 0.8\ \rho_{0.45-0.50\mu m}$, if blue a band (0.45-0.50 μm) exists.
- $\rho_{0.3-0.4\mu m} = 0.8\ \rho_{0.52-0.58\mu m}$, green band, no blue band available.

Extrapolation for the 0.40-0.45 μm region:

- $\rho_{0.4-0.45\mu m} = 0.9\ \rho_{0.45-0.50\mu m}$, if a blue band (0.45-0.50 μm) exists.
- $\rho_{0.4-0.52\mu m} = 0.9\ \rho_{0.52-0.58\mu m}$, green band, no blue band available.

The reflectance reduction factors in the blue part of the spectrum account for the decrease of surface reflection for most land covers (soils, vegetation). The extrapolation to longer wavelengths is computed as:

- If a 1.6 μm band exists
  - $\rho_{2.0-2.5\mu m} = 0.5\ \rho_{1.6\mu m}$, if $\rho_{850}/\rho_{650} > 3$ (vegetation)

  - $\rho_{2.0-2.5\mu m} = \rho_{1.6\mu m}$, else

- If no bands at 1.6 μm and 2.2 μm are available the contribution for these regions is estimated as :

  - $\rho_{1.5-1.8\mu m} = 0.50\ \rho_{0.85\mu m}$, if $\rho_{850}/\rho_{650} > 3$ (vegetation)
  - $\rho_{2.0-2.5\mu m} = 0.25\ \rho_{0.85\mu m}$, if $\rho_{850}/\rho_{650} > 3$
  - $\rho_{1.5-1.8\mu m} = \rho_{0.85\mu m}$, (else)
  - $\rho_{2.0-2.5\mu m} = \rho_{0.85\mu m}$, (else)

At least three bands in the green, red, and near-infrared are required to derive the albedo product. Wavelength gap regions are supplemented with interpolation. The contribution of the 2.5 - 3.0 μm spectral region can be neglected, since the atmosphere is almost completely opaque and absorbs all solar radiation. The output "_flx" file contains the channels SAVI, LAI, FPAR, and albedo coded as 16 bit integer with the following scale factors:

- SAVI: range 0-1000, scale factor 1000, e.g., scaled SAVI=500 corresponds to SAVI=0.5 .
- LAI : range 0-10,000, scale factor 1000, e.g., scaled LAI=5000 corresponds to LAI=5.0 .
- FPAR: range 0-1000, scale factor 1000, e.g., scaled FPAR=500 corresponds to FPAR=0.5 .
- Albedo: range 0-1000, scale factor 10, e.g., scaled albedo=500 corresponds to albedo=50% .

The next section presents a simplified treatment of the radiation and heat fluxes in the energy balance.

7.2 Surface energy balance

Surface energy balance is an essential part of climatology. The energy balance equation applicable to most land surfaces can be written as (Asrar 1989) :

$$R_n = G + H + LE \tag{7.7}$$

where, R_n is the net radiant energy absorbed by the surface. The net energy is dissipated by conduction into the ground (G), convection to the atmosphere (H) and available as latent heat of evaporation (LE). The amount of energy employed in photosynthesis in case of vegetated surfaces is usually small compared to the other terms. Therefore, it is neglected here.
The terms on the right hand side of equation (7.7) are called heat fluxes. The soil or ground heat flux (G) typically ranges from 10% to 50% of net radiation. Convection to the atmosphere is called sensible heat flux (H). It may warm or cool the surface depending on whether the air is warmer or cooler than the surface. The energy available to evaporate water from the surface (LE) is usually obtained as the residual to balance the net radiation with the dissipation terms. Net radiation is expressed as the sum of three radiation components:

$$R_n = R_{solar} + R_{atm} - R_{surface} \tag{7.8}$$

where R_{solar} is the absorbed shortwave solar radiation (0.3 - 3 μm, or 0.3 - 2.5 μm), R_{atm} is the longwave radiation (3 - 14 μm) emitted from the atmosphere toward the surface, and $R_{surface}$ is the longwave radiation emitted from the surface into the atmosphere. Downwelling radiation is

counted with a positive sign, the upwelling thermal surface radiation has a negative sign. The absorbed solar radiation can be calculated as :

$$R_{solar} = \int_{0.3\mu m}^{2.5\mu m} \{1 - \rho(\lambda)\}\ E_g(\lambda)\ d\lambda \tag{7.9}$$

where $\rho(\lambda)$ is the ground reflectance, $1-\rho(\lambda)$ is the absorbed fraction of radiation, and $E_g(\lambda)$ is the global radiation (direct and diffuse solar flux) on the ground. The numerical calculation of equation (7.9) is based on the same assumptions regarding the extrapolation of bands and interpolation of gap regions as discussed in chapter 7.1 dealing with the surface albedo. If the satellite imagery contains no thermal band(s) from which a map of ground temperature can be derived, then R_{solar} is the only surface energy component that can be evaluated. In case of flat terrain with spatially varying visibility conditions or rugged terrain imagery, a map of the global radiation is included as an additional value added channel.

$$E_g = \int_{0.3\mu m}^{2.5\mu m} E_g(\lambda)\ d\lambda \tag{7.10}$$

For flat terrain imagery with constant atmospheric conditions the global radiation is a scalar quantity and its value can be found in the "*log" file accompanying each output reflectance file. For rugged terrain imagery, the global radiation accounts for the slope/aspect orientation of a DEM surface element.

With thermal bands a ground temperature or at least a ground brightness temperature image can be derived. Then the emitted surface radiation is calculated as

$$R_{surface} = \epsilon_s\ \sigma\ T_s^4 \tag{7.11}$$

where ϵ_s is the surface emissivity, $\sigma = 5.669\ \times 10^{-8}\ Wm^{-2}K^{-4}$ is the Stefan-Boltzmann constant, and T_s is the kinetic surface temperature. For sensors with a single thermal band such as Landsat TM an assumption has to be make about the surface emissivity to obtain the surface temperature. Usually, ϵ_s is selected in the range 0.95 - 1, and the corresponding temperature is a brightness temperature. A choice of $\epsilon_s = 0.97$ or $\epsilon_s = 0.98$ is often used for spectral bands in the 10 - 12 μm region. It introduces an acceptable small temperature error of about 1-2°C for surfaces in the emissivity range 0.95 - 1. Examples are vegetated or partially vegetated fields ($\epsilon = 0.96 - 0.99$), agricultural soil ($\epsilon = 0.95 - 0.97$), water ($\epsilon = 0.98$), and asphalt / concrete ($\epsilon = 0.95 - 0.96$). Emissivities of various surfaces are documented in the literature (Buettner and Kern 1965, Wolfe and Zissis 1985, Sutherland 1986, Salisbury and D'Aria 1992).

The atmospheric longwave radiation R_{atm} emitted from the atmosphere toward the ground can be written as

$$R_{atm} = \epsilon_a\ \sigma\ T_a^4 \tag{7.12}$$

where ϵ_a is the air emissivity, and T_a is the air temperature at screen height (2 m above ground), sometimes 50 m above ground are recommended. For cloud-free conditions, Brutsaert's (1975) equation can be used to predict the effective air emissivity :

$$\epsilon_a = 1.24\ \{\frac{p_{wv}}{T_a}\}^{1/7} \tag{7.13}$$

Here, p_{wv} is the water vapor partial pressure (millibars = hPa), and T_a is the air temperature (K). Figure 7.1 shows p_{wv} as a function of air temperature for relative humidities of 20 - 100%. The partial pressure is computed as :

$$p_{wv} = RH\ e_s\ /\ 100 \tag{7.14}$$

where RH is the relative humidity in per cent, and e_s is the water vapor partial pressure in saturated air (Murray 1967) :

$$e_s(T_a) = e_{s0}\ exp\{\frac{a(T_a - 273.16)}{T_a - b}\} \tag{7.15}$$

The constants are $a = 17.26939$, $b = 35.86$, and $e_{s0} = e_s(273.16K) = 6.1078\ hPa$. An alternative to equation (7.13) is the following approximation (Idso and Jackson 1969) which does not explicitly include the water vapor and holds for average humidity conditions, compare Figure 7.2.

$$\epsilon_a = 1 - 0.261\ exp\{-7.77 \times 10^{-4}\ (273 - T_a)^2\} \tag{7.16}$$

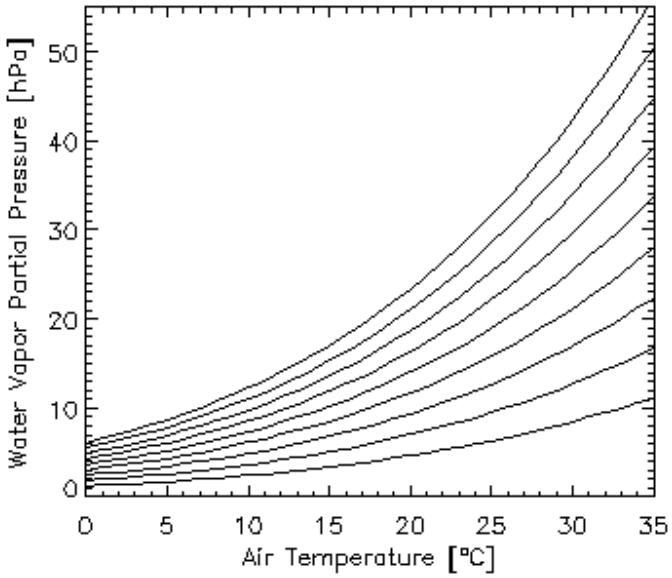

Figure 7.1: *Water vapor partial pressure as a function of air temperature and humidity. Relative humidities are 20% to 100% with a 10% increment, bottom to top curves, respectively (eq. 7.14).*

The calculation of the heat fluxes G, H, and LE on the right hand side of equation 7.7 requires different models for vegetated and man-made surfaces. For vegetated or partially vegetated surfaces, we employ a simple parametrization with the SAVI and scaled NDVI indices (Choudury 1994, Carlson et al. 1995) :

$$G = 0.4\ R_n\ (SAVI_m - SAVI)/SAVI_m \tag{7.17}$$

where $SAVI_m = 0.814$ represents full vegetation cover. The sensible heat flux is computed as :

$$H = B\ (T_s - T_a)^n \tag{7.18}$$

$$B = 286\ (0.0109 + 0.051\ NDVI^*) \tag{7.19}$$

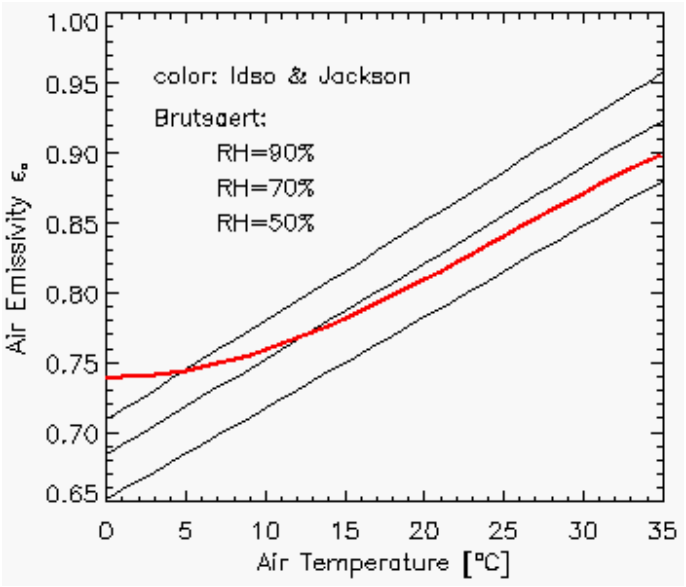

Figure 7.2: *Air emissivity after Brutsaert (eq. 7.13) and Idso/Jackson (eq. 7.16).*

$$n = 1.067 - 0.372\ NDVI^* \tag{7.20}$$

$$NDVI^* = \frac{\rho_{850} - \rho_{650}}{0.75 * (\rho_{850} - \rho_{650})} \tag{7.21}$$

Equation (7.18) corresponds to equation (1a) of Carlson et al. (1995), because G is neglected there, and so $R_n - G$ represents the energy left for evapotranspiration. The factor 286 in equation (7.19) converts the unit (cm/day) into (Wm^{-2}). $NDVI^*$ is the scaled NDVI ranging between 0 and 1, and truncated at 1 if necessary. Equation (7.21) corresponds to equation (3) of Carlson et al. (1995) with $NDVI_0 = 0$ (bare soil) and $NDVI_s = 0.75$ (full vegetation cover). The latent heat flux LE is computed as the residual:

$$LE = R_n\ -\ G\ -\ H \tag{7.22}$$

A different heat flux model is employed for urban areas with man-made surfaces (asphalt, concrete, roofs, etc.). These are defined here with the reflectance criteria

$$\rho_{650} \geq 0.10 \quad and \quad \rho_{850} \geq 0.10 \quad and \quad \rho_{650} > \rho_{850} * 0.7 \tag{7.23}$$

representing low vegetation indices with $NDVI < 0.176$. This simple spectral definition is not unambiguous, it might also apply to soils. For urban areas the latent heat is usually very small, and the fluxes G and H dominate. Therefore, the terms G, LE, and H are approximated by the following three equations (Parlow 1998):

$$G = 0.4\ R_n \tag{7.24}$$

$$LE = 0.15\ (R_n - G) \tag{7.25}$$

$$H = R_n\ -\ G -\ LE \tag{7.26}$$

For low vegetation indices ($SAVI < 0.1$) the ground heat flux G from equation (7.17), i.e., the vegetation model, agrees well with G from equation (7.24), i.e., the urban model. However, major

differences exist for the LE and H terms, see table 7.1. Parameters for this table are: $E_g = 800$, $R_n = 600$, $R_{atm} + R_{surface} = -100\ Wm^{-2}$, $T_s = 30°C$, and $T_a = 20°C$. The (veg) and (urb) indicate the heat fluxes derived from the vegetation and urban model, respectively. For the urban surfaces (asphalt, concrete) the G(veg), H(veg) and LE(veg) values are given in brackets for comparison, but the corresponding "urban" heat fluxes are valid because the "urban" criterion (equations 7.23, $\rho_{650} \geq 0.10$, $\rho_{850} \geq 0.10$, and $\rho_{650} > \rho_{850} * 0.7$) applies. The last row repeats the concrete case for $R_{solar} = 800 * (1 - 0.36) = 512, R_n = R_{solar} + R_{atm} + R_{surface} = 512 - 100 = 412\ Wm^{-2}$, a realistic reduced R_n value (compared to the asphalt where $E_g = 800, R_{solar} = 800 * (1 - 0.12) = 700, R_n = 700 - 100 = 600\ Wm^{-2}$).

surface	ρ_{650}	ρ_{850}	NDVI	G(veg)	H(veg)	LE(veg)	G(urb)	H(urb)	LE(urb)
full veget.	0.05	0.40	0.78	77	87	435	-	-	-
partial veget.	0.10	0.20	0.33	185	76	338	-	-	-
dark asphalt	0.11	0.13	0.09	(228)	(50)	(322)	240	306	54
bright concrete	0.35	0.40	0.07	(222)	(48)	(330)	240	306	54
bright concrete (*)	0.35	0.40	0.07	-	-	-	164	210	37

Table 7.1: *Heat fluxes for the vegetation and urban model. All fluxes in [Wm^{-2}].*

All radiation and heat fluxes are calculated in units of Wm^{-2}. They represent instantaneous flux values. For applications, where daily (24 h) LE values are required the following equation can be used for unit conversion:

$$LE\ [\frac{cm}{day}] = \frac{1}{286}\ LE\ [Wm^{-2}] \tag{7.27}$$

The latent heat flux LE is frequently called evapotranspiration (ET). Although LE and ET are used interchangeably the unit (cm/day) or (mm/day) is mostly employed for ET. For water surfaces the distribution of net radiation into G, LE, and H is difficult to determine, because it depends on several other parameters. Therefore, G and H are set to zero here, and so LE equals R_n.

Spatial maps (files) of air temperature and air emissivity can also be included in the processing. Usually, isolated point-like measurements of air temperature are available from meteorological stations. These have to be interpolated to generate a spatial map coregistered to the image prior to applying the ATCOR model. Data in the file containing the air temperature must have the Celsius unit, data of the air emissivity file must range between 0 and 1. Future improvements to the ATCOR model will include an air temperature map derived from the image ("triangle" or "trapezoidal" method employing the thermal band surface temperature and NDVI, Carlson et al. 1995; Moran et al. 1994).

In case of mountainous terrain, the air temperature $T_a(z_0)$ and water vapor partial pressure $p_{wv}(z_0)$ at a reference elevation z_0 have to be specified. The height dependence of air temperature is then obtained with linear extrapolation employing a user-specified adiabatic temperature gradient $\partial T/\partial z$:

$$T_a(z) = T_a(z_0)\ +\ \frac{\partial T}{\partial z}(z_0 - z) \tag{7.28}$$

where $\partial T/\partial z$ is typically in the range 0.65 - 0.9 (Celsius / 100 m). The water vapor partial pressure is extrapolated exponentially according to

$$p_{wv}(z) = p_{wv}(z_0)\ 10^{-(z-z_0)/z_s} \tag{7.29}$$

where z_s is the water vapor scale height (default 6.3 km). The list of all output channels of the value added *"*_flx.bsq"* file is :

1. Soil adjusted vegetation index (SAVI), scaled with factor 1000,
2. Leaf area index (LAI), scaled with 1000,
3. Fraction of photosynthetically active radiation FPAR, scaled with 1000,
4. Surface albedo (integrated reflectance from 0.3-2.5 μm), per cent * 10,
5. Absorbed solar radiation flux R_{solar} $[Wm^{-2}]$,
6. Global radiation E_g $[Wm^{-2}]$, omitted for constant visibility in flat terrain because it is a scalar which is put into the *"*log"* file .
   The next channels are only available in case of at least one thermal band:
7. Thermal air-surface flux difference $R_{therm} = R_{atm} - R_{surface}$ $[Wm^{-2}]$,
8. Ground heat flux G $[Wm^{-2}]$,
9. Sensible heat flux H $[Wm^{-2}]$,
10. Latent heat LE $[Wm^{-2}]$,
11. Net radiation R_n $[Wm^{-2}]$.

Chapter 8

Sensor simulation of hyper/multispectral imagery

After atmospheric correction the surface reflectance and temperature/emissivity cubes can be used to simulate new products which might be of interest:

- at-sensor radiance cubes in the solar region (0.4 - 2.5 μm) for different solar geometries and atmospheric conditions,
- at-sensor radiance cubes in the thermal region (8 - 14 μm) for different atmospheric conditions, e.g. for satellite sensor studies,
- resampling of the surface reflectance cube to an existing or new multispectral sensor,
- resampling of the surface emissivity cube to an existing or new multispectral sensor.

This is a convenient way to simulate realistic data for a spaceborne version of an airborne instrument, to obtain radiance data under differenct atmsopheric conditions, or to compare hyperspectral (hs) data with broad-band multispectral (ms) data. As a restriction, the TOA (top-of-atmosphere) or at-sensor radiance calculated with the *"TOARAD"* program assumes a nadir view. The *"hs2ms"* (hyperspectral-to-multispectral) program requires the hs and ms center wavelengths and the ms channel filter curves for resampling. In addition, noise of the ms sensor can be included as Gaussian noise with a specified amplitude, either as noise-equivalent radiance (NER) or as noise-equivalent reflectance ($NE\Delta\rho$). The hs contribution to a certain ms band is weighted with the value of the ms response curve at the corresponding hs wavelength, compare Fig. 8.1.
After summing all contributions the result is normalized with the sum of the hs filter values

$$L_{ms}(i) = \frac{\sum_{k=1}^{n_i} L_{hs}^{(k)} R_{ms}^{(i)}(\lambda_{hs}^{(k)})}{\sum_{k=1}^{n_i} R_{ms}^{(i)}(\lambda_{hs}^{(k)})} \tag{8.1}$$

where L denotes at-sensor (or TOA) radiance, $R_{ms}^{(i)}$ the ms response function of channel i, and n_i is the number of hs channels covered by the i-th ms filter function. A similar equation is used for the resampling of surface reflectance. The weight factors w_k for each hs channel are calculated with

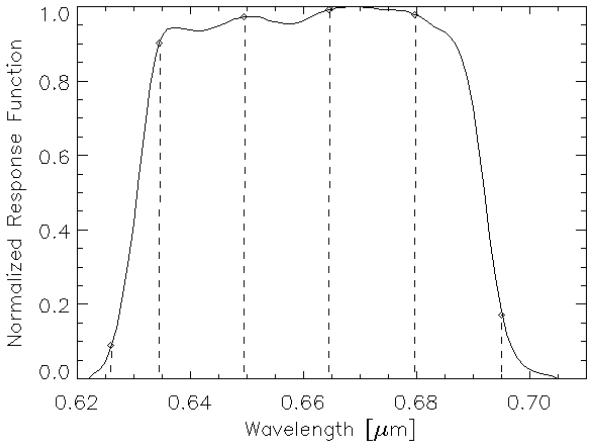

Figure 8.1: *Weight factors of hyperspectral bands.*
The solid curve shows the response function $R_{ms}^{(i)}$ of a ms channel, and the dashed lines indicate the hs center wavelengths $\lambda_{hs}^{(j)}$.

eq. 8.2, and they are documented in the corresponding *".log"* file created by program *"HS2MS"*.

$$w_k(i) = \frac{R_{ms}^{(i)}(\lambda_{hs}^{(k)})}{\sum_{j=1}^{n_i} R_{ms}^{(i)}(\lambda_{hs}^{(j)})} \tag{8.2}$$

Fig. 8.2 describes the sequence of processing for the sensor simulation in the solar region. After atmospheric correction with ATCOR the *"image_atm.bsq"* contains the surface reflectance cube. Program *"TOARAD"* then calculates the at-sensor radiance for a different solar geometry, or atmospheric parameters. All parameters not specified as keywords (see list of keywords below) are taken from the *"image.inn"* file created by ATCOR.

The program *"HS2MS"* can be started to resample the radiance cube to a ms image by specifying the ms sensor (i.e., channel filter functions) and the ms noise equivalent radiance (NER). NER = 0 is allowed, so the resampled image product will only include the noise of the hs scene, which will be reduced due to the inherent integration over several hs bands. A channel-constant NER or a file with channel-dependent NER values may also be employed.
Figure 8.3 shows the GUI panel of program *"HS2MS"*. Although the input image will usually be a hyperspectral scene with $n > 50$ channels and the output a multispectral scene with $m << n$ channels, this program can also be employed for the case of a multispectral input image with $n < 10$ channels and a panchromatic sensor with m=1 band. The program supports the four cases of resampling mentioned above, i.e., solar or thermal at-sensor radiance, surface reflectance, or emissivity.

The processing of hyperspectral thermal data is currently not supported by the satellite version of ATCOR because of the lack of commercial sensors with these channels. However, this part is already implemented in the airborne ATCOR. A detailed description of the keywords of program "toarad" follows.

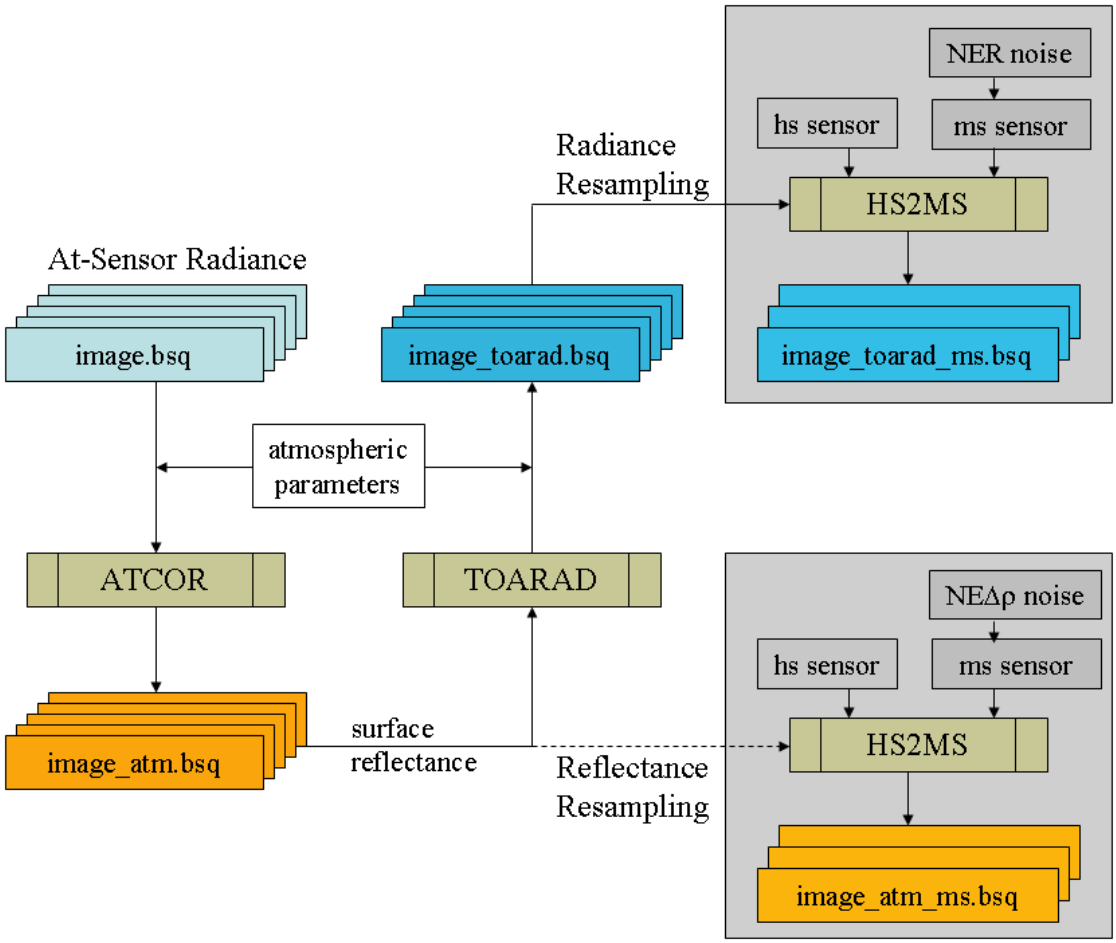

Figure 8.2: *Sensor simulation in the solar region.*

Keywords for the batch program *"toarad"*

On the IDL command line, program names can be written in lower case letters, so as an example "toarad" instead of "TOARAD" is used synonymously in this context. If "toarad" is submitted as a batch job, the following keywords can be specified:

- *toarad, input=filename, [pixelsize=pixelsize, sz=solar_zenith, atmfile=atmfile, elev=elevation, vis=visibility, adjrange=adjrange, scalef=scalef]*

The input file name must include the path, and the keywords in brackets indicate optional parameters. If a keyword is set, it will overwrite the corresponding parameter from the *".inn"* file, compare chapters 6.2 and 9.4. To perform a TOA/at-sensor radiance simulation for a given scene, the user has to resample files from the monochromatic atmospheric database:

- for the altitude 99,000 m that serves as "flight" altitude for space sensors, see chapter 4.6.

After running ATCOR for a certain scene and sensor, a surface reflectance cube is obtained which is input to the TOA/at-sensor simulation that can be performed for a flat or a mountainous terrain. A detailed description of the keywords of "toarad" follows:

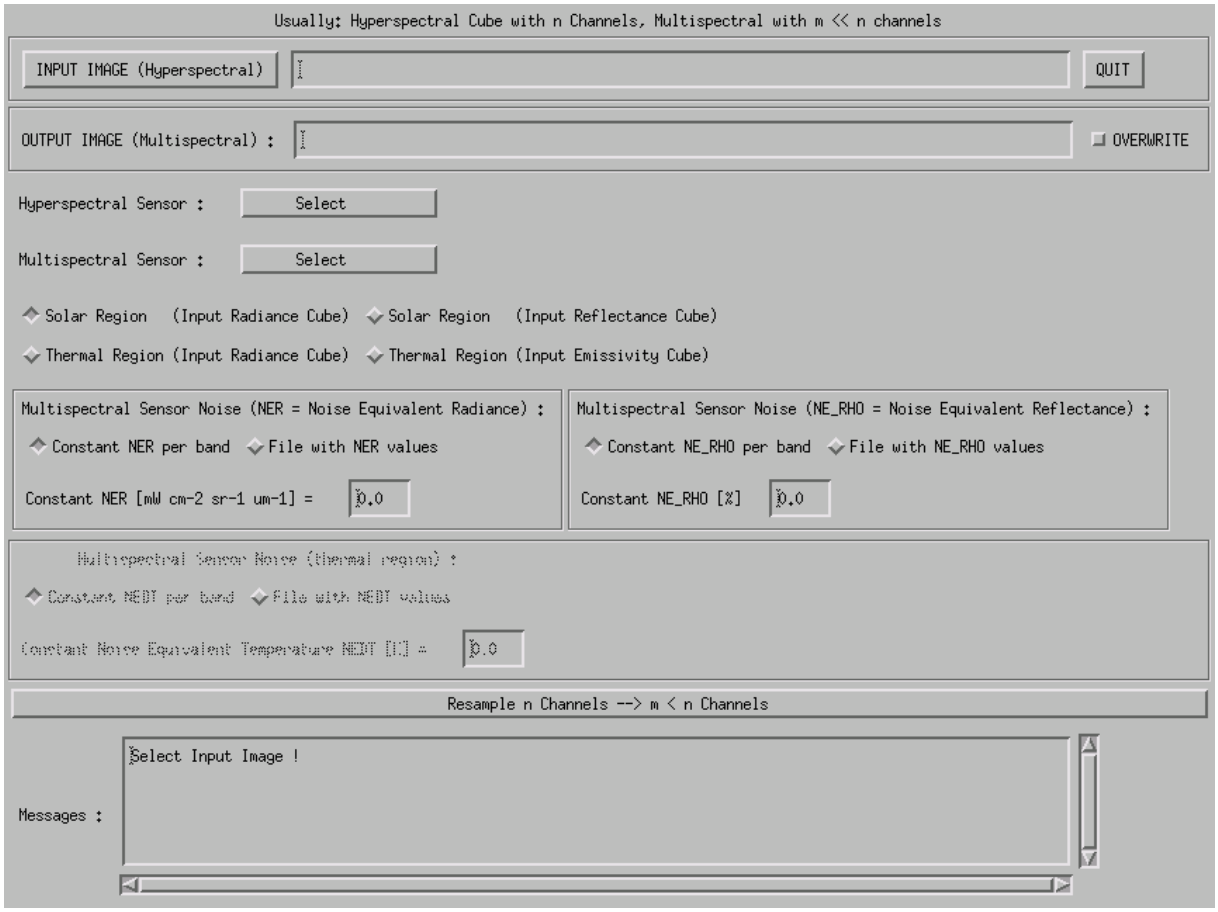
Usually: Hyperspectral Cube with n Channels, Multispectral with m << n channels
INPUT IMAGE (Hyperspectral)
QUIT
OUTPUT IMAGE (Multispectral) :
OVERWRITE
Hyperspectral Sensor :
Select
Multispectral Sensor :
Select
Solar Region (Input Radiance Cube)
Solar Region (Input Reflectance Cube)
Thermal Region (Input Radiance Cube)
Thermal Region (Input Emissivity Cube)
Multispectral Sensor Noise (NER = Noise Equivalent Radiance) :
Constant NER per band
File with NER values
Constant NER [mW cm-2 sr-1 um-1] =
0.0
Multispectral Sensor Noise (NE_RHO = Noise Equivalent Reflectance) :
Constant NE_RHO per band
File with NE_RHO values
Constant NE_RHO [%]
0.0
Multispectral Sensor Noise (thermal region) :
Constant NEDT per band
File with NEDT values
Constant Noise Equivalent Temperature NEDT [K] =
0.0
Resample n Channels --> m < n Channels
Messages :
Select Input Image !

Figure 8.3: *Graphical user interface of program "HS2MS".*

- *input='/data1/image_atm.bsq'*, the *'_atm.bsq'* indicates a surface reflectance file which is the output of an ATCOR run. The input file to ATCOR was *'/data1/image.bsq'*, and *toarad* extracts some information from the corresponding file *'/data1/image.inn'*, for example the sensor name. The output file name is *'/data1/image_toarad.bsq'*.

- *atmfile='h99000_wv29_rura'*, this is an example of an atmospheric look-up-table file with a rural aerosol and a water vapor column of 2.9 gcm^{-2}, see chapter 9.1. If the keyword *atmfile* is not specified, then *'h99000_wv10_rura'* will be taken.

- *elev=500*, an example of a ground elevation at 500 m above sea level. If *elev* is not specified, then elev=0 is assumed. However, if the keyword *elev* is not specified and the *'/data1/image.inn'* file contains file names for the DEM elevation, slope, and aspect, then the DEM files are taken, and the TOA calculation is performed for a rugged terrain. If the keyword *elev* is specified the simulation is always performed for a flat terrain regardless of any possible DEM file names in the *'*.inn'* file.

- *sz=35.5*, an example of a solar zenith angle of 35.5°.

- *vis=25*, an example of a visibility of 25 km.

- *pixelsz=4.5*, an example of a pixelsize of 4.5 m .

- *adjrange=500*, an example of an adjacency range of 500 m.
- *scalef=10,000*, scale factor for the TOA radiance. The default is *scalef=1.0* which provides the output file as float data of TOA radiance in units of $[mWcm^{-2}sr^{-1}\mu m^{-1}]$. If scalef > 1, e.g. scalef=10,000, the output TOA radiance is stored as 16 bit unsigned integer multiplied with the scale factor. The advantage is a smaller output file (compared to the 32 bit float), the drawback is that radiances will be truncated at 65,000 which might happen for bright surfaces (e.g., snow, vegetation in the NIR) with scalef=10,000, see Figure 8.4. Therefore, the easiest way to avoid scale problems is to use the default *scalef=1.0* and have a float radiance output cube.

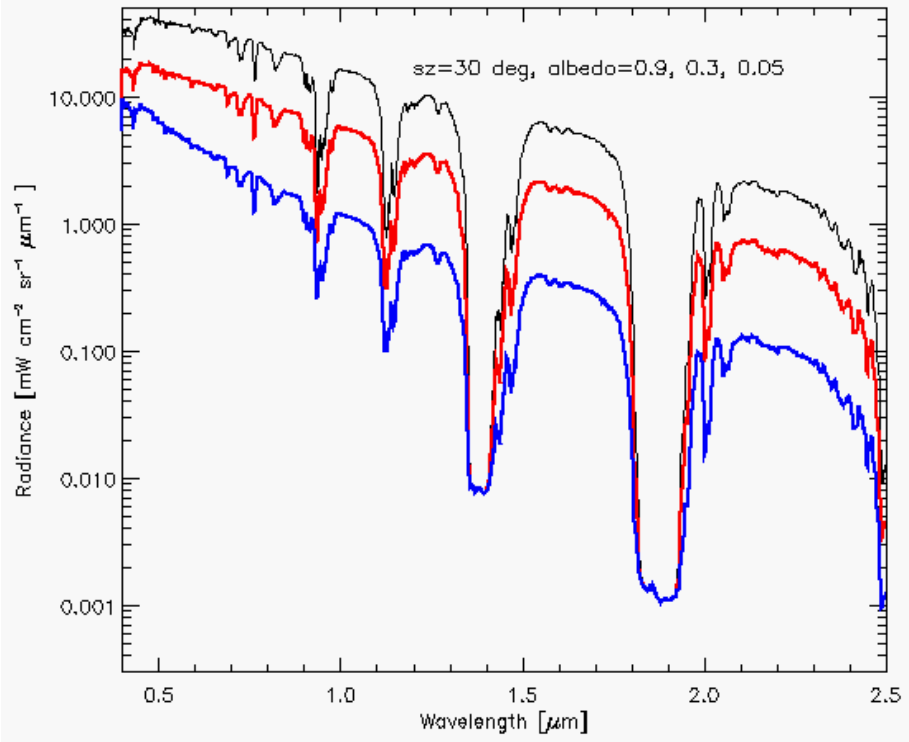

Figure 8.4: *TOA radiances for three albedos and a solar zenith angle of 30°.*
MODTRAN calculation for a mid-latitude summer atmosphere, rural aerosol, visibility 15 km, ground elevation 500 m above sea level.

For convenience, a "*.log" and an "*.ini" file are created for the documentation of the processing parameters, e.g., *'/data1/image_toarad.ini'*. In addition, the corresponding sensor calibration file will be created. Example: sensor='casi96', scalef=1000, then file *'casi96_scalef1000.cal'* will be created on the *'../atcor4/sensor/casi96/* directory with the radiometric calibration coefficient $c_1 = 0.001$ for each band.

Chapter 9

Implementation Reference and Sensor Specifics

This chapter discusses miscellaneous topics associated with the current implementation of ATCOR. First the user is acquainted with the structure and handling of the atmospheric database. Second, the supported input/output file types are given. The next item discusses the preference parameters, e.g. the definition of thresholds employed for the masking of cloud and water areas, and options for interpolating certain spectral regions. Then the parameters of the *"*.inn"* file are described which is employed for the interactive and batch processing. Last but not least a section on problems and tips is included.

9.1 The Monochromatic atmospheric database

This section presents the technical details of the atmospheric database.

To be capable of handling typical hyperspectral sensors with arbitrary spectral bands in the solar and thermal spectral regions a large database of atmospheric LUTs was compiled with the MODTRAN®5 radiative transfer code in 2010. The database is called "monochromatic" because of its high spectral resolution, compare figure 9.1. After resampling with the spectral response functions of any sensor a typical size of the sensor-specific database is 10 MB. Chapter 9.1.4 contains a description of the resampling program RESLUT.

9.1.1 Visible / Near Infrared region

In the solar spectral region (0.34 - 2.54 μm) MODTRAN® was run with different wavenumber spacings to achieve a wavelength grid spacing of approximately 0.4 nm (except for the 1400 nm and 1800 nm regions). This required the use of MODTRAN®'s *"p1_2008"* database (i.e., 0.1 cm^{-1}) in the 2.1 - 2.5 μm region. In addition, different RT algorithms were used: in atmospheric window regions the scaled DISORT algorithm with 8 streams (SD-8) was employed, in absorption regions the more accurate SD-8 with the correlated k algorithm was selected [27]. Since the wavenumber grid is not equidistant in wavelength, the LUTs were resampled with an equidistant 0.4 nm grid of Gaussian filter functions of FWHM=0.4 nm to speed up subsequent calculations. So the new LUT database should be sufficient for instruments with bandwidths > 2 nm covering the solar spectral region from 340 to 2540 nm.
The "standard" database is calculated for nadir viewing instruments. An off-nadir database with

the tilt angles 0°- 30°(in steps of 10°) is available upon request. It is intended for future hyperspectral space sensors such as EnMAP.
A separate "CHRIS/Proba" database is included in the distribution containing calculations for the tilt angles 0°, 35°, and 55° for seven equidistantly spaced relative azimuth angles (0, 30, ... 180°). CHRIS data acquisition is usually close (within ±2°) to this set of tilt angles, and interpolation is automatically performed. While the standard database is named *"atm_database"*, the CHRIS database is named *"atm_database_chris"* and it is automatically accessed if the letters *"chris"* or *"CHRIS"* are part of the user-defined sensor name, e.g., *"chris_mode5"*. While the standard database uses a 0.4 nm wavelength grid, the CHRIS database employs a 1 nm grid.

9.1.2 Thermal region

In the thermal region from 7.2 - 14.9 μm a 1 cm^{-1} grid is used, i.e., a 10 nm wavelength spacing at 10 μm, using the Isaacs's 2-stream algorithm including the correlated k algorithm. The Isaacs's algorithm is much faster than DISORT, and yields the same results for our cases in the thermal region. The spectral resolution is twice the sampling distance, and a triangular weight function with 2 cm^{-1} is employed. So the thermal region uses an equidistant wavenumber grid. In addition, all files are calculated for view or scan angles from 0° (nadir) to 40° off-nadir with a 5° increment to enable an accurate interpolation.

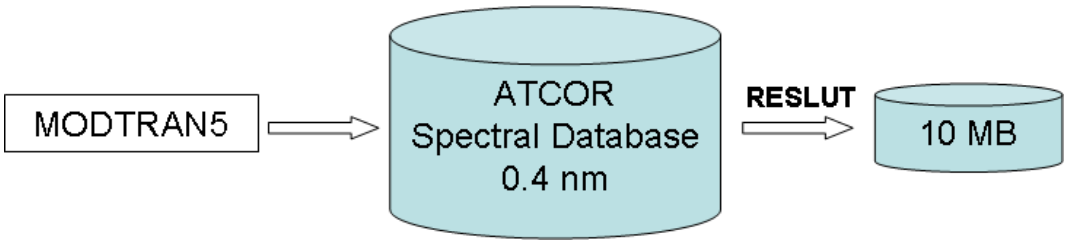

Figure 9.1: *Monochromatic atmospheric database.*

The database comprises calculations performed for a satellite altitude of 650 km, but for consistency with the airborne ATCOR the symbolic height '99,000' is used in the file names. MODTRAN®'s mid-latitude summer atmosphere was used for the air pressure and temperature height profiles at six water vapor columns (W=0.4, 1.0, 2.0, 2.9, 4.0, and 5.0 cm or or g cm^{-2}, (sea level-to-space values) and different aerosol types. These represent dry to humid atmospheric conditions [59, 6]. They are needed for the water vapor retrieval to create interpolated / extrapolated values for the range W=0.3 - 5.5 cm. In spectral regions where water vapor absorbs, the accuracy of the surface reflectance retrieval depends on the number of water vapor grid points and the interpolation method (full range of W or sub-interval pertaining to a pixel [66]). The CO_2 mixing ratio of the atmosphere is set at 400 ppmv, the ozone column is fixed at 330 DU (Dobson Units, equivalent to the former 0.33 atm-cm) for a ground at sea level. The aerosol types rural, urban, maritime, and desert have been provided in the database.

These files have to be resampled with the sensor-specific channel filter curves. The file names for the solar region include the altitude, the aerosol type, and the water vapor content. They have the extension *".atm"*. Example: *"h99000_wv04_rura.atm"* represents a file with the symbolic altitude 99,000 m, water vapor column 0.4 cm, and the rural aerosol.

Each *"*.atm"* file contains the look-up tables for the visibility range 5 - 120 km, solar zenith angles 0 - 70°, and ground elevations 0 - 2500 m (increment 500 m).

The files *"phasefct*.bin"* in the *"../atcor/bin"* directory contain the path radiance as a function of the scattering angle for the standard multispectral instruments with tilt capability, e.g. SPOT, Ikonos, Quickbird, ALOS AVNIR-2. A small field-of-view is assumed for all (hyperspectral or multispectral) instruments, i.e., the specified tilt angle and solar zenith angle holds for the whole scene.

9.1.3 Database update with solar irradiance

In the solar region any high spectral resolution database of LUTs is based on the specification of an extraterrestrial spectral solar irradiance, because the values of path radiance, direct and diffuse solar fluxes depend on solar irradiance. Other quantities (direct and diffuse atmospheric transmittances and spherical albedo) are independent of the solar spectrum. ATCOR's standard atmospheric database is calculated for a certain irradiance $E_1(\lambda)$, and the corresponding file *'e0_solar_xxx.dat'* is included in the directory *'atm_database'*.

Beginning with the ATCOR-2011 release there is an option to switch from one extraterrestrial solar irradiance source $E_1(\lambda)$ to another one $E_2(\lambda)$. The delivered high spectral resolution database of atmospheric LUTs is based on the Fontenla-2011 solar irradiance spectrum (Fontenla et al. 2009, 2011 [35, 36]). It represents the solar irradiance for a quiet or "low activity" sun and is recommended as the standard spectrum. The original $0.1 cm^{-1}$ resolution spectrum is convolved with Gaussian filter functions (FWHM=0.4 nm) and mapped on an equidistant 0.4 nm grid. The file name of this spectrum $E_1(\lambda)$ is *'e0_solar_fonten2011_04nm.dat'*. If R_1 denotes the set of quantities (path radiance, direct, diffuse solar flux) based on $E_1(\lambda)$, then the new set R_2 with the irradiance spectrum $E_2(\lambda)$ is calculated as:

$$R_2(\lambda) = R_1(\lambda)\ E_2(\lambda)/E_1(\lambda) \tag{9.1}$$

Figure 9.2 presents a schematic sketch of this conversion. The folder *'sun_irradiance'* contains a number of solar irradiance files that can be selected. The folder of the atmospheric database DB_1 pertaining to $E_1(\lambda)$ includes the corresponding irradiance file (e.g. *'e0_solar_fontan2011_04nm.dat'*) and the calculated new database DB_2 includes the $E_2(\lambda)$ file (e.g., *'e0_solar_kurucz2005_04nm.dat'*). The standard or "active" database is named *'atm_database'*, while the new database includes 10 characters from the E_2 file name, e.g. *'atm_database_kurucz2005'*.

The ATCOR "tools" panel contains the program to convert from one to another spectral irradiance database (see Figure 9.3). It enables an update of the "monochromatic" atmospheric database without the need to repeat the time-comsuming MODTRAN®5 computations (involving the correlated k algorithm in some spectral regions). The user can also provide additional solar irradiance files to the *'sun_irradiance'* folder provided the spectral range, increment, and irradiance unit agree with the template spectra.

Attention: ATCOR will always work with files in the "active" folder *'atm_database'*, therefore the old *'atm_database'* has to be renamed (or deleted) and the folder with the new database has to be renamed as *'atm_database'* before applying the sensor-specific resampling program (RESLUT). Since each *'atm_database'* folder contains its corresponding solar irradiance spectrum a unique identification is always possible. Previously generated channel-resampled *"*.atm"* files do not have

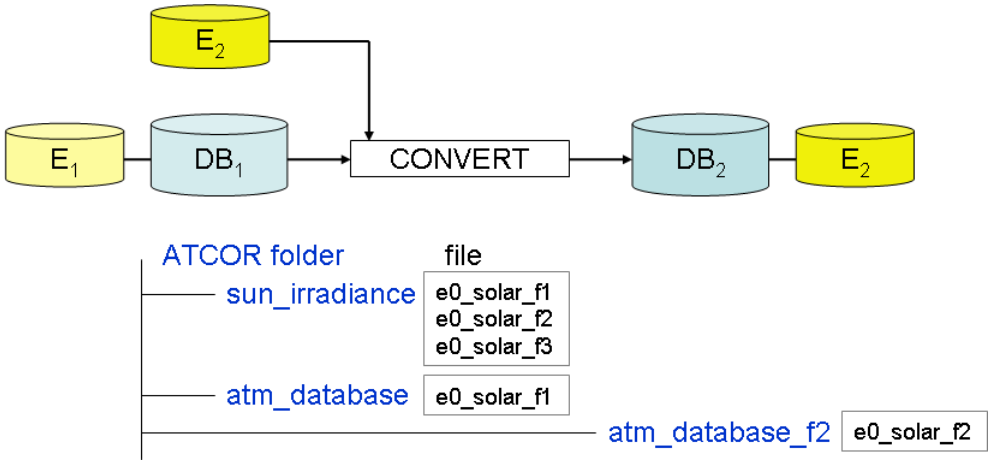

Figure 9.2: *Solar irradiance database.*

a reference to their solar irradiance file, but they are based on the *'e0_solar_kurucz1997_06nm.dat'* irradiance. Beginning with the 2011 release the directory of the *"*.atm"* files contains an ASCII file named 'irradiance_source.txt' identyfying the underlying solar irradiance file.

9.1.4 Sensor-specific atmospheric database

This sensor-specific database is created by resampling the files of the monochromatic database with the sensor's spectral response functions employing program RESLUT, see figure 9.4. An aerosol subset or all aerosol files from the monochromatic database can be selected. All water vapor files belonging to the selected aerosol type (e.g. wv04, wv10, wv20, wv29, wv40) will be resampled for hyperspectral or user-defined sensors. The folder with the ".atm" files also contains a file ""irrad_source.txt" identyfying the underlying solar irradiance spectrum.

In addition, a file of the resampled extraterrestrial solar irradiance, e.g., *"e0_solar_chris_m1.spc"*, will be created in the corresponding sensor folder, e.g., *"../sensor/chris_m1/"*.

9.1.5 Resample sensor-specific atmospheric LUTs with another solar irradiance

It is also possible to resample existing sensor-specific LUTs (".atm" files) with another solar irradiance spectrum. Input is a sensor from the "atcor/sensor/" folder (example name 'xxx') with the corresponding spectral response files (".rsp") and a high-resolution solar irradiance file from the "atcor/sun_irradiance/" directory (example: 'e0_solar_kurucz2005_04nm.dat').

Output is a new sensor subdirectory (example: "sensor/xxx_kurucz2005/") where the first 10 characters of the 'e0_solar_kurucz2005_04nm' (starting after the 'e0_solar_') are appended to the input sensor name. The contents of the input 'atcor/sensor/xxx/' are copied to the output directory, 'e0_solar_xxx.spc' is deleted (in the output directory) and replaced by the new 'e0_solar_xxx_kurucz2005.spc'. A comparison of 'e0_solar_xxx.spc' with 'e0_solar_xxx_kurucz2005.spc' shows the influence of the change of the irradiance spectrum. In addition, a new 'atm_lib/xxx_kurucz2005/' is created where all the LUTs '.atm' from the input 'atm_lib/xxx/' are replaced with the resampled selected irradiance spectrum. This new folder also contains a file ""irrad_source.txt" identifying the selected

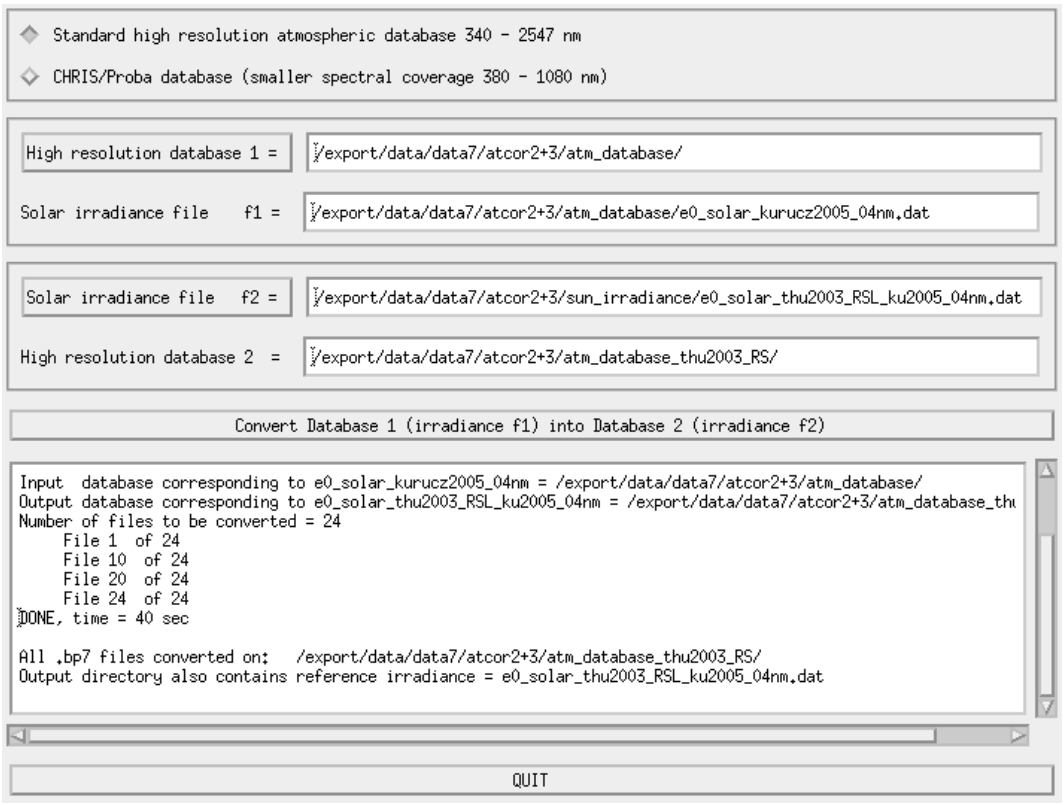
Standard high resolution atmospheric database 340 - 2547 nm
CHRIS/Proba database (smaller spectral coverage 380 - 1080 nm)
High resolution database 1 =
/export/data/data7/atcor2+3/atm_database/
Solar irradiance file f1 =
/export/data/data7/atcor2+3/atm_database/e0_solar_kurucz2005_04nm.dat
Solar irradiance file f2 =
/export/data/data7/atcor2+3/sun_irradiance/e0_solar_thu2003_RSL_ku2005_04nm.dat
High resolution database 2 =
/export/data/data7/atcor2+3/atm_database_thu2003_RS/
Convert Database 1 (irradiance f1) into Database 2 (irradiance f2)
Input database corresponding to e0_solar_kurucz2005_04nm = /export/data/data7/atcor2+3/atm_database/
Output database corresponding to e0_solar_thu2003_RSL_ku2005_04nm = /export/data/data7/atcor2+3/atm_database_thu
Number of files to be converted = 24
File 1 of 24
File 10 of 24
File 20 of 24
File 24 of 24
DONE, time = 40 sec
All .bp7 files converted on: /export/data/data7/atcor2+3/atm_database_thu2003_RS/
Output directory also contains reference irradiance = e0_solar_thu2003_RSL_ku2005_04nm.dat
QUIT

Figure 9.3: *User interface to convert database from one to another solar irradiance.*

irradiance source.

9.2 Supported I/O file types

The input image to ATCOR must have the band sequential (BSQ) ENVI format or the TIFF format. Some restrictions apply to the TIFF format as detailed below. Several data types exist for the encoding. The following data types of an input image are supported:

- byte, or unsigned 8 bit integer, ENVI data type = 1;
- signed 16 bit integer, ENVI data type = 2;
- unsigned 16 bit integer, ENVI data type = 12;
- signed 32 bit long integer, ENVI data type = 3;
- float (32 bit), ENVI data type = 4.

In case of the float input data type some restrictions exist for the image processing options. The haze and cloud shadow removal cannot be selected, because they rely on integer based histogram manipulations. The user should re-scale the float data to one of the supported integer data types in this case.

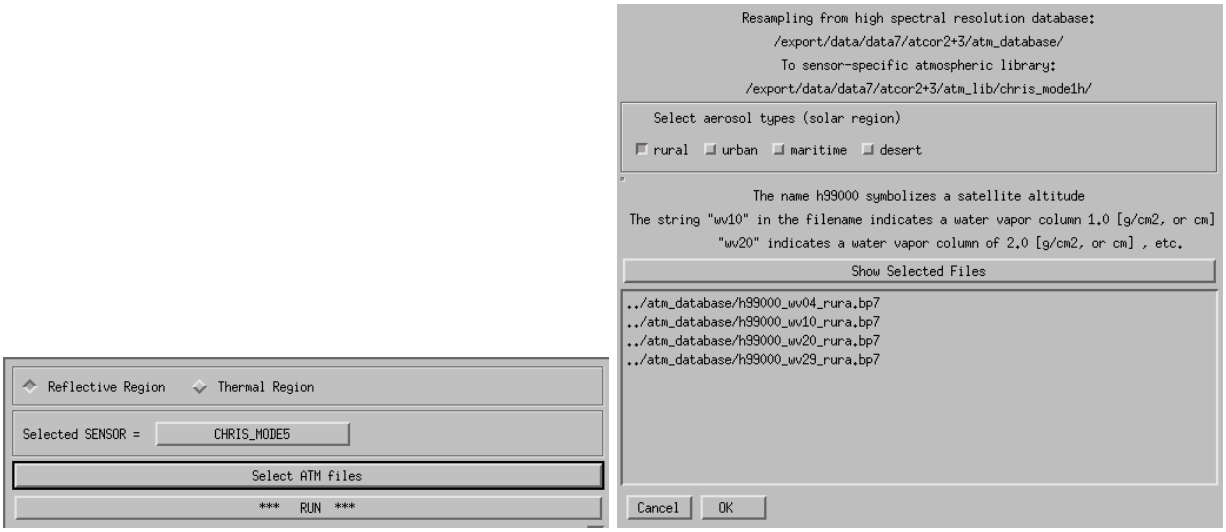

Figure 9.4: *GUI panels of the satellite version of program RESLUT.*

The default output image data type is byte if the input is byte data. Then a scale factor s=4 is employed, i.e., the per cent reflectance value of each pixel is multiplied with s=4 and rounded to byte. As an example, a surface reflectance value of 20.2% will be coded as 81. However, the user can modify the scale factor (on ATCOR's main panel). A value of s=10 to s=100 causes the output file to be coded as signed 16 bit integer, i.e., with two bytes per pixel. The specification s=1.0 produces a float output image, i.e., with 4 bytes per pixel.
Attention: The float output could be used for testing on small images. For large files and an input data type of 2 bytes per pixel the output float image would require twice the disk space of the input image.

The default output data type is signed 16 bit integer for all integer (and float) input data employing the scale factor s=100. The scale factor is always included in the output ENVI header file.

Note: Any positive value of the scale factor s is accompanied with a truncation of surface reflectance values at 0 in the output cube. So a negative reflectance, e.g., caused by a wrong choice of visibility or inaccurate radiometric calibration, will be reset to zero in the output image. In the *"SPECTRA"* module no truncation is applied. If a user wants the output reflectance cube without zero-truncation, the scale factor s should be specified with a negative value, e.g., s=-1 will provide a float output surface reflectance retaining negative reflectance values, s=-100 will provide a 16 bit integer output file. The byte scale ($-10 < s < -1$ and output data range 0-255) cannot be used to represent negative values. The negative scale factor should only be used for test purposes, since the results do not make a physical sense, and some further processing options or modules are excluded in this case, e.g. the value added calculation of surface energy balance components, the automatic spectral classification (SPECL), or the BRDF corrections.

Note: The TIFF format is also allowed for the input file. However, some restrictions apply in this case, compare chapter 6.2.

- All bands in one TIFF file: the channels in the file must have the ascending band order and the maximum number of channels is 9.

- Each band in a separate file: file names must include the band numbers, e.g., "image_band1.tif", "image_band2.tif", etc. Again, the maximum number of bands is restricted to 9. The first band is specified to ATCOR and all bands will be processed automatically.

- An optional keyword *tiff2envi* exists for the ATCOR batch and tiling modes that produces an automatic conversion of the input TIFF file (e.g., "image.tif") into the corresponding ENVI file (e.g., "image_envi.bsq"). This file is used as a temporary input file to ATCOR and it will be automatically deleted when the ATCOR run is finished. Two output surface reflectance files will be generated if *tiff2envi=1*, an ENVI file ("image_envi_atm.bsq") and a TIFF file ("image_atm.tif"). The ENVI output is needed if the spectral classification (SPECL) module is run, otherwise it may be deleted by the user.
  In the interactive ATCOR mode with GUI panels, the default for a TIFF input file is *tiff2envi=1*, i.e., a corresponding input ENVI bsq (band sequential) file is created. In the batch mode, the default for a TIFF input file is *tiff2envi=0*, i.e., the ENVI file conversion is switched off and no intermediate files are created. This will save disk space and some file conversion time. However, if the "image.ini" file specifies the de-hazing or de-shadowing option, then *tiff2envi* is reset to 1 to enable the creation of of the needed additional intermediate ENVI files. For non-TIFF files, the *tiff2envi* keyword is ignored.

Summary of output data types :

- byte (default surface reflectance scale factor = 4.0)
- 16 bit signed integer (scale factor $\geq$ 10.0, typically 10 or 100)
- float (scale factor = 1.0)
- The corresponding negative scale factors (except byte case) provide an output reflectance cube allowing negative surface reflectance values (only recommended in a test phase).

9.3 Preference parameters for ATCOR

The preference parameters are now located in a user specific HOME directory *"~/.idl/rese/atcor3/"*, so multiple users of the same license can retain their personal preference settings. The path of the last input image is saved separately for the flat and rugged terrain versions of ATCOR, i.e., *"preference_atcor2_path.txt"*, and *"preference_atcor3_path.txt"*. In addition, the file *"preference_parameters.dat"* contains a number of default parameters that can be adjusted to scene properties. This file contains the parameters with a short description.

line 1	A choice to set the water vapor values for water pixels: 1 = average water vapor value of land pixels is assigned to water pixels, 2 = line average of water vapor of land pixels is assigned to water pixels. Only available with *iwv_model* = 1, see the job control parameter section 9.4.
line 2	A cloud reflectance threshold T_c (%) in the blue-green region to define a cloud mask. Pixels belong to the cloud mask if : (a1) $\rho^*(blue) > T_c$ or (a2) $\rho^*(green) > T_c$ (asterisk: apparent reflectance) Typical values for T_c range from 15 - 35% . If the cloud reflectance threshold is too high, clouds will be included in the haze mask. This will reduce the performance of the haze removal algorithm.

line 3	A surface reflectance threshold ρ_{w1} (%) for water in the NIR band. Pixels belong to the water mask if $\rho(NIR) < \rho_{w1}$ (only NIR band available).
line 4	A surface reflectance threshold ρ_{w2} for water in the 1600 nm region (if band exists). Pixels belong to the water mask if $\rho(NIR) < \rho_{w1} \quad and \quad \rho_{1600} < \rho_{w2}$. The defaults $\rho_{w1} = 5\% \quad and \quad \rho_{w2} = 3\%$ allow some margin for turbid water.
line 5	interpolate bands in 760 nm oxygen region (0=no, 1=yes)
line 6	interpolate bands in 725 / 825 nm water region (0=no, 1=yes)
line 7	interpolate bands in 940 /1130 nm water region (0=no, 1=yes)
line 8	smooth water vapor map (box 50m*50m) (0=no, 1=yes) The water vapor map is calculated on a pixel-by-pixel basis, a moderate spatial smoothing (50m*50m or at least 3*3 pixels) reduces the noisy appearance.
line 9	interpolate bands in 1400/1900 nm nm water region (0=no, 1=yes)
line 10	cut-off limit for max. surface reflectance (default 150%)
line 11	"_out_hcw.bsq" file (haze/cloud/water/land) (0=no, 1=yes, 2=hcw + quality file)
line 12	water vapor threshold to switch off the cirrus algorithm, unit [cm]
line 13	define saturation with factor b: $DN(saturated) \geq b\ DN(max)$, b=0.9 to 1.
line 14	include non-linear influence of vegetation in water vapor calculation (yes/no)
line 15	start/stop wavelengths for interpolation in the 940 nm region
line 16	start/stop wavelengths for interpolation in the 1130 nm region
line 17	start/stop wavelengths for interpolation in the 1400 nm region
line 18	start/stop wavelengths for interpolation in the 1900 nm region
line 19	haze/sun glint over water: (apparent) NIR reflectance $T_1(clear)$, $T_2(haze)$
line 20	reduce over/under-correction in cast shadow (0=no, 1=yes)

Note on the non-linear influence of vegetation in water vapor calculations:
This option applies to the APDA-regression algorithm and only if the 940 nm region is selected for the water vapor retrieval. The retrieval is based on a linear interpolation across the absorption region, and errors can occur due to the non-linear behavior of the reflectance of vegetated surfaces in this region. A simple empirical correction to the water vapor map W is applied using the NDVI calculated with the apparent reflectances in the red/NIR channels:

$$W(new) = W(old) - 0.1\ (NDVI/0.7) \qquad (cm) \tag{9.2}$$

The correction is only performed for pixels with $NDVI \geq 0.25$ and values $NDVI > 0.7$ are reset to 0.7.

Note on cut-off limit for surface reflectance
The default limit is set to a high value (150% reflectance) to avoid a truncation in spectra of high reflectance surfaces, e.g. snow and/or surfaces with specular reflectance. The previous default cut-off (before 2012) was set to 90%.

Note on factor b:
Factor b is a relative saturation factor applied to the maximum radiometric encoding, e.g. for 8 bit data and b=1 all pixels with DN=255 will be marked as saturated in the "_out_hcw.bsq" file (color coding: red). Setting b=0.9 implies pixels with $DN > 230$ will be considered as saturated or in the non-linear radiometric range close to saturation. This factor is only used for 8 and 16 bit (signed or unsigned) data, not for float or 32 bit data.

Note on the cloud mask:
The criterion (a1) or (a2) is also coupled with the conditions:

$\rho^*(NIR)/\rho^*(red) < 2$ and $\rho^*(NIR)/\rho^*(SWIR1) > 1$ and $NDSI < 0.7$,

where NDSI is the normalized difference snow index. A quality or probability mask for clouds is generated with the above three conditions and different apparent reflectance thresholds T_c in the blue/green spectral region. For $T_c = 15\%$ we define a low probability cloud, $T_c = 25\%$ a medium probability, and $T_c = 35\%$ a high probability cloud. The result is put into a cloud map file named "image_quality.bsq" if the input scene is named "image.bsq". The cloud mask in the "image_out_hcw.bsq" file is based on the user-defined threshold T_c (in the preference parameter file) and the above three conditions.

Note on the water mask:
The NIR band *surface reflectance* threshold for a water mask is only used for sensors without visible bands. For an instrument with visible bands, better water masks are obtained with the criterion that the *TOA reflectance* ρ^* spectrum must have a negative gradient for bands in the visible to NIR :

$$\frac{d\rho^*(\lambda)}{d\lambda} < 0 \qquad for \qquad 0.4 < \lambda < 0.85\ \mu m \tag{9.3}$$

However, for a scene with a high average ground elevation (we use > 1.2 km above sea level) the *TOA reflectance* criterion is again replaced with the NIR *surface reflectance* criterion, because of the distinctly smaller path radiance. The water threshold for a 1600 nm band is always included as the second criterion (if such a band exists).
Sometimes the gradient criterion with eq. 9.3 is not adequate, and the NIR /SWIR1 reflectance thresholds yield a better water mask. This may happen in urban areas containing shadow pixels cast by buildings. Then the NIR/ SWIR1 thresholds have to be defined as negative reflectance values to overwrite the gradient criterion.

The band interpolation options are only intended for hyperspectral imagery. Linear interpolation is employed in the 760, 725, and 825 nm regions. Non-linear interpolation as a function of the vegetation index is applied in the 940 and 1130 nm parts of the spectrum to account for the leaf water content in plants. nterpolation in the strong atmospheric water vapor absorption regions around 1400 nm and 1900 nm is recommended because of the low signal and large influence of sensor noise. However, interpolation can be disabled if required, i.e., for test purposes. If enabled, non-linear interpolation is performed in the 1400 / 1900 nm regions by fitting the surface reflectance curves with a hull of a template vegetation or soil spectrum. All interpolated channels are marked with an '*' in the ENVI header of the output reflectance cube.

Haze or sunglint removal over water: the default apparent reflectance thresholds in the NIR channel for clear water and haze are $T_1(clear) = 0.04$ (or 4%) and $T_2(haze) = 0.12$ (or 12%), respectively. Pixels with values less than $T_1(clear)$ are defined as clear water, pixels with values between the thresholds $T_1(clear)$ and $T_2(haze)$ are assigned as haze (or sun glint). A lower value (i.e., $T_1(clear) < 0.04$) can be can be specified, but might cause a wrong classification of bright coastal water (sandy bottoms and bleached coral waters). If the threshold $T_1(clear)$ is too high, haze pixels might erroneously be put into the clear water category.

Cast shadow areas (mountainous terrain): these may contain over- and/or undercorrected pixels during the standard empirical BRDF correction. A reduction of these pixels is tried with the following steps:

- bright pixels in the NIR with $DN > DN(mean) - \sigma$, σ=standard deviation, are removed from the list of shadow pixels.
- a 7 x 7 pixel convolution filter is being applied to the shadow mask.
- a transition region shadow/sunlit is introduced.
- already dark pixels ($DN < DN(mean) - \sigma$ in the NIR) are not reduced in brightness during BRDF correction. The threshold is evaluated for a NIR channel, but the non-reduction of brightness (reflectance) is applied to all channels.

9.4 Job control parameters of the "inn" file (former "ini")

If the file name of the input image is *"example_image.bsq"* then a file *"example_image.inn"* is created during the interactive ATCOR session. When all image processing parameters have been defined by the user this *"inn"* file is written to the directory of the corresponding image. When the image is re-loaded during a later session, or when a batch job is submitted, all input parameters are read from this file. It is suggested not to edit this file, because it might create inconsistent input data. The file might contain empty lines when input is not required for a specific case. The IDL routine for writing this file is available on request for users who want to run ATCOR batch jobs without employing the interactive GUI panels. The contents of an *"inn"* file are:

line 1:
20/08/1989 Date (dd/mm/year) i.e., 20/08/1989 occupies the first 10 columns.

line 2:
10.0 ; scale factor reflectance

line 3:
5.0 ; pixel size [m]

line 4:
landsat4_5, Landsat-4/5 TM,
sub-directory "../atcor2+3/cal/landsat4_5", sensor text as defined in "../atcor2+3/bin/sensor.dat"

line 5:
1.0 ; gain setting
Any positive value is accepted, this gain setting g is used to replace the c_1 in the corresponding ".cal" file with c_1/g, where g is the same for all channels.

line 6:
calfile ; calibration file name

line 7:
0.9500, 0 ; iemiss, dem_unit (surface emissivity, DEM height unit)

iemiss = surface emissivity option or value, disregarded if no thermal band exists.

iemiss = 0 invokes $\epsilon = 0.98$ to be consistent with the definition of earlier ATCOR versions.
Since iemiss=1 is reserved for the cover-dependent emissivity setting below, ϵ=1.0 has to be approximated as iemiss=0.999 or iemiss=0.9999.
In case of multiple thermal bands this ϵ holds for the thermal band *itemp_band* employed for the surface temperature evaluation, see chapter 4.6.

iemiss = 1 : fixed values of surface emissivity = 0.98 (water), 0.97 (vegetation), 0.96 (soil).
iemiss = 2 : same as iemiss=3, (the iemiss=2 option of ATCOR4 is not supported here).
iemiss = 3 : NEM or ANEM method, requires multiple thermal bands, see chapter 10.1.4.
iemiss = 4 : ISAC method, requires multiple thermal bands, see chapter 10.1.4.
iemiss = 5 : both NEM and ISAC, but ISAC is currently only supported for flat terrain imagery.

dem_unit : 0 = [m], 1 = [dm], 2 = [cm] DEM height unit

line 8:
fele ; DEM elevation file name (empty line for a flat terrain calculation)

line 9:
fslp ; DEM slope file name (empty line for a flat terrain calculation)

line 10:
fasp ; DEM aspect file name (empty line for a flat terrain calculation)

line 11:
fsky ; DEM skyview file name (empty line for a flat terrain calculation)

line 12:
fshd ; DEM cast shadow file name (empty line for a flat terrain calculation, rugged terrain: empty if calculated *"on-the-fly"*)

line 13:
atmfile ; atmospheric LUT file name (reflective region)

- If the automatic aerosol type retrieval is intended for batch jobs, the usual aerosol identifier in the file name (e.g. 'rura') has to be replaced with 'auto'. Example: file name (without path) is *'aamsrura.atm'*, replace it with *'aamsauto.atm'*. The program then uses all aerosol types for the 'ms' = mid-latitude summer atmosphere in the aerosol type estimate, and selects the one with the closest match, compare chapter 10.4.2. In the example of the 'ms' case four aerosol types (rural, urban, maritime, desert) are checked. In case of the 'tr' = tropical atmosphere, only three aerosol types (rural, urban, maritime) will be found in the atmospheric library. The automatic aerosol type retrieval requires the parameter npref=1 (variable visibility, see line 20 below). If npref=0, it is reset to npref=1.
  In the interactive mode the user can just press the 'Aerosol Type' button on ATCOR's main panel to execute the aerosol type retrieval, irrespective of the '*.atm' name in the '.inn' file.

line 14:
temfile ; atmospheric LUT file name (thermal region, empty if no thermal band)

line 15:
1.0 ; adjacency range [km]

line 16:
35.0 ; visibility [km]

line 17:
0.7 ; mean ground elevation ([km asl] not used in case of rugged terrain, where elevation file applies

line 18:
33.0, 178.0 ; solar zenith, solar azimuth angle [degr.]

line 19:
10.0, 150.0 ; off-nadir sensor tilt angle , sensor view azimuth angle [degr.]
For nadir-looking sensors the tilt angle is zero and the view azimuth is an arbitrary value.

line 20:
0, 0, 1, 0, 0, 0, 1 ; npref, iwaterwv, ihaze, iwat_shd, ksolflux, ishadow, icl_shadow
seven parameters controlling the processing options:
npref = 0 : constant visibility
npref = 1 : variable visibility, based on dark reference areas in the scene
npref =-1 : variable visibility for each sub-image during batch job with tiling
iwaterwv = 0 : no water vapor correction or no water vapor bands available
iwaterwv = 1 : water vapor correction using bands in the 940 nm region
iwaterwv = 2 : water vapor correction using bands in the 1130 nm region
iwaterwv = 3 : 940 and 1130 nm bands are employed

- Haze removal is enabled by setting the parameter *ihaze>0*, no haze removal is specified with *ihaze=0*. Separate parameter values define haze removal over land, haze/sunglint removal over water, and the combination. Some criteria exist to check whether the haze/land removal is likely to yield good results. The haze/land algorithm is switched off if those criteria are not passed (*ihaze=1*). However, as these criteria might fail in certain cases, there is the option of setting *ihaze=-1* which enforces the haze removal disregarding the termination criteria.

ihaze = 0 : no haze correction
ihaze = 1 : haze/land correction, might be switched off if quality check criteria are not passed
ihaze = 2 : haze over water removal (requires clear water pixels)
ihaze = 3 : haze/land and haze/water removal
ihaze = 4 : sun glint removal over water
ihaze =-1 : haze/land correction is executed disregarding quality checks
ihaze =-2 : is treated as ihaze=2
ihaze =-3 : haze/land removal is forced, haze/water removal needs clear water pixels

Haze removal is performed for the visible bands, sun glint removal for all bands.

iwat_shd = 0 : water pixels are excluded from de-shadowing (land), default
iwat_shd = 1 : water pixels are included in de-shadowing (land)

The option *iwat_shd = 1* might be useful if the internal water classification based on purely spectral critera fails, and dark land pixels are classified as water (which is excluded from de-shadowing). So this flag is only used if the de-shadowing option is set and if no external water map is supplied. Example: scene is *"image1.bsq"*, and a file *"image1_water_map.bsq"* or *"image1_hcw.bsq"* exist in the same folder, then the flag *iwat_shd* is ignored because an external water map always has the first priority.

ksolflux = 0 : file with value added channels not calculated
ksolflux = 1 : value added channels are calculated (*.flx file)

ishadow = 0 and fshd=" (empty string): no DEM cast shadow map is used
ishadow = 0 and fshd="valid file name": pre-calculated DEM cast shadow file is used
ishadow = 1 : DEM cast shadow mask is calculated "on-the-fly"
The pre-calculated map avoids repeated on-the-fly calculations.

icl_shadow = 0 : no cloud/building shadow correction
icl_shadow > 0 : cloud/building shadow correction is performed
= 1 : de-shadowed output as DN image corresponding to input DN scene
= 2 : de-shadowed output as surface reflectance image
= 3 : de-shadowed output as surface reflectance and DN image

line 21:
0, 0.5, 0.5 : itriang, ratio_red_swir, ratio_blu_red
itriang = 0 : average vis. index of reference areas is employed for non-reference pixels
itriang = 1 : triangular interpolation of visibility index of reference areas

ratio_red_swir : ratio of surface reflectance of red to 2.2 μm band for the reference pixels
If no 2.2 μm band exists, but a 1.6 μm band, the ratio holds for the red-to-1.6 μm band.
If only VNIR bands exist (400 - 1000 nm) the ratio holds for the red-to-NIR band.
ratio_blu_red : ratio of surface reflectance of blue band to red band for the reference pixels.

line 22:
0, 65.0, 0.25 ; ibrdf, beta_thr, thr_g, parameters for BRDF correction in rugged terrain
For a flat terrain, these parameters are not used.

- ibrdf = 0 : no empirical BRDF correction (or flat terrain)
- ibrdf = 1 : correction with cosine of local solar zenith angle (eq. 10.80 with b=1)
- ibrdf = 2 : correction with sqrt(cos) of local solar zenith angle (eq. 10.80 with b=1/2)
- ibrdf = 11 : correction with cosine of local solar zenith angle (eq. 10.80 with b=1), for soil/sand. Vegetation: eq. 10.80 with exponent b=3/4 and b=1/3 for $\lambda < 720$ nm and $\lambda > 720$ nm, respectively, i.e., option (a) in the BRDF panel, see Figure 5.31 ("weak" correction),
- ibrdf = 12 : correction with cosine of local solar zenith angle (eq. 10.80 with b=1), for soil/sand. Vegetation: eq. 10.80 with exponent b=3/4 and b=1 for $\lambda < 720$ nm and $\lambda > 720$ nm, respectively, i.e., option (b) in the BRDF panel, see Figure 5.31 ("strong" correction),
- ibrdf = 21 : correction with sqrt(cos) of local solar zenith angle (eq. 10.80 with b=1/2), for soil/sand. Vegetation: eq. 10.80 with exponent b=3/4 and b=1/3 for $\lambda < 720$ nm

and $\lambda > 720$ nm, respectively, i.e., option (a) in the BRDF panel, see Figure 5.31 ("weak" correction). This is the recommended standard yielding good results in most cases.

- ibrdf = 22 : correction with sqrt(cos) of local solar zenith angle (eq. 10.80 with b=1/2), for soil/sand. Vegetation: eq. 10.80 with exponent b=3/4 and b=1 for $\lambda < 720$ nm and $\lambda > 720$ nm, respectively, i.e., option (b) in the BRDF panel, see Figure 5.31 ("strong" correction).
- beta_thr : threshold local solar illumination angle β_T where BRDF correction starts. If beta_thr=0 (and $ibrdf > 0$) then the angle β_T is calculated in ATCOR depending on the solar zenith angle and its value can be found in the corresponding "*_atm.log" file.
- thr_g : g, lower boundary of BRDF correction factor, see chapter 2.2, eq. (2.12, and chapter 10.5.1)

line 23:
1, 0.820, 0.780, 0.600 ; lai_model, a0_vi, a1_vi, a2_vi
Parameters for the LAI model to be used if ksolflux > 0, see chapter 7

line 24:
0.900, 0.950, 0.380 ; c_fpar, a_fpar, b_fpar
parameters for the fpar model to be used if ksolflux > 0, see chapter 7

line 25:
20.0, 0.83 ; air temperature (C), air emissivity, see chapter 7
Parameters for the net flux calculation (used for flat terrain, ignored for rugged terrain)

line 26:
20.0, 0.50, 0.65, 15.0, 6.3 ; t_air, z0_ref, tgradient, p_wv, zh_pwv, see chapter 7
t_air : air temperature (Celsius) at elevation z0_ref
z0_ref : reference elevation for t_air [km asl]
tgradient : air temperature gradients (Celsius per 100 m height)
p_wv : ([mb or hPa], default, water vapor partial pressure at z0_ref)
zh_pwv : ([km], scale height of water vapor, exponential decrease falls to 1/e value)
Parameters for the net flux calculation (rugged terrain, ksolflux > 0)
These are dummy values (not used) if ksolflux=0, or for a flat terrain.

line 27:
2, 2 ; ihot_mask, ihot_dynr , parameters for haze correction
ihot_mask = 1 : small area haze mask
ihot_mask = 2 : large area haze mask
ihot_dynr = 1 : thin to medium haze levels are corrected
ihot_dynr = 2 : thin to thick haze levels are corrected

line 28:
2, -0.500, 0.12, 0.08, 1 ; iclshad_mask, thr_shad, phi_unscl_max, phi_scl_min, istretch_type
Parameters for correction of cloud/building shadow effects, if icl_shadow > 0
Default values are put in this line even if icl_shadow=0
iclshad_mask = 1,2,3 : small, medium, large cloud shadow mask
thr_shad = -0.500 : threshold for core shadow areas, -999 means threshold is calculated from image histogram

phi_unscl_max : max of unscaled shadow function Φ_{max}, see chapters 2.5, 10.5.5.
phi_scl_min : min of scaled shadow function Φ^*_{min}, see chapters 2.5, 10.5.5.
istretch_type: 1=linear stretching, 2=exponential stretching of Φ into Φ^*.

line 29:
ch940(1:6) vector with 6 channel numbers for the 940 nm water vapor retrieval
ch940(1) : left window channel (850 - 890 nm)
ch940(2) : right window channel (850 - 890 nm)
ch940(3) : left absorption channel (920 - 970 nm)
ch940(4) : right absorption channel (920 - 970 nm)
ch940(5) : left window channel (1000 - 1040 nm)
ch940(6) : right window channel (1000 - 1040 nm)
The left and right channel numbers for each window or absorption region may be the same. Put in a zero channel number if not applicable.

line 30:
ch1130(1:6) vector with 6 channel numbers for the 1130 nm water vapor retrieval
ch1130(1) : left window channel (1050 - 1090 nm)
ch1130(2) : right window channel (1050 - 1090 nm)
ch1130(3) : left absorption channel (1110 - 1155 nm)
ch1130(4) : right absorption channel (1110 - 1155 nm)
ch1130(5) : left window channel (1200 - 1250 nm)
ch1130(6) : right window channel (1200 - 1250 nm)
The left and right channel numbers for each window or absorption region may be the same. Put in a zero channel number if not applicable.

line 31:
chth_w1, chth_a1, chth_a2, chth_w2 bands for thermal water vapor retrieval (9-12 μm region)
chth_w1 : left window channel (split-window covariance-variance method SWCVR)
chth_w2 : right window channel
chth_a1 : left absorption channel
chth_a2 : right absorption channel

line 32:
e_water, e_veget, e_soil, e_sand surface emissivities (adjusted NEM, channel with Tmax)

line 33:
0 iwv_model (water vapor retrieval: 1=no band regression, 2=band regression)
The choice iwv_model = 0 indicates the water vapor retrieval is disabled. Option 1 means the water vapor retrieval is performed for the selected bands, and in case of several measurement bands the one with the smallest standard deviation is selected (per 940 and 1130 nm region). Finally, if both regions are active, the average of the water vapor maps of both regions is taken. Option 2 employs a linear regression of bands which yields better results for the water vapor map if the data is noisy or not accurately calibrated. If iwv_model = 2 and channels in the 940 nm and 1130 nm regions are specified, then only the 940 nm region is evaluated with a linear regression of bands. If the regression is intended for the 1130 nm region, then the 940 nm channels (all channels in line 29) have to be specified as 0.

line 34:
0 icirrus flag for cirrus removal (0=disabled, 1=enabled, -1=forced)
The value icirrus = -1 enforces cirrus detection and removal, i.e., termination criteria are ignored.

line 35:
0 irrad0 flag for solar flux on ground (0=disabled, 1=enabled)
For *irrad0=2* the surface reflected (leaving) radiance is calculated additionally.
For a flat terrain, ASCII spectra of the direct, diffuse, and global flux on the ground are provided in the folder of the input scene, see chapter 10.1.3. In case of a flat terrain the global (i.e. direct plus diffuse) flux image is calculated. For a rugged terrain the images of the direct and diffuse fluxes are calculated. Note: as the flux files have to use a float encoding (32bits/pixel) the file size is twice or four times the size of the input scene for a 16bit/pixel and 8bit/pixel input scene, respectively.

Notice concerning visibility iterations:
ATCOR will automatically iterate the initial visibility (parameter *visib* set in the *'.inn'* file) if the number of negative reflectance pixels is larger than 1% of the scene for the red band (around 650 nm, vegetation is checked here) or the NIR band (around 850 nm, water is checked here). The specified visibility is always kept if the visibility is set to a negative value, i.e., *visib=-20* means the program performs the calculation with *visib=20 km* and does not iterate even if a large number of negative reflectance pixels occurs.

If the parameter npref is set to 1 the program computes the visibility map based on dark reference pixels in the scene and npref=1 overwrites the initial value of the *visib* parameter. With npref=1 the program still iterates the average visibility of the visibility map by checking for water pixels in the NIR band unless the specified *visib* is negative. A constant scene visibility is employed for npref=0. In case of scene tiling and npref=0 or npref=1 the iterated visibility obtained for sub-scene 1 is also applied to all other sub-scenes to avoid brightness steps for the merged sub-scenes caused by potentially different visibilities.
Attention : If scene tiling has to be performed and the aerosol map is requested for each sub-image then specify npref=-1, but this could cause different average visibilities in the sub-scenes and potentially brightness steps at the sub-scene borders.

9.5 Problems and Hints

Some often encountered problems and tips to come around are listed here.

- *Distinction of haze and cloud, when can the haze removal algorithm be applied ?*
  Ground surface information under haze areas can still be recognized in the 600-900 nm region, but the brightness contrast is low. The haze removal is only applied for channels in the 400 - 800 nm region. However, for cloud areas no ground information can be observed. If in doubt whether a certain area should be assessed as haze or cloud covered, take a look at the scene in the NIR (around 850 nm) channel: if surface features can be seen in this area, the haze algorithm might be applied. If not, the area is cloud covered and a haze removal run will not be successful.

- *The cloud mask is not appropiate.*
  The cloud mask might contain too few pixels: then decrease the cloud reflectance threshold in the *../atcor/preferences/preference_parameters.dat* file. The default threshold is 25% re-

flectance in the blue-green spectrum. The opposite case can also happen: if the cloud mask comprises too many pixels the threshold has to be raised.

- *The haze mask is not appropiate.*
  This problem may be connected with the setting of the cloud threshold. If the cloud threshold is too high, cloud pixels are counted as haze, and the results of the haze removal are bad because the haze algorithm is applied to clouds.

- *The water mask is not appropiate.*
  This might lead to problems for the haze removal as well as the cloud/building shadow removal, i.e., water is erroneously counted as land and included in the land mask. Enable the output of a haze/cloud/water map, compare Fig. 4.15, to check the water mask. Read chapter 4.8. There are two possibilities to define the water mask:

  – If the average ground elevation of the scene is below 1.2 km, the default option for calculating the water mask is the negative gradient criterion for the apparent reflectance in the VNIR region (see eq. 9.3). This yields the best water map in most cases. However, in some cases (urban areas with shadows cast by buildings) the NIR/ SWIR1 water surface reflectance thresholds (see chapter 9.3) yield better results. If the average scene elevation is below 1.2 km, one has to define negative reflectance values to both (NIR/SWIR1) thresholds to overrule the default negative gradient criterion. In the latter case, an increase/decrease of the absolute value of the thresholds will increase/decrease the number of water pixels.
    Attention concerning de-shadowing: if this option is set and if the negative gradient criterion for the water mask is enabled and if the percentage of water pixels is greater than 15% of the scene, then the de-shadowing algorithm assumes that the large percentage of water pixels is caused by the inadequate gradient criterion. Then, in the de-shadowing part the NIR/ SWIR1 water surface reflectance thresholds are used, which can be set high to reduce the percentage of (wrongly classified) water pixels, because these are likely shadow areas (and water pixels will not be de-shadowed). However, if an external water map exists (either from file *image_hcw.bsq"* or *image_water_map.bsq"* if *"image.bsq"* is the file name of the scene) and this file indicates more than 15% of water pixels then this information is regarded as reliable and this water map is excluded from de-shadowing.
  – If the average scene elevation is above 1.2 km, the gradient criterion cannot be applied and the NIR/ SWIR1 water surface reflectance thresholds apply as defined in the preference parameter file (chapter 9.3). These surface reflectance thresholds can be defined as positive values (as the gradient criterion in not valid, anyway) or as negative. An increase/decrease of the thresholds will increase/decrease the number of water pixels.

- *Rugged terrain: the slope and illumination maps show strong horizontal and vertical stripes.*
  Strong artifacts in the DEM files will immediately be visible in the atmospherically / topographically corrected surface reflectance image. This problem frequently occurs for resampled DEMs, e.g. the original DEM resolution is 30 m, which is resampled to a 5 m pixel size. Artifacts will be enhanced, especially if the stepsize of the original DEM (height resolution) is coded as integer. Float data would have smoother transitions. A simple way to get better results is the use of a larger kernel size for the slope/aspect calculation, e.g., kernel=5 or kernel=7 instead of the default kernel=3 (pixels), but this approach causes a reduction of the high frequency spatial information.
  Attention: in addition to using float data before resampling, it is recommended to calculate the slope/aspect maps on the original (coarse spatial resolution) data, followed by the

high-resolution resampling step for all DEM files (elevation, slope, aspect). Do not employ the sequence of resampling the elevation, followed by a slope/aspect calculation of the high-resolution elevation map, because this approach enhances artifacts!
Steps to reduce slope/aspect striping:

1. FLOAT(ELEVATION file) (if it is stored as integer)
2. Calculate SLOPE (and also ASPECT) with a low pass filter 5x5 pixels
3. Resize SLOPE (ASPECT) file: factor 4 larger
4. Convolve (lowpass 7x7 pixels)
5. Resize with factor 0.25 using nearest neigbor to obtain original size.

Note that the function *DEM Smoothing* 5.4.4 allows an efficient DEM smoothing.

- *Landsat and ASTER thermal band processing.*
The thermal band(s) are sensitive to the atmospheric water vapor column. However, the thermal band atmospheric LUTs (US-standard, mid-latitude summer, tropical etc) only provide a discrete set of water vapor columns (u), see chapter A. If the nearest u value from this set deviates more than 0.2-0.3 cm from measured data (e.g. radiosonde profile) the user may generate a new thermal LUT with a water vapor column u as a linear combination of two existing LUTS with water vapor contents u_1 and u_2 : $u = w_1 u_1 + (1 - w_1)\ u_2$. Example: u = 2.4 cm, $u_1 = 2.08\ cm$ (subarctic summer), $u_2 = 2.92\ cm$ (mid-latitude summer), then $w_1 = (u_2 - u)/(u2 - u_1) = 0.619$. This manipulation can be performed in the SPECTRA module after pressing the button "Mixing of Atmospheres". There, the user has to select two existing atmospheric files, defines the weight w_1, and assigns a file name to the new mixed LUTs. This file can be loaded from the main ATCOR panel.
If no atmospheric water vapor information is available, but lake temperature measurements exist, the user can define an appropriate temperature offset k_0 to match the satellite-derived temperature and the water body temperature. The corresponding panel ("Surface Radiance to Temperature Conversion") pops up when the SPECTRA module or the image processing options are entered.

9.6 Metadata files (geometry and calibration)

This section explains how the geometry and calibration information of various sensor-specific metadata files has to be interpreted for use in ATCOR. Besides the atmospheric LUTs for the nadir view, there are files for off-nadir view geometries covering tilt angles from 0° to 50° (increment 10°) and relative azimuth angles from 0° (backscatter) to 180° (forward scatter) with an increment of 30°, the *"phase_fct*.bin"* files in the ATCOR directory. A corresponding tilt/azimuth angle interpolation of the LUTs is automatically done.

9.6.1 Landsat-7 ETM+

For ETM+ two types of metadata files are distributed. The first type contains the min/max radiance for each band, e.g., Lmax_band1 = 191.6, Lmin_band1 = -6.2, from which the radiometric offset c_0 and slope or gain c_1 for ATCOR's ".cal" file are calculated as :

- $c_0 = 0.1 * Lmin$, and $c_1 = 0.1 * (Lmax - Lmin)/255$.

The factor 0.1 converts from the ETM+ radiance unit $Wm^{-2}sr^{-1}\mu m^{-1}$ into the ATCOR radiance unit $mWcm^{-2}sr^{-1}\mu m^{-1}$. The second type of meta file (fast format, metafile *.fst) specifies the "bias" and "gain" values directly (line with "biases and gains in ascending band number order"), again the factor 0.1 is required to convert into the ATCOR radiance unit: c_0 = 0.1 * bias, and c_1 = 0.1 * gain.

Different types of processing are used in the NLABS and LPGS environments, see the comprehensive article [34]. The general equations to convert the digital number DN into an at-sensor radiance are

$$L = B + G \cdot DN \tag{9.4}$$

$$B = Lmin \; - \; \Big(\frac{Lmax - Lmin}{Qmax - Qmin}\Big) \; Qmin \tag{9.5}$$

$$G = \frac{Lmax - Lmin}{Qmax - Qmin} \tag{9.6}$$

where B = bias, G = gain, and Qmin=1, Qmax=255 for LPGS processing starting at December 8, 2008, while Qmin=0 and Qmax=255 is used for the previous NLAPS processing. The factor 0.1 is required to convert into the ATCOR radiance unit, i.e., c_0 = 0.1 * B, and c_1 = 0.1 * G.

For the thermal band two files, e.g. "xxx_nn61.tif" and "xxx_nn62.tif", are included per scene, the "61" indicates the low gain, the "62" indicates the high gain data. Either one can be selected for ATCOR, but an update of the corresponding thermal "bias" and "gain" from the meta file is required in the radiometric calibration ".cal" file.
Notice: the standard negative offset values often lead to negative surface reflectances for dark targets, therefore in many cases the magnitude of the negative offset has to be decreased, typically by a factor 2 (ETM bands 1-4).

Note concerning Landsat-4/5 TM :
A difficult topic: there is no standard header format with metadata. Different formats existed in the past, depending on Landsat processing station and year of processing. The radiometric calibration is varying as a function of the day after launch, compare references [82], [33]. A file *cal_gain_table_kamstrup_hansen.dat* is available on the directory "../atcor/cal/landsat4_5" containing the gain=c1 values for 1985-2005 for bands 1-4 calculated with the regression equation of [33]. Other publications deviate 10 - 20% from the Kamstrup-Hansen c1 values. However, for reprocessed NLABS / LPGS Landsat-4 or Landsat-5 TM data, equations 9.4 to 9.6 are also valid.

9.6.2 SPOT

The metadata is specified in two files, a VOL_LIST.PDF and a METADATA.DIM. The first file is intended for a quick overview, the second file contains the complete set of specifications. The absolute calibration gains for each band can be taken from either file and should be put into the corresponding ".cal" file as they are. In the METADATA.DIM file the calibration gains are named *PHYSICAL_GAIN*. The SPOT unit is $1/\left[Wm^{-2}sr^{-1}\mu m^{-1}\right]$, but it is automatically converted into the ATCOR radiance unit. The standard offset values are zero. Occasionally however, for SPOT-4/5 data a slightly negative offset has to be introduced for band 4 (1.6 μm) in cases when the scene water reflectance is too high (it should be close to zero).

The geometry of data acquisition is described in the the METADATA.DIM file. The solar geometry is specified with the solar elevation and azimuth angle. The sensor tilt geometry is defined by the incidence angle θ_I at the earth's surface, or the corresponding sensor tilt/view angle θ_V at the orbit altitude h, see Fig. 9.5. Both angles are specified in the METADATA.DIM, but the tilt angle is input to ATCOR. The tilt/view angle is not included in old versions of METADATA.DIM, but was added later. For a given incidence angle the corresponding tilt/view angle can be calculated as :

$$\theta_V = arcsin\Big[\frac{R_E}{R_E + h} sin(\theta_I)\Big]\ 180/\pi \tag{9.7}$$

where $R_E = 6371$ (km) is the earth radius and h=832 (km) is the SPOT orbit altitude. Example: incidence angles of 5°, 10°, 20°, 30° correspond to view angles of 4.4°, 8.8°, 17.6°, and 26.2°, respectively.

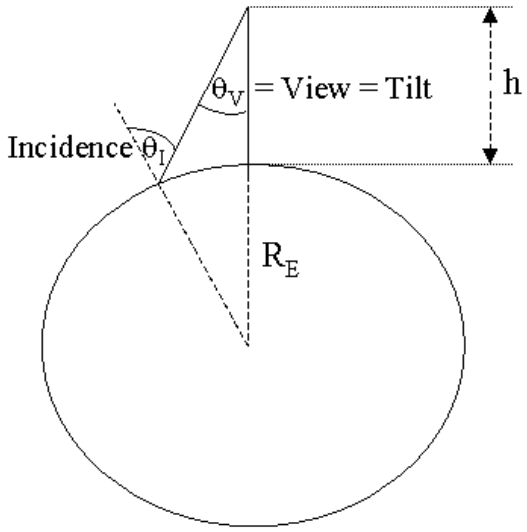

Figure 9.5: *SPOT orbit geometry.*

In addition to the tilt angle the view direction with respect to the flight path is specified. Nearly all SPOT data (99.9%) is recorded in the descending node, i.e., flying from the north pole to the equator (indicated by a negative value of the velocity vector for the Z component in the METADATA.DIM). Then a positive incidence (tilt) angle in METADATA.DIM means the tilt direction is left of the flight direction ("east" for the descending node). This is indicated by an "L" in the incidence angle in VOL_LIST.PDF, e.g. incidence angle L20.6 degree. A negative incidence angle means the sensor is pointing to the "west" (coded as R=right in the VOL_LIST.PDF, e.g. incidence angle R20.6 degree). For ATCOR the satellite azimuth as seen from the recorded image has to be specified. If α denotes the scene orientation angle with respect to north (see Fig. 9.6) then the satellite azimuth angle ϕ_V as viewed from the scene center is :

- $\phi_V = \alpha + 270°$ if tilt/incidence angle is positive (L=left case, "east")
- $\phi_V = \alpha + 90°$ if tilt/incidence angle is negative (R=right case, "west")

Attention:

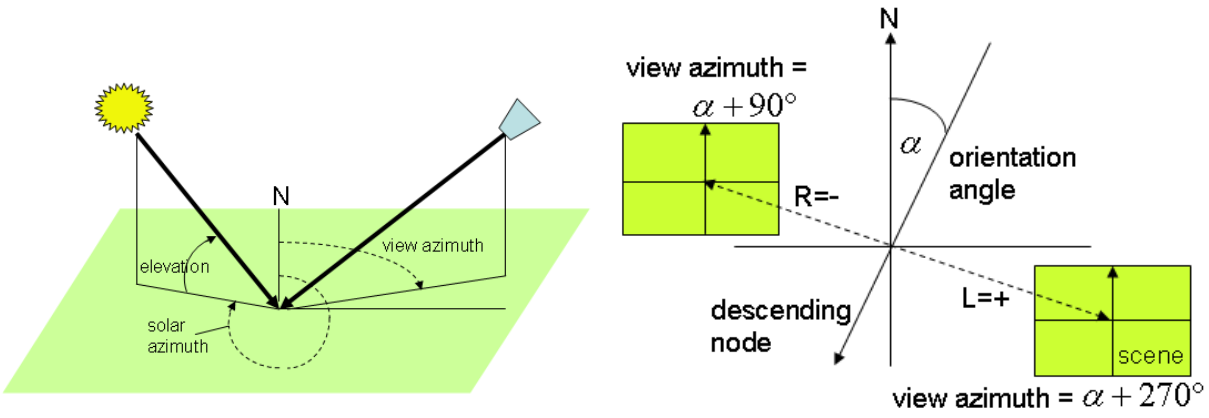

Figure 9.6: *Solar and view geometry.*

- Tricky: The orientation angle is specified in the VOL_LIST.PDF, but does not show if the METADATA.DIM is viewed with an XML browser. However, it is included in the METADATA.DIM and can be found when the file is opened with an editor. On the other hand, the view angle is not included in the VOL_LIST.PDF, but is displayed with an XML browser applied to METADATA.DIM .
- SPOT-4/5 imagery is usually delivered in the DIMAP format, a tif file with the band sequence 3/2/1/4, NIR/Red/Green and 1.6 μm. The wavelength increasing sequence has to be created before offering the file to ATCOR.

Attention:
Old SPOT-2 imagery are usually distributed in the CAP format. For this old format the SPOT leader file and the voldir.pdf indicate: "L - instrument looks to west" and "R - instrument looks to east". This is a header coding error, it is just vice versa, so interpret L = east, R = west.

9.6.3 ALOS AVNIR-2

The ALOS satellite has a sun-synchronous orbit of 690 km and among other instruments carries the AVNIR-2 optical payload. AVNIR-2 has four spectral channels (blue, green, red, NIR) with a nadir resolution of 10 m. The instrument has a ±44° across-track tilt capability. Different metafiles are available, one is in the DIMAP format. It contains the relevant geometric and radiometric parameters. The convention for the tilt and orientation angles is similar to SPOT, compare Fig. 9.6, i.e., a tilt left (with respect to flight direction) is coded as 'L' (tilt angle > 0), a tilt right is coded as 'R' (tilt angle < 0). The radiometric calibration coefficients are given in the unit $mWm^{-2}sr^{-1}nm^{-1}$, thus they have to be multiplied with 0.1 to convert them into the unit $mWcm^{-2}sr^{-1}\mu m^{-1}$ used by ATCOR.

9.6.4 Ikonos

Ikonos metadata files look like "po_3964_metadata.txt" where the po indicates the project order and the following number the project number. The meta data include the geographic coordinates and the solar elevation and azimuth angles. The sensor can tilt into any direction, and the satellite geometry as viewed from the scene center is specified with :

- Nominal Collection Azimuth : absolute azimuth view angle, e.g.. east = 90°.
- Nominal Collection Elevation.

ATCOR's tilt angle can be calculated from equation 9.7 with the Ikonos orbit altitude 680 km. The tilt angle is close to the "incidence=90-elevation", see Table 9.1.

elevation (degree)	incidence (degree)	tilt (degree)
90	0	0.0
85	5	4.5
80	10	9.0
75	15	13.5
70	20	18.0
65	25	22.4
60	30	26.9
55	35	31.2

Table 9.1: *Elevation and tilt angles for Ikonos.*

Ikonos offers a radiometric calibration L = DN / calcoef where calcoef is specified in the in-band radiance unit $mWcm^{-2}sr^{-1}$, see http://www.spaceimaging.com/products/ikonos/spectral.htm. For post 22 February 2001 scenes with 11 bit data calcoef is specified as 728, 727, 949, and 843 (blue, green, red, NIR band, respectively). These values have to be converted into c1 = 1 / (calcoef*bandwidth) and are stored in the "ikonos_2001_std.cal" standard calibration file.

9.6.5 Quickbird

The metadata files are named "*.IMD". They contain the geographic coordinates. The "sunEl" and "sunAz" keywords (or "meanSunEl" and "meanSunAz") specify the solar elevation and azimuth angle, respectively. Similar to Ikonos, the sensor can tilt into any direction. The satellite geometry as viewed from the scene center is specified with "satEl" or "meanSatEl" (satellite elevation angle), and "satAz" or "meanSatAz" (absolute azimuth angle). ATCOR's tilt angle can be calculated from equation 9.7 with the Quickbird orbit altitude 450 km. The tilt angle is close to the "incidence=90-satEl" value, see Table 9.2. Depending on the processing date, the tilt angle may also be included in the ".IMD" file, then it is named "offNadirViewAngle" or "meanOffNadirViewAngle".

elevation (degree)	incidence (degree)	tilt (degree)
90	0	0.0
85	5	4.7
80	10	9.3
75	15	14.0
70	20	18.6
65	25	23.2
60	30	27.8
55	35	32.4

Table 9.2: *Elevation and tilt angles for Quickbird.*

The Quickbird sensor uses the radiance unit $Wm^{-2}sr^{-1}$ (in-band radiance) which can be converted into a spectral (band-average) radiance employing the effective bandwidth of each channel,

specified as $\Delta\lambda = 0.068$, 0.099, 0.071, and 0.114 μm for the blue, green, red, and NIR band, respectively (reference [46] from http://www.digitalglobe.com). The calibration is different for compressed 8-bit data and the original 11-bit data. ATCOR contains a template for an 8 bit .cal file ("quickb_8bit_std.cal") and an 11 bit file ("quickb_16bit_std.cal"). However, it is recommended to use only the 11 bit data for ATCOR. The ".IMD" metadata file contains the absolute calibration factor (absCalFactor) for each multispectral channel in the unit $Wm^{-2}sr^{-1}$. Depending on processing date, the "effectiveBandwidth" $= \Delta\lambda$ (μm unit) is also included. The nominal offset is $c_0 = 0$ in each channel, and the ATCOR gain c_1 has to be specified in the unit $Wcm^{-2}sr^{-1}\mu m^{-1}$ which requires the following conversion equation for Quickbird:

- $c_1 = \frac{absCalFactor * 0.1}{\Delta\lambda}$.

Therefore, the template calibration file has to be updated, i.e., copied to a new file name, and edited according to the absCalFactor of the scene IMD file and the above spectral bandwidth values $\Delta\lambda$.

9.6.6 IRS-1C/1D Liss

The metadata file contains the geographic coordinates as well as the solar elevation and azimuth angles. It also includes the radiometric calibration coefficients, the bias $B = L_{min}$ and gain $G = L_{max}$ in the ATCOR radiance unit $mWcm^{-2}sr^{-1}\mu m^{-1}$. The radiometric coefficients for ATCOR's ".cal" file have to be calculated as

- $c_0 = Lmin$, and $c_1 = (Lmax - Lmin)/255$.

9.6.7 IRS-P6

The IRS-P6 platform carries three optical sensors: the AWiFS (advanced wide-field-of-view sensor), the Liss-3, and the Liss-4. AWiFS (60 m resolution) and Liss-3 (20 m) have the same spectral bands (green, red, NIR, and SWIR1 at 1.6 μm), the LISS-4 (red band) serves as the high-resolution camera (5 m). Similar to the IRS-1C/1D, the radiometric calibration coefficients are included in the meta file: the bias $B = L_{min}$ and gain $G = L_{max}$ are specified in the unit $mWcm^{-2}sr^{-1}\mu m^{-1}$, and the nominal value of L_{min} is zero. For each sensor (AWiFS, Liss-3, Liss-4) the calibration coefficients seem to be constant with time, i.e., independent of the scene, based on laboratory calibration. The radiometric coefficients for ATCOR's ".cal" file have to be calculated as

- $c_0 = Lmin$, and $c_1 = (Lmax - Lmin)/b$.

where b=1023 for AWiFS (10 bit data encoding), and b=255 for Liss-3 and Liss-4 (8 bit encoding). The analysis of a couple of scenes showed that a non-zero bias c_0 is required to obtain reasonable surface reflectance spectra. Therefore, typical average bias values are included in the standard "*.cal" file for each sensor. A fine tuning of the calibration coefficients may be necessary to obtain better agreement between scene-derived surface reflectance spectra and library or ground measured spectra.

9.6.8 ASTER

ASTER has 9 reflective and 5 thermal bands. ATCOR calculates surface reflectance and a surface (brightness) temperature (from band 13). ASTER has four gain settings (high=H, normal=N, and low1=L1, low2=L2) for the reflective bands. Table 9.3 contains the c1 values for the different reflective bands and gain settings in the ATCOR radiance unit $mWcm^{-2}sr^{-1}\mu m^{-1}$. It was taken from the ASTER user's guide ([18]). The thermal band 13 has a calibration gain of c1=5.693E-4.

band	high gain	normal gain	low gain 1	low gain 2
1	0.0676	0.1688	0.225	N/A
2	0.0708	0.1415	0.189	N/A
3	0.0423	0.0862	0.115	N/A
4	0.01087	0.02174	0.0290	0.0290
5	0.00348	0.00696	0.00925	0.0409
6	0.00313	0.00625	0.00830	0.0390
7	0.00299	0.00597	0.00795	0.0332
8	0.00209	0.00417	0.00556	0.0245
9	0.00159	0.00318	0.00424	0.0265

Table 9.3: *Radiometric coefficients c1 for ASTER.*

9.6.9 DMC (Disaster Monitoring Constellation)

DMC is a constellation of several orbiting satellites with an optical payload intended for rapid disaster monitoring. All DMC sensors have three spectral bands (green, red, NIR) with a spatial resolution of 32 m and a swath of 600 km. The metadata file (*.dim and *.htm formats) pertaining to each scene contains the solar geometry and the radiometric calibration coefficients. The bias and gain specified in the metadata are defined as:

$$L = bias + DN/gain \tag{9.8}$$

using the radiance unit $Wm^{-2}sr^{-1}\mu m^{-1}$. Since ATCOR uses the radiance unit $mWcm^{-2}sr^{-1}\mu m^{-1}$ and the equation

$$L = c_0 + c_1 DN \tag{9.9}$$

the calibration coefficients have to be calculated as :

$$c_0 = 0.1 * bias \tag{9.10}$$

$$c_1 = 0.1/gain \tag{9.11}$$

Note: analysis of some DMC data from 2007 indicates that the specified bias in the NIR band is too high, and better results are obtained if bias(NIR) = 0 is employed.

9.6.10 RapidEye

The RapidEye constellation consists of 5 identical instruments in different orbits enabling a high temporal revisit time for any area. The sensor has 5 multispectral bands covering the blue to NIR region, with the specialty of a red-edge band (at 710 nm, bandwidth 40 nm). In addition, the instruments can be tilted in the across-track direction. The nadir spatial resolution is 6.5 m. The .xml metafile contains information on the solar elevation angle ("illuminationElevationAngle"), solar azimuth ("illuminationAzimuthAngle)", and the view geometry, i.e. the "acrossTrackIncidenceAngle" and the view azimuth ("azimuthAngle").

ATCOR requires the sensor tilt angle θ_V , which is close to the across-track incidence angle θ_I on the ground. The exact calculation can be done with eq. 9.7 using the RapidEye orbit height 630 km.

9.6.11 GeoEye-1

GeoEye-1 provides optical data with four multispectral channels in the 480 - 840 nm region with a spatial resolution of about 1.7 m. In addition, panchromatic data with a resolution of about 0.5 m is available. The radiometric encoding is 11 bits per pixel. The metafile for each scene contains the radiometric offset and gain values. These values are given in the same unit as used by ATCOR (i.e. $mWcm^{-2}sr^{-1}\mu m^{-1}$), so they can be directly taken, i.e.,

$$c_1 = Gain \tag{9.12}$$

The Offset = c_0 is usually zero.

9.6.12 WorldView-2

WorldView-2 provides optical data with 8 multispectral channels in the VNIR region (428 - 923 nm) at a spatial resolution of 1.8 m (nadir) with a dynamic range of 11 bits per pixel. The instrument has selectable radiometric gain factors ("absCalFactor") specified in the metafile (*.IMD). The offset c_0 is zero for all channels and the gain c_1 for ATCOR has to be calculated as:

$$c_1 = 0.1\ AbsCalFactor\ /\ FWHM \tag{9.13}$$

where FWHM is the effective bandwidth ("effectiveBandwidth" in μm) as specified in the metafile. Although the bandwidth is constant per channel, the gain c_1 might have to be updated, because the absCalFactor can vary from scene to scene. Additionally, panchromatic images with a 0.5 m resolution are available.

Chapter 10

Theoretical Background

Standard books on optical remote sensing contain an extensive presentation on sensors, spectral signatures, and atmospheric effects where the interested reader is referred to (Slater 1980 [80], Asrar 1989 [2], Schowengerdt 2007 [78]). This chapter contains a description of the concepts and equations employed for the atmospheric correction.
We start with the basic equations in the solar and thermal spectral region for clear sky conditions (standard case), then move on to non-standard conditions comprising bidirectional reflectance (BRDF) effects, hazy scenes, and a treatment of shadow areas caused by clouds or buildings. Standard atmospheric conditions include the option of a constant visibility (aerosol optical thickness) and water vapor content per scene, as well as the retrieval of a visibility and water vapor map if the required spectral bands are available for the specific sensor. Water vapor correction on a pixel-by-pixel basis is usually necessary for hyperspectral imagery.
The section on the non-standard conditions contains a short discussion on empirical correction methods for bidirectional effects. It continues with the description of a statistical haze removal method. The third section presents a technique to compensate shadow effects, i.e. cloud or building shadow areas are masked and de-shadowed. Then, an overview is presented of all major processing steps involved in the atmospheric correction.
After atmospheric correction, the surface reflectance cube can be used for classification. A simple automatic method is included here based on template reflectance spectra of different surface covers. Finally, the accuracy of the atmospheric correction is discussed.

10.1 Basics on radiative transfer

This chapter presents the basic concepts and the terminology. The full set of equations is documented here as implemented in ATCOR. We start with the radiative transfer equation in the solar spectral region (0.4 - 2.5 μm) for a flat terrain under clear sky conditions. First, the equation for an infinite plane of uniform reflectance is presented. Then the case of a small uniform surface embedded in a large homogeneous background of different reflectance is discussed. We continue with the rugged terrain, and finally discuss the equations for the thermal spectral region (8-14 μm).

10.1.1 Solar spectral region

For a cloud-free sky and a uniform ground of reflectance ρ, the radiance signal received at the sensor consists of scattered solar radiation and ground reflected radiation. The scattered radiation component is also called path radiance. It depends on the solar and viewing geometry as sketched

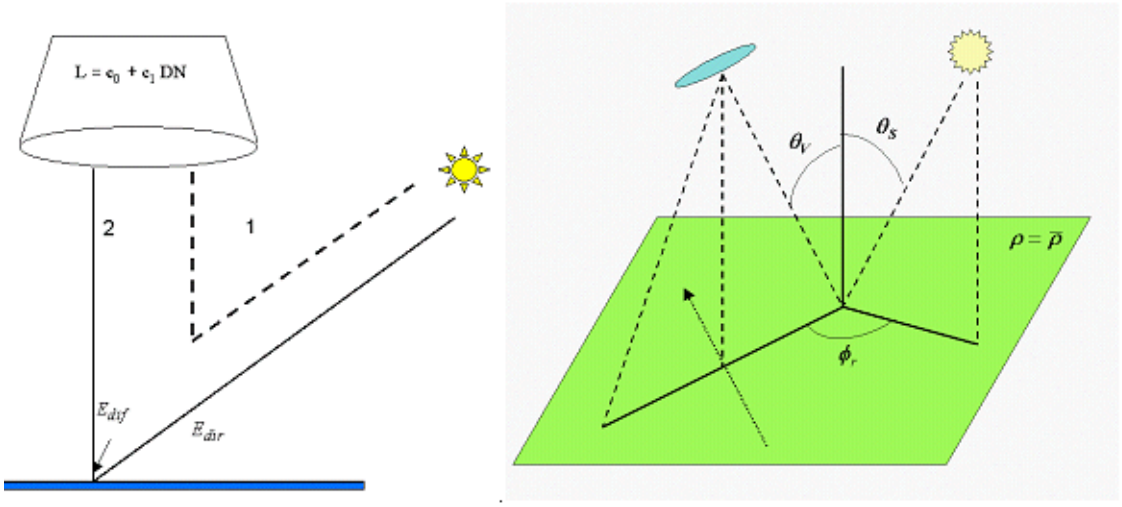

Figure 10.1: *Radiation components, illumination and viewing geometry.*

in Fig. 10.1. In case of a flat terrain, the at–sensor radiance L can be written as (Asrar 1989, chapter 9):

$$L = L_p(\Theta_v, \Theta_s, \phi) + \tau_v(\Theta_v)\frac{\rho}{\pi}\frac{E_g(0)}{1-\rho_r s} \tag{10.1}$$

L	at-sensor radiance for surface reflectance ρ ;
L_p	path radiance ;
τ_v	total ground-to-sensor atmospheric transmittance, sum of direct τ_{dir} and diffuse τ_{dif} transmittance;
E_g	global flux on a horizontal surface, sum of direct (E_{dir}) and diffuse (E_{dif}) flux, $E_g(0)$ is calculated for a ground surface with $\rho = 0$;
ρ_r	large scale reference background reflectance determining the effective global flux (ρ_r=0.15 is used for ATCOR) ;
s	spherical albedo of the atmosphere, accounts for atmospheric backscattering to the ground.

The geometry is described by the angles Θ_v (view zenith), and Θ_s, ϕ (solar zenith and relative azimuth angles), compare figure 10.1. Since ρ and ρ_r are not known for image data and can vary within a scene, equation (10.1) has to be solved for ρ iteratively, compare equations (10.9 - 10.15). In a strict sense, the reflectance ρ used here should be called *hemispherical-directional reflectance factor (HDRF)*, because most surfaces show an anisotropic reflectance behavior characterized by the bidirectional reflectance distribution function (BRDF, Nicodemus 1970, Slater, 1985). The ground is illuminated *hemispherically* by the direct and diffuse solar flux and the reflected radiation is recorded from a certain *direction*, i.e., *hemispherical* input radiation, *directional* reflected radiation. Since the reflected radiation is always measured in a small cone, the term *hemispherical-conical reflectance factor HCRF* is also used, but for small instantaneous field-of-view sensors,

"directional" is a sufficiently accurate geometrical description. However, for simplicity we will use the abbreviation *reflectance* in this manual.

In spectral regions dominated by scattering effects, the terms of equation (10.1) are calculated with the scaled DISORT option (discrete ordinate radiative transfer [51]), in regions with strong atmospheric absorption the more accurate correlated k algorithm is used in combination with DISORT [5]. The results are stored in look-up tables (LUT). Since MODTRAN calculates the path radiance including the diffuse reflected ground radiation in the form

$$L_{path}(\rho) = L_{path}(0) + \frac{\tau_{dif}\ E_g(0)\ \rho/\pi}{1-\rho s} = L_{path}(0) + \tau_{dif}\ E_g(\rho)\ \rho/\pi \tag{10.2}$$

two MODTRAN runs with surface reflectance $\rho = 0$ and $\rho_r = 0.15$ are required to calculate the diffuse ground-to-sensor transmittance τ_{dif} and spherical albedo s from equation (10.2)

$$\tau_{dif} = \frac{[L_{path}(\rho_r) - L_{path}(0)]\ \pi}{\rho_r\ E_g(\rho_r)} \tag{10.3}$$

$$E_g(\rho_r) = \frac{E_g(\rho = 0)}{1-\rho_r s} \tag{10.4}$$

$$s = [1 - \frac{E_g(0)}{E_g(\rho_r)}]/\rho_r \tag{10.5}$$

For image data, the pixel reflectance ρ may differ from the background reflectance $\bar{\rho}$. In this case the signal at the sensor consists of three components as sketched in Fig. 10.2:

- component 1: scattered radiance, path radiance,
- component 2: radiation reflected from pixel under consideration,
- component 3: radiation reflected from the neighborhood and scattered into the viewing direction ("adjacency" effect).

Only component 2 contains information on the surface properties of the pixel, the other components have to be removed during the atmospheric correction. As detailed in [65] the adjacency radiation L_3 consists of two components (atmospheric backscattering and volume scattering) which are combined into one component in Fig. 10.2.
The radiometric calibration assigns to each digital number (DN) the corresponding at-sensor radiance L

$$L(k) = c_0(k) + c_1(k)DN(k) \tag{10.6}$$

where k indicates the channel number, and c_0 , c_1 are the calibration coefficients (offset and slope). For sensors with adjustable gain settings the equation is

$$L(k) = c_0(k) + c_1(k)DN(k)/g(k) \tag{10.7}$$

where $g(k)$ is the gain setting in channel k. The atmospheric correction has to be performed iteratively, since the surface reflectance and large-scale (0.5-1 km neighborhood) background reflectance are not known. So three steps are employed in the ground reflectance calculation:

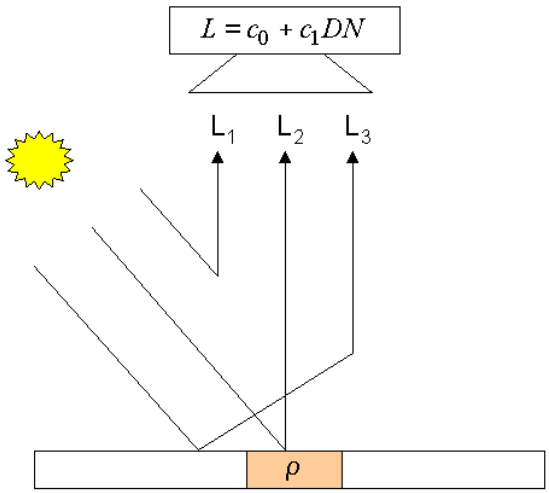

Figure 10.2: *Schematic sketch of solar radiation components in flat terrain.*

Step 1: The influence of the neighborhood (adjacency effect) is neglected and the surface reflectance is obtained from

$$\rho^{(1)} = \frac{\pi[d^2(c_0 + c_1 DN) - L_p]}{\tau_v E_g(\rho_r = 0.15)} \tag{10.8}$$

where the spectral band index is omitted for clarity. The factor d^2 takes into account the sun-to-earth distance (d is in astronomical units) since the LUTs with path radiance and global flux are calculated for d=1 in ATCOR.
Step 2: The second step calculates the average reflectance in a large neigborhood of each pixel (range R=0.5-1 km)

$$\bar{\rho} = \frac{1}{N^2} \sum_{i,j=1}^{N} \rho_{i,j}^{(1)} \tag{10.9}$$

where N corresponds to the number of pixels for the selected range R of the adjacency effect [58], [65]. The exact choice of R is not critical since the adjacency influence is a second-order effect. Instead of the range-independent weighting in eq. (10.9), a range-dependent function can be selected with an exponential decrease of the weighting coefficients [59]. The range-dependent case requires more execution time, of course. Except for special geometries, the difference between both approaches is small, because the average reflectance in a large neighborhood usually does not vary much and the influence is a second-order effect.

$$\rho^{(2)}(x,y) = \rho^{(1)}(x,y) + q\{\rho^{(1)} - \bar{\rho}(x,y)\} \tag{10.10}$$

The function q indicates the strength of the adjacency effect. It is the ratio of the diffuse to direct ground-to-sensor transmittance. The range-dependent version of eq. (10.10) is:

$$\rho^{(2)}(x,y) = \rho^{(1)}(x,y) + q\{\rho^{(1)}(x,y) - \int_0^R \rho^{(1)}(r) A(r) exp(-r/r_s) dr\} \tag{10.11}$$

Here, R is the range where the intensity of the adjacency effect has dropped to the 10% level (i.e. r=R=2.3x r_s, where r_s is a scale range, typically r_s=0.2-0.4 km, R=0.5-1 km), ρ(r) is the reflectance at range r from the (x,y) position and A(r) is the area of a circular zone from r to r+dr. Now we approximate the circular regions by square regions to obtain the discrete version of eq. (10.11) with exponentially decreasing weighting coefficients w_i:

$$\rho^{(2)}(x,y) = \rho^{(1)}(x,y) + q\{\rho^{(1)}(x,y) - \sum_{i=1}^{n_R} \bar{\rho}_i w_i\} \tag{10.12}$$

$$w_i = \frac{1}{\sum_{i=1}^{n_R} W_i} W_i \qquad and \qquad W_i = \int_{r_{i-1}}^{r_i} A(r) exp(-r) dr \approx \int_{r_{i-1}}^{r_i} (2r)^2 exp(-r) dr \tag{10.13}$$

ATCOR supports up to n_R=5 regions. Since the sequence of moving digital low pass filters works with square filters of size $2r_i$ * $2r_i$, the area A(r) is approximated as the corresponding square region $A(r) = (2r)^2$.
Step 3: it includes the spherical albedo effect on the global flux that was initially calculated with the reference background reflectance $\rho_r = 0.15$ and is finally adapted to the scene-dependent value $\bar{\rho}$ by correcting with the difference $\bar{\rho} - \rho_r$:

$$\rho^{(3)}(x,y) = \rho^{(2)}(x,y)[1 - (\bar{\rho}(x,y) - \rho_r)s] \tag{10.14}$$

Radiation components in rugged terrain :

Figure 10.3 shows a sketch of the radiation components in a rugged terrain [59]. Compared to the flat terrain one additional component is taken into account in the ATCOR model. It is an approximation of the terrain reflected radiation. It is obtained by weighting the reflected radiation in a 0.5 km surrounding of a pixel with the terrain view factor. The terrain view factor is $V_{terrain}(x,y) = 1 - V_{sky}(x,y)$, and the sky view factor $V_{sky}(x,y)$ is calculated from the DEM as explained below. The sky view factor is normalized to 1 for a flat terrain.
The reflectance is calculated iteratively. The first step neglects the adjacency effect and starts with a fixed terrain reflectance of $\bar{\rho}^{(0)}_{terrain} = 0.1$ [62] :

$$\rho^{(i)}(x,y) = \frac{\pi\ [d^2(c_0 + c_1 DN(x,y)) - L_p(z,\Theta_v,\phi)]}{\tau_v(z,\Theta_v)[b(x,y)E_s\tau_s(z)cos\beta(x,y) + E^*_d(x,y,z) + E^{i)}_t(z,\rho_r)\bar{\rho}^{(i-1)}_{terrain}V_{terrain}(x,y)]} \tag{10.15}$$

The terms are defined as :

x, y	horizontal coordinates, corresponding to the georeferenced pixel positions;
z	vertical coordinate, containing the elevation information from the DEM;
DN(x,y)	digital number of georeferenced pixel;
$L_p(z,\theta_v,\phi)$	path radiance, dependent on elevation and viewing geometry;
$\tau_v(z,\Theta_v)$	ground-to-sensor view angle transmittance, direct plus diffuse components;
$\tau_s(z)$	Sun-to-ground beam (direct) transmittance;
$\beta(x,y)$	angle between the solar ray and the surface normal (illumination angle);
b(x,y)	binary factor: b=1 if pixel receives direct solar beam, otherwise b=0;
E_s	extraterrestrial solar irradiance (earth-sun distance d=1 astronomical unit);
$E^*_d(x,y,z)$	diffuse solar flux on an inclined plane (see equation 10.18);
$E_g(z)$	global flux (direct plus diffuse solar flux on a horizontal surf. at elevation z);

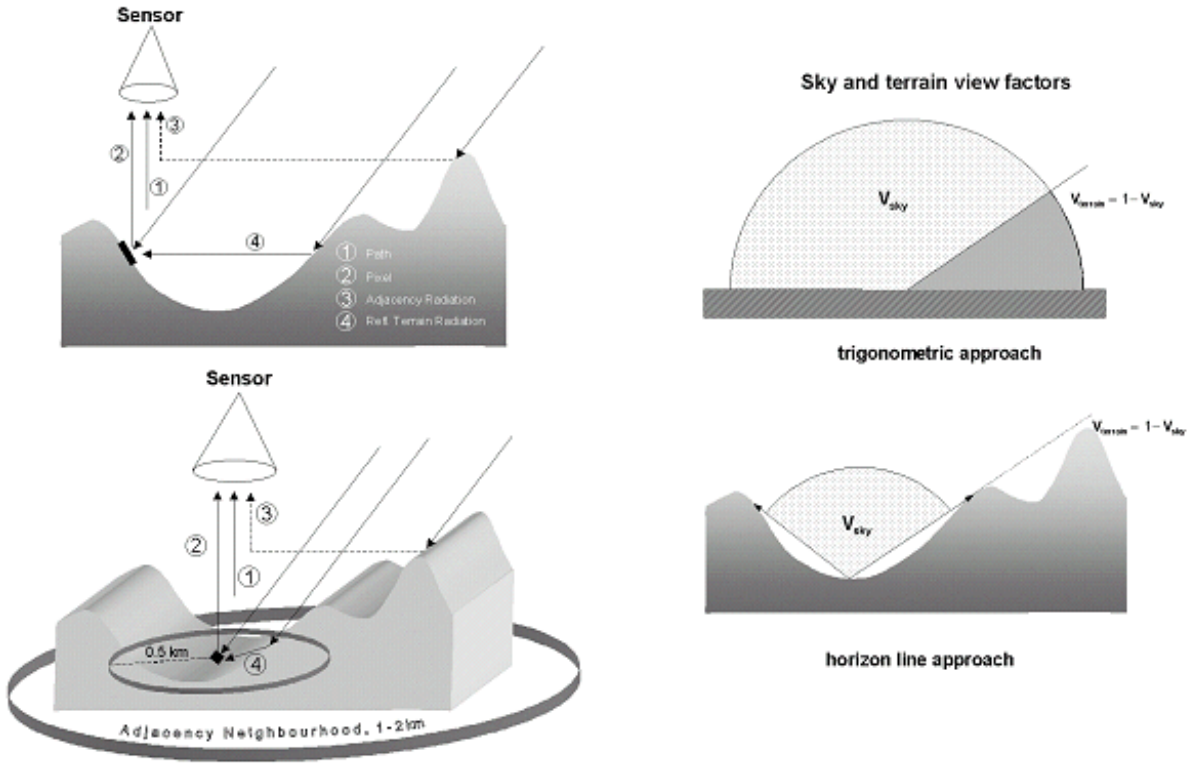

Figure 10.3: *Radiation components in rugged terrain, sky view factor.*
Left: schematic sketch of radiation components in rugged terrain; 1 : path radiance; 2 : pixel reflected radiance; 3 : adjacency radiance; 4 : reflected terrain radiance. Right: sky and terrain view factor.

$E_t(z)$	radiation incident upon adjacent slopes;
$\rho_{terrain}^{(0)}$	= 0.1, initial value of average terrain reflectance;
$\bar{\rho}_{terrain}^{(i)}(x,y)$	locally varying average terrain reflectance, calculated iteratively (i=1,2,3);
$V_{terrain}(x,y)$	terrain view factor (range 0-1).

The solar and DEM geometry is shown in figure 10.4 as well as the three solar radiation components taken into account for rugged terrain: direct and circumsolar irradiance, and diffuse hemispherical sky flux. It can be shown that these three components are equivalent to the direct and diffuse solar flux components in flat terrain. In case of a shadow pixel the direct and circumsolar components are set to zero, i.e. the binary factor b=0.

The next step iterates eq. 10.15 averaging the reflected terrain radiation over a square box of 0.5 × 0.5 km. If equation (10.15) is used with $E_t = E_g$ then three iterations are usually sufficient to be independent of the start value of the terrain reflectance [59]. However, for highly reflective surfaces, e.g. snow, and high terrain view factors, more than three iterations are necessary, and a faster convergence of $\bar{\rho}_{terrain}^{(i)}$ can be achieved with a geometric series for the terrain reflected

radiation E_t as proposed in [79] :

$$E_t^{(i)} = E_g \frac{\bar{\rho}_{terrain}^{(i-1)} V_{terrain}}{1 - \bar{\rho}_{terrain}^{(i-1)} \bar{V}_{terrain}} \tag{10.16}$$

The next steps include the adjacency correction (eq. 10.9, 10.10) and the spherical albedo effect (eq. 10.14).

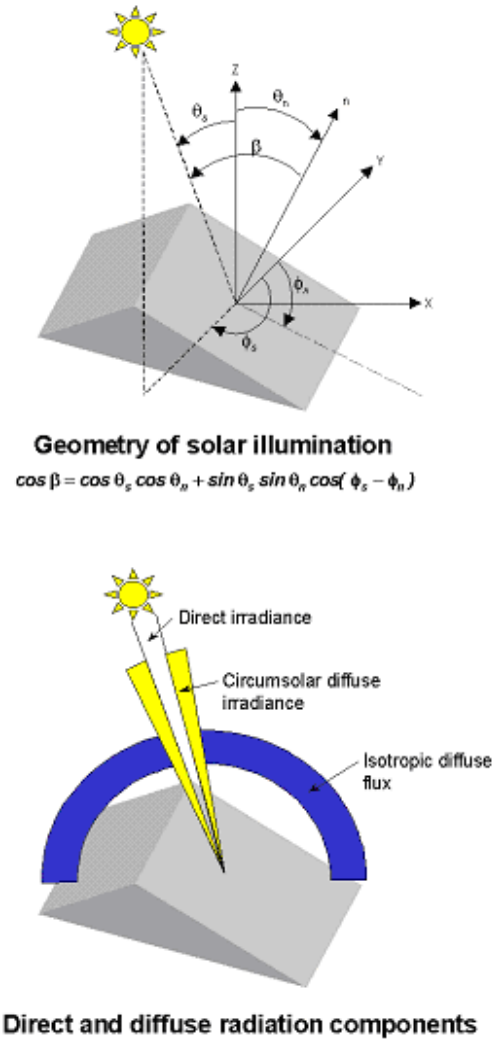

Figure 10.4: *Solar illumination geometry and radiation components.*

If $\Theta_s, \Theta_n, \phi_s, \phi_n$ denote solar zenith angle, terrain slope, solar azimuth and topographic azimuth, respectively, the illumination angle β can be obtained from the DEM slope and aspect angles and the solar geometry:

$$cos\beta(x,y) = cos\Theta_s cos\Theta_n(x,y) + sin\Theta_s sin\Theta_n(x,y) cos\{\phi_s - \phi_n(x,y)\} \tag{10.17}$$

The illumination image $cos\beta(x,y)$ is calculated within ATCOR and stored as a separate map. The

diffuse solar flux on an inclined plane is calculated with Hay's model (Hay and McKay 1985, also see Richter 1998 for the enhancement with the binary factor b):

$$E_d^*(x,y,z) = E_d(z)[b\tau_s(z)cos\beta(x,y)/cos\Theta_s + \{1 - b\tau_s(z)\}V_{sky}(x,y)] \tag{10.18}$$

The sky view factor can be computed from local information as $V_{sky}(x,y) = cos^2(\Theta_n(x,y)/2)$ based on the local DEM slope angle Θ_n. ATCOR uses the horizon algorithm that provides a more accurate value of the sky view factor by considering the terrain neighborhood of each pixel (Dozier et al. 1981). V_{sky} and $V_{terrain}$ are related by :

$$V_{sky}(x,y) = 1 - V_{terrain}(x,y) \tag{10.19}$$

10.1.2 Integrated Radiometric Correction (IRC)

The IRC method was published by Kobayashi and Sanga-Ngoie [40, 41] to provide a combined atmospheric and topographic correction. The algorithm is briefly outlined here, more details can be found in the original papers.

The first step is the orthorectification of the scene using a digital elevation model (DEM). Then the slope and aspect maps are calculated. The next step is the calculation of the sky view factor, see chapter 10.1.1. The original paper uses the simple equation based solely on the slope angle, but with ATCOR a more accurate calculation based on a ray tracing can also be used in case of a steep terrain. Then the following quantities are computed (keeping the original notation of Kobayashi in most cases):

$$h_0 = \frac{(\pi + 2\theta_s)}{2\pi} \tag{10.20}$$

Here θ_s is the solar zenith angle in radian. IF s denotes the slope map (in radian) then the simple version of the skyview is obtained with

$$h = 1 - s/\pi \tag{10.21}$$

The cosine of the local solar zenith (illumination angle β) is given in eq. 10.17. Then the surface radiance for each channel L_s is calculated by subtracting the path radiance L_p from the at-sensor radiance L:

$$L_s(x,y) = L(x,y) - L_p(x,y,z) \tag{10.22}$$

In the ATCOR version of the IRC algorithm the path radiance varies spatially, particularly due to the DEM height variation, while a constant value (per channel) is used in the original IRC paper. Then a regression analysis (per channel) of L_s versus $cos\beta$ is applied to calculate the slope m and intercept b. After defining $C = m/b$ the topographic correction map A is calculated:

$$A(x,y) = \frac{cos\theta_s + C/h_0}{cos\beta(x,y) + C\ h(x,y)/h_0} \tag{10.23}$$

Finally, the surface reflectance ρ is computed according to:

$$\rho(x,y) = \frac{\pi\ L_s(x,y,z)\ A(x,y)}{T(x,y,z)\ \{E_{dir}(x,y,z)\ cos\theta_s + E_{dif}(x,y,z)\}} \tag{10.24}$$

where T is the total ground-to-sensor transmittance, and E_{dir}, E_{dif} are the direct irradiance and diffuse solar flux on the ground, respectively.

So the ATCOR version of IRC contains some improvements with respect to the original method: the path radiance varies spatially, mainly caused by terrain height variations, possibly also due to visibility variations, and the sky view factor can be provided from a ray tracing analysis instead of the local slope angle.

Note: the IRC method usually performs well. However, due to the statistical evaluation of the regression analysis unphysically large ($>$ 1 reflectance unit) or small ($<$ 0) surface reflectance values might happen for some pixels, usually in areas with topographic shadow or low local sun elevations.

10.1.3 Spectral solar flux, reflected surface radiance

The spectral solar fluxes on the ground can be calculated by setting the parameter *irrad0 = 1* in the *.inn* file or using the graphical user interface. The fluxes depend on solar geometry, terrain elevation, topography, and atmospheric conditions. For a flat terrain, ATCOR provides spectra of the direct, diffuse, and global flux for the selected visibility / water vapor. In case of variable visibility / water vapor the spectra are calculated for the average scene visibility / water vapor. The direct flux is just the beam irradiance on the ground times the cosine of the local solar zenith angle. The diffuse flux spectrum E_{dif} is evaluated for a surface reflectance of $\rho = 0$, and the global flux for $\rho = 0.15$, i.e., $E_g = (E_{dir} + E_{dif}(0))/(1 - s \cdot 0.15)$, where s is the spherical albedo. The spectral band index is omitted for brevity. For a flat terrain these fluxes are provided in the directory of the input file (e.g. *'scene.bsq'*):

- the direct spectral flux on the ground: *'scene_edir.dat'*
- the diffuse spectral flux on the ground: *'scene_edif.dat'* for surface reflectance $\rho = 0$.
- the global spectral flux on the ground: *'scene_eglo.dat'* for a typical average surface reflectance $\rho = 0.15$.

These spectra will already give a realistic description for a flat terrain, but they lack the dependence on the spectral reflectance variations in the scene. Therefore, an image of the global flux is also provided that accounts for the spatial reflectance and visibility / water vapor patterns (VIS, named *'scene_eglobal.bsq'*:)

$$E_g(x,y) = \frac{E_{dir}(VIS(x,y)) + E_{dif}(\rho = 0, VIS(x,y))}{1 - s(x,y)\ \bar{\rho}(x,y)} \tag{10.25}$$

Here, $\bar{\rho}$ indicates a spatial averaging with a filter size corresponding to the specified adjacency range. The unit of the global flux is $mWcm^{-2}\mu m^{-1}$ and it is stored as float data (32 bits/pixel). Therefore, its file size will be twice or four times the size of the input scene if the scene is encoded as 16bit/pixel and 8bits/pixel, respectively.

For a rugged terrain, images of the direct and diffuse fluxes will be calculated using the available DEM information on height (z), slope and aspect (i.e. local solar illumination angle β), and atmospheric conditions (visibility / water vapor VIS). The direct flux on the ground is :

$$E_{dir}(x,y) = b(x,y)\ E_0\ T_{sun}(VIS(x,y,z))\ cos\beta(x,y) \tag{10.26}$$

where E_0, T_{sun} are extraterrestrial solar irradiance and sun-to-ground transmittance, respectively, and b is the topographic shadow mask (0=shadow, 1=sunlit pixel).

The diffuse flux in mountainous terrain accounts for the adjacency effect and multiple reflection effects from the surrounding topography. Using the terrain view factor V_t from the last section and the effective terrain reflectance $\rho_t = V_t(x,y)\ \bar{\rho}(x,y)$ and $\bar{\rho}_t = \bar{V}_t(x,y)\ \bar{\rho}(x,y)$ the diffuse flux is approximated as:

$$\begin{aligned} E_{dif}(x,y) \quad = \quad & E_{dif,flat}\ \{b\ T_{sun}(x,y,z)\ cos\beta/cos\theta_s + \ [1 - b(x,y)\ T_{sun}(x,y,z)]\ V_{sky}(x,y)\} \\ & + \{E_{dir,flat}(x,y,z)\ +\ E_{dif,flat}(x,y,z)\}\ \rho_t(x,y)\ /\ (1 - \bar{\rho}_t(x,y)) \end{aligned} \tag{10.27}$$

The first line describes the anisotropic and isotropic components of the diffuse flux, the second line accounts for multiple terrain reflection effects.

Related quantities to the global spectral solar flux on the ground are the wavelength-integrated global flux and the absorbed solar flux (Wm^{-2}). These play a role in the surface energy balance and they are available as part of the value added channels, see chapter 7.2, equations 7.9, 7.10.

Surface reflected radiance

The ground reflected (or ground leaving) radiance per band can be obtained in addition to the spectral solar fluxes by setting the parameter irrad0=2. It is calculated corresponding to the surface reflectance cube $\rho(x,y)$, named *'scene_surfrad.bsq'*. For a flat terrain it is:

$$L(surf,x,y) = E(global)\ \rho(x,y)\ /\ \pi \tag{10.28}$$

In case of a mountainous terrrain the direct and diffuse reflected radiation maps from the equations 10.26 and 10.27 are used:

$$L(surf,dir,x,y) = (E_{dir}\ +\ E_{dif})\rho(x,y)\ /\ \pi \tag{10.29}$$

Again, the same output file name is used (*'scene_surfrad.bsq'*).

10.1.4 Thermal spectral region

Similar to the solar region, there are three radiation components: thermal path radiance (L_1), i.e., photons emitted by the atmospheric layers, emitted surface radiance (L_2), and reflected radiance (L_3). The short form of the radiance equation in the thermal region can be written as [32], [24] :

$$L = L_p + \tau\ \varepsilon\ L_{BB}(T) + \tau\ (1 - \varepsilon)\ F/\pi \tag{10.30}$$

where

L	at-sensor radiance,
$L_1 = L_P$	thermal path radiance,
τ	ground-to-sensor atmospheric transmittance,
ε	surface emissivity,
T	surface temperature,
L_{BB}	blackbody radiance at temperature T, weighted with the channel's filter curve,
F	thermal downwelling flux on the ground.

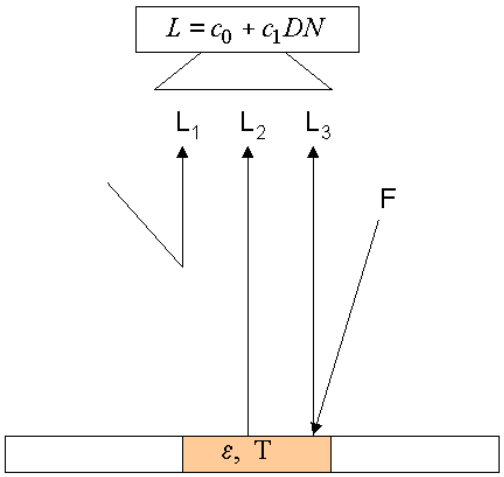

Figure 10.5: *Radiation components in the thermal region.*
$L_1 = L_P$, $L_2 = \tau\ \epsilon\ L_{BB}(T)$, $L_3 = \tau\ (1-\epsilon)\ F/\pi$.

The second term on the right-hand side of equation (10.30) is emitted surface radiance reaching the sensor, the third term is the atmospheric radiance reflected at the surface and attenuated by the surface-to-sensor path. The spectral band index, elevation, and angular dependence is omitted for brevity.

The $L_{BB}(T)$ term is Planck's blackbody radiance $B(\lambda, T)$ weighted with the spectral channel response function $R(\lambda)$:

$$L_{BB}(T) = \frac{\int_{\lambda_1}^{\lambda_2} B(\lambda, T) R(\lambda) d\lambda}{\int_{\lambda_1}^{\lambda_2} R(\lambda) d\lambda} \tag{10.31}$$

For a discrete temperature interval $T = (T_1, T_2)$ and increment (e.g. $T_1 = 270K, T_2 = 330K$, increment 1 K) equation (10.31) is solved numerically. Temperature and radiance are then approximated by an exponential fit function function with channel dependent coefficients a_1, a_2:

$$L_{BB} = exp[(\frac{1}{T} - a_1)/a_2] \tag{10.32}$$

$$T = \frac{1}{a_1 + a_2 ln L_{BB}} \tag{10.33}$$

For convenience, an offset a_0 is introduced with default $a_0 = 0$. The offset term can be used to adjust a temperature bias in a scene. Example: if scene temperatures are too low by 3K they can be raised by setting $a_0 = 3$.

$$T = a_0 + \frac{1}{a_1 + a_2 ln L_{BB}} \tag{10.34}$$

Remark:
The computer implementation of the channel-resampled radiance equations is coded to minimize

spectral resampling effects [60], [61].

Temperature / emissivity separation

For a sensor with n thermal channels there are n equations of (10.30) with n+1 unknowns, namely the n surface emissivities plus a surface temperature. So, the system of equations (10.30) is always underdetermined. Several possibilities exist to address this problem (Gillespie et al. 1998). Four options are offered by the satellite version of ATCOR:

- a constant emissivity (default ϵ=0.98 independent of surface cover type, 10-12 μm region) for sensors with a single thermal channel. For user-defined sensors with multiple thermal bands the parameter *itemp_band* described in 4.6.1) defines the channel employed for the surface temperature calculation.

- fixed emissivity values assigned for 3 classes for the selected surface temperature band (parameter *itemp_band* described in 4.6.1): $\epsilon(soil)$=0.96, $\epsilon(vegetation)$=0.97, else ϵ=0.98 (water and undefined class). The assignment to the vegetation / soil class is performed on-the-fly in memory employing the vegetation index (red and NIR bands required), and the 3-class emissivity map is available (file *'image_atm_emi3.bsq'*, compare chapter 4.5). In the airborne ATCOR version [69] a pre-classification with more emissivity classes can be used as already suggested in [55].

- for multispectral thermal bands the normalized emissivity method (NEM) or adjusted NEM are also implemented. In the NEM [23], the surface temperature is calculated for all channels with a constant user-defined emissivity, and for each pixel the channel with the highest temperature is finally selected. In the adjusted NEM (ANEM) [12] the assigned emissivity is surface cover dependent. Here, we define four surface cover classes (water, vegetation, soil/dry vegetation, sand/asphalt) based on the following criteria:

  - vegetation: $\rho_{nir}/\rho_{red} > 2$ and $\rho_{nir} > 0.20$.
  - soil/dry vegetation: $\rho_{nir}/\rho_{red} \geq 1.4$ and $\rho_{nir}/\rho_{red} < 2.0$ and $\rho_{red} > 0.09$.
  - sand/asphalt : $\rho_{nir}/\rho_{red} < 1.4$ and $\rho_{red} > 0.09$.
  - water : $\rho_{nir} < 0.05$ and $\rho_{1.6\mu m} < 0.03$.

  To each class the user can assign an emissivity valid for the channel with the highest temperature. There is only one common emissivity class in case of night data or data from purely thermal channels.
  The ANEM method provides accurate channel emissivities and surface temperatures if the classes are assigned correctly and the emissivity value assigned to the channel with the maximum temperature is close to the actual channel emissivity. Maximum surface emissivities usually lie in the 10.5 - 13 μm region. After calculating the surface temperature, the emissivities for all channels are computed.

- for thermal band imagery with at least 5 channels the ISAC (In-Scene Atmospheric Compensation) method is available. A detailed description is given by Young et al. [89]. The

method does not require ancillary meteorological data or atmospheric modeling. It neglects the downwelling thermal flux and employs the equation

$$L = L_p + \tau\ \varepsilon\ L_{BB}(T) = L_p + \tau\ L_{surface} \tag{10.35}$$

This approximation is justified for pixels with a high emissivity close to 1, i.e. "blackbody" pixels. First, the highest brightness temperature T_{max}^{sensor} for each pixel in each channel is computed based on the at-sensor radiance L converted into brightness temperature. In the current implementation, only channels in the spectral region 8 - 13 μm are employed for the maximum brightness temperature search, because the spectral regions $\lambda < 8\ \mu m$ and $\lambda > 13\ \mu m$ are strongly affected by atmospheric water vapor absorption. Next, a reference channel is defined where most pixels with maximum brightness temperature occur. Only those blackbody pixels are retained which have the maximum brightness temperature in this reference channel ("most hits" method). For these selected blackbody pixels the scatterplot of measured at-sensor radiance L versus blackbody radiance corresponding to $L_{BB}(T_{max}^{sensor})$ is computed for each channel. This means the surface radiance of eq. 10.35 is approximated as $L_{surface} = L_{BB}(T_{max}^{sensor})$. The final step is a least squares regression of the scatterplot data L versus $L_{surface}$, yielding the intercept (path radiance L_p) and slope (transmittance τ) of eq. 10.35. Care has to be taken to apply the regression only to the points near the top edge of all cluster points, but allow some margin, so the fitting line is allowed to sink by an amount of the sensor noise equivalent spectral radiance (NESR). The quality of the regression is significantly increased by allowing only those pixels in the scatterplot that had their maximum temperatures in the reference channel.

Two comments: first, because of the involved assumptions, the obtained intercept is not the physical path radiance, and the slope not the physical atmospheric transmittance. Both quantities may be negative in some channels, therefore they are referred to as unscaled path radiance $L_p^{(u)}$ and unscaled transmittance $\tau^{(u)}$. They might be rescaled to proper atmospheric path radiance and transmittance spectra, e.g. using a radiative transfer code. Second: the ISAC method requires an adequate spread in surface temperatures in the scene, and surface temperatures higher than the atmospheric radiation temperature. So, results for night-time imagery will likely be degraded.

The compensated unscaled surface radiance spectrum is calculated as

$$L_{surface}^{(u)}(\lambda) = \frac{L(\lambda) - L_p^{(u)}(\lambda)}{\tau^{(u)}(\lambda)} \tag{10.36}$$

and the unscaled ISAC surface emissivity can be obtained with

$$\epsilon_{isac}(\lambda) = L_{surface}^{(u)}(\lambda)\ /\ L_{BB}(\lambda, T_{ref}) \tag{10.37}$$

where T_{ref} is the brightness temperature image in the reference channel. The compensated surface radiance spectrum $L_{surface}^{(u)}(\lambda)$ can be converted into the equivalent compensated brightness temperature spectrum where most of the atmospheric absorption features are removed. Both the compensated surface radiance and compensated brightness temperature are spectrally consistent with the data and represent the best estimate for the spectral shape.

The emissivity spectrum $\epsilon_{isac}(\lambda)$ may exceed the value 1 in certain channels if the maximum brightness temperature of a pixel does not occur in the selected reference channel. However, a common reference channel is needed in this method to obtain a consistent pixel-independent spectrum of unscaled path radiance $L_p^{(u)}$ and transmittance $\tau^{(u)}$.

10.2 Masks for haze, cloud, water, snow

A useful first step before executing an atmospheric correction is the calculation of a pixel map for haze, cloud, water snow, etc. Such a pre-classification has a long history in atmospheric correction methods [37, 38, 55, 56, 57, 39, 44]. It is also employed as part of NASA's automatic processing chain for MODIS [45] using the classes land, water, snow/ice, cloud, shadow, thin cirrus, sun glint, etc. A similar approach is taken here.
The calculation is done "on-the-fly" and if the scene is named "scene.bsq", then the corresponding map is named "scene_out_hcw.bsq". There is also the possibility to provide this information from an external source: if a file ""scene_hcw.bsq" exists in the same folder as the "scene.bsq" then this information is taken and the internal ATCOR calculations for this map are skipped. In this case, the coding of the surface types has to agree with the ATCOR class label definition, of course, see Table 10.1. This file is written if the corresponding flag is set to 1, see chapter 9.3 and figure 5.9 in chapter 4.

label	class
0	geocoded background
1	shadow
2	thin cirrus over water
3	medium cirrus over water
4	thick cirrus over water
5	land
6	saturated (blue/green band)
7	snow / ice
8	thin cirrus over land
9	medium cirrus over land
10	thick cirrus over land
11	thin haze over land
12	medium haze over land
13	thin haze over water
14	medium haze over water
15	cloud over land
16	cloud over water
17	water

Table 10.1: *Class labels in the hcw file.*

Depending on the available spectral channels, it may not be possible to assign certain classes. Table 10.1 contains one class for cloud (over land, meaning water cloud), whereas the low optical thickness cloud is put into the thin and medium thickness haze class. Thin and medium haze can often be corrected successfully. Of course, there is no clear distinction between thick haze and cloud.

We take a pragmatic view, and if the haze removal is successful in areas with thick haze, then these pixels can be included in the haze mask. Since this is not clear at the beginning, it might be necessary to run the program twice, with and without haze removal. A check of the results will reveal whether the haze removal was successful. ATCOR contains a number of criteria to assess the probability of a successful haze removal, and will switch off the haze option if the chances are not good. This automatic haze termination works in most cases, but a success cannot always be guaranteed. There are three cirrus classes: thin, medium, and thick. Thin and medium cirrus can be included in the cirrus removal. The classes are currently defined with the following criteria:

Water class:

If the surface elevation of a pixel is lower than 1.2 km above sea level, then a water pixel has to fulfill the criteria:

$$\begin{aligned} \rho^*(blue) \leq 0.20 \qquad & and \qquad \rho^*(blue) > \rho^*(green) - 0.03 \\ \rho^*(NIR) < \rho^*(green) \qquad & and \qquad \rho^*(1.6\mu m) < T_{water,SWIR1} \end{aligned} \tag{10.38}$$

where $T_{water,SWIR1}$ is the water threshold reflectance in the SWIR1 band (around 1.6 μm) as defined in the preference parameter file, see chapter 9.3. Basically, the gradient of the apparent water reflectance has to be negative.

If the pixel elevation is higher than 1.2 km, the criterion of a negative gradient for the apparent reflectance does not properly work (as the path radiance in the visible, especially in the blue, becomes small), and the following criterion based on surface reflectance instead of apparent reflectance is used:

$$\rho(NIR) \leq |T_{water,NIR}| \qquad and \qquad \rho(SWIR1) \leq |T_{water,SWIR1}| \tag{10.39}$$

where $T_{water,NIR}$ is the water reflectance threshold for the NIR band (around 850 nm). Equation 10.39 is also applied if any threshold $T_{water,NIR}$ or $T_{water,SWIR1}$ is set to a negative value. In this case the elevation criterion (pixel below 1.2 km) is overruled.

Saturated pixels:

These pixels fulfill the criterion

$$DN(blue) \geq T_{saturation} \tag{10.40}$$

where $DN(blue)$ is the digital number in a blue band (around 470 nm) and the threshold $T_{saturation}$ is defined in the preference parameter file. If a blue band does not exist, a green band (around 550 m) is used as a substitute. If a green band also does not exist, a red band (around 650 nm) is used. $T_{saturation} = b \cdot encoding$, default b=0.9, e.g. 0.9*255=230 for 8 bit sensors with encoding=255. The value b=0.9 is used as default instead of the obvious b=1.0, because saturation or nonlinear effects often occur at these lower radiance levels.
As saturation usually occurs in the blue-to-red part of the spectrum, channels in this region are checked and assigned to the class 'saturated', false color coded red in the *"*_out_hcw.bsq"* file. However, the *"*_atm.log"* file contains the percentage of saturated pixels for each channel.

Cloud over land:

Pixels must satisfy the conditions:

$$\rho^*(blue) > T_c \quad and \quad \rho^*(red) > 0.15 \quad and \quad \rho^*(NIR) \,/\, \rho^*(red) < 2$$
$$and \quad \rho^*(NIR) > 0.8\ \rho^*(red) \quad and \quad \rho^*(NIR) \,/\, \rho^*(SWIR1) > 1$$
$$and \quad NDSI < 0.7 \quad or \quad DN(blue) > T_{saturation} \tag{10.41}$$

where $\rho^*(blue)$ is the apparent reflectance in a blue band, T_c is the cloud threshold as defined in the preference parameter file, and $DN(blue)$ is the corresponding digital number. If no blue band is available, a green band (around 550 nm) is taken as a substitute. If no green band exists, a red band (around 650 nm) is taken. NDSI is the normalized difference snow index:

$$NDSI = \frac{\rho^*(green) \ - \ \rho^*(SWIR1)}{\rho^*(green) \ + \ \rho^*(SWIR1)} \tag{10.42}$$

Note that saturated pixels in visible bands are automatically counted as cloud although they might be something else (e.g., snow, or a specular reflection from a surface). If a thermal band exists, the following cloud criterion must also be fulfilled:

$$(1 \ - \ \rho^*(SWIR1))\ T_{bb} < 225\ (Kelvin) \quad and\ exclude \quad T_{bb} > 300\ (Kelvin) \tag{10.43}$$

where T_{bb} is the at-sensor blackbody temperature in the selected thermal band.

Cloud over water:

The following criteria have to be fulfilled:

$$0.20 < \rho^*(blue) < 0.40\ , \quad \rho^*(green) < \rho^*(blue)$$
$$\rho^*(NIR) < \rho^*(green)\ , \quad \rho^*(SWIR1) < 0.15\ , \quad NDSI < 0.2 \tag{10.44}$$

For optically thick clouds it is not possible to distinguish clouds over water from clouds over land if only spectral criteria are used.

Cloud shadow:

Pixels must satisfy the conditions:

$$0.04 < \rho^*(NIR) < 0.12 \qquad and \qquad \rho^*(SWIR1) < 0.20 \tag{10.45}$$

and they should not belong to the water class. This may also include building shadow pixels.

Snow / ice:

Pixels must satisfy the conditions:

$$\rho^*(blue) > 0.22 \quad and \quad NDSI > 0.6 \quad and \quad DN(blue) < T_{saturation} \tag{10.46}$$

The condition $DN(blue) < T_{saturation}$ means that saturated pixels in the blue spectral band are not included in the snow mask, instead they are put into the cloud class. If no blue band exists, a green band (around 550 nm) is taken. However, if the blue or green band is saturated and $NDSI > 0.7$ then this pixel is assigned to the snow class because of the very high probability. If a green band and a SWIR2 band (around 2.2 μm) exist the following relationships are used:

$$DN(blue) < T_{saturation} \quad and \quad (\ (\rho^*(blue) > 0.22\ , \quad NDSI > 0.6)$$
$$or \quad (\rho^*(green) > 0.22\ , \quad NDSI > 0.25\ , \quad \rho^*(SWIR2)/\rho^*(green) < 0.5\ )\ ) \tag{10.47}$$

Again, if the blue or green band is saturated and $NDSI > 0.7$ then the snow class is assigned.

Cirrus over land:

The apparent reflectance is calculated in the cirrus band (1.38 μm) and additionally in a band around 1.24μm. If the latter does not exist a NIR channel is used.
Thin cirrus over land is calculated with

$$1.0\% < \rho^*(cirrus) < 1.5\% \tag{10.48}$$

employing the percent reflectance unit. Medium thickness cirrus is calculated as

$$1.5\% < \rho^*(cirrus) < 2.5\% \tag{10.49}$$

and the thick cirrus class consists of pixels with

$$\rho^*(cirrus) \geq 2.5\% \tag{10.50}$$

and the pixels have to belong to the land class.

Cirrus over water:

The same spectral criteria (eq.'s 10.48, 10.49, 10.50) hold, but the pixels have to belong to the water class.

Haze over land: see chapter 10.5.2

The the mean of the tasseled cap transformation (TC) is calculated. Clear pixels are those with $TC < mean(TC)$ and $\rho^*(blue) < T_c$ (cloud over land threshold) and $\rho^*(NIR) > T_{water}(NIR)$ (water reflectance threshold, defined in "preference_parameters.dat"). Next, the mean and standard deviation σ of the HOT transformation are calculated. Pixels are assigned to the compact haze mask if $HOT > mean(HOT)$, and to the large haze mask if $HOT > mean(HOT) - 0.5\ \sigma(HOT)$. Then the HOT histogram of all haze pixels is calculated. Pixels with values less than 40% of the cumulative histogram are assigned to thin-medium haze, pixels with higher values to medium-thick haze. This distinction is arbitrary and has no effect on the subsequent processing.

Haze over water:

Pixels must belong to the water mask, and the NIR apparent reflectance $\rho^*(NIR)$ must be greater than the NIR clear water threshold $T_{clear_water_NIR}$ defined in the preference parameter file (chapter 9.3). Thin haze over water is defined as:

$$T_{clear_water_NIR} \geq \rho^*(NIR) \geq 0.06 \tag{10.51}$$

Medium haze over water is defined as:

$$0.06 < \rho^*(NIR) \leq T_2 \tag{10.52}$$

where T_2 (default=0.12) is another editable parameter in the preference file. The method of haze removal over water is described in chapter 10.5.3. The same technique is also employed to remove sun glint.

10.3 Quality layers

The previous section defined a coarse pixel classification which is useful for an atmospheric correction. In addition, it supports an assessment of the quality of the processing. For example, a large error in the radiometric calibration could cause a scene classification with all pixels labeled as water. In this case, a user can immediately identify the problem. Of course, a more detailed assessment is possible with an analysis of the reflectance spectra. Nevertheless, the classification map (land, water, haze, cloud, etc) is a useful product and the quality of the atmospheric correction may depend on the correct class assignment, at least for some classes.

The previous (haze, cloud, water, land) pixel classifyer is a binary decision: a pixel belongs to a certain class or not. In reality the decision is typically not unique and a class assignment has only a certain probability. As the absolute probability of a class assignment is very difficult to assess, we define three probability levels: low, medium, and high coded 30, 60, 90, respectively. These numbers might be interpreted as a percent probability, but the numbers are relative and arbitrary. Currently there are three quality layers, cloud, water, and snow, which are solely calculated with spectral criteria. The quality file is written if the corresponding flag is set to 2, see chapter 9.3 and figure 5.9 in chapter 4.

Cloud probability:

- low cloud probability (coded 30):

$$\begin{aligned} \rho^*(blue) > 0.15 \quad and \quad \rho^*(red) > 0.15 \quad and \quad \rho^*(NIR) \;/\; \rho^*(red) < 2 \\ and \quad \rho^*(NIR) > 0.8\,\rho^*(red) \quad and \quad \rho^*(NIR) \;/\; \rho^*(SWIR1) > 1 \\ and \quad NDSI < 0.7 \quad or \quad DN(blue) > T_{saturation} \end{aligned} \tag{10.53}$$

  where $\rho^*(blue)$ is the apparent reflectance in a blue band, and $DN(blue)$ is the corresponding digital number. If no blue band is available, a green band (around 550 nm) is taken as a substitute. If no green band exists, a red band (around 650 nm) is taken. Note that saturated pixels in visible bands are counted as cloud although they might be something else (e.g., snow, or a specular reflection from a surface). Only saturated pixels with a very high $NDSI > 0.7$ are assigned to the snow class.

- medium cloud probability (coded 60): same as for low probability, but with

$$\rho^*(blue) > 0.25 \qquad and \qquad \rho^*(red) > 0.18 \tag{10.54}$$

  This is similar to the standard cloud assignment in the *"*_out_hcw.bsq"* file where $\rho^*(blue) > T_c$, $T_c = 0.25$ (or 25%), and $\rho^*(red) > 0.15$. The 25% reflectance threshold in the blue (or green) band is the default value in the preference parameter file.

- high cloud probability (coded 90): same as for medium probability, but with

$$\rho^*(blue) > 0.35 \qquad and \qquad \rho^*(red) > 0.25. \tag{10.55}$$

If a thermal band exists, the relationships 10.43 must also be fulfilled.

Water probability:

The criteria for the water class are described in the previous section. The following water probability rules are employed:

- low water probability (coded 30): water pixels fulfilling the above criteria (eq.'s 10.38, 10.39). This is the water assignment in the *"*_out_hcw.bsq"* file.

- medium water probability (coded 60): same as for low probability, but with a more stringent NIR reflectance threshold. If no SWIR1 band (around 1.6 μm) exists, the criterion is:

$$\rho^*(NIR) \leq 0.04 \tag{10.56}$$

  Note: the default threshold $T_{water,NIR}$ is 0.05 (or 5% in the reflectance percent unit), defined in the preference parameter file, yielding more low probability water pixels than medium probability pixels (eq. 10.56). If a SWIR1 band exists the apparent NIR reflectance threshold is relaxed (first line of eq. 10.57) because of the additional SWIR1 surface reflectance threshold.

$$\begin{aligned} &\rho^*(NIR) \leq 0.05 \quad and \quad \rho(SWIR1) \leq 0.03 \\ &\qquad\qquad\qquad\qquad or \\ &\rho^*(NIR) \leq 0.03 \quad or \quad \rho(SWIR1) \leq 0.03 \end{aligned} \tag{10.57}$$

  The relationships on the second line of eq. 10.57 assign the water probability based on the smaller reflectance value in the NIR or SWIR1.

- high water probability (coded 90): same as for medium probability, but with lower NIR, SWIR1 thresholds.

$$\begin{aligned} &\rho^*(NIR) \leq 0.03 \quad (no\ SWIR1\ band) \\ &\rho^*(NIR) \leq 0.03 \quad or \quad \rho(SWIR1) \leq 0.02 \end{aligned} \tag{10.58}$$

  Note: the default threshold $T_{water,SWIR1}$ is 0.03 (or 3% in the reflectance percent unit), defined in the preference parameter file.

Snow /ice probability:

The criteria for the snow-ice class are described in the previous section. As mentioned before, if pixels are saturated in the blue-green spectral bands they are counted as cloud unless the $NDSI > 0.7$. The following probability rules are employed for snow:

- low snow/ice probability (coded 30):

$$\rho^*(blue) > 0.22 \quad and \quad NDSI > 0.4 \quad and \quad DN(blue) < T_{saturation} \tag{10.59}$$

  If no blue band exists, a green band is used as a substitute. If a green band and a SWIR2 band exist, the rules are:

$$\begin{aligned} &DN(blue) < T_{saturation} \quad and \quad (\ (\rho^*(blue) > 0.22\ , \quad NDSI > 0.4) \\ &or \quad (\rho^*(green) > 0.22\ , \quad NDSI > 0.25\ , \quad \rho^*(SWIR2)/\rho^*(green) < 0.5\ )\ ) \end{aligned} \tag{10.60}$$

- medium snow/ice probability (coded 60): same as for low probability, but with a more stringent NDSI threshold of 0.6. This is the snow assignment in the *"hcw.bsq"* file.

$$\rho^*(blue) > 0.22 \quad and \quad NDSI > 0.6 \quad and \quad DN(blue) < T_{saturation} \tag{10.61}$$

If no blue band exists, a green band is used as a substitute. If a green band and a SWIR2 band exist, the rules are:

$$\begin{aligned} DN(blue) < T_{saturation} \quad and \quad & (\ (\rho^*(blue) > 0.22 \quad and \quad NDSI > 0.6) \\ or \quad & (\rho^*(green) > 0.22 \quad and \quad \rho^*(SWIR2)/\rho^*(green) < 0.3 \ ) \ ) \end{aligned} \tag{10.62}$$

This is very similar to the snow assignment in the *"hcw.bsq"* file, except for the threshold for $\rho^*(SWIR2)/\rho^*(green)$.

- high snow/ice probability (coded 90): same as for medium probability, but with a more stringent NDSI threshold of 0.7.

$$\rho^*(blue) > 0.22 \quad and \quad NDSI > 0.7 \quad and \quad DN(blue) < T_{saturation} \tag{10.63}$$

If no blue band exists, a green band is used as a substitute. Again, if a green band and a SWIR2 band exist, the rules are:

$$\begin{aligned} DN(blue) < T_{saturation} \quad and \quad & (\ (\rho^*(blue) > 0.22 \quad and \quad NDSI > 0.7) \\ or \quad & (\rho^*(green) > 0.22 \quad and \quad \rho^*(SWIR2)/\rho^*(green) < 0.2 \ ) \ ) \end{aligned} \tag{10.64}$$

10.4 Standard atmospheric conditions

Standard conditions comprise scenes taken under a clear sky atmosphere. This means the visibility (aerosol optical thickness) can be assumed as constant over a scene, or it might vary within a certain range (excluding haze) and a visibility map can be calculated. It also includes situations with constant or spatially varying water vapor column contents.

10.4.1 Constant visibility (aerosol) and atmospheric water vapor

This is the easiest case for atmospheric correction. Still, it can often be applied if homogeneous atmospheric conditions exist. These might be encountered for small area scenes, i.e., high spatial resolution imagery. If the sensor has no channels in atmospheric water vapor regions, results of atmospheric correction are not sensitive with respect to the selected water vapor content, and a climatological value (e.g., midlatitude summer, US standard, or tropical water vapor profile) is usually sufficient. For hyperspectral instruments, the processing has to include the image-derived pixel-by-pixel water vapor map.

The program performs a check whether the specified visibility leads to negative reflectance pixels for dark surfaces in the red band (660 nm, vegetation) and NIR band (850 nm, water). If this is the case, the visibility is iteratively increased (up to VIS=80 km) to reduce the percentage of negative reflectance pixels below 1% of the scene pixels. During an interactive ATCOR session the user is notified, and can continue with the recommended visibility update or with the initial visibility. During batch mode operation the program continues with the updated visibility and the

initial value is disregarded. A corresponding notice is given in the "*atm.log" output file. The final iterated visibility depends slightly on the initial value, because a coarse set of visibility grid points is used to restrict the number of iterations ($n \leq 8$), see Table 10.2.

Example 1: start VIS = 15 km, potential visibility iterations = 19, 24, 34, 44, 54, 64, 74 km, and the next step of 84 km is reset to VIS = 80 km. If the number of negative reflectance pixels (red, NIR bands) is already less than 1% of the number of scene pixels for VIS = 34 km, the program will terminate the visibility loop after three iterations.
Example 2: start VIS=23 km, potential visibility iterations = 28, 38, 48, 58, 68, 78 km, and the next step of 88 km is reset to VIS = 80 km. If the criterion (threshold of 1% negative reflectance pixels) is already fulfilled for VIS = 28 km, the program will terminate the visibility loop after the first iteration. If the criterion is fulfilled for the start visibility, no iteration is executed.

The upper visibility threshold of 80 km is a trade-off: although higher visibilities are possible they are not very likely, and even if a situation with a higher visibility (say VIS=120 km) is encountered, results of a calculation with vis = 80 km do not differ much from the results with VIS = 120 km. So the iteration capability is most important for low visibility start values.

visibility [km]	vis. increment [km]
5 - 15	3
15 - 20	4
20 - 28	5
28 - 60	10
60 - 80	10, but max VIS=80 km

Table 10.2: *Visibility iterations on negative reflectance pixels (red, NIR bands).*

10.4.2 Aerosol retrieval and visibility map

If a sensor has the appropriate spectral bands the aerosol type and visibility or optical thickness of the atmosphere can be derived, provided the scene contains reference areas of known reflectance behavior (Kaufman and Sendra 1988, Kaufman et al. 1997). The minimum requirements are spectral bands in the red and near IR. If the scene contains dense dark vegetation (coniferous type) the reflectance values in the red band can be obtained from a correlation with the SWIR band reflectance as detailed below. The visibility of each reference pixel can then be calculated in the red band as the intersection of the modeled at-sensor radiance curve with the measured radiance, see figure 10.6.

The measured radiance for a reference pixel of digital number DN is $L = c_0 + c_1 DN$, which is a constant value indicated by the dashed line in figure 10.6. The curve indicates the modeled radiance. It employs the reflectance of the reference surface (e.g., $\rho_{ref} = 0.02$) and uses values of path radiance, atmospheric transmittance, and global flux for the current solar and viewing geometry stored in precalculated LUTs.

Automatic masking of reference areas (1.6 or 2.2 μm band required, or at least red/NIR bands)

If the sensor has a SWIR band (at 1.6 or 2.2 μm), then the scene can be searched for dark pixels in this band and a correlation of the SWIR reflectance with the reflectance in the red and blue band

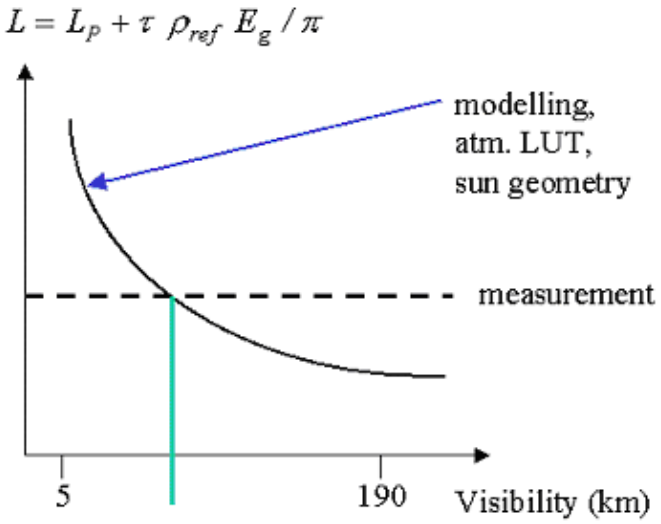

Figure 10.6: *Schematic sketch of visibility determination with reference pixel.*

can be employed to estimate the visibility automatically (Kaufman et al. 1997). For this purpose, we use a modified version of the original idea for the following algorithm.
If a SWIR band exists the SWIR reflectance is calculated assuming a visibility of 23 km (instead of the original version of top of atmosphere reflectance). Then, water pixels are excluded by employing only those pixels with SWIR reflectance values above 1% and an NDVI > 0.1. For the 2.2 μm band the upper threshold of the reflectance of the dark pixels is selected as 5%. If the number of reference pixels is less then 1% of the image pixels, then the upper threshold is increased to 10% or finally 12%. If a 1.6 μm band exists, but no 2.2 μm band, the corresponding upper thresholds are selected as 10% and 15%, or finally 18%, respectively. The reflectance ratios for the red and blue band are then calculated as :

$$\rho_{red} = 0.5\ \rho_{2.2} \qquad and \qquad \rho_{blue} = 0.5\ \rho_{red} \tag{10.65}$$

$$\rho_{red} = 0.25\ \rho_{1.6} \qquad and \qquad \rho_{blue} = 0.5\ \rho_{red} \tag{10.66}$$

This situation is sketched in figure 10.7. The correlation factor of 0.5 between the 2.2 μm and the red region is not a universal constant, but may typically vary between 0.4 and 0.6. The correlation actually also works for dark soils. So the dark pixels may also include soil areas. For narrow band hyperspectral sensors a band close to 2.13 μm is used instead of a 2.20 μm band.
The red band is then used to calculate the visibility (compare figure 10.6) as the intersection of the measured radiance with the simulated visibility-dependent at-sensor radiance curve. Since the same visibility is employed for the blue spectral band this provides an opportunity to adjust the spectral behavior of the path radiance (which is essentially the aerosol path radiance, since the Rayleigh path radiance is known) in the blue spectral region.

$$L_{p,blue}^{update} = L_{blue} - \tau_{blue}\rho_{blue}E_{g,blue}/\pi \tag{10.67}$$

The question of an automatic aerosol type calculation is addressed next.

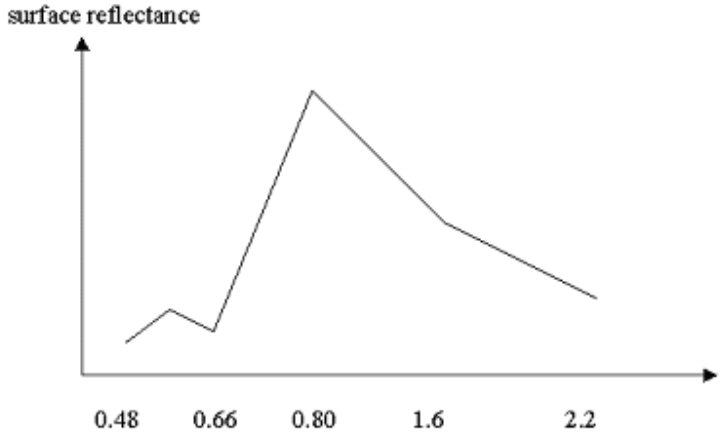

Figure 10.7: *Correlation of reflectance in different spectral regions.*

Aerosol type estimation

After calculation of the scene path radiance in the blue and red region (as total minus reflected radiance, using the average values obtained for the dark reference pixels) the ratio of $L_p(blue, scene)$ to $L_p(red, scene)$ can be compared to the corresponding ratio for the MODTRAN standard aerosols (rural, urban, maritime, desert) :

$$d_p = \frac{L_p(blue, scene)/L_p(red, scene)}{L_p(blue, MODTRAN)/L_p(red, MODTRAN)} \tag{10.68}$$

The aerosol type for which the double ratio (d_p) is closest to 1 is the best approximation for the scene. It approximates the corresponding MODTRAN aerosol type. However, some fine tuning is subsequently performed to be able to modify the wavelength behavior of the path radiance compared to the standard aerosol types. If $L_p(blue, scene)$ deviates more than 5% from $L_p(blue, MODTRAN)$ then $L_p(blue, scene)$ is used as the valid path radiance. In addition, the path radiance for any other bands in the blue to red region is linearly re-scaled with the factor $L_p(blue, scene)/L_p(blue, MODTRAN)$, see Figure 10.8. Here, the path radiance in the red band is used as a fixed tie point. For wavelengths greater than 700 nm a posssible typical 10% difference in path radiance between the selected aerosol type (after fine tuning) and the actual aerosol is usually not important, because path radiance contributes only a small fraction to the total radiance.

If the sensor has no blue spectral band, but a green band, than the green band is substituted and for the dense dark vegetation the surface reflectance relationship is used:

$$\rho(green) = 1.3\ \rho(red) \tag{10.69}$$

Now eq. 10.67 is again employed for the green band instead of the blue band to calculate the path radiance, the best match to a MODTRAN aerosol type, and possibly a fine tuning of the path radiance.

Aerosol retrieval for VNIR sensors

If no SWIR bands exist, but at least a red band (around 660 nm) and a NIR band (around 850 nm) a different approach has to be taken, see reference [64] for details. It starts with the assumption of

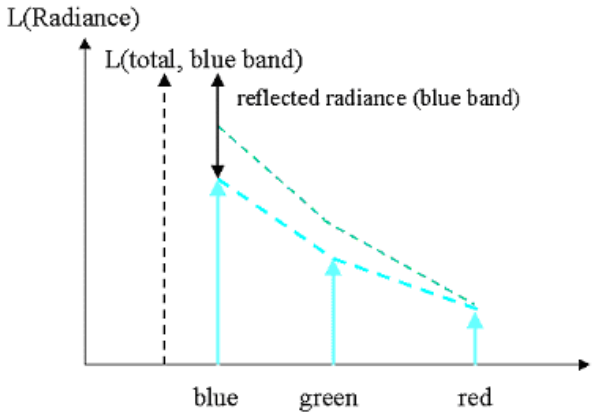

Figure 10.8: *Rescaling of the path radiance with the blue and red band.*
After subtraction of the reflected radiance from the total radiance in the blue band the remaining signal is the updated path radiance in the blue band. The path radiance of bands in the blue to red region is then rescaled with interpolation.

average clear atmospheric conditions (visibility VIS=23 km) to calculate the surface reflectance in the red and NIR bands which is appropriate for situations of clear atmospheres (VIS = 15 - 40 km). The second step derives a mask of dark vegetation pixels using the ratio vegetation index rvi of the red and near-infrared surface reflectance, $rvi = \rho_{nir}/\rho_{red}$, and multiple reflectance thresholds:

- The mask pixels have to fulfill: $rvi \geq 3$ and $\rho_{nir} \geq 0.10$ and $\rho_{nir} \leq 0.25$ and $\rho_{red} \leq 0.04$.

Water pixels are automatically excluded from this mask because of the $\rho_{nir} \geq 0.10$ condition, and soil pixels are excluded with the combination of all four conditions. If the percentage of reference pixels is smaller than 2% of the scene the search is iterated with VIS=60 km (covering the very clear conditions of visibility = 40 - 100 km). Again, if the percentage is smaller than 2%, the search is iterated with VIS=10 km to cover higher aerosol loadings (VIS = 8 - 15 km). Each visibility iteration is supplemented with an iteration of the threshold ρ_{red} which is decreased in steps of 0.005 down to $\rho_{red} = 0.025$ to include only the darkest vegetation pixels (see [64] for details). Currently, the algorithm terminates if less than 2% reference pixels are found after these two iterations. In this case, the user has to employ the constant visibility option specifying the value of the visibility for the scene. During batch mode operation the program takes the specified visibility (from the ".inn" file). Then a check for negative reflectance pixels is performed with dark pixels in the red band (660 nm, vegetation) and the NIR band (850 nm, water), and the visibility is iteratively increased (up to VIS=60 km) to reduce the percentage of negative reflectance pixels below 1% of the scene pixels. A corresponding notice is given in the "*atm.log" output file.
The third step calculates the surface reflectance in the red band as a fraction α of the NIR band reflectance:

$$\rho_{red} = \alpha * \rho_{nir} = 0.1 * \rho_{nir} \tag{10.70}$$

Similar to the empirical SWIR relationships the coefficient $\alpha = 0.1$ is an average empirical value yielding results in close agreement with the SWIR method in many cases. However, deviations from the nominal value $\alpha = 0.1$ can vary about 30% depending on biome. Before the final step of atmospheric correction takes place the visibility of non-reference pixels in the scene can be set to

the average value of the reference pixels or a spatial interpolation can be applied.

The visibility calculated for each reference pixel (range 5 - 190 km in ATCOR) is converted into an integer, called visibility index vi, with range 0-182. The visibility index is closely related to the total optical thickness δ at 550 nm, the equidistant optical thickness spacing is 0.006 for a ground at sea level, and smaller for increasing elevations.

$$\delta = 0.185 + 0.006 * vi \tag{10.71}$$

It is easy to calculate the aerosol optical thickness (AOT) from a known total optical thickness by subtracting the Rayleigh optical thickness and a very small trace gas optical thickness, compare Fig. 2.1 in chapter 2.
With the MODTRAN code the AOT (at 550 nm) can be calculated from a given visibility VIS (km) as

$$AOT = exp\,(a(z) + b(z)\ ln(VIS)) \tag{10.72}$$

where z is the surface elevation, and a(z), b(z) are coefficients obtained from a linear regression of $ln(AOT)$ versus $ln(VIS)$.

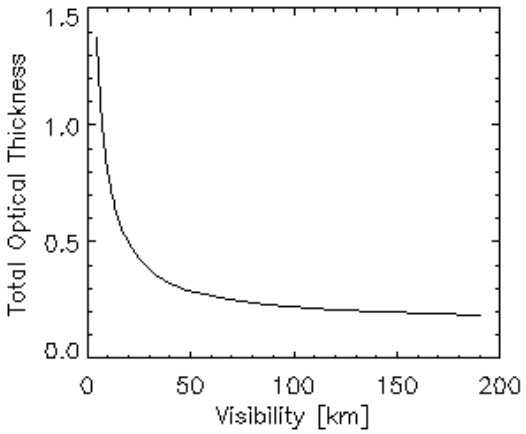

Figure 10.9: *Optical thickness as a function of visibility and visibility index.*

10.4.3 Water vapor retrieval

A water vapor retrieval can be included after the aerosol retrieval because the aerosol retrieval does not use water vapor sensitive spectral bands, but the water vapor algorithm (employing bands around 940 or 1130 nm) depends on aerosol properties. The water vapor retrieval over land is performed with the APDA (atmospheric precorrected differential absorption) algorithm [75]. In its simplest form, the technique uses three channels, one in the atmospheric water vapor absorption region around 940 or 1130 nm (the "measurement" channel), the others in the neighboring window regions ("reference" channels). The depth of the absorption feature is a measure of the water vapor column content, see figure 10.10.
In case of three bands the standard method calculates the water vapor dependent APDA ratio as :

$$R_{APDA}(\rho, u) = \frac{L_2(\rho_2, u) - L_{2,p}(u)}{w_1(L_1(\rho_1) - L_{1,p}) + w_3(L_3(\rho_3) - L_{3,p})} \tag{10.73}$$

where the index 1 and 3 indicates window channels (e.g. in the 850-890 nm region and 1010-1050 nm region), respectively. Index 2 indicates a channel in the absorption region (e.g., 910-950 nm). L and L_p are the total at-sensor radiance and path radiance, respectively. The symbol u indicates the water vapor column. The weight factors are determined from

$$w_1 = (\lambda_3 - \lambda_2)/(\lambda_3 - \lambda_1) \qquad and \qquad w_3 = (\lambda_2 - \lambda_1)/(\lambda_3 - \lambda_1) \tag{10.74}$$

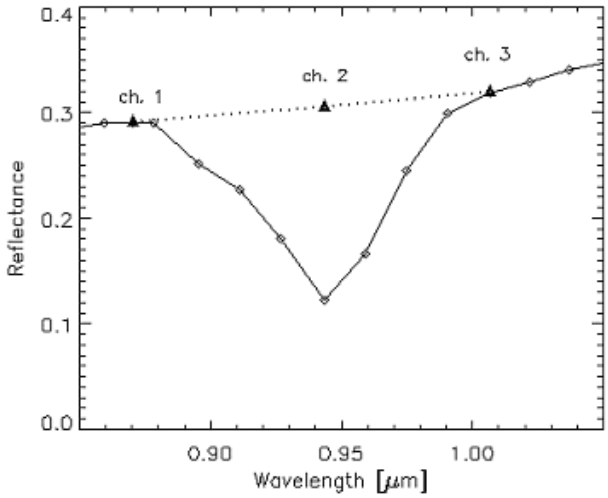

Figure 10.10: *Reference and measurement channels for the water vapor method. The at-sensor radiance is converted into an at-sensor reflectance.*

The problem is the estimation of the surface reflectance ρ_2 in the absorption band (eq. 10.73). The technique tries to estimate the reflectance ρ_2 with a linear interpolation of the surface reflectance values in the window channels (ch. 1, 3) that are not or only slightly influenced by the water vapor content: Therefore, the reflectance ρ_2 is calculated as

$$\rho_2 = w_1\rho_1 + w_3\rho_3 \tag{10.75}$$

Then equation (10.73) can be written as

$$R_{APDA}(u) = \frac{\rho_2\tau_2(u)E_{g2}(u)}{\rho_2\tau_2(u=0)E_{g2}(u=0)} = \frac{\tau_2(u)E_{g2}(u)}{\tau_2(u=0)E_{g2}(u=0)} \tag{10.76}$$

where $E_{g2}(u)$ is the global flux on the ground for the measurement channel (index 2). ATCOR employs 4 to 5 water vapor columns (u=0.4, 1.0, 2.0, 2.9, 4.0 cm, sea-level-to space geometry) to calculate an exponential fit function

$$R_{APDA}(u) = exp(-\alpha + \beta\sqrt{u}) \tag{10.77}$$

which can be solved for the water vapor column u , see Fig. 10.11, where the diamonds in the figure mark the calculated water vapor grid points (u= 0.4, 1.0, 2.0, 2.9 cm) :

$$u = (\frac{\alpha + lnR_{APDA}}{\beta})^2 \tag{10.78}$$

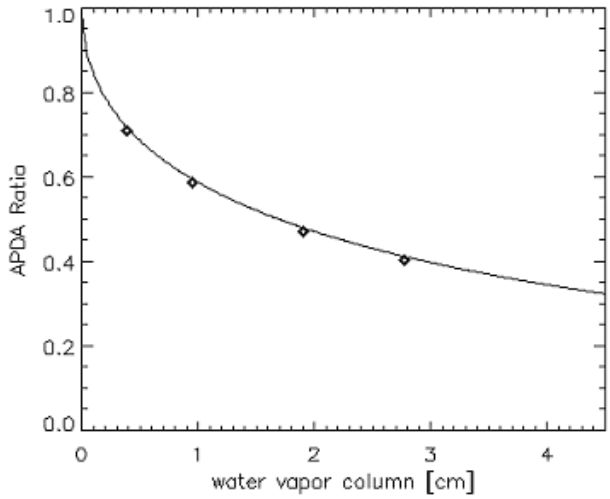

Figure 10.11: *APDA ratio with an exponential fit function for the water vapor.*

Equations (10.73, 10.75 to 10.78) are iterated, starting with u=1.0 cm, calculating R_{APDA}, updating u, $L_{i,p}(u)$, ρ_1, ρ_3 and repeating the cycle. A minimum of two channels (one reference, one measurement channel) is required. The advanced APDA method can take into account multiple absorption channels in the 910-960 nm and 1110-1150 nm regions. Two water vapor retrieval algorithms are available in ATCOR (compare chapter 9.4, parameter iwv_model = 1, 2):

1. The water vapor maps with the smallest standard deviation in the 940 nm and 1130 nm region are selected. Finally, if both regions are available, the average of these two water vapor maps is taken (parameter iwv_model=1 in the ".ini" file).

2. A linear regression ratio (LIRR) is applied to multiple bands (parameter iwv_model=2). This water vapor map might be more accurate, because the regression reduces sensor noise and may partially compensate calibration problems in lucky cases. Although the water vapor map might be less noisy, the retrieved surface reflectance spectrum will always retain any channel calibration problems.

Remarks:

1. The APDA algorithm is relatively fast. Its disadvantage is that it is not stable numerically for very low reflectance targets (water, shadow regions). The transmittance slope ratio method [72] might work better in these cases, so it is an interesting alternative water vapor algorithm. However, since the required processing time is much higher than for the APDA method, it is currently not implemented in the ATCOR environment. In addition, the method requires data with a very accurate spectral and radiometric calibration, otherwise its potential advantage will be lost.

2. Five water vapor grid points at 0.4, 1.0, 2.0, 2.9, and 4.0 cm are sufficient to cover the 0.5 - 5.0 cm range with an accuracy of about 5-10 % [66].

10.5 Non-standard conditions

The non-standard situations refer to bidirectional reflectance (BRDF) effects and scenes with a substantial amount of haze and shadow areas. Although bidirectional surface reflectance effects are independent of the atmospheric conditions, the subject is included here, because the isotropic reflector is used for the standard conditions. We present some empirical methods of BRDF correction in flat and rugged terrain. The non-standard atmospheric conditions treat the haze removal and de-shadowing employing spectral and statistical algorithms.

10.5.1 Empirical methods for BRDF correction

ATCOR offers two different methods of correcting BRDF effects. The first method is mainly intended for flat terrain and normalizes the off-nadir reflectance values to the corresponding nadir values. The second method is exclusively dedicated to rugged terrain imagery. The reflectance values of areas with low local sun elevation angles, i.e. large local solar zenith angles, are often overcorrected by the assumption of isotropically reflecting surfaces, and the method reduces these high overcorrected values depending on the illumination and/or viewing angles. In some cases of rugged terrain imagery it is useful to apply both methods of empirical BRDF correction.

1. Nadir normalization method

A simple algorithm was implemented as part of the ATCOR package to normalize the scan angle dependent brightness values to the nadir value. It is recommended to apply the method to imagery after atmospheric correction, i.e., to reflectance data. However, if only the across-track illumination gradients shall be removed without any further atmospheric correction, the algorithm can also be applied to radiance (DN) data. In this case, the brightness gradient may be caused by a combination of surface BRDF and atmospheric BRDF (left/right asymmetry in path radiance).
The algorithm is intended for large field-of view sensors (minimum FOV=20^o). It computes the column means with a certain angular sampling interval (1^o or 3^o). The input image may be geocoded, or not. If it is not geocoded the total field-of-view FOV corresponds to the number n of across-track image pixels per line. If geocoded, the scan angle for each pixel must be provided in a separate file ("_sca"). It contains the scan angle in degree scaled with a factor of 100, and coded with 16 bits per pixel. This definition is taken from the airborne ATCOR/PARGE interface (Schläpfer and Richter 2002). Scan angles on the right hand side with respect to flight heading are defined as negative, those on the left side as positive, e.g., a value of -2930 represents a scan angle of 29.3°on the right side.

The nadir region is defined here as the $\pm 3^o$ scan angle range. Usually, a 3^o angular sampling interval, from $+3^o$ to +FOV/2 on the left side and -3^o to -FOV/2 on the right side, is adequate, except for geometries close to the hot spot geometry. In the latter case, a 1^o sampling interval can be selected.
If $\bar{b}_{nadir}$ denotes the averaged brightness value for the nadir region, i.e., reflectance or radiance, then the nadir normalized brightness value of a pixel with column number j is calculated as:

$$b_{norm}(j) = b(j)\frac{\bar{b}_{nadir}}{f_2(j)} \tag{10.79}$$

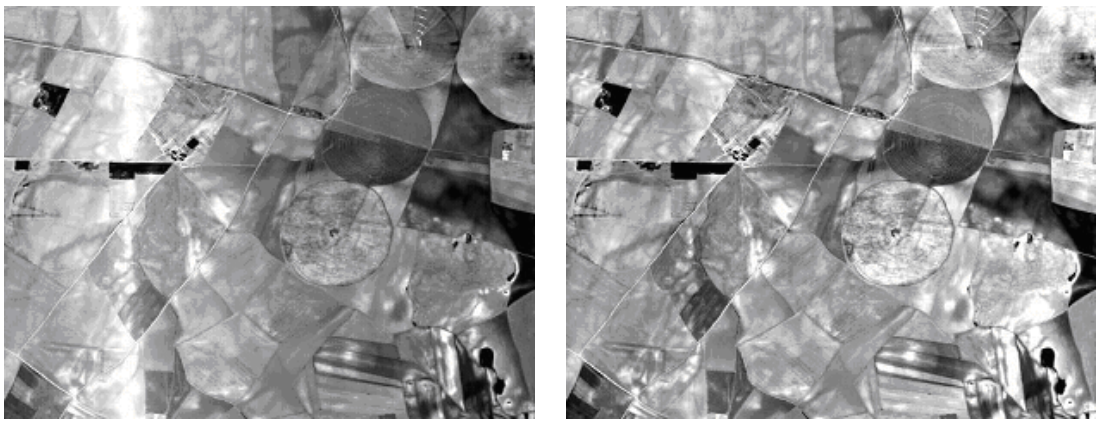

Figure 10.12: *Nadir normalization of an image with hot-spot geometry.*
Left: reflectance image without BRDF correction. Right: after empirical BRDF correction.

where the function f_2 is obtained with three processing steps:

- The first step is the averaging over each interval (3°or 1°). It yields a function f_1 with m+1 grid points for the m off-nadir intervals plus the nadir interval.
- Two cases are distinguished now: if the image is not geocoded, an interpolation from function $f_1(m+1)$ to a function $f_2(ncols)$ is performed where ncols is the number of column pixels of the image. If the image is geocoded, an interpolation from the 3° grid to the 1° grid is performed (no hot spot case).
- The third step is a filter with a moving average window applied to the f_2 function. The following cases are distinguished: if the image is not geocoded the window is 9 pixels (without hot spot) and 3 pixels (with hot spot option). If the image is geocoded, the moving window extends over a 5° angular interval (no hot spot) and over a 3° interval (with hot spot option).

Figure 10.12 shows part of a HyMap image (acquired 3 June 1999, Barrax, Spain, 12:09 UTC) containing the hot spot geometry. The solar azimuth was 181^o and the sensor scan line azimuth was 179^o, almost exactly pointing into the solar azimuth. The left image shows HyMap band 30 at 868 nm after atmospheric correction. The right image is the result after nadir normalization with a 1^o sampling interval. In this example, the column means were calculated globally, i.e. surface cover independent. The algorithm also contains an option to compute the column means separately for 4 surface covers. It can currently only be selected if the input imagery is reflectance data and not geocoded. The processing time is much larger than for the global, cover-independent method. The four surface classes are:

- bright vegetation (ratio vegetation index NIR/RED > 10);
- medium/dark vegetation (6 < ratio vegetation index < 10);
- dry vegetation or mixed vegetation/soil (3 < vegetation index < 6);
- soil (vegetation index < 3).

The reflectance of off-nadir water pixels (criterion: near infrared reflectance < 5 %) is not modified.

2. Empirical BRDF correction in rugged terrain

For many surface covers the reflectance increases with increasing solar zenith and / or viewing angle [47]. Scenes in mountainous regions often exihibit a large variation of terrain slopes, and thus bidirectional brightness variations for a certain surface cover, e.g., meadow or forest. This behavior cannot adequately be eliminated with the Lambertian assumption of equation (10.15). This equation leads to overcorrected reflectance values in faintly illuminated areas (having small values of $cos\beta$). Several approaches have been pursuit to solve this problem :

- an empirical coefficient C is calculated based on a regression of brightness values and the local ilumination angle derived from the DEM. The coefficient depends on scene content and wavelength ([85], [54]).
- the sun-canopy-sensor (SCS) geometry is employed in forested terrain instead of the solely terrain-based geometry [25].
- the SCS method is coupled with the C-correction [83].

These approaches produced good results on sample scenes with uniform cover types presented in the above papers. When applying the methods to a wider range of areas, some of the practical problems are:

- mountainous scenes often contain a number of different covers, e.g., deciduous forest, coniferous forest, mixed forest, shrubs, meadow, rocks, etc.
- the computation of the C coefficients for different surface covers would require a pre - classification.
- the correlation obtained for the C coefficients is often less than 0.7, yielding unreliable results with this method.

These remarks are supported by reference [54]. These authors applied different correction approaches to a TM scene containing different cover types and noted that there is no optimum method for all cover types. A drawback of the Minnaert and empirical C-methods is that they do do not distinguish between the direct and diffuse solar illumination as opposed to the physically based approach of ATCOR. Nevertheless, the latter approach also cannot avoid problems in faintly illuminated areas. Therefore, it is supplemented by an empirical method with three adjustable parameters (β_T, b, and g) as explained below. This approach was tested on different rugged terrain scenes with vegetated and arid landscapes and usually yields satisfactory results. It reduces overcorrected reflectance values starting at a threshold local solar zenith angle β_T greater than the scene's solar zenith angle Θ_s. Equation (10.80 defines the implemented basic geometric correction

function which depends on the local solar incidence angle (solar illumination β_i) and the threshold angle β_T. The exponent b (= 1/3, 1/2, 3/4, or 1) is the second parameter and can be selected by the user. Some guidelines on the choice of b are are discussed below. The third adjustable parameter is the lower bound g of the correction function, see Figure 10.13.

$$G = \{cos\beta_i / cos\beta_T\}^b \qquad \geq g \tag{10.80}$$

The threshold illumination angle β_T should have some margin to the solar zenith angle to retain the original natural variation of pixels with illumination angles close to the solar zenith angle. The threshold angle can be specified by the user and the following empirical rules are recommended:

- $\beta_T = \theta_s + 20°$ if $\theta_s < 45°$
- If $45 \leq \theta_s \leq 20°$ then $\beta_T = \theta_s + 15°$
- If $\theta_s > 55°$ then $\beta_T = \theta_s + 10°$

These rules are automatically applied if $\beta_T = 0$, e.g., during batch processing.

The geometric function G needs a lower bound g to prevent a too strong reduction of reflectance values. Values of G greater than 1 are set to 1, and values less than the boundary g are reset to g. This means the processing works in the geometric regime from β_T to 90°and the updated reflectance is

$$\rho_g = \rho_L G \tag{10.81}$$

where ρ_L is the isotropic (Lambert) value.

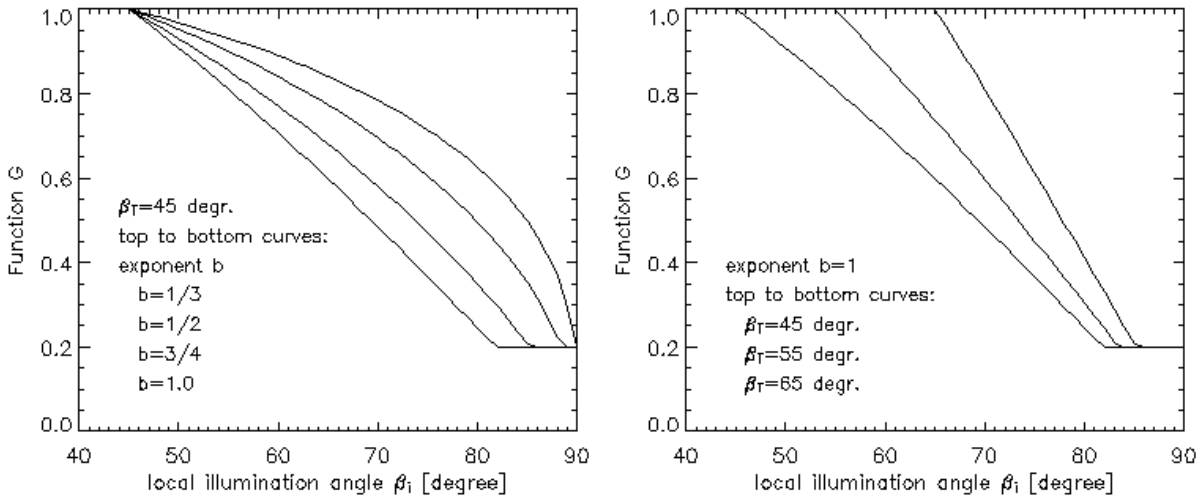

Figure 10.13: *Geometric functions for empirical BRDF correction.*
Left: Functions G eq. (10.80) for different values of the exponent b.
Right: Functions G of eq. (10.80) for b=1 and different start values of β_T.
The lower cut-off value is g=0.2 .

Figure 10.13 shows a graphical presentation of equation (10.80). The left part displays the function G for different values of the exponent b. For b=1 the decrease with β_i is strong with a constant gradient. For smaller values of b the decrease with β_i is moderate initially, but the gradient increases

with larger β_i. Currently, different functions G for soil/sand and vegetation can be selected in ATCOR (compare the graphical user interface of Figure 5.31). The function G for soil / sand is applied with a wavelength - independent exponent b. After testing a large number of vegetated mountainous scenes two vegetation modes were finally selected because of their good performance:

1. b=0.75 for channels with $\lambda < 720$ nm and b=0.33 for $\lambda > 720$ nm ("weak" correction),
2. b=0.75 ($\lambda < 720$ nm) and b=1 ($\lambda > 720$ nm), ("strong" correction).

In most of the tested cases, the first mode was appropriate. A simple criterion (vegetation index $\rho_{850nm}/\rho_{660nm} > 3$) is used to distinguish soil/sand and vegetation.
The right part of Figure 10.13 shows the effect of shifting the threshold illumination angle β_T. For larger values of β_T the decline of function G starts later with a larger gradient, and the lower bound g is met at slightly higher values of β_i. In most cases, g=0.2 to 0.25 is adequate, in extreme cases of overcorrection g=0.1 should be applied.

10.5.2 Haze removal over land

In many cases of satellite imagery the scene contains haze and cloud areas. The optical thickness of cloud areas is so high that the ground surfaces cannot be seen, whereas in hazy regions some information from the ground is still recognizable. In ATCOR the scene is partitioned into clear, hazy, and cloud regions. Here we will treat the low altitude boundary layer (0 - 3 km) haze as opposed to high altitude cirrus. Thin boundary layer haze can be detected with broad-band multispectral instruments, while a detection of thin cirrus requires specific narrow bands around 1.38 μm or 1.88 μm, compare chapter 10.5.4. As a first approximation, haze is an additive component to the radiance signal at the sensor. It can be estimated and removed as described below. Cloud areas have to be masked to exclude them from haze areas and to enable a successful haze removal. The treatment of cloud shadow regions is discussed in chapter 10.5.5.
The haze removal algorithm runs fully automatic. It is a combination of the improved methods [57], [90] and consists of five major steps :

1. Masking of clear and hazy areas with the tasseled cap haze transformation [15].

$$TC = x_1 * BLUE + x_2 * RED \tag{10.82}$$

   where BLUE, RED, x_1, and x_2 are the blue band, red band, and weighting coefficients, respectively. The clear area pixels are taken as those pixels where TC is less than the mean value of TC.

2. Calculation of the regression between the blue and red band for clear areas ("clear line" slope angle α), see figure 10.14. If no blue band exists, but a green spectral band, then the green band is used as a substitute.

3. Haze areas are orthogonal to the "clear line", i.e., a haze optimized transform (HOT) can be defined as (Zhang et al. 2002):

$$HOT = BLUE * sin\alpha - RED * cos\alpha \tag{10.83}$$

4. Calculation of the histogram of HOT for the haze areas.

5. For bands below 800 nm the histograms are calculated for each HOT level j. The haze signal Δ to be subtracted is computed as the DN corresponding to HOT(level j) minus the DN corresponding to the 2% lower histogram threshold of the HOT(haze areas). The de-hazed new digital number is (see figure 10.14):

$$DN(new) = DN - \Delta \tag{10.84}$$

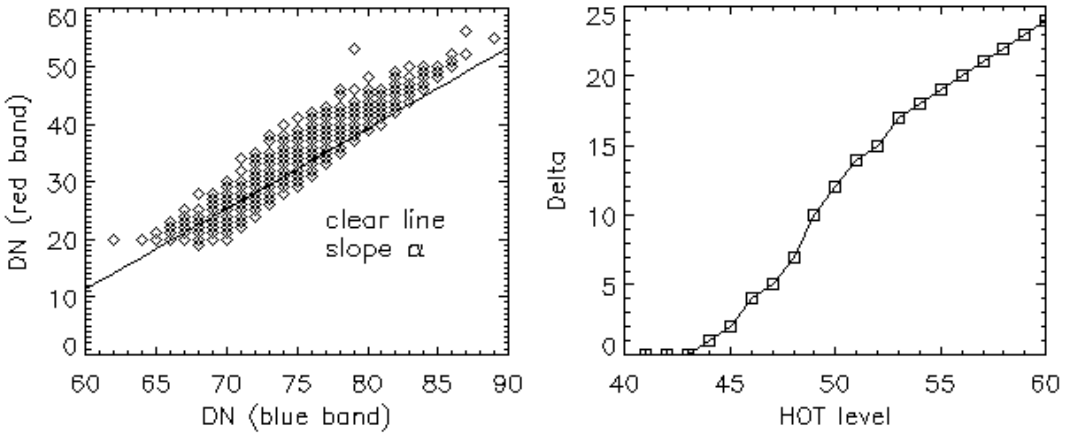

Figure 10.14: *Haze removal method. Left: regression between red and blue band for clear areas. Right: calculation of Delta=Δ as a function of the HOT haze level (example Landsat TM band 1).*

So the haze removal is performed before the surface reflectance calculation. Two options are available: the use of a large area haze mask (eq. 10.85), which is superior in most cases, or a compact smaller area haze mask (eq. 10.86).

$$HOT > mean(HOT) - 0.5 * stdev(HOT) \tag{10.85}$$

$$HOT > mean(HOT) \tag{10.86}$$

In addition, the user can select between haze removal of "thin / medium haze" or "thin to moderately thick haze", the last option is superior in most cases.

The algorithm only works for land pixels, so the near infrared band (NIR) is used to exclude water pixels. The current implementation provides a mask for haze-over-land (coded with 110 in the visibility index channel). The haze-over-water mask (to be coded with 111) is difficult to determine, leaving room for future research and improvements. The cloud mask is coded with 112. The remaining numbers (0 to 109) of the visibility index channel ("*_visindex.bsq" file) are reserved for the coding of the optical optical thickness channel are reserved for the coding of the optical depth or visibility index itself, compare chapter 10.4.2 on the derivation of the visibility map.

Figure 10.15 shows an example of a subset of an Ikonos scene of Dresden where the haze removal algorithm was applied. More images with the results of the haze removal method are shown on ATCOR's web page, http://www.rese.ch or http://www.op.dlr.de/atcor.

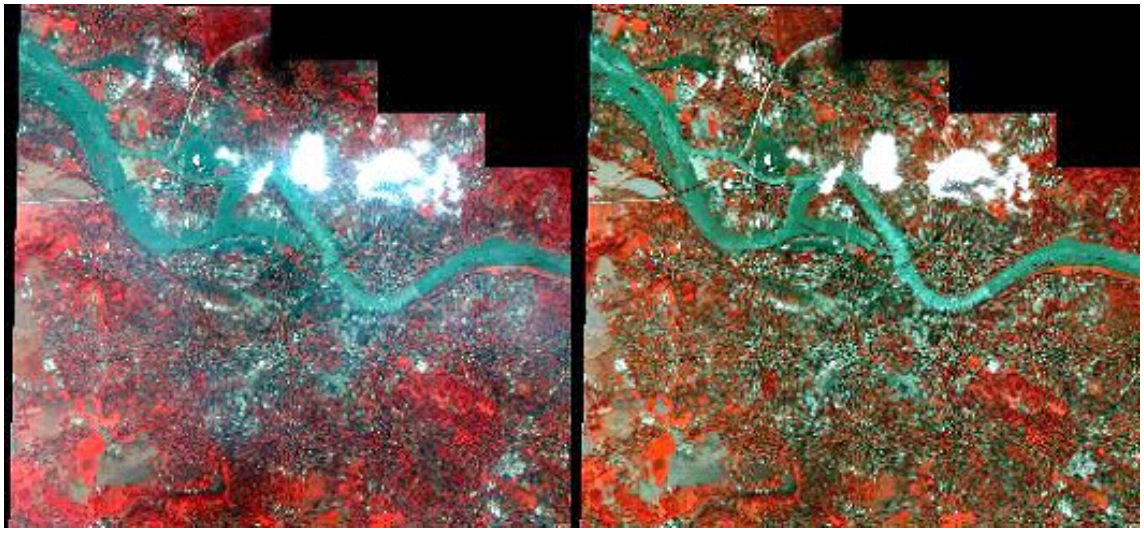

Figure 10.15: *Subset of Ikonos image of Dresden, 18 August 2002. ©Space Imaging Europe 2002. Left: original scene, right: after haze removal. Color coding: RGB=4/2/1 (NIR/Green/Blue bands)*

10.5.3 Haze or sun glint removal over water

The haze removal over water uses a near infrared (NIR) band to estimate the spatial distribution of haze. The principal method is described in [43]. We use a modified version of this approach without an interactive definition of haze polygons. First, the water pixels are masked either using spectral criteria or taking an external water map. If the scene is named *"scene1.bsq"* the external map must be named *"scene1_water_map.bsq"*, a 1-channel 8-bit/pixel or 16-bit/pixel file where water is coded with an arbitrary positive number. The external map is automatically taken if it is placed in the same folder as the scene. The second step is the definition of clear water pixels using the apparent reflectance in the NIR band. Pixels are labeled as clear if

$$\rho^*(NIR) < T_1(clear) \qquad clear\ pixels \tag{10.87}$$

The default value is $T_1(clear) = 0.04$ (i.e. 4%). The value is one of the editable preference parameters (see chapter 9.3). Thin haze over water is defined as:

$$T_1(clear) \leq \rho^*(NIR) \leq 0.06 \qquad thin\ haze \tag{10.88}$$

Medium haze over water is defined as:

$$0.06 < \rho^*(NIR) \leq T_2(haze) \qquad medium\ haze \tag{10.89}$$

The default value is $T_2(haze) = 0.12$ (i.e. 12%). This value is also one of the editable preference parameters. The third step is a linear regression between haze pixels in the NIR band and each other (reflective) band. The regression is iterated with only those pixels deviating less than half a standard deviation from the average. If α_j and β_j denote offset and slope of the regression line, respectively, the de-hazed pixel for each channel j can be calculated as

$$DN(corrected, j) = DN(original, j) - (\alpha_j + \beta_j DN_{NIR} - DN(clear, j)) \tag{10.90}$$

where $DN(clear, j)$ is the average of all clear water pixels in channel j. The same technique is also employed to remove sun glint. The main problem is the specification of the clear water threshold.

If the threshold is too low, clear water pixels are included in the haze mask, if it is set too high haze or sun glint pixels will be included in the clear pixel class. There is no unique solution, because sandy bottoms over shallow water can have a similar spectral reflectance behavior as haze, so the clear water threshold is scene-dependent. In addition, the upper threshold defining haze (or sun glint) might be scene-dependent. However, the default values usually provide good results and a solid basis for a possible iteration of these two parameters.
Figure 10.16 presents an example of haze removal over water with the two default values of $T_1(clear) = 0.04$ and $T_2(haze) = 0.12$. The de-hazing over water is successful to a large extent, however, some artifacts appear close to the land border (image center) where haze pixels over water are classified as land or cloud. This is due to a simple spectral classification of the land / water mask, an external water map would lead to better results.

Figure 10.16: *Haze removal over water, ALOS-AVNIR2 true color image, northern Germany, 16 April 2007. Left: part of original scene, right: after haze removal.*

10.5.4 Cirrus removal

On the first glance, images contaminated by cirrus appear similar to hazy scenes discussed in the previous section. However, haze usually occurs in the lower troposphere (0-3 km) while cirrus clouds exist in the upper troposphere and lower stratosphere (8 - 16 km). The effect of boundary layer haze can be observed in the visible region, but seldom in longer wavelength channels > 850 nm. However, cirrus also affects the NIR and SWIR spectral regions. Thin cirrus clouds are difficult to detect with broad-band multispectral satellite sensors in the atmospheric window regions, especially over land, because land scenes are spatially inhomogeneous and this type of cloud is partially transparent. On the other hand, water vapor dominates in the lower troposphere and usually 90% or more of the atmospheric water vapor column is located in the 0 - 5 km altitude layer. Therefore,

if a narrow spectral band is selected in a spectral region of very strong water vapor absorption, e.g., around 1.38 μm or 1.88 μm, the ground reflected signal will be totally absorbed, but the scattered cirrus signal will be received at a satellite sensor or a sensor in a high-altitude aircraft (e.g., 20 km AVIRIS scenes).

So a narrow channel at 1.38 μm is able to detect cirrus clouds, and if a correlation of the cirrus signal at this wavelength and other wavelengths in the VNIR and SWIR region can be found, then the cirrus contribution can be removed from the radiance signal to obtain a cirrus-corrected scene. The basic ideas of cirrus correction were presented in several papers ([19], [20], [22], [71]). The algorithm differs for water and land pixels. For water, a scatterplot of the 1.38 μm versus the 1.24 μm channel is used, for land the band-correlation is determined from a scatterplot of the 1.38 μm versus a red channel (around 0.66 μm). To obtain a high sensitivity, only vegetation pixels are taken because they have a low reflectance in the red spectral region, so the cirrus contribution is easily traced. The scatterplot is computed in terms of the apparent (TOA or at-sensor) reflectance of $\rho_{1.38}$ versus ρ_{red} where the apparent reflectance is defined as:

$$\rho^* = \frac{\pi L}{E_s \; cos\theta_s} \tag{10.91}$$

where L is the recorded radiance signal, E_s the extraterrestrial solar irradiance for the selected band, and θ_s is the solar zenith angle. Following [19] the method can be described by the following set of equations:

$$\rho^*(\lambda) = \rho_c(\lambda) \; + \; \frac{T_c(\lambda) \; \rho(\lambda)}{1 \; - s_c(\lambda) \; \rho(\lambda)} \tag{10.92}$$

Here, ρ_c is the reflectance of the cirrus cloud, T_c the two-way transmittance (direct plus diffuse) through the cloud, ρ the reflectance of the *"virtual"* surface (land or water surface including all effects of molecular and aerosol scattering below the cirrus), and s_c is the cloud base reflectance of upward radiation. Eq. 10.92 can be simplified, because of $s_c \; \rho << 1$, yielding

$$\rho^*(\lambda) = \rho_c(\lambda) \; + \; T_c(\lambda) \; \rho(\lambda) \tag{10.93}$$

With the assumption that the cirrus reflectance $\rho_c(\lambda)$ is linearly related to the cirrus reflectance at 1.38 μm we obtain

$$\rho^*(\lambda) = \rho_c(1.38\mu m) \; / \; \gamma \tag{10.94}$$

where γ is an empirical parameter derived from the scene scatterplot of $\rho_{1.38}$ versus ρ_{red} (land) or $\rho_{1.24}$ (water). It depends on the scene content, cirrus cloud height, and solar and viewing angles. Fig. 10.17 shows an example of such a scatterplot. The red line is the left-side boundary of data points that are not influenced by ground surface reflection, i.e. cirrus-contaminated pixels are clustered around this line, and its slope represents the correlation coefficient γ (the blue line represents the first of several iterations). Papers on the cirrus algorithm often restrict eq. 10.94 to the wavelength interval $0.4 < \lambda < 1 \; \mu m$, but we will extend this relationship into the SWIR region. Substituting eq. 10.94 into eq. 10.93 yields

$$T_c(\lambda) \; \rho(\lambda) = \rho^*(\lambda) \; - \; \rho_c(1.38\mu m) \; / \; \gamma \tag{10.95}$$

Neglecting the cirrus transmittance T_c (i.e., setting $T_c = 1$), we obtain the *"cirrus path radiance corrected"* apparent reflectance image (index 'cc'):

$$\rho^*_{cc}(\lambda) = \rho^*(\lambda) \; - \; \rho_c(1.38\mu m) \; / \; \gamma \tag{10.96}$$

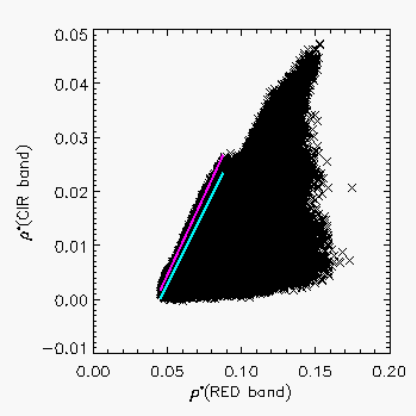

Figure 10.17: *Scatterplot of apparent reflectance of cirrus (1.38 μm) band versus red band.*

As the cirrus is almost on top of the atmosphere we have $\rho_c(1.38\mu m) = \rho_c^*(1.38\mu m)$ and the apparent cirrus reflectance can be calculated with eq. 10.91. Cirrus removal is conducted as the first step during atmospheric correction, followed by the aerosol and water vapor retrievals. If the average water vapor column W of a scene is less than some threshold (default W=0.6 cm) then the cirrus removal algorithm is switched off, to avoid a misinterpretation of bright surfaces as cirrus in the 1.38 μm channel. Normally, atmospheric water vapor completely absorbs surface features in the 1.38 μm channel, but the channel might become partly transparent to surface features for very low water vapor values. This water vapor threshold can be set by the user, see chapter 9.3.

The file *'xxx_out_hcw.bsq'* (haze, cloud, water) corresponding to a scene *'xxx.bsq'* contains three relative levels of cirrus optical thickness (thin, medium, and high). The corresponding thresholds are arbitrarily set depending on the statistics (mean, standard deviation) of the apparent reflectance $\rho_c^*(1.38\mu m)$ map. The file *'xxx_out_hcw.bsq'* is intended as a visual aid or quicklook, therefore, the cirrus level maps of different scenes cannot be compared quantitatively. As an example, a certain scene setting could be:

- thin cirrus thickness, color coded as light yellow, with $0.010 < \rho^*(cirrus) \leq 0.015$,
- medium thickness, color coded as darker yellow, with $0.015 < \rho^*(cirrus) \leq 0.025$,
- high thickness, color coded as bright yellow, with $\rho^*(cirrus) > 0.025$ (reflectance units).

In addition to the 1.38 μm cirrus channel, another channel (index w1) around 1.24 μm (or as a substitute a NIR channel from the 800 to 900 nm region) is employed with a ratio criterion to define cirrus pixels:

$$\rho^*(cirrus)/\rho^*(w1) > T(cir) \tag{10.97}$$

Reference [21] proposes a threshold of T(cir) = 0.3 to distinguish tropospheric aerosols due to dust storms from cirrus clouds. However, in the absence of dust storms, this threshold is too high and predicted no cirrus in a number of test scenes containing a lot of cirrus clouds. Therefore, we use much lower values of T(cir) ranging from 0.01 (for water vapor columns W > 1 cm) to T(cir)=0.15 (for W < 0.5 cm). So with these thresholds, tropospheric aerosols might be misclassified as cirrus in situations with dust storms, but this is a necessary trade-off. In any case, those cloud areas are

excluded from the map of pixels employed for the aerosol retrieval, which is the main purpose.

The cirrus and (boundary layer) haze removal options are exclusive, i.e., only one of them can be selected per run.

10.5.5 De-shadowing

Remotely sensed optical imagery of the Earth's surface is often contaminated with cloud and cloud shadow areas. Surface information under cloud covered regions cannot be retrieved with optical sensors, because the signal contains no radiation component being reflected from the ground. In shadow areas, however, the ground-reflected solar radiance is always a small non-zero signal, because the total radiation signal at the sensor contains a direct (beam) and a diffuse (reflected skylight) component. Even if the direct solar beam is completely blocked in shadow regions, the reflected diffuse flux will remain, see Figure (10.18). Therefore, an estimate of the fraction of direct solar irradiance for a fully or partially shadowed pixel can be the basis of a compensation process called de-shadowing or shadow removal. The method can be applied to shadow areas cast by clouds or buildings.

The proposed de-shadowing technique works for multispectral and hyperspectral imagery over land acquired by satellite / airborne sensors. The method requires a channel in the visible and at least one spectral band in the near-infrared (0.8-1 μm) region, but performs much better if bands in the short-wave infrared region (around 1.6 and 2.2 μm) are available as well. The algorithm consists of these major components: (i) the calculation of the covariance matrix and zero-reflectance matched filter vector, (ii) the derivation of the unscaled and scaled shadow function, (iii) a histogram thresholding of the unscaled shadow function to define the core shadow areas, (iv) a region growing to include the surroundings of the core shadow areas for a smooth shadow/clear transition, and (v) the de-shadowing of the pixels in the final shadow mask. Details are published in [63].

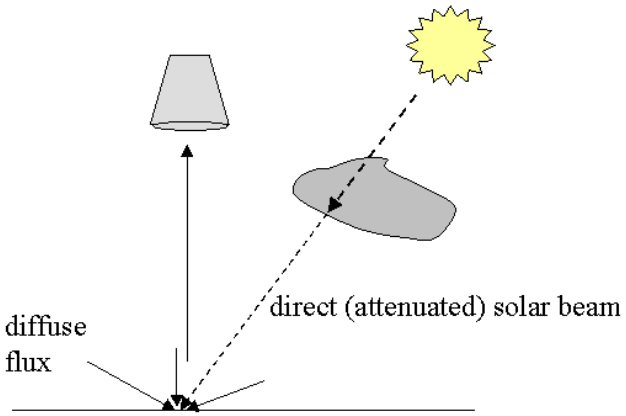

Figure 10.18: *Sketch of a cloud shadow geometry.*

The method starts with a calculation of the surface reflectance image cube $\rho_i = \rho(\lambda_i)$, where three spectral bands around $\lambda_i = 0.85$, 1.6, and 2.2 μm are selected. These bands from the near and shortwave infrared region are very sensitive to cloud shadow effects, because the direct part

of the downwelling solar radiation flux at the ground level is typically 80% or more of the total downwelling flux. Channels in the blue-to-red region (0.4-0.7 μm) are not used for the detection of shadow regions because they receive a much larger diffuse radiation component, making them less sensitive to partial shadow effects. Instead, visible channels serve to define a potential cloud mask.

The surface reflectance is first computed with the assumption of full solar illumination, i.e., the global flux on the ground consists of the direct (E_{dir}) and diffuse (E_{dif}) component. If DN denotes the digital number of a pixel, L_P the path radiance, and τ the atmospheric transmittance (ground-to-sensor) the surface reflectance can be obtained as:

$$\rho_i(x,y) = \frac{\pi(d^2\{c_0(i) + c_1(i)DN_i(x,y)\} - L_{p,i})}{\tau_i\{E_{dir,i} + E_{dif,i}\}} \tag{10.98}$$

Here, d is the Earth-Sun distance at the image acquisition time in astronomical units, c_0 and c_1 are the radiometric calibration coefficients (offset and slope) to convert the digital number into the corresponding at-sensor radiance L, i.e., $L = c_0 + c_1 DN$, and i is the channel index.

The proposed de-shadowing algorithm consists of a sequence of eight processing steps as sketched in Fig. 10.19. It starts with the atmospheric correction. The next step is the masking of water bodies and cloud areas with simple spectral criteria as detailed below. Water pixels have to be excluded as far as possible to avoid their assignment as shadow pixels.
Step 3 calculates the covariance matrix $C(\rho)$ where ρ is the surface reflectance vector comprising only the non-water and non-cloud pixels. For each pixel, this vector holds the reflectance values in the 3 selected channels (around 0.85, 1.6, 2.2 μm). The matched filter is a vector tuned to a certain target reflectance spectrum ρ_t to be detected [1] :

$$V_{mf} = \frac{C^{-1}(\rho_t - \bar{\rho})}{(\rho_t - \bar{\rho})^T C^{-1}(\rho_t - \bar{\rho})} \tag{10.99}$$

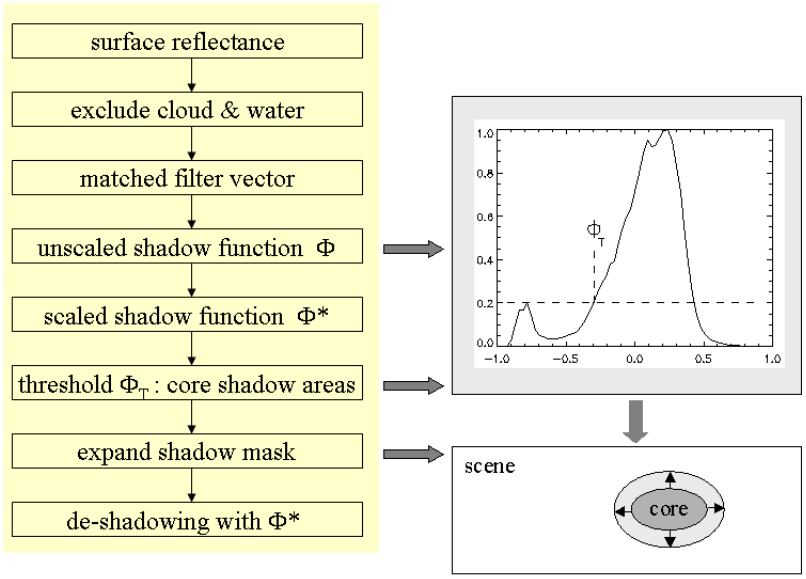

Figure 10.19: *Flow chart of processing steps during de-shadowing.*

Here, $\bar{\rho}$ is the scene-average spectrum, without the water/cloud pixels. Selecting $\rho_t = 0$ for a shadow target yields a special simplified form of the matched filter, where the 'sh' index symbolizes shadow:

$$V_{sh} = -\frac{C^{-1}\bar{\rho}}{\bar{\rho}^T C^{-1}\bar{\rho}} \tag{10.100}$$

The shadow matched filter vector is then applied to the non-water/non-cloud part of the scene and yields the still un-normalized values ϕ that are a relative measure of the fractional direct illumination, also called *unscaled shadow function* here:

$$\Phi(x,y) = V_{sh}^T(\rho(x,y) - \bar{\rho}) \tag{10.101}$$

The matched filter calculates a minimum RMS shadow target abundance for the entire (non-water/non-cloud) scene. Therefore, the values of Φ are positive and negative numbers. The arbitrary, image-depending range of Φ has to be rescaled to the physical range from 0 to 1, where 0 indicates no direct illumination (full shadow), and 1 means full direct illumination. The histogram of Φ is used to rescale the image data. Fig. 10.20 shows a schematic sketch of such a histogram with a smaller peak (at Φ_2) representing the shadow pixels and the main peak (at Φ_{max}) representing the majority of the fully illuminated areas. The statistical assumption is used that full direct solar illumination is already obtained for pixels with $\Phi(x,y) = \Phi_{max}$. Then the values Φ are linearly mapped from the unscaled (Φ_{min}, Φ_{max}) interval onto the physically scaled (0,1) interval, where the *scaled shadow function* is named Φ^*:

$$\Phi^* = \frac{\Phi - \Phi_{min}}{\Phi_{max} - \Phi_{min}} \qquad if \quad \Phi \leq \Phi_{max} \tag{10.102}$$

$$\Phi = 1 \qquad if \quad \Phi > \Phi_{max} \tag{10.103}$$

The smallest value of the scaled shadow function is $\Phi^*_{min} = 0$, which means no direct illumination. However, to avoid overcorrection and to cope with scenes containing merely partial shadow areas, it is advisable to set Φ^*_{min} at a small positive value. This value of Φ^*_{min}, i.e., the minimum fractional direct illumination (deepest shadow in a scene, typically ranging between 0.05 and 0.10) is scene-dependent, see the detailed discussion below.
In principle, the de-shadowing could now be performed with the physically scaled function Φ^*, which represents the fraction of the direct illumination for each pixel in the ρ vector, i.e., the complete scene without cloud and water pixels. However, since the matched filter is not a perfect shadow transformation, it is much better to restrict its application to the potential, most-likely shadow areas. This is an important processing step to reduce the number of mis-classifications or false-alarms. If omitted it will cause strange 'shadow' pixels scattered all over the image. An example can be found in the central part of Fig. 10.21 where the standard shadow map contains a lot of artifact shadow areas.
Therefore, the proposed method tries to find the core shadow areas in a scene, and subsequently expands the core regions to obtain the final mask that includes a smooth shadow/clear transition. The physically scaled shadow function Φ^* is then applied only to the pixels in the final mask.

The histogram of the unscaled shadow function Φ can be employed to separate regions of low values of Φ from the moderate-to-high values, compare Fig. 10.20. A threshold Φ_T can be set in the vicinity of the local histogram minimum (Φ_1) and the core shadow mask is defined by those pixels with $\Phi(x,y) < \Phi_T$. The details of the choice of Φ_T are discussed below. As always with thresholding, some arbitrariness is involved in the final selection.

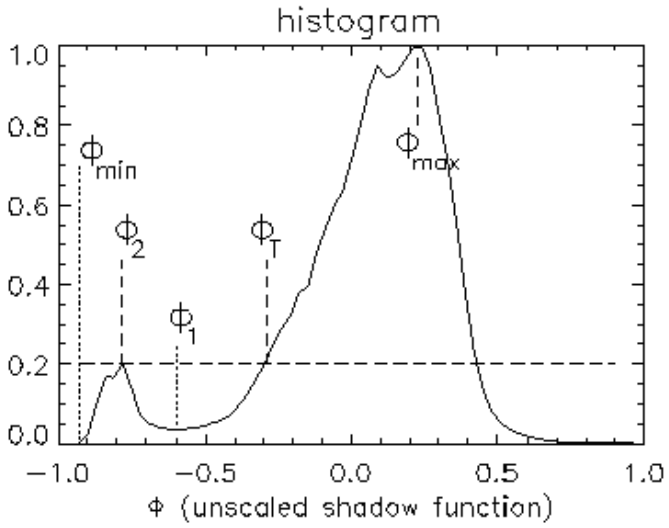

Figure 10.20: *Normalized histogram of unscaled shadow function.*

Once the core shadow mask has been defined, it is expanded to include the surrounding shadow / clear transition zone of 100 m width. De-shadowing with the scaled shadow function Φ^* is then exclusively applied to the pixels in this final mask. This means the direct solar flux (E_{dir} term in eq. 10.98) has to be multiplied with $\Phi^*(x, y)$:

$$\rho_i(x, y) = \frac{\pi(d^2\{c_0(i) + c_1(i)DN_i(x, y)\} - L_{p,i})}{\tau_i\{E_{dir,i}\Phi^*(x, y) + E_{dif,i}\}} \tag{10.104}$$

In equations (10.98, 10.104) the aerosol optical thickness or visibility required for the atmospheric terms (path radiance, transmittance, direct and diffuse flux) can be derived from the image provided the necessary bands in the visible and shortwave infrared region exist and the scene contains dark reference areas [39]. Otherwise, the user has to specify an estimated visibility. The second important atmospheric parameter is the water vapour column. For instruments with bands in the atmospheric water vapour regions this information can be derived from the image data [75], otherwise an estimate has to be provided by the user. In summary, three channels (around 0.85, 1.6, and 2.2 μm) are used to define a matched filter vector with three elements per pixel. For each image pixel the surface reflectance in these three channels and the scene-average reflectance of these channels are calculated to obtain the unscaled shadow function, and finally the scaled shadow function. The same shadow function is employed to de-shadow the imagery not only in the initial three channels but for all channels of the sensor (eq. 10.104).

Details of the method:

One of the most important parameters is the available number of spectral channels during the covariance matrix and matched filter part of the algorithm. The minimum requirement is a band in the near-infrared region (0.8 - 1.0 μm). The performance usually increases significantly if two additional bands (at 1.6 μm and at 2.2 μm) are available, i.e., a Landsat TM type of multispectral sensor. Even for hyperspectral imagery these three bands (around 0.85, 1.6, 2.2 μm) are sufficient for the matched filter calculation. The usage of a hundred bands would not be helpful, but only cause numerical problems during the inversion of the covariance matrix (eq. 10.100).

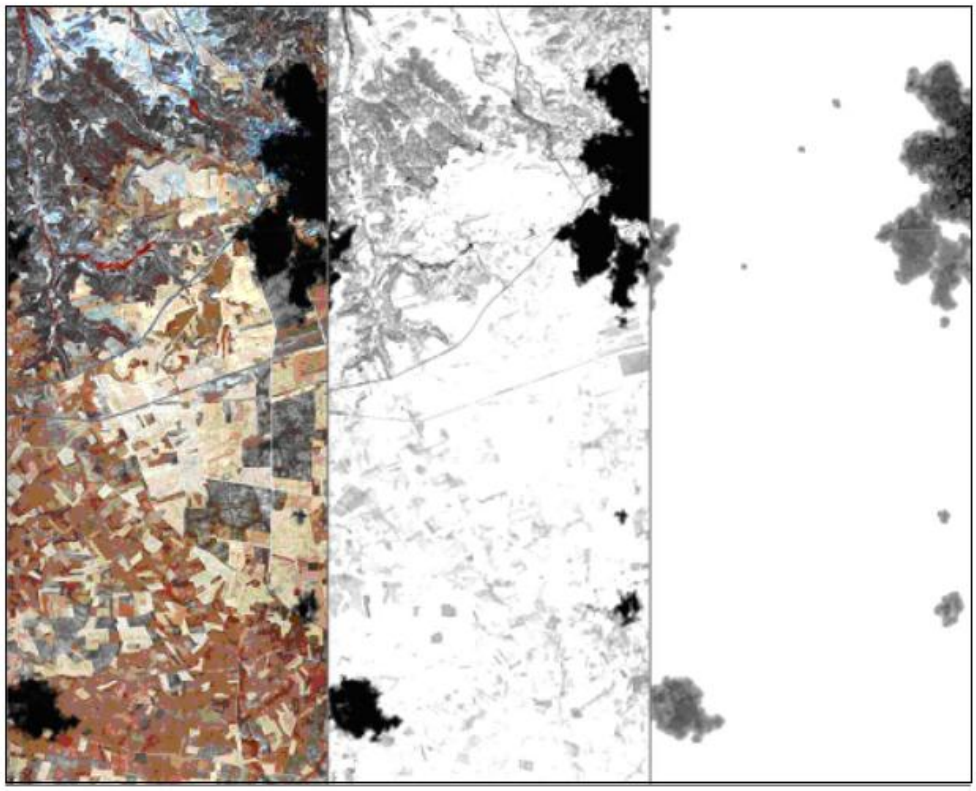

Figure 10.21: *Cloud shadow maps of a HyMap scene.*
Left: surface reflectance image of HyMap at Chinchon, Spain, 12 July 2003. Colour coding: RGB=878, 646, 462 nm channels. Center: standard shadow map showing a lot of artifact shadow areas (grey patches) which do not appear with the core shadow approach (right part). Right: improved cloud shadow map derived from core shadow regions.

Spectral channels from the visible region are merely employed for the masking of cloud regions, not for the matched filter part, because water, vegetation, dark soils, and shadowed pixels all range within a few percent reflectance. In addition, the visible region is not very sensitive to partial shadow effects, because of its larger fraction of diffuse radiation component as compared to wavelengths longer than 0.8 μm.

The distinction of water bodies from cloud shadow areas may be difficult or impossible if it is based merely on spectral reflectance shape and amplitude information. Water bodies should be excluded as far as possible to improve the performance of the de-shadowing algorithm. Currently, water and cloud pixels are masked with the spectral criteria:

$$\rho(0.85\mu m) \leq 5\% \qquad and \qquad \rho(1.6\mu m) \leq 1\% \qquad (water) \tag{10.105}$$

$$\rho(0.48\mu m) \geq 30\% \qquad and \qquad \rho(1.6\mu m) \geq 30\% \qquad (cloud) \tag{10.106}$$

If no channel in the blue region is available, a channel in the green (0.5-0.6 μm) or red part of the spectrum (0.6-0.68 μm) could be used as a substitute. Both criteria do not uniquely define the

corresponding class. The water criteria allow some margin for turbid water in the NIR region. The more restrictive criterion $\rho(0.85\ \mu\text{m}) < 3\%$ would perform better for clear water bodies. However, it would fail for moderately turbid or muddy waters. Other common water classification criteria such as average reflectance over all bands $\bar{\rho} \leq 3\%$ or $\rho(0.4 - 0.6\mu m) < 6\%$ may also fail. So one has to compromise and tolerate a certain amount of misclassification for a fully automatic algorithm. The scaled shadow map $\Phi^*(x, y)$ is written to an output file.

The histogram of the unscaled shadow function Φ (Fig. 10.20) typically has a main peak at Φ_{max}, a smaller secondary peak (at Φ_2) due to shadow pixels, and a local minimum (at Φ_1). The secondary peak can be determined by level-slicing the normalized histogram. We arbitrarily define a threshold Φ_T as the intersection of this slice line at the level of $h(\Phi_2)$ with the normalized histogram h(Φ) for $\Phi_1 < \Phi < \Phi_{max}$. The approach with a main peak and a smaller secondary peak is restricted to cases where the percentage of shadow pixels in the scene is less than about 25%. This applies to the fully automatic processing mode. If the secondary peak at Φ_2 is not clearly defined numerically, i.e., no local minimum found at Φ_1, or histogram difference $h(\Phi_2) - h(\Phi_1) < 0.03$, then Φ_T is defined as the intersection of the slice level 0.10 with h(Φ) for $\Phi < \Phi_{max}$. More flexibility exists in the interactive mode, see chapter 2.5, figure 5.25.

Masking of the core shadow areas with $\Phi < \Phi_T$ (Fig. 10.20) is critical like any thresholding process: a large threshold could potentially include non-shadow areas, a low threshold could miss shadow areas. The current automatic algorithm has the three user-selectable options of a small, medium, or large core shadow mask corresponding to thresholds set at $\Phi_T - 0.1, \Phi_T$, and $\Phi_T + 0.1$, respectively. The default value for the fully automatic algorithm is the medium-size mask. In addition, an interactive mode for adjusting the threshold is also available.

A second tunable parameter is the minimum fractional direct illumination Φ^*_{min}, also called depth of shadow. Theoretically, it can be zero, i.e., a completely shadowed pixel receiving only diffuse solar illumination. However, a too low estimate close to zero will boost the surface reflectance, especially for channels in the 1.5 - 2.5 μm region (eq. 10.104), since the diffuse solar radiation term E_{dif} is very small. Therefore, small positive values of Φ^*_{min} are recommended. The range of Φ^*_{min} is typically from 0.05 to 0.1, with the default set at $\Phi^*_{min} = 0.08$. The third tunable parameter is Φ_{max} providing the range of stretching of the unscaled shadow function into the scaled function. The default of Φ_{max} is the location of the maximum of the histogram of Φ, but it could be set at a greater value if the corrected image is too dark in the expanded shadow regions, which indicates the histogram maximum does not represent fully illuminated areas.

The advantage of the presented method is its fast processing performance, because it relies exclusively on spectral calculations and avoids time-consuming geometric cloud/shadow pattern considerations. The drawback is that useful geometric information is neglected.

In some cases it is useful to have the de-shadowed digital number (DN) image in addition to the surface reflectance product. This facilitates a comparison with the originally recorded DN imagery. The conversion from reflectance to the corresponding at-sensor radiance is performed with eq. (10.1). Then eq. (10.6) is employed to compute the de-shadowed DN image for channel k:

$$DN(k) = \frac{L(k) - c_0(k)}{c_1(k)} \tag{10.107}$$

Figure 10.22 shows an example of de-shadowing. More images with the results of the de-shadowing

method can be found on ATCOR's web page, http://www.rese.ch or http://www.op.dlr.de/atcor .

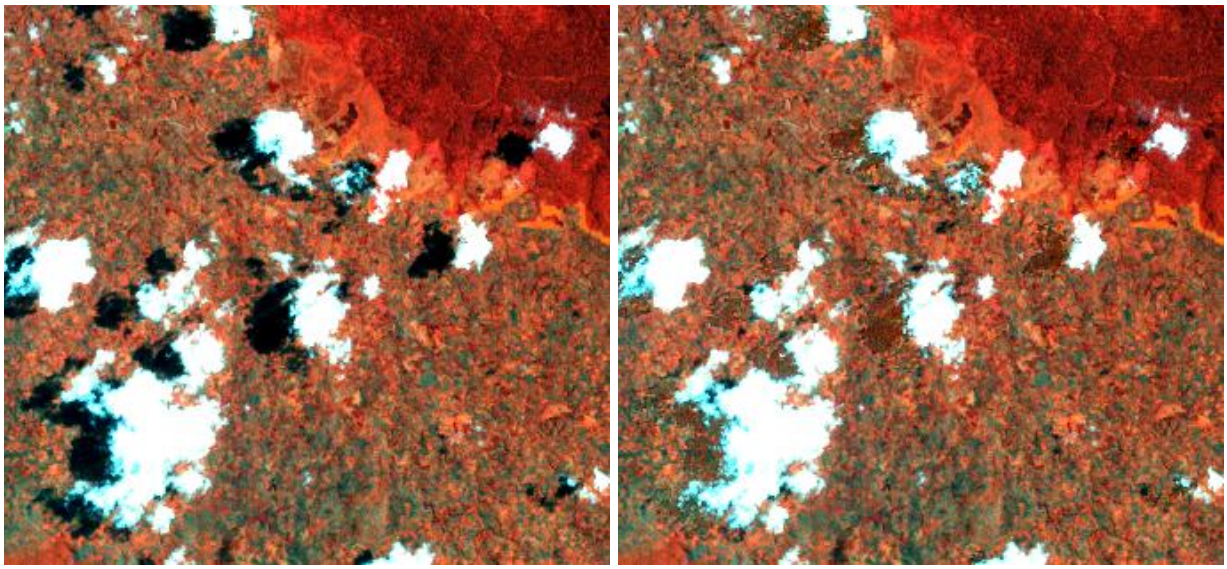

Figure 10.22: *De-shadowing of a Landsat-7 ETM+ scene.*
Subset of a Landsat-7 ETM+ scene from Kenia, 10 April 2001. Color coding: RGB = bands 4/2/1 (830, 560, 480 nm). Left: original scene, right: after de-shadowing.

10.6 Summary of atmospheric correction steps

Although the case of a flat terrain could be treated as a special case of a rugged terrain with the same elevation everywhere this is not an efficient solution, because the rugged terrain algorithm runs 3 to 4 times slower than the flat terrain code. Therefore, the coding is done in separate modules as discussed below.

10.6.1 Algorithm for flat terrain

The complete sequence of processing for sensors with water vapor bands and a short wave IR band (1.6 or 2.2 μm region) consists of the following steps:

- masking of haze, cloud, water, and clear pixels
- haze removal
- de-shadowing
- masking of reference pixels
- calculation of visibility or optical thickness for reference pixels. The optical thickness for the remaining pixels can be defined as the average of the reference pixels or a spatial (triangular) interpolation is employed to fill the gaps. Finally, a moving low pass window with a box size of $3km \times 3km$ is applied to smooth sensor noise and small scale variations of the spectral correlation coefficient for the DDV reference pixels. The resulting visibility index and AOT

maps are stored as separate files. The visibility calculation based on the reference pixels has to account for the adjacency effect, because reference areas are embedded in non-reference areas, see the sketch below. Since the weighting fraction of reference to non-reference area within the adjacency range is not known for each pixel, the visibility calculation is performed with an average adjacency weighting factor of 0.5 q :

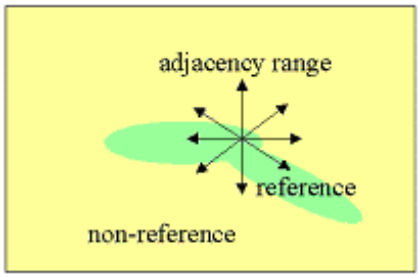

Figure 10.23: *Weighting of q function for reference pixels.*

$$L_{adj.cor} = c_0 + c_1 DN + 0.5q(DN - DN_{av,clear}) \tag{10.108}$$

$$L(VIS) = L_p + \tau \rho_{ref} E_g / \pi = L_{adj.cor} \tag{10.109}$$

Next the visibility is converted into the nearest visibility index vi (range 0-54), compare Fig. 10.9, to store the visibility index map as byte data. Spatial interpolation is performed to fill the gaps for non-reference pixels or the average vi value can be taken to close the gaps. A moving average window of 500 m × 500 m is employed to reduce the influence of noise. In addition, the haze-over-land, haze-over-water, and cloud pixels are coded with 55, 56, and 57 in the visibility index map, respectively. The cloud / building shadow map is stored separately ("fshd.bsq" file, containing the fraction of direct solar irradiance per pixel, scaled with the factor 1000). The scaled value 1000 indicates full solar irradiance, smaller values a corresponding fractional value.

- an update of the path radiance in the blue-to-red spectral region is performed, if required, provided a blue spectral band exists.
- water vapor retrieval using the previously calculated visibility map. If the scene contains no reference areas the user has to specify a constant visibility that enters the water vapor calculation.
- reflectance spectrum retrieval with pixel-based water vapor and visibility map. Iterations for adjacency effect and spherical albedo are included. For the adjacency correction, the reflectance of cloud pixels is replaced with the scene average reflectance to avoid an overcorrection of the adjacency effect.
- temperature / emissivity retrieval if thermal bands exist.

10.6.2 Algorithm for rugged terrain

The algorithm for rugged terrain basically consists of the same processing step as in the flat terrain, but every step has to take into account some or all DEM information:

- During the calculation of the visibility index map the DEM information (elevation, slope, aspect, skyview factor) is taken into account.
- The retrieval of the water vapor map has to include the terrain elevation.
- The empirical BRDF correction is based on the local illumination map (local solar zenith angle) derived from the slope, aspect and shadow channels.
- The retrieval of the spectral reflectance cube consists of the steps
  1. three iterations for terrain reflectance,
  2. empirical BRDF correction depending on illumination map, if enabled,
  3. adjacency correction, including proper treatment of cloud areas,
  4. spherical albedo correction.
- The retrieval of surface temperature and emissivity includes the maps of visibility index, water vapor (if water vapor bands exist), elevation, and scan angle. No slope/aspect correction is performed in the thermal region.

10.7 Spectral classification of reflectance cube

The SPECL code performs a spectral preclassification of the reflectance cube based upon template spectra at the Landsat Thematic Mapper reference wavelengths (i.e., 0.48, 0.56, 0.66, 0.83, 1.6, 2.2 μm) and returns a map of class indices for each pixel. The template spectra consist of typical vegetation covers, soil, sand, and water, see figure 10.24. If the spectral reflectance signature agrees within a 10% margin at the reference wavelengths with one of the class template spectra it is put into this class, otherwise it belongs to the class undefined.

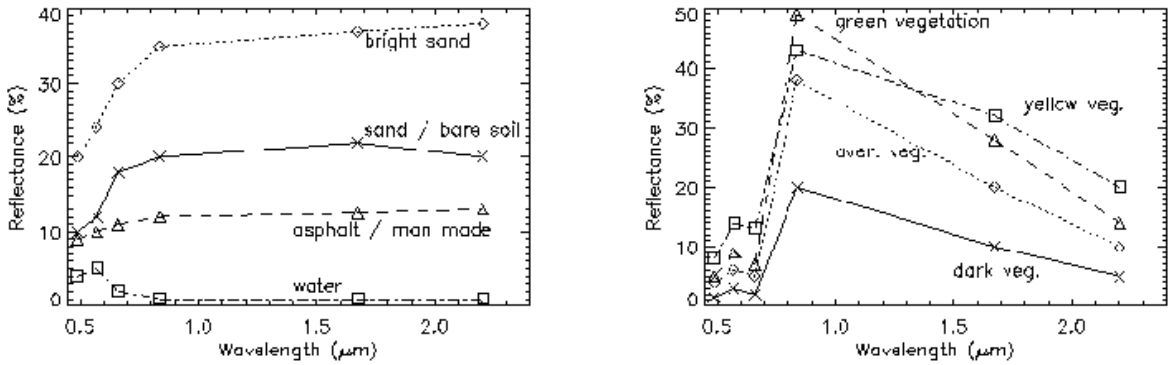

Figure 10.24: *Examples of template reflectance spectra employed by the SPECL code.*

10.8 Accuracy of the method

There is not a single figure that can be given to summarize the accuracy for all situations, because the radiometric accuracy of the method depends on several factors: the calibration accuracy of

the sensor, the quality of geometric co-registration of the spectral bands, the algorithm for ortho-rectification relying on auxiliary information such as attitude and GPS/DGPS, the accuracy of the radiative transfer code (MODTRAN 5), the correct choice of atmospheric input parameters, the terrain type (flat or rugged), and the surface cover.

Solar region:
In the solar region (wavelength < 2.5 μm), assuming a flat terrain, and avoiding the specular and backscattering regions, an accuracy of the retrieved surface reflectance of $\pm 2\%$ (for reflectance $< 10\%$) and $\pm 4\%$ reflectance units (for reflectance $> 40\%$) can be achieved [62]. For rugged terrain, the most important parameter is an adequate spatial resolution of the DEM or DSM (digital surface model) and the exact ortho-rectification of the imagery. It would be desirable to have a DEM of a quarter of the sensor's spatial resolution or at least the resolution of the sensor's footprint which is seldom available [59]. Even in the latter case, errors in the matching of imagery and DEM can lead to large relative reflectance errors exceeding 100% for critical geometries (principal plane, e.g. a mountain ridge with half a pixel offset between imagery and DEM [59]). Thus, the quality of the required DEM will limit the final accuracy of the geo-atmospheric image product in many cases. For a flat terrain and larger off-nadir view angles, BRDF effects may have to be accounted for, and the appropriate surface-cover dependent BRDF model will influence the accuracy.

Thermal region:
In the thermal wavelength region beyond 8 μm, the surface temperature retrieval additionally depends on the correct choice of the surface emissivity. In the ATCOR model the emissivity in one thermal band is based on a classification of the reflective bands if the sensor collects co-registered reflective and thermal band data. Depending on the surface cover classification (vegetation, soil, sand, asphalt, water, etc.), a typical emissivity value is assigned to each class [73]. If the deviation of the true surface emissivity to the assumed emissivity is less than 0.02 (a typical error margin), then the temperatures will be accurate to about 1-1.5 K. A rule of thumb is a surface temperature error of about 0.5-0.8 K per 0.01 emissivity error if the surface temperature is much higher than the boundary layer air temperature [80]. An accuracy of 1-2 K can be achieved if the emissivity estimate is better than 2% [12].

Bibliography

[1] Adler-Golden, S.M., Matthew, M. W., Anderson, G. P., Felde, G. W., and Gardner, J. A., 2002, An algorithm for de-shadowing spectral imagery, *Proc. 11th JPL Airborne Earth Science Workshop, 5-8 March 2002*, JPL-Publication 03-04, Pasadena, U.S.A.

[2] Asrar, G., Fuchs, M., Kanemasu, E. T., and Hatfield, J. L., "Estimating absorbed photosynthetically active radiation and leaf area index from spectral reflectance in wheat", *Agron. J.*, Vol. 76, 300-306, (1984).

[3] Asrar, G. "Theory and Applications of Optical Remote Sensing", J. Wiley, New York, (1989).

[4] Baret, F., and Guyot, G., 1991, "Potentials and limits of vegetation indices for LAI and APAR assessment", *Remote Sensing of Environment*, Vol. 35, 161-173, (1991).

[5] Berk, A., Bernstein, L.S., Anderson, G.P., Acharya, P.K., Robertson, D.C., Chetwynd, J.H., and Adler-Golden, S.M., "MODTRAN cloud and multiple scattering upgrades with application to AVIRIS", *Remote Sensing of Environment*, Vol. 65, 367-375 (1998).

[6] Berk, A., Anderson, G.P., Acharya, P.K., and Shettle, E.P., "MODTRAN5.2.0.0 User's Manual", Spectral Sciences Inc., Burlington MA, Air Force Research Laboratory, Hanscom MA (2008).

[7] Brutsaert, W., "On a derivable formula for long-wave radiation from clear skies", *Water Resources Research*, Vol. 11, 742-744, (1975).

[8] Buettner, K. J. K., and Kern, C. D., "The determination of infrared emissivities of terrestrial surfaces, *Journal of Geophysical Research*, Vol. 70, 1329-1337, (1965).

[9] Carlson, T. N., Capehart, W. J., and Gillies, R. R., "A new look at the simplified method for remote sensing of daily evapotranspiration", *Remote Sensing of Environment*, Vol. 54, 161-167, (1995).

[10] Choudhury, B. J., "Synergism of multispectral satellite observation for estimating regional land surface evaporation", *Remote Sensing of Environment*, Vol. 49, 264-274, (1994).

[11] Choudhury, B. J., Ahmed, N. U., Idso, S. B., Reginato, R. J., and Daughtry, C. S. T., "Relations between evaporation coefficients and vegetation indices studied by model simulations", *Remote Sensing of Environment*, Vol. 50, 1-17, (1994).

[12] Coll, C., Caselles, V., Rubio, E., Sospreda, F., and Valor, E., "Temperature and emissivity separation from calibrated data of the Digital Airborne Imaging Spectrometer", Remote Sens. Environm., Vol. 76, 250-259, (2001).

[13] Coll, C., Richter, R., Sobrino, J. A., Nerry, F., Caselles, V., Jimenez, J. C., Labed-Nachbrand, J., Rubio, E., Soria, G., and Valor, E., "A comparison of methods for surface temperature and emissivity estimation", In *Digital Airborne Spectrometer Experiment*, ESA- SP-499 p. 217-223, Nordwijk, Netherlands (2001).

[14] Corripio, J. G., "Vectorial algebra algorithms for calculating terrain parameters from DEMs and the position of the sun for solar radiation modelling in mountainous terrain", Int. J. of Geographical Information Science, Vol. 17, 1-23 (2003).

[15] Crist, E. P., and Cicone, R. C., "A physically-based transformation of Thematic Mapper data - the Tasseled Cap", *IEEE Trans. Geosci. Remote Sensing*, Vol. GE-22, 256-263 (1984).

[16] Dozier, J., Bruno, J., and Downey, P., "A faster solution to the horizon problem", *Computers & Geosciences*, Vol. 7, 145-151 (1981).

[17] Dell'Endice, F., Nieke, J., Schläpfer, D., and Itten, K. I., "Scene-based method for spatial misregistration detection in hyperspectral imagery", *Applied Optics*, Vol. 46, 2803-2816 (2007).

[18] ERSDAC. "ASTER User's Guide, Part II, (Vers. 3.1)", (2001).

[19] Gao, B.-C., Kaufman, Y.J., Han, W., and Wiscombe, W.J., "Correction of thin cirrus path radiances in the 0.4 - 1.9 μm spectral region using the sensitive 1.375 μm cirrus detecting channel", *J. Geophys. Res.*, Vol. 103, D24, 32,169-32,176 (1998).

[20] Gao, B.-C., Yang, P., Han, W., Li, R.-R., and Wiscombe, W.J., "An algorithm using visible and 1.38 μm channels to retrieve cirrus cloud reflectances from aircraft and satellite data", *IEEE Trans. Geosci. Remote Sens.*, Vol. 40, 1659-1668 (2002).

[21] Gao, B.-C., Kaufman, Y. J., Tanre, D., and Li, R. R., "Distinguishing tropospheric aerosols from thin cirrus clouds for improved aerosol retrievals using the ratio of $1.38-\mu m$ and $1.24-\mu m$ channels", *Geophys. Res. Letters*, Vol. 29, No. 18, 1890, 36-1 to 36-4 (2002).

[22] Gao, B.-C., Meyer, K., and Yang, P., "A new concept on remote sensing of cirrus optical depth and effective ice particle size using strong water vapor absorption channels near 1.38 and 1.88 μm", *IEEE Trans. Geosci. Remote Sens.*, Vol. 42, 1891-1899 (2004).

[23] Gillespie, A. R., "Lithologic mapping of silicate rocks using TIMS", *In Proc. TIMS Data User's Workshop*, JPL Publ. 83-38 (Pasadena, CA), pp. 29-44 (1986).

[24] Gillespie, A., et al., "A temperature and emissivity separation algorithm for Advanced Spaceborne Thermal Emission and Reflection Radiometer (ASTER) images", *IEEE Trans. Geosc. Remote Sensing*, Vol. 36, 1113-1126 (1998).

[25] Gu, D., and Gillespie, A., "Topographic normalization of Landsat TM images of forest based on subpixel sun - canopy - sensor geometry", *Remote Sensing of Environment*, Vol. 64, 166-175 (1998).

[26] Guanter, L., Richter, R., and Moreno, J., "Spectral calibration of hyperspectral imagery using atmospheric absorption features", *Applied Optics*, Vol. 45, 2360-2370 (2006).

[27] Guanter, L., Richter, R., and Kaufmann, H., "On the application of the MODTRAN4 atmospheric radiative transfer code to optical remote sensing", accepted for publication, *Int. J. Remote Sensing*, 30(6), 14071424, doi:10.1080/01431160802438555 (2009).

[28] Hay, J. E., and McKay, D. C., "Estimating solar irradiance on inclined surfaces: a review and assessment of methodologies", *Int. J. Solar Energy*, Vol. 3, 203-240 (1985).

[29] Huete, A. R., "A soil adjusted vegetation index (SAVI)", *Remote Sensing of Environment*, Vol. 25, 295-309, (1988).

[30] Idso, S. B., and Jackson, R. D., "Thermal radiation from the atmosphere", *J. Geophysical Research*, Vol. 74, 5397-5403, (1969).

[31] Isaacs, R. G., Wang, W-C., Worsham, R. D., and Goldberg, S., "Multiple scattering LOWTRAN and FASCODE models", *Applied Optics*, Vol. 26, 1272-1281, (1987).

[32] Kahle, A. B., et al., "Middle infrared multispectral aircraft scanner data analysis for geological applications", *Applied Optics*, Vol. 19, 2279-2290 (1980).

[33] Kamstrup, N., and Hansen, L. B., "Improved calibration of Landsat-5 TM applicable for high-latitude and dark areas", *Int. J. Remote Sensing*, Vol. 24, 5345-5365 (2003).

[34] Chander, G., Markham, B. L., and Helder, D. L., "Summary of current radiometric calibration coefficients for Landsat MSS, TM, ETM+, and EO-1 ALI sensors", *Remote Sens. Environm.*, Vol. 113, 893-903 (2009).

[35] Fontenla, J. M., Curdt, W and Haberreiter, M., Harder J., and Tian, H.,"Semiempirical Models of the Solar Atmosphere. III. Set of Non-LTE Models for Far-Ultraviolet/Extreme-Ultraviolet Irradiance Computation *The Astrophysical Journal*, 707:482-502 (2009).

[36] Fontenla, J. M., Harder, J., Livingston, W., Snow, M., and Woods, T., "High-resolution solar spectral irradiance from extreme ultraviolett to far infrared", J. Geophys. Res., Vol. 116, D20108, 31pp., (2011).

[37] Fraser, R. S., Bahethi, O.P., and Al-Abbas, A. H., "The effect of the atmosphere on classification of satellite observations to identify surface features", *Remote Sens. Environm.*, Vol. 6, 229-249 (1977).

[38] Kaufman, Y. J., and Sendra, C., "Algorithm for automatic atmospheric corrections to visible and near-IR satellite imagery", *Int. J. Remote Sensing*, Vol. 9, 1357-1381 (1988).

[39] Kaufman, Y. J., et al. "The MODIS 2.1 μm channel - correlation with visible reflectance for use in remote sensing of aerosol", *IEEE Transactions on Geoscience and Remote Sensing*, Vol. 35, 1286-1298 (1997).

[40] Kobayashi, S., and Sanga-Ngoie, K., "The integrated radiometric correction of optical remote sensing imageries" *Int. J. Remote Sensing*, Vol. 29, 5957-5985 (2008).

[41] Kobayashi, S., and Sanga-Ngoie, K., "A comparative study of radiometric correction methods for optical remote sensing imagery: the IRC vs. other image-based C-correction methods", *Int. J. Remote Sensing*, Vol. 30, 285-314 (2009).

[42] Irish, R. R., Barker, J. L., Goward, S. N., and Arvidson, T., "Characterization of the Landsat-7 ETM+ automated cloud-cover assessment (ACCA) algorithm", *Photogr. Eng. Remote Sens.* Vol. 72, 1179-1188 (2006).

[43] Yi, C. Y., "Haze reduction from the visible bands of Landsat TM and ETM+ images over a shallow water reef environment", *Remote Sens. Environm.*, Vol. 112, 1773-1783 (2008).

[44] Liang, S., Falla-Adl, H., Kalluri, S., Jaja, J., Kaufman, Y. J., and Townshend, J. R. G., "An operational atmospheric correction algorithm for Landsat Thematic Mapper imagery over the land", *J. Geophys. Res.*, Vol. 102, D14, 17,173-17,186 (1997).

[45] Ackerman, S. A., Strabala, K. I., Menzel, W. P., Frey, R. A., Moeller, C. C., and Gumley, L. E., "Discriminating clear sky from clouds with MODIS", *J. Geophys. Res.*, Vol. 103, D24, 32,141-32,157 (1998).

[46] Krause, K., "Radiance conversion of QuickBird data", Technical note RS_TN_radiometric_radiance_4002, http://www.digitalglobe.com, Digital Globe, 1900 Pike Road, Longmont, CO 80501, USA (2003).

[47] Kriebel, K. T., "Measured spectral bidirectional reflection properties of four vegetated surfaces", *Applied Optics*, Vol. 17, 253-259 (1978).

[48] Mouroulis, P., Green, R. O., and Chrien, T. G., "Design of pushbroom imaging spectrometers for optimum recovery of spectroscopic and spatial information", *Applied Optics*, Vol. 39, 2210-2220 (2000).

[49] Moran, M. S., Clarke, T. R., Inoue, Y., and Vidal, A., "Estimating crop water deficit using the relation between surface-air temperature and spectral vegetation index", *Remote Sensing of Environment*, Vol. 49, 246-263 (1994).

[50] Murray, F. W., "On the computation of saturation vapor pressure", *J. Applied Meteorology*, Vol. 6, 203-204, (1967).

[51] Stamnes, K., Tsay, S. C., Wiscombe, W. J., and Jayaweera, K., "Numerically stable algorithm for discrete-ordinate-method radiative transfer in multiple scattering and emitting layered media", *Applied Optics*, Vol. 27, 2502-2509 (1988).

[52] Nicodemus, F. E., "Reflectance nomenclature and directional reflectance and emissivity", *Applied Optics*, Vol. 9, 1474-1475 (1970).

[53] Parlow, E., "Net radiation of urban areas", Proc. 17th EARSeL Symposium on Future Trends in Remote Sensing, Lyngby, Denmark, 17-19 June 1997, pp. 221-226, Balkema, Rotterdam (1998).

[54] Riano, D., Chuvieco, E., Salas, J., and Aguado, I., "Assessment of different topographic corrections in Landsat-TM data for mapping vegetation types", *IEEE Trans. Geoscience and Remote Sensing*, Vol. 41, 1056-1061 (2003).

[55] Richter, R., "Derivation of temperature and emittance from airborne multispectral thermal infrared scanner data", *Infrared Phys. Technol.*, Vol. 35, 817-826 (1994).

[56] Richter, R., "A spatially adaptive fast atmospheric correction algorithm", *Int. J. Remote Sensing*, Vol. 17, 1201-1214 (1996).

[57] Richter, R., "Atmospheric correction of satellite data with haze removal including a haze/clear transition region", *Computers & Geosciences*, Vol. 22, 675-681 (1996).

[58] Richter, R., "On the in-flight absolute calibration of high spatial resolution spaceborne sensors using small ground targets", *Int. J. Remote Sensing*, Vol. 18, 2827-2833 (1997).

[59] Richter, R., "Correction of satellite imagery over mountainous terrain", *Applied Optics*, Vol. 37, 4004-4015 (1998).

[60] Richter, R., "Bandpass-resampling effects on the retrieval of radiance and surface reflectance", *Applied Optics*, Vol. 39, 5001-5005 (2000).

[61] Richter, R., and Coll, C., "Bandpass-resampling effects for the retrieval of surface emissivity", *Applied Optics*, Vol. 41, 3523-3529 (2002).

[62] Richter, R., and Schläpfer, D., "Geo-atmospheric processing of airborne imaging spectrometry data. Part 2: atmospheric / topographic correction.", *Int. J. Remote Sensing*, Vol. 23, 2631-2649 (2002).

[63] Richter, R., and Müller, A., "De-shadowing of satellite/airborne imagery", *Int. J. Remote Sensing*, Vol. 26, 3137-3148 (2005).

[64] Richter, R., Schläpfer, D., and Müller, A., "An automatic atmospheric correction algorithm for visible/NIR imagery", *Int. J. Remote Sensing*, Vol. 27, 2077-2085 (2006).

[65] Richter, R., Bachmann, M., Dorigo, W., Mueller, A., "Influence of the adjacency effect on ground reflectance measurements", *IEEE Geoscience Remote Sensing Letters*, Vol. 3, 565-569 (2006).

[66] Richter, R., and Schläpfer, D., "Considerations on water vapor and surface reflectance retrievals for a spaceborne imaging spectrometer", *IEEE Trans. Geoscience Remote Sensing*, Vol. 46, 1958-1966 (2008).

[67] Richter, R., Kellenberger, T., and Kaufmann, H., "Comparison of topographic correction methods", *Remote Sensing*, Vol. 1, 184-196 (2009).

[68] Richter, R., "Atmospheric / topographic correction for satellite imagery: ATCOR-2/3 User Guide", DLR IB 565-01/11, Wessling, Germany (2011).

[69] Richter, R., "Atmospheric / topographic correction for airborne imagery: ATCOR-4 User Guide", DLR IB 565-02/12, Wessling, Germany (2012).

[70] Richter, R., Schläpfer, D., and Müller, A., "Operational atmospheric correction for imaging spectrometers accounting the smile effect", *IEEE Trans. Geoscience Remote Sensing*, Vol. 49, 1772-1780 (2011).

[71] Richter, R., Wang, X., Bachmann, M., and Schläpfer, D., "Correction of cirrus effects in Sentinel-2 type of imagery", *Int. J. Remote Sensing*, Vol.32, 2931-2941 (2011).

[72] Rodger, A., and Lynch, M. J., "Determining atmospheric column water vapour in the 0.4-2.5 μm spectral region", Proceedings of the AVIRIS Workshop 2001, Pasadena, CA (2001).

[73] Salisbury, J. W., and D'Aria, D. M., "Emissivity of terrestrial materials in the 8-14 μm atmospheric window", *Remote Sensing of Environment*, Vol. 42, 83-106 (1992).

[74] Santer, R., et al., "SPOT Calibration at the La Crau Test Site (France)", *Remote Sensing of Environment*, Vol. 41, 227-237 (1992).

[75] Schläpfer, D., Borel, C. C., Keller, J., and Itten, K. I., "Atmospheric precorrected differential absorption technique to retrieve columnar water vapor", *Remote Sensing of Environment*, Vol. 65, 353-366 (1998).

[76] Schläpfer, D., and Richter, R., "Geo-atmospheric processing of airborne imaging spectrometry data. Part 1: parametric orthorectification.", *Int. J. Remote Sensing*, Vol. 23, 2609-2630 (2002).

[77] Schläpfer, D. "PARGE, User Guide, Version 3.0", ReSe Applications Schlpfer, Wil, Switzerland, (2010).

[78] Schowengerdt, R. A., "Remote Sensing, Models and Methods for Image Processing", 3rd Edition, Elsevier (Academic Press), (2007).

[79] Sirguey, P., "Simple correction of multiple reflection effects in rugged terrain", *Int. J. Remote Sensing*, Vol. 30, 1075-1081 (2009).

[80] Slater, P. N., "Remote Sensing, Optics and Optical Systems", Addison-Wesley, London (1980).

[81] Slater, P. N., "Radiometric considerations in remote sensing", *Proc. IEEE*, Vol. 73, 997-1011 (1985).

[82] Slater, P. N., et al., "Reflectance and radiance-based methods for the in-flight absolute calibration of multispectral sensors", *Remote Sensing of Environment*, Vol. 22, 11-37 (1987).

[83] Soenen, S., A., Peddle, D. R.,and Coburn, C. A., "SCS+C: a modified sun - canopy - sensor topographic correction in forested terrain", *IEEE Trans. Geoscience and Remote Sensing*, Vol. 43, 2148-2159 (2005).

[84] Sutherland, R. A., "Broadband and spectral emissivities (2-18 μm) of some natural soils and vegetation, *Journal of Atmospheric and Oceanic Technology*, Vol. 3, 199-202, (1986).

[85] Teillet, P. M., Guindon, B., and Goodenough, D.G., "On the slope-aspect correxion of multispectral scanner data", *Canadian J. Remote Sensing*, Vol. 8, 84-106, (1982).

[86] Wiegand, C. L., Gerbermann, A. H., Gallo, K. P., Blad, B. L., and Dusek, D., "Multisite analyses of spectral-biophysical data for corn", *Remote Sensing of Environment*, Vol. 33, 1-16, (1990).

[87] Wiegand, C. L., Richardson, A. J., Escobar, D. E., and Gerbermann, A. H., "Vegetation indices in crop assessments", *Remote Sensing of Environment*, Vol. 35, 105-119, (1991).

[88] Wolfe, W. L., and Zissis, G. J., "The Infrared Handbook", Office of Naval Research, Washington, DC., (1985).

[89] Young, S. J., Johnson, B. R., and Hackwell, J. A., "An in-scene method for atmospheric compensation of thermal hyperspectral data", *J. Geophys. Research*, Vol. 107, No. D24, 4774-4793 (2002).

[90] Zhang, Y., Guindon, B., and Cihlar, J., "An image transform to characterize and compensate for spatial variations in thin cloud contamination of Landsat images", *Remote Sensing of Environment*, Vol. 82, 173-187 (2002).

Appendix A

Altitude Profile of Standard Atmospheres

This chapter contains the altitude profiles of ATCOR's standard atmospheres that are based on the MODTRAN code. Only the lower 5 km altitudes are shown, since this region has the largest influence on the radiative transfer results and usually comprises about 90-95% of the total water vapor column. For multispectral sensors without water vapor bands, e.g., Landsat TM or SPOT, the selection of the atmosphere should be coupled to the season of the image data acquisition. The influence of a large error in the water vapor estimate (e.g., 50%) on the reflectance retrieval is usually very small (about 1-2% reflectance at a reflectance level of 40% for Landsat TM band 4).

However, for sensors with water vapor bands (e.g., MOS-B or hyperspectral sensors) the water vapor content plays an important role. For these sensors the database contains files with four water vapor columns (2.9, 2.0, 1.0, 0.4 cm). These are used to generate interpolated and extrapolated values for the LUTs. In analogy to the files for the airborne version of ATCOR the file names are *"h99000_wv29_rura.atm"*, *"h99000_wv20_rura.atm"*, etc., where the h99000 indicates the symbolic height of 99000 m used for satellites, the water vapor column content wv (cm or g cm^{-2}) is scaled with 10, and the aerosol type is included in the last part of the name.

altitude (km)	pressure (mbar)	temperature (°C)	rel. humidity (%)	abs. humidity (gm^{-3})
0	1013	26.4	7.5	1.9
1	904	20.4	7.3	1.3
2	805	14.4	7.4	0.9
3	715	10.4	4.8	0.5
4	633	3.8	3.5	0.2
5	559	-3.0	3.8	0.1

Table A.1: *Altitude profile of the dry atmosphere. Total (ground-to-space) water vapor content = 0.41 (cm or g cm^{-2}).*

altitude (km)	pressure (mbar)	temperature (°C)	rel. humidity (%)	abs. humidity (g/m^{-3})
0	1018	-1.0	77	3.5
1	897	-4.5	70	2.5
2	789	-8.0	65	1.8
3	694	-11.5	57	1.2
4	608	-17.5	50	0.7
5	531	-23.5	47	0.4

Table A.2: *Altitude profile of the midlatitude winter atmosphere. Total (ground-to-space) water vapor content = 0.85 (cm or g cm^{-2}).*

altitude (km)	pressure (mbar)	temperature (°C)	rel. humidity (%)	abs. humidity (g/m^{-3})
0	1013	10.0	56	5.2
1	902	3.0	47	2.8
2	802	-1.0	41	1.9
3	710	-5.0	40	1.4
4	628	- 9.0	40	1.0
5	554	-14.0	40	0.6

Table A.3: *Altitude profile of the fall (autumn) atmosphere. Total (ground-to-space) water vapor content = 1.14 (cm or g cm^{-2})*

altitude (km	pressure (mbar)	temperature (°C)	rel. humidity (%)	abs. humidity (g/m^{-3})
0	1013	15.0	46	5.9
1	900	8 .5	49	4.2
2	795	2.0	52	2.9
3	701	-4.5	51	1.8
4	616	-11.0	50	1.1
5	540	-17.5	48	0.6

Table A.4: *Altitude profile of the 1976 US Standard. Total (ground-to-space) water vapor content = 1.42 (cm or g cm^{-2}).*

altitude	pressure	temperature	rel. humidity	abs. humidity
(km)	(mbar)	(°C)	(%)	(g/m^{-3})
0	1010	14.0	75	9.1
1	896	8.5	70	6.0
2	792	3.1	70	4.2
3	700	-2.3	65	2.7
4	616	-7.7	60	1.7
5	541	-13.1	53	1.0

Table A.5: *Altitude profile of the subarctic summer atmosphere. Total (ground-to-space) water vapor content = 2.08 (cm or g* cm^{-2}*).*

altitude	pressure	temperature	rel. humidity	abs. humidity
(km)	(mbar)	(°C)	(%)	(g/m^{-3})
0	1013	21.0	76	13.9
1	902	16.5	66	9.3
2	802	12.0	55	5.9
3	710	6.0	45	3.9
4	628	0.0	39	1.9
5	554	-6.0	31	1.0

Table A.6: *Altitude profile of the midlatitude summer atmosphere. Total (ground-to-space) water vapor content = 2.92 (cm or g* cm^{-2}*).*

altitude	pressure	temperature	rel. humidity	abs. humidity
(km)	(mbar)	(°C)	(%)	(g/m^{-3})
0	1013	26.4	75	18.9
1	904	20.4	73	13.0
2	805	14.4	74	9.3
3	715	10.4	48	4.7
4	633	3.8	35	2.2
5	559	-3.0	38	1.5

Table A.7: *Altitude profile of the tropical atmosphere. Total (ground-to-space) water vapor content = 4.11 (cm or g* cm^{-2}*).*

Appendix B

Comparison of Solar Irradiance Spectra

The following two plots show the relative differences between two extraterrestrial solar irradiance sources:

- Kurucz 1997 (distributed with MODTRAN, Berk et al. 2008 [6]). The previous high-resolution (*"monochromatic"*) databases of ATCOR were calculated with this spectrum.
- Fontenla 2011 (Fontenla et al., 2009, 2011 [35, 36]). The new ATCOR release uses the improved quiet sun spectrum of Fontenla and co-workers, also referred to as "low activity sun".

As explained in chapters 5.7.10, 5.7.11 the user can convert the database of atmospheric look-up tables from one solar irradiance source to another one, provided that the spectral range and sampling distance agrees with the template spectra in the *"sun_irradiance"* directory of ATCOR. Currently, irradiance spectra of Kurucz 1997, Kurucz 2005 (distributed with MODTRAN [6]), and Fontenla 2011 are offered.

The plots show the detailed information (line structure) contained in the Fontenla spectrum. The curves with 2.8 nm and 10 nm represent results based on a moving average of the the 0.4 nm data over 7 and 25 spectral points, respectively.

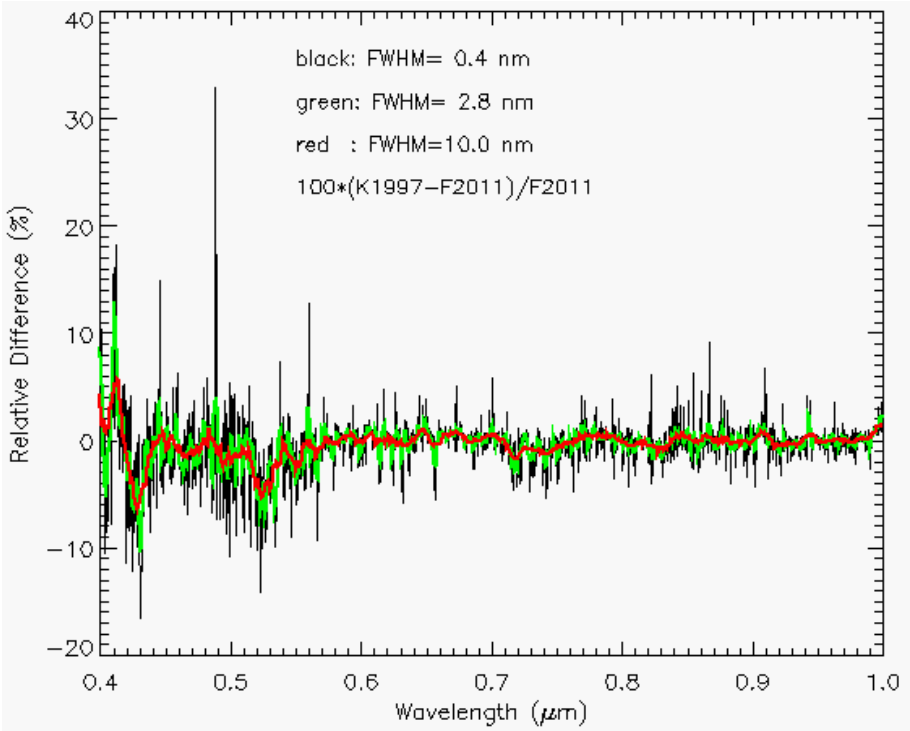
black: FWHM= 0.4 nm
green: FWHM= 2.8 nm
red : FWHM=10.0 nm
100*(K1997−F2011)/F2011
Relative Difference (%)
Wavelength (μm)
40
30
20
10
0
−10
−20
0.4
0.5
0.6
0.7
0.8
0.9
1.0

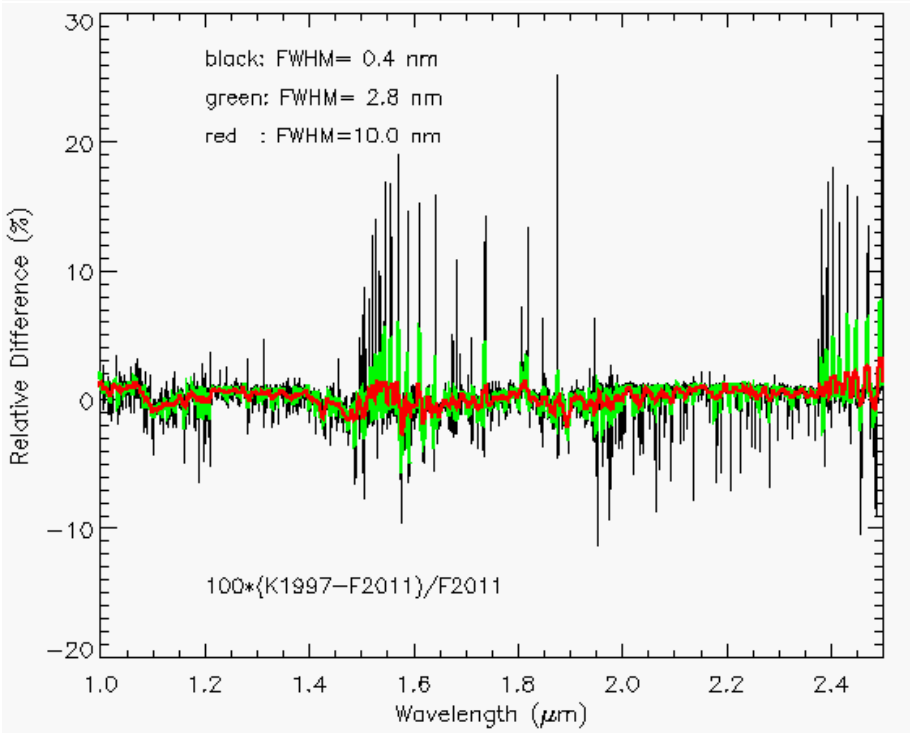
black: FWHM= 0.4 nm
green: FWHM= 2.8 nm
red : FWHM=10.0 nm
100*(K1997−F2011)/F2011
Relative Difference (%)
Wavelength (μm)
30
20
10
0
−10
−20
1.0
1.2
1.4
1.6
1.8
2.0
2.2
2.4